DIFFERENTIATION OF THE CAV1.2 AND CAV1.3 PHARMACOLOGY AND ROLE OF RYR2 IN PANCREATIC BETA-CELL ELECTROPHYSIOLOGY

by

Shiqi Tang

A Dissertation

Submitted to the Faculty of Purdue University

In Partial Fulfillment of the Requirements for the degree of

Doctor of Philosophy

Department of Medicinal Chemistry and Molecular Pharmacology

West Lafayette, Indiana

August 2021

THE PURDUE UNIVERSITY GRADUATE SCHOOL
STATEMENT OF COMMITTEE APPROVAL

Dr. Gregory H. Hockerman, Chair

Department of Medicinal Chemistry and Molecular Pharmacology

Dr. Val Watts

Department of Medicinal Chemistry and Molecular Pharmacology

Dr. Yang Yang

Department of Medicinal Chemistry and Molecular Pharmacology

Dr. Riyi Shi

Department of Neuroscience and Biomedical Engineering

Approved by:

Dr. Andy Hudmon

I dedicate this dissertation to my lovely parents, Lihong Wen and Yongqiang Tang, who have been providing the best support they could and unconditional love throughout my life, even when they were under enormous financial burden. Their unconditional love helps me conquer every critical challenge I have faced. I also dedicate this to my favorite grandpa, Changbao Wen, who came to my undergraduate graduation on a 13-hour flight in his late 80s and wanted to come for my Ph.D. defense even though he does not speak English. Finally, at last, to my boyfriend Mark Hyde if he still dates me.

ACKNOWLEDGMENTS

I cannot express how grateful I am for Dr. Gregory Hockerman to accept me into the lab to continue studying ion channels and membrane proteins. More importantly, because of this wonderful lab, I sincerely believe that I had a much happier graduate student life than average, that I was asked so many times why I always looked so happy in the hallway and the lab by undergrads and other PIs. The electrophysiology skills Dr.H taught me step-by-step and all the great advice on academia and life shine a light on my current and future path. Not to mention the mini slang lecture series over the years, along with old-fashioned academic story dragging me back to the time when retro journals were printed on A6, and the excellent examples to pursue a meaningful life without giving up passion for research. He can always tell you more about the world and always available in his welcoming office. Sorry if I dragged along here, but I would like to show more solid proof that Dr. H has been such an inspirational idol in life besides an exceptional investigator and lecturer in academia, as no one in our lab has given vivid talks in this tiny section of their thesis. I would like to acknowledge the members of my advisory committee, Dr. Val Watts, Dr. Yang Yang, and Dr. Riyi Shi, who are extraordinary in their fields and always supportive of electrophysiology and writing suggestions. I would also like to thank Dr. Park for allowing us to take over his student office and lab equipment. Without him, we could not finish our graduate studies. I also would like to thank Dr. van Rijn, my undergraduate PI, for leading me to graduate school, teaching me the proper way to practice science in membrane proteins and calcium pathways, and support my preliminary exam, and Dr. Pelaez, who led me to the world of calcium eight years ago.

Next, I owe a lot of “thank you” to our current and past members. Thanks to Amy Salyer, our lovely and only lab manager, for making the most excellent protocols and keeping everything so organized, plus the best home-made macaroons, the most fantastic lab art so we could win all the art contests in the department, and all the nerdy interest sharing outside the nerdy lab talks. And so many thanks to Dr. Kyle Harvey, who is the lab angel/mom in our lab, doing the most complicated experiments, filling the heaviest DI water tanks, taking care of the whole building (even the buildings across the campus). He is the most creative scientist in my generation, thanks to his brilliant experimental ideas, delicious vegetarian food invites, game nights, fluffy kids, and two life-long friends. Thanks to Emily Rantz, who is also so kind and offering help and care all

the time. She is a smart, strong lady and also shares her armors with people near her. Thanks to Dr. Evan Pratt for accepting my drinking tickets in my undergrad and graduate conferences and how to do plate assays. Thanks to our forever 18-year-old undergraduate, Paxton Sample, for being cool in the lab. Thanks to our past lab members for building the solid scientific path for our current research, especially Dr. Yuchen Wang and Dr. Rachel Jarrard, for their extraordinary effort and guidance. I have to thank all the senior friends from MCMP, Nook Doungakamol, Remah Ali, Shaminie Athinarayanan, Trevor and Meridith Doyle, Chen Chen, and MeeJung Ko, for providing precious suggestions on academia and life.

I would like to thank the staff in the college of pharmacy. Nine years in this college have taught me very well and educated me from a foreign teenager who knew nothing about scientific methods and a well-prepared scientist ready to solve critical puzzles independently and collaboratively. I have been feeling very supported since I was enrolled in this college as a ready-to-be bachelor of pharmaceutical science back in 2012, and my opinion still stayed the same in 2021. I would like to thank my friends through the years for sharing my happiness and sadness. I could not survive on my own without any of the help provided around me. I have to thank Ying Huang and Qin Dong (and her parents) for helping with my TA. I have to thank Yue Peng and Yuan Gao for providing the most professional mental support. I have to nominate my dearest ex-roommate Yu Wang for sabotaging my fitness plan but becoming the one best homie in my grad life. I do not know how I can thank my parents, Lihong Wen and Yongqiang Tang, for supporting my study abroad, which took almost everything my family had. The three of us cried over the free internet call with a 12-hour difference for not being good enough parents or kids, as we all struggled for a long time in poverty to pay off the tuition without letting each other know. All this time, I thought that, without me, my parents would have a rich and comfortable life, but they said: without you, we would not achieve what we have today. They also said: no matter where you go, where three of us being together is home. At last, I have to thank my boyfriend, Mark Hyde, for being so supportive of my every critical decision, proofreading my thesis, organizing the list of tables and figures, and stealing the interesting names of these excellent scientists in my references to color his novels. Most importantly, he provided a home for me away from my home, that I can strive to fight for what I am dreaming of without worrying about where I will end up alone the next day.

TABLE OF CONTENTS

LIST OF TABLES

LIST OF FIGURES

LIST OF ABBREVIATIONS

6-OHDA	hydroxylated dopamine
ABC	transporter ATP-binding cassette transporter
Ach	acetylcholine
AD	Alzheimer's disease
ADHD	attention deficit-hyperactivity disorder
ADP	diphosphate
AHP	Ca^{2+}-dependent K^{+}-mediated afterhyperpolarization
AID	α interacting domain
AKAP15	A-kinase anchoring protein
ALS	amyotrophic lateral sclerosis
AMPR	α-amino-3-hydroxy-5-methyl-4-isoxazole propionic acid receptor
AP	action potential
apoCam	Ca^{2+}- free CaM
AR	androgen receptor
ASD	autism spectrum disorders
ATP	triphosphate
BAPTA	1,2-bis(o-aminophenoxy)ethane-N,N,N′,N′-tetraacetic acid
Bay K 8644	methyl 2,6-dimethyl-5-nitro-4-[2-(trifluoromethyl)phenyl]-1,4-dihydropyridine-3-carboxylate
BDNF	Brain-derived neurotrophic factor
BID	β interacting domain
BPTI	bovine pancreatic trypsin inhibitor
Bsol	bridging α-solenoid repeats
BTZ	benzothiazepines
C/EBPs	CCAAT enhancer-binding proteins
CaC	calcicludine
cADPR	cyclic ADP-ribose
CaM	calmodulin
CaMKII	calcium/calmodulin-dependent kinase II
CaMKIV	calcium/calmodulin-dependent kinase IV
cAMP	cyclic adenosine monophosphate
CaS	calciseptine
CAZ	cytomatrix in the active zone
CCAAT	Cytidine-Cytidine-Adenosine-Adenosine-Thymidine
CCAT	calcium channel associated transcription regulator
CCB	calcium channel blocker
CCD	central core disease
CDI	calcium-dependent inactivation

CFTR	cystic fibrosis transmembrane conductance regulator
CICR	calcium-induced calcium release
CRF_1s	corticotropin-releasing factor 1 receptors
CREB	cAMP response element-binding protein
CRISPR	Clustered Regularly Interspaced Short Palindromic Repeats
Cryo-EM	cryo-electron microscopy
CSNB2	congenital stationary night blindness type-2
CT	C-terminus
DA	dopamine
DAG	diacylglycerol
DCM	dilated cardiomyopathy
DH5α	E.coli cells engineered by Dr. Douglas Hanahan
DHP	dihydropyridines
DHPi	dihydropyridine insensitive
D-MEM	Dulbecco's Modified Eagle's Medium
E2	The predominant biologic effects of estradiol
EC	endometrial carcinoma
EGTA	Ethylene glycol tetra acetic acid
ENZ	enzalutamide, an androgen receptor antagonist
EPAC2	exchange protein directly activated by cAMP
ER	endoplasmic reticulum
ERK1/2	Extracellular Signal-Regulated Kinase 1/2
ERs	estrogen receptors
FACS	Fluorescence Activated Cell Sorting
FBS	Fetal bovine serum
FFA	free fatty acids
FK-506	tacrolimus
FKBP	FL506 binding protein 12
FKBP12	Calstabn1, Ca^{2+} channel-binding and -stabilizing protein 1
FKBP12.6	Calstabn1, Ca^{2+} channel-binding and -stabilizing protein 2
FPL	2,5-dimethyl-4-[2-(phenylmethyl)benzoyl]-1H-pyrrole-3-carboxylic acid methyl ester
FRB	fragment of mTOR that binds rapamycin
GABA	gamma-aminobutyric acid
GCK	glucokinase
GFP	green fluorescence protein
GIP	gastric inhibitory peptide
GLP-1	glucagon-like peptide 1
GLUT	glucose transporters
GPCR	G-protein coupled receptor
GSIS	glucose-stimulated insulin secretion

GWA	genome-wide association
Hap1	Huntingtin-associated protein 1
HCC	Hepatocellular carcinoma
HCN	hyperpolarization-activated cation channel
HD	Huntington's disease
HEK	Human Embryonic Kidney Cells
HEPES	4-(2-hydroxyethyl)piperazine-1-ethanesulfonic acid
HVA	high-voltage activated
HVCC	high voltage-gated calcium channel
IAA	antibodies to insulin
IB	immunoblotting
ICA	islet cell autoantibodies
IGF-1	insulin-like growth factor-1
IHC	inner hearing cells
II-III loop	Intracellular loop between domain II and III
INS-1	insulin-secreting cell line
InsP	Inositol phosphate
IP	immunoprecipitation
IP4	D-myo-inositol 1, 3, 4, 5-tetrakisphosphate
IPR3	inositol 1,4,5-triphosphate receptor
iPSCs	induced pluripotent stem cells
IRBIT	IP3R-binding protein
IRP	immediately releasable pool
K_{ATP}	ATP-sensitive K^+ channel
Kir6.2	inward rectifying K^+ channel
LBs	Lewy bodies
LNCaP	androgen-sensitive human prostate adenocarcinoma cells
LTD	long-term depression
LTP	long-term potentiation
LVA	low-voltage activated
M3	muscarinic receptor
MCS	membrane contact sites
MEF	type M resistance determinant
MH	malignant hyperthermia
MIDAS	metal ion-dependent adhesion site
NAADP	nicotinic acid dinucleotide phosphate
NCX1	Na^+/Ca^{2+} exchanger 1
NEFA	Non-esterified fatty acids
NFAT	Nuclear factor of activated T-cells
NGS	Next-Generating Sequencing

Nifedipine	1,4-dihydro-2,6-dimethyl-4-(2-nitrophenyl)-3,5-pyridinecarboxylic acid dimethyl ester
NM	neuromelanin
NMDA	N-methyl-D-aspartate
NMDG	N-methyl-D-glucamine
NT	N-terminus
Opti-MEM	Reduced serum media
P2Y	purinergic receptor
PAA	phenylalkylamine
PACAP	pituitary adenylate cyclase-activating peptide
PCLO	cytoskeletal matrix protein piccolo
PCR	Polymerase Chain Reaction
PD	Parkinson's disease
PDE	phosphodiesterase
PEI	polyethyleneimine
PH	pleckstrin homology
PI	phosphatidylinositol
PI4P	phosphatidylinostiol 4-phosphate
PIP_2	phosphatidylinositol-4,5-biphosphate
PJ	pseudojanin
PJ-D	pseudojanin-dead
PKA	protein kinase A
PKC	protein kinase C
PKG	protein kinase G
PLC	phosphplipase C
PMA	phorbol ester
PMA	Phorbol 12-myristate 13-acetate
PMCA	plasmalemma membrane Ca^{2+} ATPase
PP	pancreatic polypeptide
R10	the tail current remaining 10 milliseconds after reaching peak
RCC	rat chromaffin cells
RDA	recommended dietary allowance
RNA	Ribonucleic acid
RPMI	Roswell Park Memorial Institute
RRP	readily releasable pool
RyR	Ryanodine receptor
RyR2	type 2 ryanodine receptor
SAN	sino-atrial node
SANDD	sinoatrial node dysfunction and deafness
SCAs	spinocerebellar ataxias
SDS-PAGE	SDS-polyacrylamide gel electrophoresis

SERCA	sarco/endoplasmic reticulum (sER) Ca2+-ATPases
SFA	spike-frequency adaptations
SH3	Src homology 3
SHR	spontaneously hypertensive
SLCT	sodium-dependent glucose transporters
SNAP	Soluble NSF attachment protein
SNARE	SNAP Receptor
SNc	substantia nigra pars compacta
SNP	single nucleotide polymorphism
SOCE	store-operated calcium entry
SR	sarcoplasmic reticulum
STIM	stromal interaction molecules
SUR1	sulfonylurea receptor
T1DM	type 1 diabetes mellitus
T2DM	type 2 diabetes mellitus
TARPs	transmembrane AMPA receptor regulatory proteins
TH	tyrosine hydroxylase
TRP	channel transient receptor potential channel
TS	timothy syndrome
tsA	A transformed human kidney cell line stably expressing an SV40 temperature-sensitive T antigen
TTX	tetrodotoxin
VDI	voltage-dependent inactivation
VGCC	voltage-gated calcium channel
VIP	vasoactive intestinal polypeptide
VMA	Von Willbebrand Factor-A
VRAC	volume-regulated anion channels
VSD	voltage-sensing domain
VTA	ventral tegmental area
VTA-NAc	ventral tegmental area-nucleus accumbens
WKY	normotensive Wistar-Kyoto

ABSTRACT

The L-type VGCC subtypes, including subtypes $Ca_v1.1$-1.4, have been shown to play critical roles in various cellular activities, including muscle contraction, hormone secretion, and neurotransmitter release. Recent research indicates the potential involvement of $Ca_v1.3$ in various neurological and psychiatric disorders, such as the early onset of Parkinson's disease and substance abuse disorders. Non-selective L-VGCC subtype blockers such as dihydropyridines (DHPs) are used to treat hypertension and angina because they potently inhibit $Ca_v1.2$, but no selective $Ca_v1.3$ inhibitors have been developed yet. We resolved the molecular determinants to differentiate $Ca_v1.2$ and $Ca_v1.3$ in response to DHP nifedipine. Nifedipine IC_{50} for $Ca_v1.2$ and $Ca_v1.3$ are 22nM and 289nM determined by whole-cell patch-clamp. We found that this 12-fold difference in potency was largely accounted for by amino acid sequence divergence within the DHP binding pocket originally mapped in $Ca_v1.2$. Specifically, we identified two significant amino acids, $Ca_v1.3$/M1030 to $Ca_v1.2$/V1036 in the transmembrane IIIS5 and $Ca_v1.3$/S1100 $Ca_v1.2$/A1106 in the extracellular IIIS-3P loop, to differentiate the subtype affinity to nifedipine. We generated a $Ca_v1.3$ mutant channel containing both the M/V switch in IIIS5 and the IIIS5-3P loop of $Ca_v1.2$, which was blocked by nifedipine with an IC_{50} of 42nM. Furthermore, we found that switching amino acids at positions F1052, Q1089, D1092, N1094, and S100 within the Cav1.3 IIIS-3P loop to the corresponding amino acids in $Ca_v1.2$, reduced the EC_{50} of the L-type channel agonist FPL 64176 from 854nM to 133nM, essentially close to that of $Ca_v1.2$ at 103nM.

Developing L-VGCC subtype-selective inhibitors based on existing small molecules has been challenging. Therefore, we asked if the intracellular loops of $Ca_v1.2$ and $Ca_v1.3$, which are highly divergent, could be targeted for selective modulation of these two subtypes. First, we found that the $Ca_v1.3$/II-III loop fused to eGFP decreased glucose-activated action potential (GSAP) frequency by ~80% in the pancreatic β-cell. Next, we expressed $Ca_v1.3/\beta_3/\alpha_2\delta_1$ in tsA-201 cells and found that overexpression of the $Ca_v1.3$ II-III loop selectively shifts $Ca_v1.3$ inactivation by -15mV, but not $Ca_v1.2$. To refine the significant residues in the $Ca_v1.3$ II-III loop, we created GFP fusions with the N and C-terminal (NT and CT) half of the $Ca_v1.3$/II-III loop co-expressed with $\alpha_2\delta_1$ and β_3 and found that both could shift the inactivation of $Ca_v1.3$ to hyperpolarizing potentials. We introduced several synthetic peptides, and peptide P3-1 from CT induced a -16mV shift in $V_{1/2}$ inactivation with an EC_{50} of 231nM. P3-1 contains a protein kinase G (PKG) phosphorylation site

(RRISE) required for PKG inhibition of $Ca_v1.3$ current but not conserved in $Ca_v1.2$. We found that the shift in $V_{1/2}$ inactivation induced by co-expression of $Ca_v1.3$ with the $Ca_v1.3$/II-III loop/GFP requires the presence of a $Ca_v\beta$ subunit, and $Ca_v\beta_3$ also exhibits selectivity over other β subunits. Significantly, P3-1 shifts the $Ca_v1.2$ inactivation to a more positive voltage when co-expressed with either $Ca_v\beta_{2a}$ or $Ca_v\beta_3$, demonstrating the ability of P3-1 to differentiate $Ca_v1.2$ and $Ca_v1.3$ in a $Ca_v\beta$-dependent manner.

Failure of pancreatic β-cells to secrete enough insulin to maintain glucose homeostasis is a hallmark of Type 2 diabetes. VGCCs play critical roles in β-cell function. However, the consequences of the dysregulation of the endoplasmic reticulum (ER) Ca^{2+} channel ryanodine receptor-2 (RyR2) in pancreatic β-cells are not fully understood. Therefore, we characterized the electrical activity in INS-1 in which RyR2 has been deleted via CRISPR/Cas9 gene editing. We observed a decreased level of IP_3 receptor binding protein (IRBIT) in $RyR2^{KO}$ INS-1 cells and generated $IRBIT^{KO}$ INS-1 cells. VGCC current density in $RyR2^{KO}$ doubled compared to controls and was also elevated in $IRBIT^{KO}$ compared to control cells. All HVA Ca^{2+} channels were upregulated, determined by fractional current blocked by nifedipine. We also found that GSAP frequency is doubled by RyR2 deletion due to failure to activate apamin sensitive SK (small conductance calcium-activated potassium) channels. Additionally, we examined the role of increased plasma membrane PIP_2 levels in the upregulation of Ca_v current density with a PIP_2 phosphatase, pseudojanin, which rapidly translocates to the plasma membrane upon rapamycin binding. Activation of phosphatase, but not a phosphatase dead variant in INS-1 cell lines inhibited a higher percentage of current in $RyR2^{KO}$ compared to the controls, suggesting that an increase in plasma membrane PIP_2 content may be responsible for the increased current density in $RyR2^{KO}$ cells.

CHAPTER 1. INTRODUCTION

1.1 Calcium

Calcium is a ubiquitous chemical element with the symbol Ca. It is the third most abundant metal on earth and the most abundant mineral in the body. It is the principal constituent of bones and teeth and a dietary supplement and medicine in daily life. The recommended dietary allowance (RDA) for calcium is 1000-1200 mg/day for adults (Linus Pauling Institute 2021). An adequate calcium intake is crucial for maintaining a healthy skeleton, in which we can find 99% of the calcium in our body.

Besides the indispensable role in body structure, its vital roles in the physiological and biochemical processes in the body have been studied, and the list keeps going on. It acts as electrolytes to modulate homeostasis, as cofactors in enzymes, and as a second messenger to regulate signal transduction pathways such as neurons and muscles (Rajagopal and Ponnusamy 2017) (Figure 1.1). Researchers have done extensive studies over the past decades considering the fundamental role of calcium in the human body. However, the more we study the multiple roles of Ca^{2+}, the more questions there are to answer. Regarding the fluctuating environmental risks we are exposed to, we will keep exploring the hidden stories of calcium.

1.2 Calcium channel and transporter overview

1.2.1 Calcium channel

The divalent Ca^{2+} requires calcium channels or other transporters with Ca^{2+} conductance to mobilize and carry out its essential functions. By definition, calcium channels are ion channels that show selective permeability to Ca^{2+}. Two major types of calcium channels were identified based on activation: voltage-gated calcium channel activated by membrane potential change and ligand-gated calcium channel activated by ligand binding (Nature portfolio 2021).

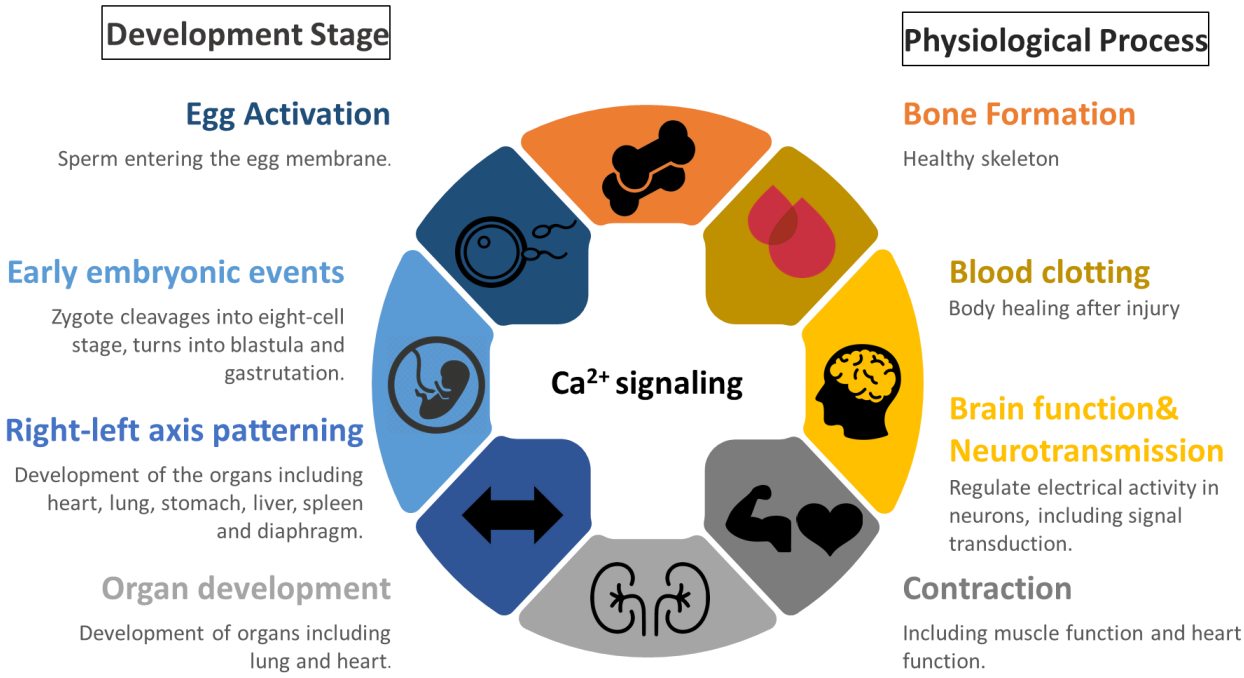

Figure 1.1. Involvement of Ca^{2+} in critical developmental processes and physiological function. (Rajagopal and Ponnusamy 2017)

1.2.2 Voltage-gated calcium channels regulating Ca^{2+} influx

Voltage-gated calcium (Ca_v) channels (VGCCs) are ubiquitously expressed in prokaryotes and eukaryotes (Anderson and Greenberg 2001). Ca_v channels are distributed in both excitable and non-excitable cells in the mammalian body (Yang and Berggren 2005). They are located in the plasma membrane and function as Ca^{2+} -conducting pores, undergoing conformational switches upon plasma membrane potential change. The channels change from an inactivated and impermeable state to an activated and highly permeable pore. This specific permeability allows Ca^{2+} influx, facilitates electrical signaling, and induces Ca^{2+} -dependent protein-protein interactions and enzymatic responses (Catterall 2000). Vital functions in excitable cells require the VGCCs involved in various cellular processes, including excitation-transcription coupling during developmental stages, apoptosis, exocytosis, and endocytosis (Wheeler et al., 2012), excitation-contraction coupling in muscle tissues (Bannister and Beam, 2013), and transmitter release and hormone secretion for proper endocrine and neuronal function (Catterall et al., 2013).

In the early stage of VGCC discovery, two types of Ca_v currents were identified from fertilized starfish eggs (Hagiwara et al., 1975) with distinct voltage-dependent activation and

inactivation properties. They were firstly termed channel I (low-voltage activated (LVA)) and channel II (high-voltage activated (HVA)). Researchers have devoted extensive effort to creating a well-accepted nomenclature based on their biophysical and pharmacological properties as the technology and methodology developed. L-, P/Q-, N- and R-type Ca_v currents have high thresholds for activation and are referred to as HVA Ca^{2+} currents, and T-type Ca_v currents are referred to as LVA Ca^{2+} currents (Tsien et al., 1988).

As for the auxiliary subunits, researchers used Greek letter-based nomenclature to describe Ca_v channel subunits as α_1 (approximately 170 kDA), β (approximately 150 kDa), γ (approximately 32 kDa) and $\alpha_2\delta$ subunits (α_2 approximately 150 kDa and δ approximately 17-25 kDa) (Curtis et al., 1984; Takahashi et al., 1987), corresponding to the alphabetic system as CACNA1, CACNAB, CACNG, and CACNA2D. Later on, a more comprehensive nomenclature of Ca_v channels based on sequence analysis won popularity (Ertel et al., 2000). Three families of Ca_v, Ca_v1, Ca_v2, and Ca_v3 were identified and will be introduced in the subsequent chapters.

Table 1.1. Physiological types of Ca_v channels (Refs. Varadi et al., 1999; Yang and Berggren 2006; Zamponi et al., 2015; Dolphin 2018).

VGCCs	Type	Gene	Protein	α_1 name	Blocker	Localization
HVA	L-type	CACNA1S	$Ca_v1.1$	α_1S	DHPs PAAs BTZs	Skeletal muscles
		CACNA1C	$Ca_v1.2$	α_1C		Cardiac cells
		CACNA1D	$Ca_v1.3$	α_1D		Hearing, SA node
		CACNA1F	$Ca_v1.4$	α_1F		Retina
	P/Q-type	CACNA1A	$Ca_v2.1$	α_1A	ω-Aga IVA	CNS
	N-type	CACNA1B	$Ca_v2.2$	α_1B	ω-CTX GVIA	PNS/ early CNS
	R-type	CACNA1E	$Ca_v2.3$	α_1E	SNX 482	Cerebellar granule cells
LVA	T-type	CACNA1G	$Ca_v3.1$	α_1G	Ethosuximide	Brain
		CACNA1H	$Ca_v3.2$	α_1H		Kidney, liver, heart
		CACNA1I	$Ca_v3.3$	α_1I		Brain

1.2.2.1 L-type VGCCs

L-type voltage-gated calcium channels (L-VGCCs) were designated "L" due to their long-lasting inward currents during depolarization, and they have high unitary Ba^{2+} conductance (Tsien et al., 1988). The Ca_v1 channel family consists of four pore-forming α_1 subunit isoforms $Ca_v1.1$ to $Ca_v1.4$, predominantly distributed in skeletal muscles, cardiac cells, neuron and endocrine cells, and retina, respectively (Yang and Berggren 2006, Table 1.1). Besides the pore-forming α1 subunit, the auxiliary subunits β and $\alpha_2\delta$ subunits are co-expressed to maintain Ca_v1 function (Figure 1.2). Unlike $Ca_v1.1$ and $Ca_v1.4$, which are exclusively expressed in skeletal muscles and retina, $Ca_v1.2$ and $Ca_v1.3$ are widely expressed in neuronal and endocrine cells and cardiac cells with electric excitability (Koschak et al., 2001). Their relative abundance associated with a physiological and pathological difference will be compared and discussed in Chapter 1.7.

Ca^{2+} influx through L-VGCCs regulates numerous physiological functions, including developmental progression, cardiac pacemaking, hormone release, muscle contraction, neuronal firing, plasticity, and sensory function (Catterall 2000), corresponding to the earlier mentioned tissue distribution (Table 1.1).

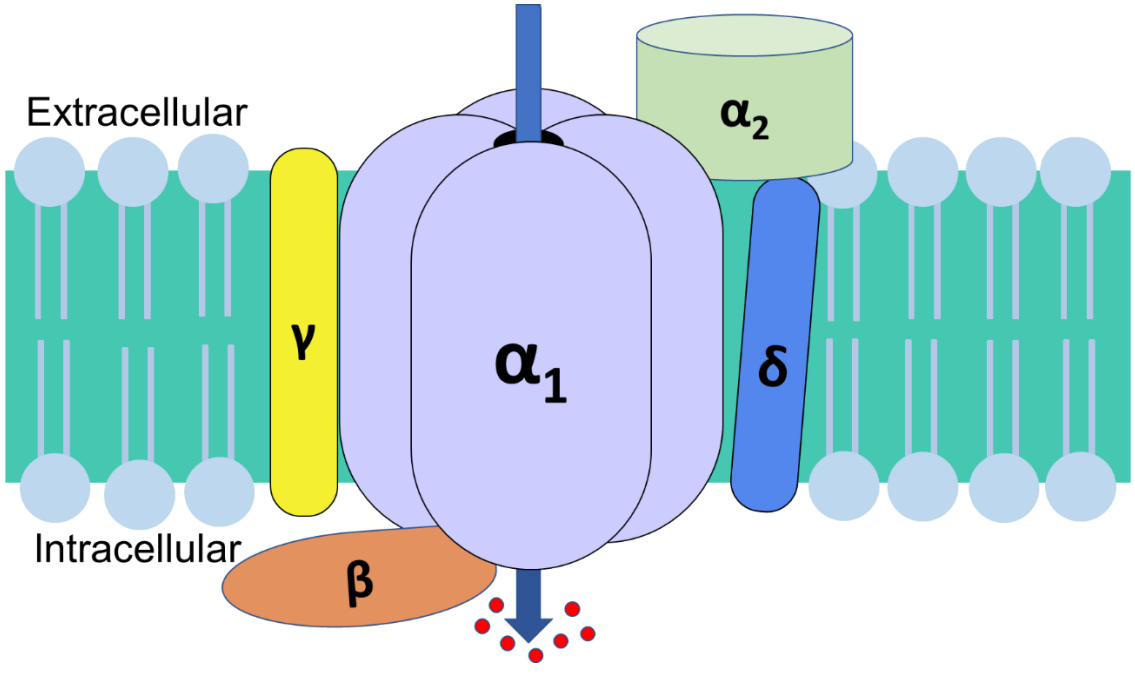

Figure 1.2. A subunit composition of voltage-gated calcium channels (VGCCs). Ca_v channel subunits co-express on the membrane: pore-forming subunit α_1 (purple) with four homologous transmembrane domains (I to IV), auxiliary subunit β (orange), γ (yellow), $\alpha_2\delta$ (green/ blue). The Blue arrow indicates the Ca^{2+} influx (represented in red).

1.2.2.2 P/Q-type VGCCs

$Ca_v2.1$ channel, one of the three members in Ca_v2 channel family, mediates P/Q-type Ca_v currents. P-type Ca_v currents were first identified using ω-agatoxin IVA (ω-Aga IVA) in neuronal Purkinje cells in the cerebellum (Llinas et al., 1989), and Q-type Ca_v currents were reported in cerebellar granule cells and also blocked by a higher concentration of ω-Aga IVA (Randall and Tsien 1995). These two types of $Ca_v2.1$ channels can be discriminated by their voltage-dependent inactivation rate and sensitivity to ω-Aga IVA (Randall and Tsien 1995). However, they are now combined as P/Q-type Ca_v currents because the same pore-forming subunit $Ca_v2.1$ conducts both currents (Yang and Berggren 2005; Catterall 2000) and are coupled to neurotransmitter release.

1.2.2.3 N-type VGCCs

$Ca_v2.2$ channel conducts N-type Ca_v currents, very similar to those of P/Q type currents. N-type Ca_v currents display smaller unitary Ba^{2+} conductance, a lower activation threshold, and faster inactivation kinetics compared to L-type Ca_v currents. Inactivation rates in $Ca_v2.2$ are still slower than those of T-type Ca_v currents (Tsien et al., 1988). $Ca_v2.2$ channels were initially discovered in neurons and are selectively antagonized by the peptide blocker ω-conotoxin GVIA (ω-CTX GVIA) but not Ca_v1 blockers. $Ca_v2.2$ channels, similar to $Ca_v2.1$, trigger neurotransmitter release by mediating Ca^{2+} influx into the active zone.

1.2.2.4 R-type VGCCs

$Ca_v2.3$ channels were also discovered in cerebellar granule cells. They are termed R-type, representing the current resistance to all existing VGCC blockers in the early discovery stage (Randall and Tsien 1995). Later, a novel toxin SNX-482 was discovered to have a higher affinity for $Ca_v2.3$ channels than other Ca_v channels (Newcomb et al., 1998). R-type currents have a faster inactivation rate than other HVA calcium channels and play essential roles in generating Ca^{2+} -dependent action potentials and neurotransmitter release (Yang and Berggren 2005; Catterall 2000).

1.2.2.5 T-type VGCCs

Ca_v3 channels display a low threshold for activation and comprise three members, $Ca_v3.1$, $Ca_v3.2$, and $Ca_v3.3$, according to the pore-forming subunits (Yang and Berggren 2005; Catterall 2000; Rizzuto and Pozzan 2003). Ca_v3 currents are also termed T-type Ca_v currents because they are characterized by transient currents due to rapid inactivation and a tiny unitary Ba^{2+} conductance (Tsien et al., 1988). Ca_v3 channels are found in a wide range of cell types, including endocrine cells, muscle cells, neurons, sperm cells, and even non-excitable cells (Yunker et al., 2003). Ca_v3 channels are believed to be only comprised the α_1 subunit because α_1 expression shows the same activity as natural T-type VGCCs (Perez-Reyes et al., 2003). T-type currents support repetitive firing in excitable cells and mediate steady Ca^{2+} influx in non-excitable cells (Tsien et al., 1988; Catterall 2000; Yang and Berggren 2005; Yunker et al., 2003).

1.2.3 Ligand-gated calcium channels regulating intracellular Ca^{2+} homeostasis

Among all the emerging repertoire of Ca^{2+} signaling proteins in the cytoplasmic compartments, there are two major classes of Ca^{2+} calcium interacting macromolecules on the endoplasmic/sarcoplasmic reticulum (ER/SR) membrane: Ca^{2+} releasing channels from Ca^{2+} stores into the cytosol and Ca^{2+} pumps moving cytosolic Ca^{2+} back into the ER/SR. Ryanodine receptors (RyRs) and 1,4,5-trisphosphate receptors (IP_3Rs) are the two prominent families of Ca^{2+} release channels to regulate cytoplasmic Ca^{2+} homeostasis (Seo et al., 2014; Cremer et al., 2020). Another ligand-gated calcium channel located in the plasma membrane is responsible for store-operated calcium entry (SOCE) (Putney et al., 2017) (Figure 1.3).

1.2.3.1 Ryanodine receptors

Ryanodine receptors (RyRs) are intracellular ion channels for regulating the release of stored Ca^{2+} from ER/SR and were first identified by isolation of the enormous cytoplasmic “foot” structure (Inui et al., 1987). Its characterization was facilitated by recognizing the interaction with a poisonous plant alkaloid ryanodine, used as an insecticide. RyR is the largest ion channel known to date, with a tetrameric arrangement of ~560 kDa subunits totaled to ~2.2 MDa (Williams et al., 2018). Three different variants (RyR1-3) have been identified. RyR1 is predominantly found in the skeletal muscle (Inui et al., 1987; Marks et al., 1989; Takeshima et al., 1989). RyR2 makes up

the primary form in cardiac muscle (Brillantes et al., 1989; Nakai et al., 1990; Otsu et al., 1990), but is found in the brain and associated with cognitive function (Liu et al., 2012), and appears to be involved in insulin secretion from pancreatic β cells (Santulli et al., 2015). RyR3 was initially thought to be restricted to brain and smooth muscle but was later shown to be widely distributed throughout the body (Hakamata et al., 1992; Nakashima et al., 1997; Zhang et al., 2011).

RyR1 is found to interact with $Ca_v1.1$ on specialized invaginations of the sarcolemma (transverse tubules) to rapidly release Ca^{2+} in skeletal muscle cells (Rios and Brum 1987; Nelson et al., 2013). RyR2 is activated by Ca^{2+} influx through $Ca_v1.2$ following cardiac muscle depolarization, termed as Ca^{2+}-induced Ca^{2+} release (Fabiato and Fabiato 1975). The open probability (P_o) of RyR is extremely low at ~100-200nM cytosolic Ca^{2+} and increases at sub-micromolar levels, reaching a maximal P_o at ~10μM, and goes lower when concentration increases more (Bezprozavanny et al., 1991). A variety of functional ligands, proteins, and small molecules, including ions (primarily Ca^{2+} and Mg^{2+}), calmodulin, L-VGCCs, and caffeine, can activate RyRs (See Santulli et al., 2017 for review). Structural studies supported two Ca^{2+} binding sites with different affinities (activation and inhibition) (des Georges et al., 2016). Additionally, because of the high concentration in skeletal muscle, ATP (adenosine triphosphate) is consistently bound and activating RyR, with Ca^{2+} and ATP having synergistic effects on RyR gating (Kushmerick et al., 1992).

Due to the gigantic size of the channel, the solution of the RyR structure has been challenging. In the 1980s, cryo-electron microscopy (cryo-EM) was intensively used to obtain low-resolution information. As the technology advanced over the years, many strategies to gain structural information were pursued (See Stantulli et al., 2008 and Williams et al., 2018 for review). In the mid-2010s, high-resolution cryo-EM structures of RyR1 (Efremov et al., 2015; Yan et al., 2015; Zalk et al., 2015; des Georges et al., 2016; Wei et al., 2016; Bai et al., 2016; Clarke and Hendrickson 2016) and RyR2 (Peng et al., 2016) have been published, providing new insights on their dynamic mechanism of channel activation and gating.

A wide range of factors can modulate RyR dynamics and gating. Calstabin1 and Calstabin2 (FKBP12 and FKBP12.6), the Ca^{2+} channel-binding and -stabilizing proteins, preferentially bind to RyR1/2 and stabilize the closed state the channels, preventing Ca^{2+} leakage coupled gating (Santulli and Marks 2015). They are proposed to bind to the N-terminus of Bsol (bridging α-solenoid repeats), rigidify the interface, and stabilize the link between the pore and cytoplasmic

region (des Georges et al., 2016; Zalk et al., 2015; Yan et al., 2015). A cryo-EM study further supported these findings (Peng et al., 2016). Additionally, they are the targets for the immunosuppressant drugs rapamycin (sirolimus) and FK506 (tacrolimus) (Lombardi et al., 2017a & b). Several post-translational modifications also regulate RyR function, including phosphorylation, oxidation, and nitrosylation (See Santulli et al., 2018 for review). RyRs can act as both signal amplifiers and integrators via coupled gating with adjacent channels upon activation.

RyR1 channelopathies are associated with malignant hyperthermia (MH) and central core disease (CCD) (Quane et al., 1993), and mutations in RyR2 have been implicated in cardiac arrhythmias (Lehnart et al., 2004, 2008; Vest et al., 2005). Downregulation of RyR2 or cGMP equivalently inhibits unfolded protein response and ER stress, leading to early-onset cone protection and rescuing the cGMP/PKG signaling-induced cone degeneration in cyclic nucleotide-gated channel deficiency (Yang et al., 2020). Several studies have revealed RyR function and autophagy regulation by RyR-interacting proteins, and a role for RyRs in neurodegenerative diseases has been proposed (Vervliet 2018).

1.2.3.2 IP_3 receptors

IP_3Rs (inositol 1,4,5-trisphosphate receptors, also called $InsP_3$Rs) are closely related to RyRs, found in most cell types, and activated by the second messenger IP_3 and Ca^{2+} (Harnick et al., 1995; Yuan et al., 2016; Santulli et al., 2017). They also mediate Ca^{2+} release from intracellular stores, mainly ER (Berridge 1993) and Golgi apparatus (Pizzo et al., 2011; Wong et al., 2013; Rodrigues-Prados et al., 2015), and nuclear envelope and nucleoplasmic reticulum (Echevarrría et al. 2003). Both Ca_v channels and intracellular IP_3R share the standard function to regulate intracellular Ca^{2+} supply (Catterall 2000; Taylor et al., 2004). Intracellular Ca^{2+} signaling is established with a time course and spatial arrangement by the Ca_v-regulated Ca^{2+} influx and IP_3-mediated efflux from intracellular stores. (Berridge et al., 2000, 2003).

The IP_3R is comprised of ~2,700 amino acid residues (human type 1: 2,695; 2: 2,701; 3:2,671) (Yamamato-Hino et al., 2994; Yamada et al., 1994). Each IP_3R subunit has an IP_3 binding site in the N-terminus, a modulatory domain in the middle, and six membrane-spanning helices in the C-terminus. The Ca^{2+} conducting pore only accounts for a tiny portion in IP_3R. However, its large cytoplasmic region harbors a variety of recognition sites for proteins and small molecules besides IP_3 and Ca^{2+}, including calmodulin, nucleotides, protein kinases (PKA, PKB, and PKC),

phosphatases, apoptotic proteins, G-protein coupled receptors (GPCRs), and transient receptor potential (TRP) channels (Taylor et al., 2004). Several IP_3R antagonists were identified to study the channel physiology and pathology, including heparin, caffeine, and xestospongin. However, they all lack specificities as some of them also activate RyRs (Saleem et al., 2014; Prole and Taylor 2019).

IP_3Rs and RyRs share about 40% homology in the core regions, implying a common region for Ca^{2+} release channels, but IP_3R does not express much of the cytoplasmic shell or the large Bsol. C-terminal and activation domains are conserved between these two intracellular channels, suggesting a very similar calcium activation mechanism, and the C-terminal is further extended and linked to the N-terminal domain and IP_3 binding site in IP_3R (Fan et al., 2015; Baker et al., 2021). IP_3R mutations have been shown to be associated with diseases including heart disease, ataxia, exocrine secretion defects, taste perception malfunction, cancers, and neurodegenerative diseases (Seo et al., 2014).

1.2.3.3 Store-operated channels

Store-operated channels, Orai1, Orai2, and Orai3, are another type of ligand-gated calcium channel located in the plasma membrane and provide calcium signaling into the cytoplasm (Putney et al., 2016). Depleting Ca^{2+} stores primarily in ER activates a biphasic signaling mechanism, including releasing Ca^{2+} from ER and Ca^{2+} entry from the plasma membrane. Store-operated Ca^{2+} entry (SOCE) is activated when less Ca^{2+} binds to the luminal Ca^{2+} -binding sites of stromal interaction molecule 1 (STIM1), which is a dimeric protein anchored in ER membranes (Liou et al., 2005; Gudlur et al., 2019). A small cluster of mobilized STIM1 directly binds to the Orai1 channel at membrane contact sites (MCS) and induces the Ca^{2+} entry from the plasma membrane (Shen et al., 2021).

Even though the SOCE mechanism by Orai1-STIM1 interaction is better documented now, IP_3R and TRP channels were thought to tightly associate with this pathway during the early studies (Streb et al., 1983). The exploration of SOCE was initiated when a plant toxin, thapsigargin, induced intracellular Ca^{2+} release independent from IP_3R activation (Jackson et al., 1988). TRP channel activation, phospholipase C (PLC) coupling, IP_3 formation, and Ca^{2+} -induced Ca^{2+} release from IP_3R was originally proposed to explain this thapsigargin activity (Putney et al., 2005). Interestingly, the canonical TRP (TRPC) channels are involved in SOCE, interacting with STIM1

together with Orai1 in different mechanisms, also contributing to cytoplasmic Ca^{2+} hemostasis (Lopez et al., 2020).

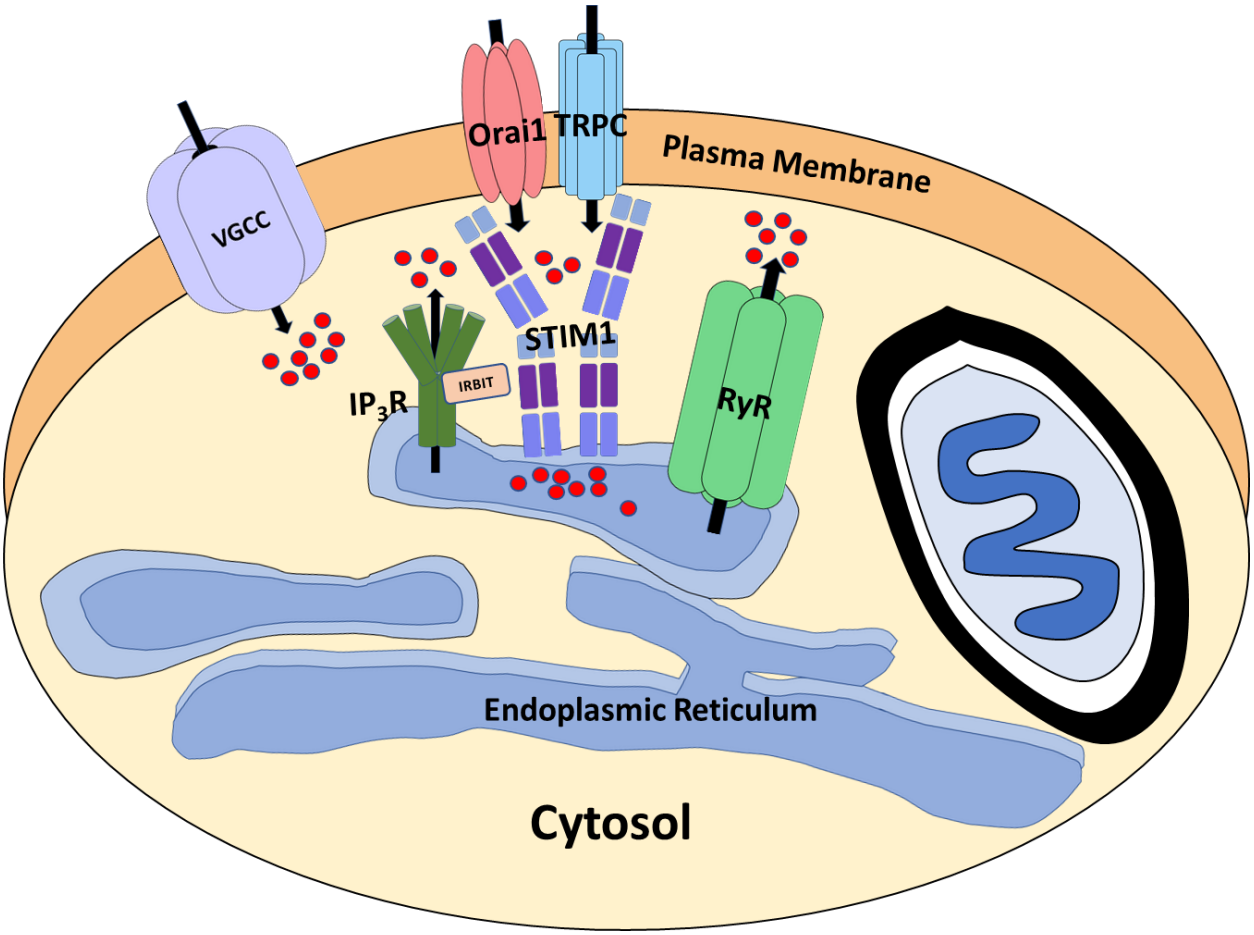

Figure 1.3. Calcium channels regulating cytosolic Ca^{2+} homeostasis. Voltage-gated calcium channels are activated by membrane potential depolarization. Ca^{2+} influx through VGCCs activates the ligand-gated calcium channels, such as RyR and IP_3R, to induce calcium-induced calcium release (CICR). Both RyR and IP_3R release Ca^{2+} from primarily the endoplasmic reticulum and other organelles (not shown) to elevate the cytosolic Ca^{2+} concentration. Depleting Ca^{2+} stores from ER induces STIM1 activation and direct interaction with Orai1 and TRPC to induce more Ca^{2+} entry across the plasma membrane (SOCE).

1.3 L-VGCC subunits

The skeletal muscle Ca_v channel $Ca_v1.1$ was first extensively studied and identified as a hetero-multimer composed of a pore-forming α_1 subunit and regulatory β and $\alpha_2\delta$ subunits (Jones 1998; Catterall 2000). Subsequently, other subtypes of pore-forming and auxiliary subunits were

purified, screened, and characterized (Catterall 2000; Ertel et al., 2000). In the subsequent sections, we will talk about the structure of L-VGCC subunits specifically, briefly introduce the properties of auxiliary subunits, and focus on biophysiological and pharmacological properties in Chapters 1.4 and 1.5.

1.3.1 Pore-forming α_1 subunit

To date, four Ca_v1 subunits have been identified (Table 1.1). $Ca_v\alpha_1$ is the largest subunit and spans at least 250 kb and contains up to 50 exon-intron boundaries, with at least ten alternative splicing sites in intron transcripts (Lipscombe et al., 2002). The variety of $Ca_v\alpha_1$ isoforms explain the diverse VGCC-mediated signaling pathways.

The α_1 subunit comprises four homologous domains from DI to DIV, each containing six transmembrane helices from S1 to S6 (segment 1 to segment 6) (Tanabe et al., 1987). The Ca^{2+} selectivity filter comprises four conserved glutamic acids (EEEE locus) located in the transmembrane region of every pore-lining (P-) loop between S5 and S6 in every domain (Yang et al., 1993). Three intracellular linkers (I-II, II-III, and III-IV loop) and N- and C-termini are all located on the cytoplasmic face of the plasma membrane (Figure 1.4). Voltage sensors allow these four homologous repeat structures to form a Ca^{2+} -conducting pore and modulate activation and inactivation gates. The large, intracellular carboxy tail contains an EF-hand and an IQ calmodulin-binding motif, critical for accelerating the inactivation rate in Ca^{2+} relative to Ba^{2+} (i.e., Ca^{2+}-dependent inactivation, CDI) (Peterson et al., 1999; Zuhlke et al., 1999). We will expand this section in section 1.4 and section 1.5.

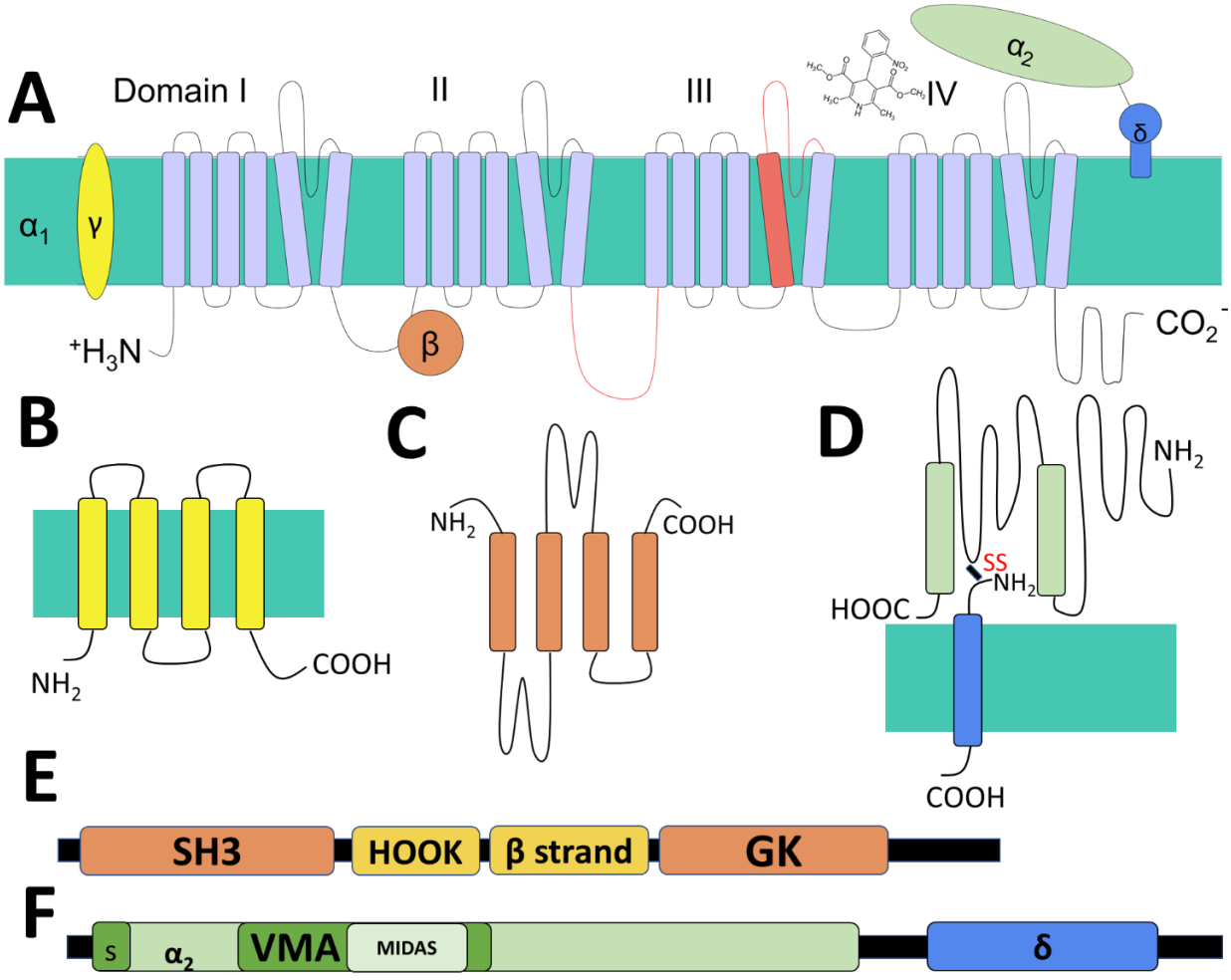

Figure 1.4. Subunit structure of L-type voltage-gated calcium channels. **(A)** L-type calcium channel contains up to 5 different subunits: α_1 (purple, 170–240 kDa), α_2 (green, 150kDa), δ (blue, 17-25 kDa), β (orange, 50-78 kDa), and γ (yellow, 32 kDa) subunits. The α_2, δ, and β subunits are noncovalently bound to the α1 subunit and modulate trafficking, expression, and biophysical properties of the α1 subunit. The α_2 is in the extracellular space, and δ and γ subunits are in the transmembrane and β subunits in the cytosolic space. The structure of nifedipine, the prototypical L-type selective blocker, is shown; Red segments: Intracellular II-III loop and transmembrane & extracellular IIIS5-3P loop. (**B**) $Ca_v\gamma$ spans the plasma membrane with four homologous transmembrane and intracellular N- and C- termini. (**C**) $Ca_v\beta$ is entirely cytosolic with four homologous helices. (**D**) $Ca_v\alpha_2\delta$ is a dimer consisting of an extracellular $Ca_v\alpha_2$ polypeptide and a transmembrane $Ca_v\delta$ polypeptide linked via a disulfide bond. (**E**) Structural motifs within the $Ca_v\beta$ subunit. (**F**) Structural motifs within $Ca_v\alpha_2\delta$ subunit. (Yang and Berggren 2005; Dolphin 2018).

1.3.2 Auxiliary β subunit

$Ca_v\beta$ subunits were first isolated from the purified $Ca_v1.1$ complex (Ruth et al., 1989), and four distinct $Ca_v\beta$ subunit genes ($Ca_v\beta1$-4) have been identified so far (Dolphin 2003b; Buraei and Yang 2010). Numerous alternative splices of these $Ca_v\beta$ subunit gene structures have been observed and studied, and exon-intron organization is essential in different protein-protein interactions (Yang and Berggren 2005). $Ca_v\beta$ are cytoplasmic proteins binding to the intracellular I-II loop of Ca_v1 and Ca_v2 α1 subunits with high affinity, and a binding motif with 18 amino acids in I-II linker is termed the α-interaction domain (AID) (Pragnell et al., 1994).

$Ca_v\beta$ subunits can be divided into five domains (D1-5). D2 and D4 domains are highly conserved, but N-terminal D1, middle D3, and C-terminal D5 domains are highly variable (Dolphin 2003a). $Ca_v\beta$ subunits contain a conserved Src homology 3 (SH3) domain and a guanylate kinase (GK) domain (Hanlon et al., 1999) linked by a flexible loop comprised of HOOK domain and fifth β strand (Richards et al., 2007) (Figure 1.4.C & E). Several studies have solved the crystal structures of different β subunit subtypes (Chen et al., 2004; Opatowsky et al., 2004; Van Petegem et al., 2004). They showed that β-interaction domain (BID) peptide locates in a groove in the GK-like domain (Van Petergem et al., 2004), and AID was predicted to locate at the carboxy end of IS6 of Ca_v channels (Opatowsky et al., 2004). In addition to the BID, the C-terminal region also directly associate with the $Ca_v\alpha_1$ subunit (Walker and De Waard 1998).

$Ca_v\beta$ subunits exert two significant functions, enhancing $Ca_v\alpha1$ subunit trafficking to the plasma membrane and regulating Ca_v channel biophysical properties through interaction with the $Ca_v\alpha_1$ subunit (Arikkath and Campbell 2003). All of the $Ca_v\beta$ subunits were examined and found to increase the channel open probability, leading to increased current magnitude through individual channels and increased macroscopic current density (Matsuyama et al., 1999; Meir et al., 2000; Neely et al., 2004) but might also exert opposite effects. Interestingly, co-expression of the $Ca_v\beta_2$ subunit slows inactivation while the $Ca_v\beta_3$ subunit makes the inactivation faster (Arikkath and Campbell 2003; Hullin et al., 1992). More importantly, $Ca_v\beta$ may protect $Ca_v\alpha_1$ from endoplasmic reticulum-associated proteasomal degradation and promote forward trafficking of the channels to the plasma membrane (Zamponi et al., 2015).

$Ca_v\beta$ subunit carries several potential PKA and PKC phosphorylation sites within SH3 and GK domains. S182 and T205 in $Ca_v\beta_{1a}$ subunits have been identified as critical for PKA and PKC phosphorylation, respectively (Ruth et al., 1989; De Jongh et al., 1989). S478 and S479

phosphorylated by PKA in $Ca_v\beta_{2a}$ were shown to regulate the activity of truncated $Ca_v1.2$ channels (Bunemann et al., 1999).

$Ca_v\beta$ subunit pathology has been implicated in multiple diseases, including epilepsy, cardiac dysfunction (Yang and Berggren 2010), and diabetes (Lee et al., 2018). The interruption of α_1 and β interactions has been proposed as a potential therapeutic strategy (Young et al., 1998). Considering the mobility of $Ca_v\beta$ subunits within the plasma membrane, scientists also reported the calcium channel-independent function of $Ca_v\beta$. A nonconventional β_4 function is in the nucleus, contributing to the ataxic phenotype in activity-dependent gene regulation (Etemad et al., 2014).

1.3.3 Auxiliary $\alpha_2\delta$ subunit

The role of $Ca_v\alpha_2\delta$ has been well-established, especially by Dolphin's group (Dolphin 2016; Dolphin 2018). $Ca_v\alpha_2\delta$ is a single polypeptide encoded by one gene (Ellis et al., 1988; De Jongh et al., 1990). Four isoforms ($Ca_v\alpha_2\delta_{1-4}$) were isolated (Klugbauer et al., 1999; Qin et al., 2002) and have a similar structure (Figure 1.4D). A signal sequence at the N-terminus directs the protein into extracellular space. Following the signal sequence, the $Ca_v\alpha_2$ subunit is completely extracellular, including a Von Willebrand Factor-A (VWA) domain which contains a strong motif, the metal ion-dependent adhesion site (MIDAS) (Whittaker and Hynes 2002) necessary for protein-protein interactions (Figure 1.4.F). The transmembrane $Ca_v\delta$ polypeptide is connected to a hydrophobic C-terminal (Ellis et al., 1988). The two polypeptides, $Ca_v\alpha_2$ and $Ca_v\delta$, connect via a disulfide bond and contain multiple glycosylation sites and cysteine residues (Calderon-Rivera et al., 2012).

$Ca_v\alpha_2\delta$ positively modulates $Ca_v\alpha_1$ in its trafficking, expression, and voltage-dependent kinetic properties (Dolphin 2018). However, there is debate on the combinational effect of $Ca_v\alpha_1/Ca_v\beta/Ca_v\alpha_2\delta$ expression in different tissues. $Ca_v\alpha_2\delta$ has become a novel therapeutic target for various diseases such as neuropathic pain, epilepsies, night blindness, neuropsychiatric disorders, and cardiac and endocrine dysfunction because of its vital role in correct VGCC function (Dolphin 2018). One example in pancreatic β-cell activity shows the genetic deletion of dominant subtype $\alpha_2\delta$-1 in mouse pancreatic islets resulting in glucose intolerance and diabetes, without affecting insulin sensitivity, by reducing Ca_v current through all high voltage-gated Ca^{2+} channels (HVCC) isoforms in a sex-dependent manner (Mastrolia et al., 2017).

Table 1.2. Distribution and mutational effects of known auxiliary subunits $\alpha_2\delta$ and β (Refs. Varadi et al., 1999; Taylor et al., 2014; Hofmann et al., 2013).

Subunit	Gene	Localization	Mutation effect
α2δ-1	cacna2d1	Global	Decreased myocardial contractility Neuropathic phenotype
α2δ-2	cacna2d2	Global	Premature death Epileptic and ataxic phenotype
α2δ-3	cacna2d3	Global/ Brain	Decreased startle reflex Increased aggression & hyperactivity
α2δ-4	cacna2d4	Global	Loss of retinal signaling Cone-rod dysfunction
β1	cacnb1	Skeletal muscle/ Brain	Paralysis/ Reduced skeletal muscle mass Transverse tubule expression
β2	cacnb2	Global/ Heart/ Lung/ Brain	Embryonic lethal Small reduction in calcium current
β3	cacnb3	Global/ Brain	Increased GSIS, decreased pain perception Decreased L-, P/Q-, N-type current
β4	cacnb4	Global/ Brain	Lethargic phenotype: seizures, ataxia Mediate TCR-mediated calcium response Decreased Ca^{2+} current in cochlea inner hair cells

1.3.4 Auxiliary γ subunit

The $Ca_v\gamma$ subunits have the smallest size and showed the most minor effect on regulating $Ca_v\alpha_1$ subunits. Eight isoforms ($Ca_v\gamma_{1\text{-}8}$) were identified, and they all comprise a conserved four-transmembrane domain with intracellular N and C terminals (Buraei and Yang 2010) (Figure 1.4B). A conserved N-glycosylation site (GLWXXC) forms a disulfide bridge with cysteine residues in the first extracellular loop (Arikkath and Campbell 2003; Kang and Campbell 2003). The C-terminal in most $Ca_v\gamma$ subtypes (except $Ca_v\gamma_1$ and $Ca_v\gamma_6$) carries a PDZ-like domain (Chu et al., 2001). In contrast to $Ca_v\beta$ and $Ca_v\alpha_2\delta$, the $Ca_v\gamma$ subunits inhibit Ca_v channel current by generating a positive shift in voltage-dependent activation and a negative shift in inactivation. Moreover, $Ca_v\gamma$ shows no effect on Ca_v channel trafficking (Arikkath and Campbell 2003). Interestingly, the discovery of $Ca_v\gamma_2$ mutation in stargazer mouse phenotype (Letts et al., 1998) inducing epilepsy and cerebellum and inner ear defects revealed $Ca_v\gamma$s regulation of other proteins. Subunits $Ca_v\gamma_{2,3,4,8}$ are referred to as transmembrane AMPA (α-amino-3-hydroxy-5-methyl-4-isoxazole propionic acid receptor) receptor regulatory proteins (TARPs) because $Ca_v\gamma$ regulates AMPA receptor trafficking, localization, and biophysical properties (Buraei and Yang 2010).

1.4 L-VGCC biophysical properties

In the previous section, we discussed the five subunits in L-VGCCs, and the largest pore-forming α_1 subunit contributes the most to the biophysical properties of the voltage-gated channels. This section will focus on essential amino acid motifs in α1 subunits associated with channel gating.

1.4.1 Ca^{2+} selectivity filter

Calcium channels have an exceptional selectivity for conductance over other ions, and selectivity is mediated by the Ca^{2+} selectivity filter. The Ca^{2+} selectivity filter contains four conserved glutamic acid residues (Table 1.3), and this EEEE locus is located in the four extracellular Pore-lining (P-) loops between transmembrane helices S5 and S6 of HVA Ca^{2+} channels (Sather et al., 2003; Stephens et al., 2015). The Ba^{2+} conductance of L-VGCCs is higher than that of Ca^{2+} because Ba^{2+} binds less tightly to the pore Glu residues and flows with higher mobility (Almers and McCleskey, 1984). Identification of these essential amino acids was based on testing single point mutations. In the LVA Ca^{2+} channel, the lower Ca^{2+} affinity can be explained by two glutamic acid residues replaced by aspartic acid residues (Perez-Reyes et al., 1998; Talavera et al., 2001). In HVA Ca^{2+} channels, the Ba^{2+}/Ca^{2+} permeation can be reduced when one or multiple glutamic residues are substituted by alanine, glutamine, or aspartic acid residues (Mikala et al., 1993; Tang et al., 1993; Chen and Tsien 1997; Kim et al., 1993;). These observations strongly support the necessity of this EEEE locus to filter Ca^{2+} influx.

The early discovery of the ion permeation mechanism believed that Ca^{2+} interacting sites display different affinities (Varadi et al., 1999). Among four glutamic acid residues, two are deprotonated, and two are not. The higher-affinity site is preoccupied with a Ca^{2+} and locates at the cytoplasmic site. When the lower-affinity site is bound with incoming Ca^{2+}, the Ca^{2+} at higher-affinity sites are driven away into the cell by cationic repulsive forces (Hess and Tsien 1984; Almers and McCleskey 1984). Moreover, two main factors determine Ca_v channel selectivity for Ca^{2+}: the size of the selectivity filter and dynamic interactions with Ca^{2+} (Yang et al., 1993). In this case, Ca^{2+} presence largely excludes monovalent cations interactions with the filter.

A more recent study converted the homo-tetrameric bacterial Na_vAb channel into a Ca_vAb channel with high calcium selectivity by adding negatively charged aspartic acids. This new channel revealed two high-affinity sites and one low-affinity site coordinating Ca^{2+} movements

(Tang et al., 2013). Interestingly, another novel Ca^{2+} selectivity filter with essential glycine residues was found in native prokaryotes and conserved in eukaryotic VGCC subdomains (Shimomura et al., 2020).

Table 1.3. Ca^{2+} selectivity filter sequence containing conserved glutamic acid residues (shaded) in four homologous domains of three L-type Ca_vs (Ca_v1.1-1.3: Skeletal: Ca_v1.1; Cardiac: Ca_v1.2; Brain: Ca_v1.3) isolated from different tissues.

Repeats	Cav	Sequence	Amino acid location
Domain I	Cav1.1	T M E G W T D V L Y	316-325
	Cav1.2	T M E G W T D V L Y	391-400
	Cav1.3	T M E G W T D L L Y	290-299
Domain II	Cav1.1	T G E D W N E V M Y	666-675
	Cav1.2	T G E D W N E V M Y	734-743
	Cav1.3	T G E D W N E V M Y	612-621
Domain III	Cav1.1	T G E G W P Q V L K	1763-1722
	Cav1.2	T F E G W P Q V L K	1443-1453
	Cav1.3	T F E G W P Q V L K	1321-1330
Domain IV	Cav1.1	T G E A W H E I M L	1467-1476
	Cav1.2	T G E A W H D I M L	1143-1152
	Cav1.3	T G E A W H N I M L	1012-1021

1.4.2 Voltage-sensing domain

Besides Ca^{2+} permeability, the ability to sense the membrane potential change caused by ion flux is vital for VGCCs in excitable cells. The voltage sensors, a string of negatively charged residues in each homologous domain, have been the object of intense study to understand how VGCCs sense the membrane potential change (Hill 1978 & 2021). The voltage sensors are highly conserved in S4 segments, which contain positively charged amino acids such as arginine or lysine, reappearing at every third or fourth position among all documented voltage-gated ion channels (Table 1.4) (Payandeh et al., 2011; Shen et al., 2017; Wang et al., 2017; Hering et al., 2018; Hill 2021). The L-VGCC voltage sensors were confirmed to locate in Ca_v1.1 S4 segments due to the recently revealed Cryo-EM structure (Wu et al., 2016).

Even though the voltage sensors only take up a short region in S4, the voltage-sensing domains (VSDs), S4 carrying positive chares and S1-S3 carrying countercharges, can induce the

movement of their own domains and neighboring domains because of the intercrossed assembly of four homologous domains (Yan et al., 2017). The four intracellular loops connecting S4 and S5 surround the pore at the intracellular side so that a hydrophobic interaction can form between S4 of one domain and S5 of the neighboring domain (Demers-Giroux et al., 2013).

A novel dynamic model of $Ca_v1.1$ VSDs provides a mechanism underlying specific ion-pair formation in characterizing the biophysiological properties (Fernández-Quintero et al., 2021). The structurally similar VSDs showed divergent functions by controlling gate-opening speed in different orders. A rate-limiting step was first observed when disrupting molecular interactions by ionic pairs in the first activated VSD, followed by a faster process for subsequent VSDs. Voltage sensors in individual voltage-gated channels provide fine-tuning and pass on various signaling. The underlying mechanism to complete the story of every single channel is still under exploration.

Table 1.4. S4 segment sequence containing conserved arginine and lysine residues (shaded) for voltage sensing in four homologous domains of three L-type Ca_vs ($Ca_v1.1$-1.3).

Domain	Cav	S4 sequence
IS4	Cav1.1	G L D V K A L R A F R V L R P L R L V S G
	Cav1.2	G F D V K A L R A F R V L R P L R L V S G
	Cav1.3	G F D V K A L R A F R V L R P L R L V S G
IIS4	Cav1.1	P L G I S V L R C I R L L R L F K I T K Y
	Cav1.2	P L G I S V L R C V R L L R L F K I T K Y
	Cav1.3	P L G I S V F R C V R L L R I F K V T H W
IIIS4	Cav1.1	I S V V K I L R V L R V L R P L R A I N R
	Cav1.2	I N V V K I L R V L R V L R P L R A I N R
	Cav1.3	I S V V K I L R V L R V L R P L R A I N R
IVS4	Cav1.1	R I S S A F F R L F R V M R L V K L L S R
	Cav1.2	R I S I T F F R L F R V M R L V K L L S R
	Cav1.3	R I S I T F F R L F R V M R L V K L L S R

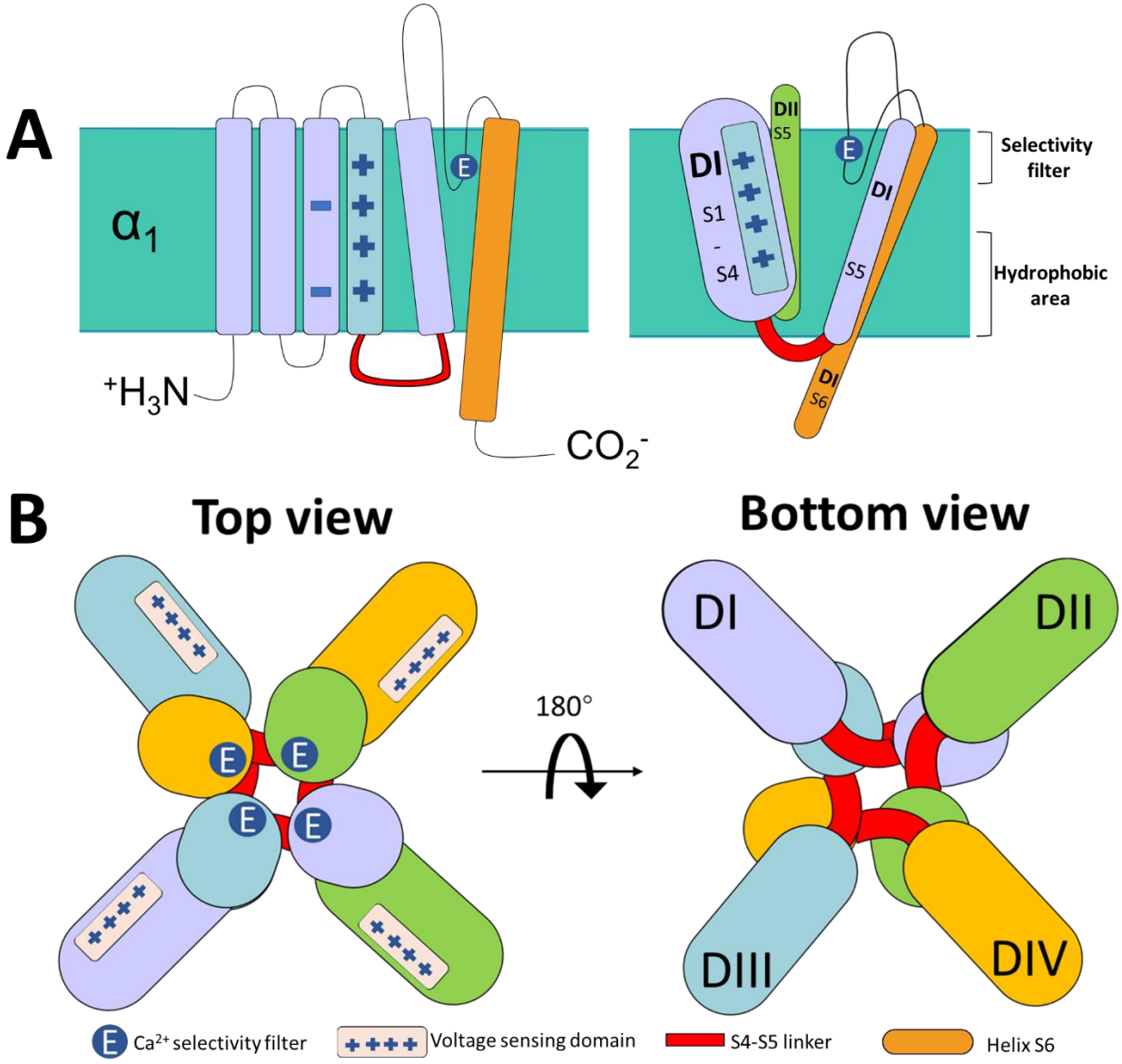

Figure 1.5. Model of $Ca_v\alpha_1$ subunits with essential structural elements. (**A**) The 2D and 3D transmembrane representations of a single homologous domain with labeled voltage sensors in S4, counter charges in S3, intracellular S4-S5 linker, a calcium selectivity filter in P-loop between S5 and S6, and a hydrophobic pore-lining part in lower S6. S5 helix in domain II is shown in 3D representation to show the relative localization of voltage-sensing domain and adjacent S5. (**B**) The topic and bottom view of the four opposing domains in a clock-wise assembly. The top view includes the Ca^{2+} selectivity filter, and the bottom view shows the support of the S4-S5 linker at the pore lining. (Ref. Hering et al., 2018; Tikhonov and Zhorov 2020; Fernandez-Quintero et al., 2021).

1.4.3 Voltage-gated activation

1.4.3.1 Molecular mechanism of the activation gate

The involvement of four VSDs in voltage-gated channel gating and modulation has been extensively studied. Each VSD contributes differentially to the gating kinetics (Flucher 2016; Fernández-Quintero et al., 2021). The detailed molecular mechanism is better explained in voltage-gated sodium and potassium channels than calcium channels, but a popular sliding-helix model with the conformational change of S6 has been proposed for all the voltage-gated channels (Sackin et al., 2006; Zhao et al., 2004; Catterall 2010 & 2020). Before activation, the pore-lining S6 helices are induced to bend and diverge from the neighboring S6 helices by VSD movements from the closed state, allowing the ions to flow through into the intracellular space (Xie et al., 2005).

However, the specific residues responsible for the activation gate vary among different structures (Lenaeus et al., 2017; Zubcevic et al., 2014). The conserved glycine residue in S6, often found in potassium channels to provide flexibility (Jacob et al., 1999; Magidovich et al., 2004; Ding et al., 2005), does not alter current kinetics or shift voltage-dependent activation of $Ca_v1.2$. In contrast, a unique amino acid, I781 in IIS6, with adjacent residues, L779, A780, and A782, regulates the $Ca_v1.2$ channel activation gate (Hohaus et al., 2005). Corresponding mutations in $Ca_v2.3$ determine the essential gating motifs, suggesting a similar mechanism for most HVA channels (Raybaud et al., 2007; Zhao et al., 2004).

In addition to the pore-lining of S6 segments, the other helices also play essential roles in supporting the sliding-helix model. The ion-pair interactions between the external gating charges in VSD and negative countercharges in S1-S3 facilitate S4 translocation through the lipid bilayer (Groome and Bayless-Edwards 2020). The roles of S1-S3 have been well-examined in voltage-gated potassium (Kuang et al., 2015) and sodium channels (Yarov-Yarovoy et al., 2012). Studies of L-VGCC subtype $Ca_v1.2$ and $Ca_v1.3$ (Pantazis et al., 2014; Coste de Bagneaux et al., 2018; Tuluc et al., 2016 a & b), and a dynamic simulation of Cryo-EM $Ca_v1.1$ (Fernández-Quintero et al., 2021) revealed the supporting interactions of S1-S3 in response to S4 movements.

1.4.3.2 Four states of VGCC activation

Voltage sensors have two states, resting and activated, and the activation pores have two states, open and closed. In this case, a 4-state cycle (Figure 1.6) was proposed for the VGCC activation (Beyl et al., 2009). Unlike the previous 2-state models based on the shaker potassium channel model (Yang et al., 1995 & 1996; Zagotta et al., 1994a & 1994b), this 4-state cycle includes an additional deactivated state and expands one open state into two transitional states of activation and opening.

When the VGCC is in the hyperpolarized membrane potential, both the resting voltage sensor and closed channel pore make the channel stay in the non-activated state R (resting). Once the depolarization activates the voltage sensor, the pore has not fully opened due to S6 guarding at the activation gate, keeping the channel in a transient state A (activation) with a voltage-dependent rate constants *x(V)* and *y(V)*. When the voltage sensors finally mobilize all four S6 at the pore, the channel starts to open, resulting in a transient state O (open). The transition between the state A and O is more frequently reversed and is represented by the voltage-dependent rate constants α and β. When the channel is opened for a sufficient period to permit Ca^{2+} influx, the hypopolarization moves the voltage sensor back into the resting mode. Opened pore with resting voltage sensors results in the channel in a deactivated state D (deactivation). The transition between state D and state O is modeled with voltage-independent *u(V)* and *w(V).* The cycle restarts when state D transits back to state R with the voltage-dependent constants δ and γ.

Even though this model can explain the functional property of VGCC activation, it is simplified and excludes multi-exponential and asymmetrical information (Hering et al., 2018). A more complicated model for potassium channels with 16 individual states considered the asymmetrical voltage-sensors and pore-lining S6 with sequential transitions (Pathak et al., 2005). In conclusion, both VSD and adjacent helices (especially S2, S3 for countercharges and S6 for pore-opening) with correct charges are required to stabilize the open state of the channel.

Pore	Voltage Sensor	States	Description
Closed	Resting	R	Resting closed state
Closed	Activated	A	Activated closed state
Open	Activated	O	Activated open state
Open	Resting	D	Deactivated open state

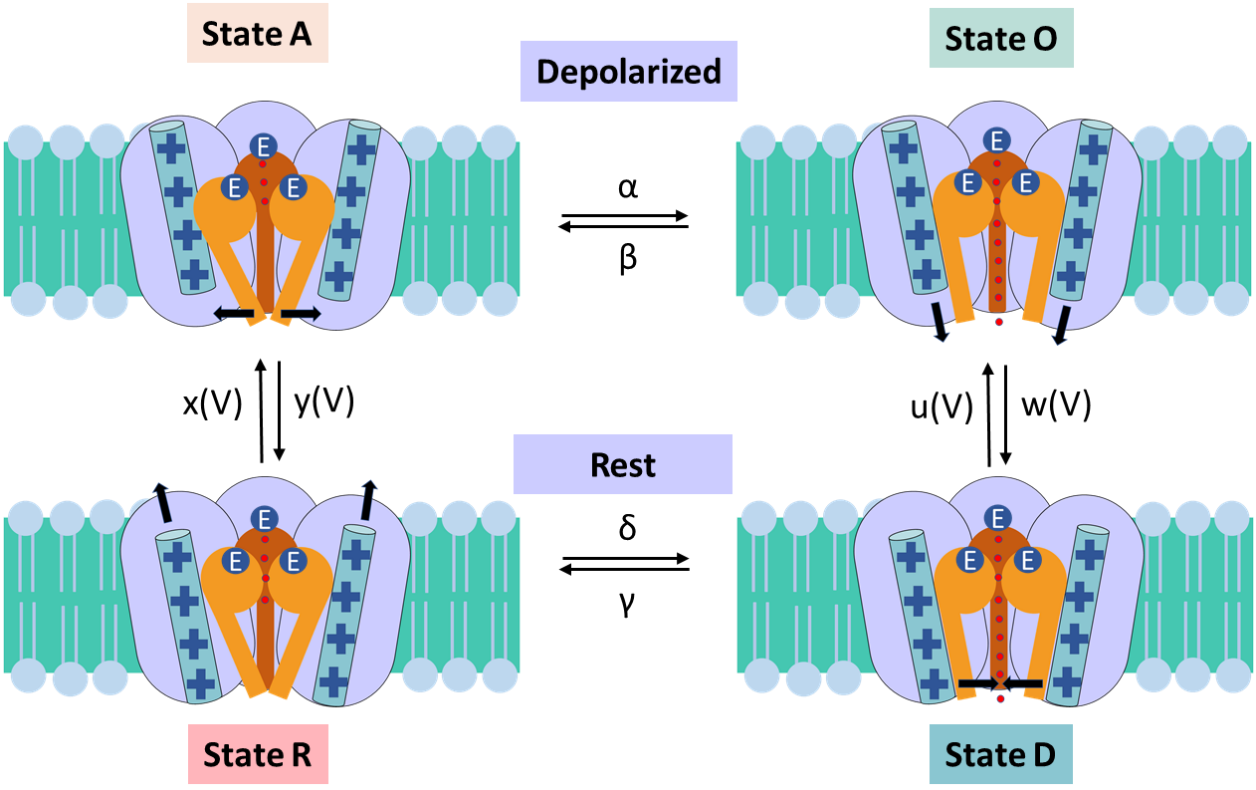

Figure 1.6. The four-states during Ca_v activation with double locking mechanism. This simplified 4-state model explains the gating functions of most Ca_vs. Three (out of four) homologous domains are shown to reveal the vertical inner-lining of the channel. The homologous domain is shown in purple. Each contains a voltage sensor domain with an S4 segment (labeled with four positive charges) and a pore-lining domain in orange (or brown in the back) with S6 guarding the intracellular gating and a Ca^{2+} selectivity filter near the extracellular side. The voltage sensor has two states: activated (up) and resting (down). Pore opening has two states: Open or close. All combinational states result in four channel-activation states summarized in the table. α, β, γ, and δ are rate constants to measure voltage-independent pore opening and closing. Rate constants x, y, u, and w measure voltage-dependent voltage-sensing activation. Annotation refers to Figure 1.5 (Ref. Beyl et al., 2009; Hering et al., 2018).

1.4.4 Voltage-dependent inactivation

Inactivation of VGCCs is both voltage and Ca^{2+} dependent. Voltage-dependent inactivation (VDI) is observed when Ba^{2+} is the permeant ion, but Ca^{2+} -dependent inactivation (CDI) is not (See section 1.4.5). VDI displays a reduced current magnitude and Ca^{2+} permeability and happens in response to prolonged single or repetitive depolarization (Hofmann et al., 2014). VDI is an intrinsic Ca_v property, divided into fast and slow VDI based on their inactivation kinetics, and other auxiliary subunits also play a role in modulating this property (Hering et al., 2000). Voltage sensor-dependent rearrangement of S6 potentially changes the conformation of VGCCs, and numerous studies made point mutations on S6 and neighboring helices to modulate VDI by causing an asymmetrical collapse of the pore (Depil et al., 2011; Hohaus et al., 2005). S6 defects in $Ca_v1.2$ are associated with Timothy syndrome (Splawski et al., 2004 & 2005), and mutations in $Ca_v1.3$ S6 are associated with autism spectrum disorders and epilepsy (Pinggera et al., 2015 & 2017 & 2018). The intracellular loops connecting the homologous domains also contain significant VDI determinants (Stuhmer et al., 1989; Bezprozvanny et al., 1995; Zhong et al., 1999; Degtiar et al., 2000; Hering et al., 2000). A mutation in segment IS4 in $Ca_v1.2$ (Andranovits et al., 2017) shifted the voltage-dependent inactivation to a more negative state than mutations in other domains. These observations further support the role of VSD movement in stabilizing the inactivation state of VGCCs.

1.4.5 Calcium-dependent inactivation

Ca^{2+} -dependent inactivation (CDI or Ca^{2+}/calmodulin-dependent inactivation) is a crucial negative feedback mechanism to tune the Ca^{2+} entry kinetics and avoid Ca^{2+} overload (Peterson et al., 1999; Pitt et al., 2001; Alseikhan et al., 2002; Ghosh et al., 2017). The ubiquitous calcium-modulated protein, calmodulin (CaM), mediates this process by binding to the IQ domain of the C-terminus of Ca_v channels (Zühlke et al., 1999; Peterson et al., 1999). Under basal calcium conditions, Ca^{2+}-free CaM (apo-calmodulin, apoCaM) pre-binds to the IQ domain of the C-terminus and enhances channel openings (Adams et al., 2014). Once the level of cytoplasmic level of Ca^{2+} increases, the bound CaM relocates onto the intracellular permeation path, inducing C-terminus movement by interacting with Ca^{2+}/CaM binding sites (Bazzazi et al., 2013; Johny et al., 2013) (Figure 1.7). This C-terminus conformational change in response to calmodulin fluctuations

modulates Ca^{2+} homeostasis, antagonizes drastic channel opening, and induces CDI. Like VDI, CDI serves as an essential protective process to prevent excessive Ca^{2+} entry during repetitive or prolonged depolarization. Disruption of this process in the cardiac myocytes is associated with lethal cardiac arrhythmias (Splawski et al., 2004, 2005).

However, this stereotypic behavior is not observed among all L-VGCC. $Ca_v1.3$ CDI varies in neuronal tissues, and $Ca_v1.2$ has divergent basal strength of CDI (Liu et al., 2010). Endogenous $Ca_v1.4$ in retina displays minimal CDI (Griessmeier et al., 2009; Haeseleer et al., 2016), and $Ca_v1.3$ in inner hair cells lack CDI (Yang et al., 2016). Researchers found that the alternative splicing of distal C-terminus in $Ca_v1.3$ and $Ca_v1.4$ might explain why these two subtypes intrinsically diminish CDI (Wahl-Schott et al., 2006). Mutations of $Ca_v1.2$/Iso1624 in the IQ motif disrupt the CaM binding and disables CDI in *Xenopus* oocytes (Zühlke et al., 1999 & 2000), but standard CDI and disturbed VDI are observed in HEK cells (Barrett et al., 2008). This mutation is also lethal during embryonic development (Poomvanicha et al., 2011), accompanied by dilated cardiomyopathy (DCM). Additionally, a conserved aspartate in domain II at the pore was found to modulate CDI (Abderemane-Ali et al., 2019). The most recent study found the CDI- inhibiting region with a lower affinity in binding to $Ca_v1.2$ IQ domain than $Ca_v1.3$ IQ domain, resulting in a more significant CDI decrease in $Ca_v1.3$ (Sang et al., 2021).

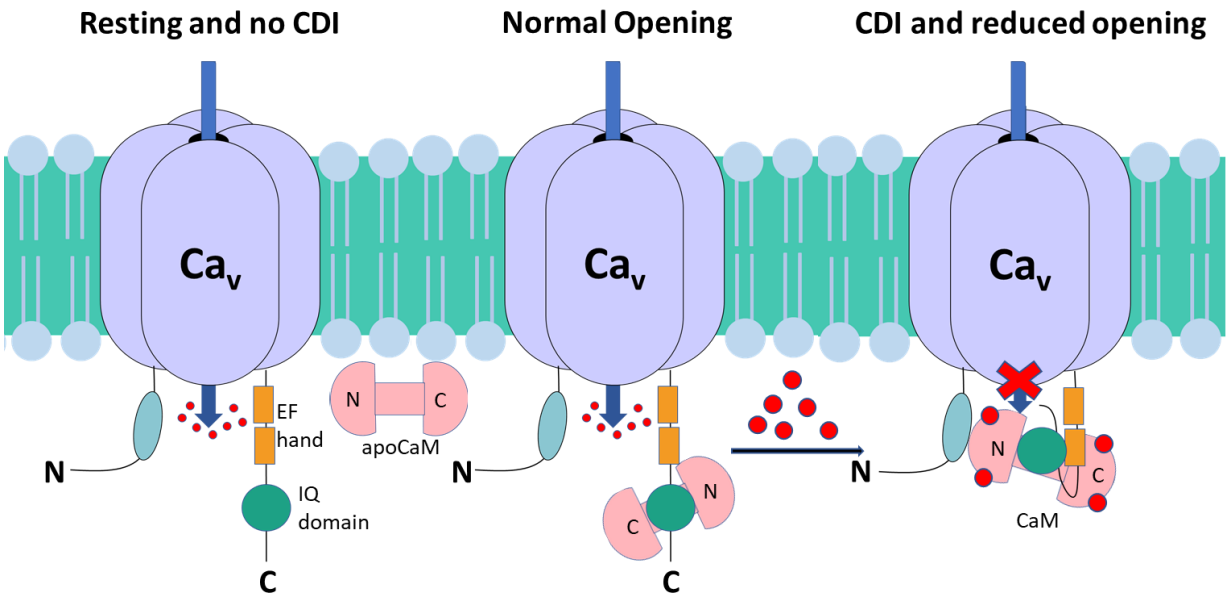

Figure 1.7. Model of calcium/calmodulin-dependent inactivation in the voltage-gated calcium channels. An amino (N) and a carboxy (C) tail are added to this model to show intracellular interaction. The C-terminus contains ~160 a.a, including an IQ domain spanning ~30 a.a and a dual vestigial EF-hand that spans ~100a.a. Three states during CDI were hypothesized: (1) Intracellular Ca^{2+} level is low and Free apoCaM is not bound to Ca^{2+}; (2) apoCaM pre-binds to IQ domain and acts as Ca^{2+} sensors; (3) Excessive Ca^{2+} influx induces the bound CaM to associate with the N-terminal, thus blocking the pore (Ref. Bazzazi et al., 2013).

1.4.6 Phosphorylation sites in $Ca_v\alpha_1$

L-VGCCs are involved in the signaling cascade of plasma membrane protein phosphorylation, and they also carry various phosphorylation sites. Phosphorylation of L-VGCCs increases the Ca^{2+} permeability and increases the channel activity (Yamakage and Namiki 2002). Early *In silico* simulations predicted the phosphorylation of $Ca_v1.1$ by protein kinase A (PKA), C (PKC), G (PKG), calcium/calmodulin-dependent kinase II (CaMKII), and casein kinase II (Jahn et al., 1988; Curtis et al., 1985; Sieber et al., 1987). A wide range of both *in vitro* and *in vivo* experiments determined multiple serine residues for PKA phosphorylation in $Ca_v1.1$ (Rohrkasten et al., 1988a & b; Rotman et al., 1992), $Ca_v1.2$ (Rotman et al., 1995; De Jongh et al., 1996; Leach et al., 1996; Weiss et al., 2012), $Ca_v1.3$ (Ramadan et al., 2009) and $Ca_v1.4$ (Sang et al., 2016). Several threonine residues for PKC phosphorylation were also identified in $Ca_v1.2$ (Kamp et al., 2000; McHugh et al., 2000) and $Ca_v1.3$ (Baroudi et al., 2006; Qu et al., 2005; Marshall et al., 2011).

Moreover, the cGMP-PKG pathway modulates $Ca_v1.3$ regulation of insulin secretion (Sandoval et al., 2017). Moreover, GPCRs can form signaling complexes with VGCCs (Altier 2012) and effectively modulate $Ca_v1.2$ and $Ca_v1.3$ in membrane micro-domains (Albillos et al., 1996; Carabelli et al., 1996; Hernández-Guijo et al., 1999; Hernández et al., 2011; Roberts-Crowley and Rittenhouse 2018). GPCR pathways, cAMP/PKA and NO/cGMP/PKG, regulate channel gating of $Ca_v1.2$ and $Ca_v1.3$ in a competitive manner (Carbone et al., 2001; Carabelli et al., 2001, 2002; Cesetti et al., 2003; Marcantoni et al., 2007, 2008, 2009; Mahapatra et al., 2012).

1.4.7 C-terminal functions

Besides the role in Ca^{2+}/calmodulin-dependent inactivation, the carboxy tail of Ca_V channels exhibits numerous functions. Multiple phosphorylation sites of Ca_v channels exist on the C-terminal tail of VGCCs, and several studies revealed the role of C-terminus cleavage involved in phosphorylation. An A-kinase anchoring protein (AKAP15) associates with the distal VGCC C-terminus, initiates the anchoring of cyclic AMP-dependent protein kinase (PKA) and increases Ca^{2+} current (McDonald et al., 1994; Hulme et al., 2003).

1.4.7.1 Proteolytic cleavage of C-terminus

Alternative splicing has been implied to modulate L-type Ca_V biophysical and pharmacological properties. We will briefly discuss the proteolytic cleavage of different L-type Ca_v channels and the functional roles of alternative splicing variants.

In skeletal muscle calcium channel $Ca_v1.1$, the cleavage site was identified at alanine 1664 (Sculptoreanu et al., 1993; Johnson et al., 1994, 1997; Hulme et al., 2005). The cleaved $Ca_v1.1$ channel has a higher Ca^{2+} conductance, suggesting profound effects of C-terminus cleavage on electrical activities.

In cardiac myocytes and neurons, proteolytical cleavage of $Ca_v1.2$ C-terminus happens at serine 1928 and facilitates phosphorylation by PKA in the distal C-terminus (Hell et al., 1993; De Jongh et al., 1994 &1996; Gerhardstein et al., 2000). Deletion of the distal C-terminus increases $Ca_v1.2$ channel activity like $Ca_v1.1$ (Wei et al., 1994). The C-terminus peptides mimicking the cleavage can directly bind to and weakly inhibit the truncated $Ca_v1.2$ (Gao et al., 2001; Hulme et al., 2006). The $Ca_v1.2$ C-terminal fragment may remain noncovalently associated with the channel

(Hulme et a., 2006) or may translocate from the cytoplasm to the nucleus (Gomez-Ospina et al., 2006).

Some evidence shows the C-terminal proteolytical processing in neuronal $Ca_v1.3$ (Singh et al., 2008; Bock et al., 2011). However, $Ca_v1.3$ was distinguished from $Ca_v1.2$ as going through a specific post-translational proteolytic cleavage step (Hell et al., 1993). Both $Ca_v1.3$ and $Ca_v1.4$ channels exhibit inhibitory C-terminus alternative splicing variants (Sang et al., 2021). Alternative splicing of $Ca_v1.3$ α_1 subunit yields a long ($Ca_v1.3_{42}$) and a short form ($Ca_v1.3_{42A}$), expressed in multiple rodent and human models and suggesting an intramolecular protein-protein interaction resulting in substantial gating differences and channel activity tuning. $Ca_v1.3_{42A}$ showed enhanced CDI, a hyperpolarized activation than $Ca_v1.3_{42}$, perhaps fine-tuning $Ca_v1.3$ for its role in modulating neuronal firing and SA node pacemaking (Catterall et al., 2005; Singh et al., 2008).

$Ca_v1.4$ is predominately expressed in rod photoreceptors and retina bipolar synapses. Its channelopathies have been associated with night blindness (especially human congenital stationary night blindness type-2, CSNB2) (Strom et al., 1998; Bech-Hansen et al., 1998; Boycott et al., 2000). Electrophysiology studies also showed $Ca_v1.4$ mediating neurotransmitter release at the synapse (Miyake et al., 1986). The distal C-terminus of $Ca_v1.4$ can control activation, VDI, and CDI (Singh et al., 2006; Striessnig et al., 2010). However, $Ca_v1.4$ displays the absence of CDI and slow VDI due to the autoinhibitory domain (Koschak et al., 2003; McRory et al., 2004; Baumann et al., 2004). A later study proposed that alternative splicing variants of $Ca_v1.4$ C-terminus and cytoplasmic Ca^{2+} protein buffering can explain the different CDI and VDI of native $Ca_v1.4$ channels and heterologous expression system (Tan et al., 2012).

A cross-channel cleavage and inhibitory interactions are proposed to occur, as the cleaved $Ca_v1.2$ C-terminal tail could regulate other channels or proteins within myocytes and neurons. C-terminal truncated versions of $Ca_v2.1$ (Kubodera et al., 2003) and $Ca_v2.2$ (Westenbroek et al., 1992) were detected in neurons. Similar to $Ca_v1.2$, the cleaved C-terminal tail of $Ca_v2.1$ was found in the nucleus of Purkinje cells of the cerebellum (Kordasiewicz et al., 2006). This observation suggests a common feature of VGCC C-terminal cleavage, and this process potentially produces transcriptional regulators in other calcium channel families.

1.4.7.2 Transcription Factor

Calcium influx through L-VGCCs activates a variety of transcription factors, including CREB, MEF, and NFAT (Sheng et al., 1990; Mao et al., 1999; Graef et al., 1999), which regulate gene expression, including *c-fo*s and *BDNF* (Morgan & Curran, 1986, Murphy et al., 1991, Zafra et al., 1990). Calcium influx may trigger increases in nuclear Ca^{2+} concentrations and activates CaMKIV (a nuclear calcium-dependent enzyme), modulating the activity of transcription factors and cofactors (Hardingham et al., 2001). Besides CaMKIV, calcium can activate calcium-dependent signaling proteins adjacent to the channel pore and amplify the nuclear signal (Deisseroth et al., 1998, Dolmetsch et al., 2001). The C-terminal of $Ca_v1.2$ was reported to encode a transcription factor, translocating to the nucleus upon cleavage to regulate transcription (Gomez-Ospina et al., 2006). These studies failed to find a transcription regulatory effect of $Ca_v1.3$ or $Ca_v2.1$ C-terminus in cortical neurons when fused with Gal4 to recruit proteins to DNA. However, other types of neurons may exhibit the C-terminal domain repressing neuron transcriptional signals or regulating chromatin structures (Gomez-Ospina et al., 2006).

1.5 L-VGCC pharmacological properties

1.5.1 L-VGCCs in cardiovascular disease

The most well-known L-VGCC modulators were developed to treat cardiovascular disease well before the subunit composition, or structures of L-VGCC were known. Cardiovascular disease ranks as the top cause of death in the United States (*CDC High Blood Pressure*, 2020). Thirty percent of American adults are estimated to suffer from hypertension, a precursor to most cardiovascular diseases (Bendyopadhyay et al., 2017). Ca^{2+} influx via L-VGCC subtype $Ca_v1.2$ in cardiac and vascular smooth muscle cells initiates contractions and contributes to the cardiac action potentials (Bers and Perez-Reye, 1999). Three distinct chemical classes of small-molecule drugs with FDA approval showed a potent block of $Ca_v1.2$: 1,4-dihydropyridines (DHPs), phenylalkyamines (PAAs), and benzothiazepines (BZPs) (Hockerman et al., 1997b). All three classes treat hypertension and angina pectoris by inducing vasodilation and reducing vascular resistance (Fleckenstein and Fleckenstien-Grun, 1980). In addition, phenylalkylamines and benzothiazepines are also used to treat supraventricular arrhythmia.

1.5.2 Dihydropyridines

1,4-dihydropyridines (DHPs) have a flattened boat-like six-membered ring structure with a stern (NH group), a bowsprit (aromatic moiety), and the port and starboards (substituents). The relative localization of aromatic moiety and substituents are critical for the modulation of VGCCs (Tikhonov and Zhorov 2009). A variety of DHPs has been identified as agonists or antagonists (Figure 1.8). Ca^{2+} bindings in the selectivity filter Glu residues and adjacent Phe residues are proposed to enhance DHP affinity (Peterson and Catterall 1995). L-type channel "agonists" prolong the activated, open conformation of the channel before transitioning to the inactivated states. On the other hand, L-type channel blockers bind to the closed state of the channel and prevent it from opening (Josephson and Sperelakis 1990; Affolter and Corondado 1985; Bechem and Schramm 1987; Peterson and Catterall 1995). Multiple generations of DHP have been developed for decades, and many are still commercially available (Acosta and Santa Cruz 2018).

Numerous early studies including *in vitro*, *in vivo* and *in silico* modulations of L-VGCCs suggested a binding site within IIIS6, IVS6, and IIIS5-3P loop (the extracellular pore-loop connecting S5 and S6 in domain III) (Hockerman et al., 1997c; Peterson et al., 1996; Sanguinetti and Kass, 1984; Janis et al., 1984; Mitterdorfer et al., 1996; Yamaguchi et al., 2000 & 2003). However, the precise binding mechanism was not fully understood. The crystal structures of the engineered bacterial homotetrameric Ca_vAb channel revealed the DHP binding sites at the subunit interface, but this channel did not have a high amino acid identity with eukaryotic VGCCs (Tang et al., 2016). In the same year, the Cryo-EM structure of rabbit $Ca_v1.1$ ($rCa_v1.1$) was solved at 3.6Å (Wu et al., 2015 & 2016) and remains the only available eukaryotic VGCCs. A recent study determined the Cryo-EM structure of $Ca_v1.1$ complex with DHP antagonist nifedipine or agonist Bay K 8644 at around 3Å (Zhao et al., 2019; Gao et al., 2020), confirming the role of previously identified L-type residues T935, Q939, and S1011 in drug binding (Figure 1.10). A couple of structural Cav1.2 models were simulated to understand the DHP binding interactions based on previously identified residues (Tikihonov and Zhorov 2009; Xu et al., 2016; Saddala et al., 2017; Ozer et al., 2017; Schaller et al., 2018; Mosa et al., 2021). These well-developed models shared consensus binding motifs with the results of the cryo-EM structural basis of rabbit $Ca_v1.1$ but not in other subtypes and species. Moreover, DHP drugs selectivity inhibit $Ca_v1.2$ in the vasculature at therapeutic doses, causing reflex tachycardia and sympathetic and renin-angiotensin system stimulation (Bandyopadhyay et al., 2017). Developing selective Ca_v1-subtype channel blockers

based on DHP derivatives might be challenging because of their high affinities to $Ca_v1.2$ and side effects in cardiovascular systems.

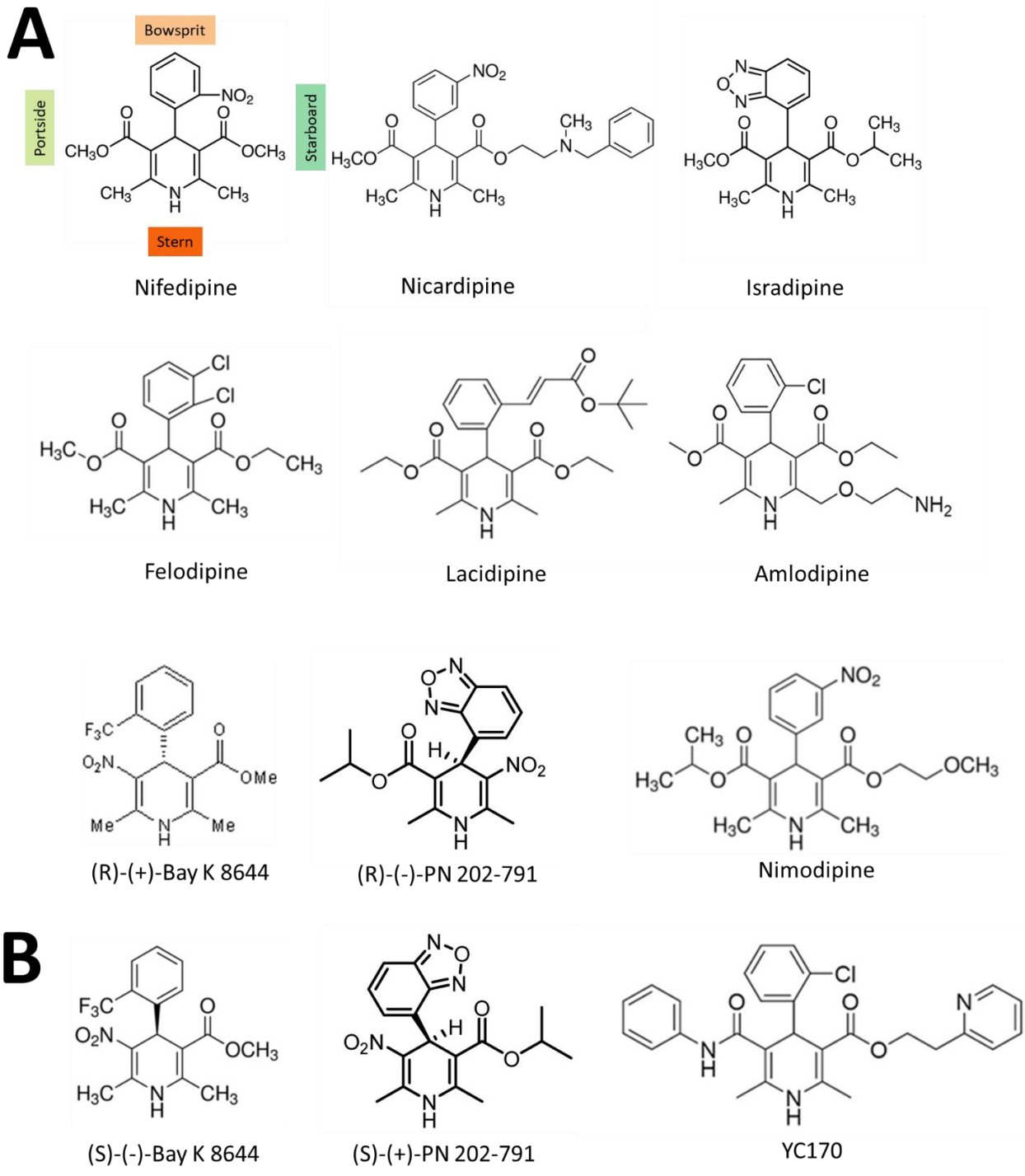

Figure 1.8. Examples of dihydropyridines. (**A**) Antagonistic DHPs. (**B**) Agonistic DHPs.

1.5.3 Phenylalkylamines

Like dihydropyridines, phenylalkylamines (PAAs) are widely used to treat cardiovascular disease. However, unlike DHPs, PAAs bind to Ca_v channels through a different route and show different chronic effects (Catterall and Swanson 2015; Lund-Johansen et al., 1987). The clinically relevant PAA member is verapamil. Verapamil does not have high selectivity for L-type channels, as it also blocks voltage-gated K^+ channels (Wang et al., 2008).

Verapamil blocks $Ca_v1.2$ with high potency in both primary cardiac myocytes (Lee and Tsien 1983) and heterologous expression systems (Johnson et al., 1996), with no selectivity among $Ca_v1.2$, $Ca_v2.1$, and $Ca_v2.3$ (Cai et al., 1997). Verapamil, methoxy-verapamil, and desmothoxy-verapamil block $Ca_v1.2$ via different routes. Verapamil and methoxy-verapamil block $Ca_v1.2$ only from the cytoplasmic side, but desmothoxy-verapamil blocks $Ca_v1.2$ from both sides (Berjukov et al., 1996). Transmembrane IIIS6 and IVS6 in L-VGCCs exhibit specific amino acids for desmothoxy-verapamil to block the closed channels (Hockerman et al., 1995, 1997a; Döring et al., 1996). PAAs exhibit the property of frequency-dependent block to antagonize $Ca_v1.2$ during high-frequency depolarizations (Lee and Tsien 1983), explaining the higher drug affinity for the inactivated state of the channel (Johnson et al., 1996; Nawrath and Wegener, 1997). PAA binding sites were proposed to be conserved and later proved, making two Glu/Gln mutations at $Ca_v1.2$ selectivity filter in domain III and IV, resulting in a reduced affinity (Hockerman et al., 1995 & 1997a). Additional mutations in domain III and the C-terminal displayed altered verapamil sensitivity in $Ca_v1.2$ (Dilmac et al., 2004). With the help of the cryo-EM structure of $Ca_v1.1$, two verapamil binding sites with different affinities were revealed, and verapamil shows direct blocking of the Ca^{2+} permeation path (Zhao et al., 2019). Verapamil inhibits DHP binding allosterically, confirmed by affinity assays and structural building (Gould et al., 1983; Ferry et al., 1995; Hockerman et al., 1997b; Zhao et al., 2019).

1.5.4 Benzothiazepines

The benzothiazepine (BZT) class has one clinically approved compound, diltiazem. An extracellular route was proposed in the early studies (Hering et al., 1993; Seydl et al., 1993). However, the molecular modeling of Cav1.2 implicated a III-V fenestration with favorable energy (Tikhonov and Zhorov 2008). The binding sites in VGCCs are also located in domain III and

domain IV, especially the selectivity filter Glu resides and adjacent Phe residues (Hockerman et al., 2000; Dilmac et al., 2003), overlapping with several identified amino acids in DHP and PAA binding. Three conserved amino acids in L-type VGCCs support the higher diltiazem sensitivity over other VGCCs (Hering et al., 1996). Previous studies have shown overlapping binding sites between PAAs and BZTs (Kraus et al., 1996; Hockerman et al., 2000). Some labs believed that no competition between verapamil and diltiazem is reported even though they both function as a pore blocker (Porzig and Becker 1988; Catterall et al., 2015) or simple competitive behavior (Murphy et al., 1983). However, diltiazem inhibits verapamil in a non-competitive mechanism (Ferry et al., 1984; Glossmann and Striessnig 1990; Brauns et al., 1997). Like verapamil, diltiazem displays frequency-dependent block, with weaker effects (Lee and Tsien 1983; Lund-Johansen 1987). The cryo-EM structure also confirmed these critical amino acids with M1057 in IIIS6 positioning inward, opposite from nifedipine binding (Zhao et al., 2019). Even though the rCa_v1.1 structure showed that diltiazem is not compatible with simultaneous binding of nifedipine because of M1057 (Zhao et al., 2019), (+)-cis-diltiazem stimulates DHP binding while (-)-cis-diltiazem shows no effect in Ca_v1.2 affinity assays (Ferry et al., 1984).

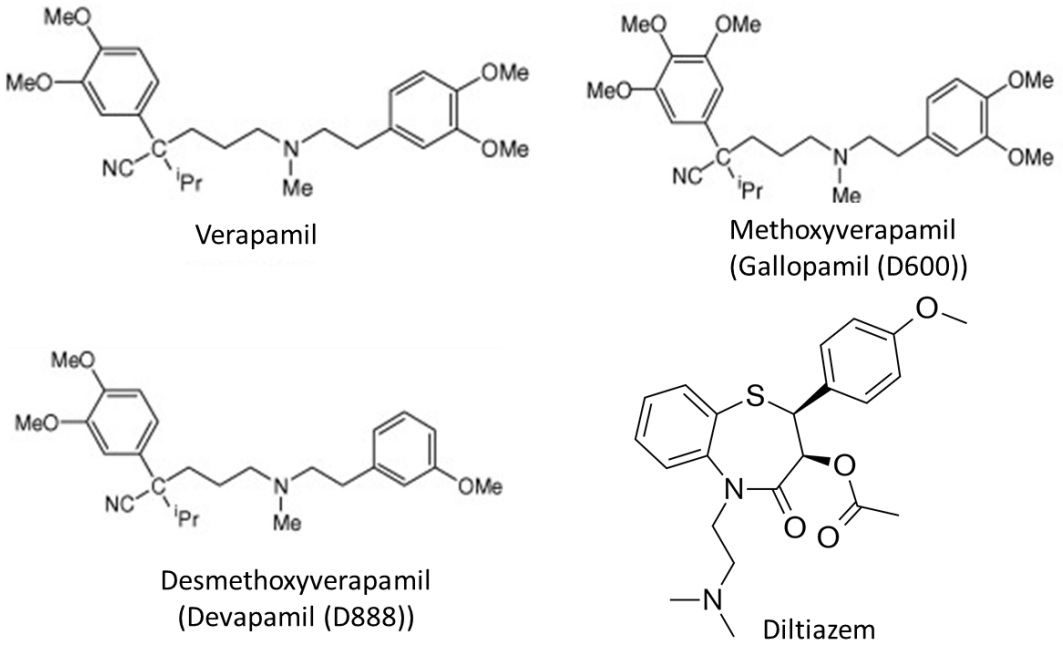

Figure 1.9. Examples of phenylalkylamines (verapamil, methoxy-verapamil, and desmothoxy-verapamil) and benzothiazepine (diltiazem).

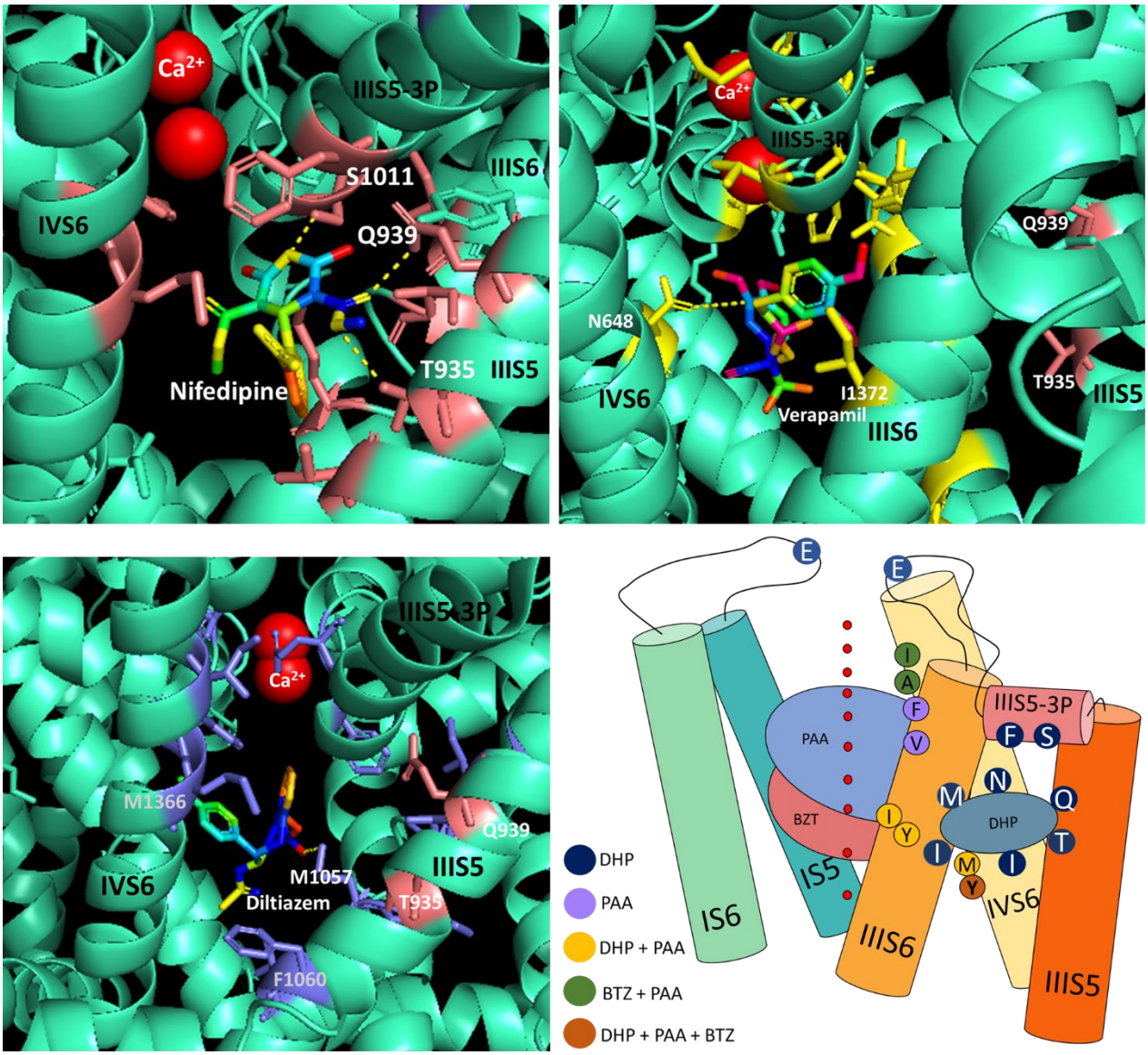

Figure 1.10. Binding pockets of Cryo-EM $Ca_v1.1$ (green) (Zhao et al., 2019) with nifedipine (pink residues), verapamil (yellow residues), and diltiazem (blue residues), and hydrated calcium is colored in red. Schematic of binding motifs of dihydropyridines (DHP; grey) (IIIS5: Mitterdorfer et al., 1996; III/IVS6: Peterson et al., 1997; IIIS5-IIIP loop: Yamaguchi et al., 2000 & 2003), phenylalkylamines (PAA; blue) (Hockerman et al., 1995 & 1997; Dilmac et al., 2004), and benzothiazepines (BZT; red) (Hockerman et al., 2000; Dilmac et al., 2003) share overlapped regions in voltage-gated calcium channels. Individual molecular determinants and combinational binding motifs are labeled with different colors. Calcium in the permeation path is labeled with red circles. (Additional Ref. Lacinová 2005; Wu et al., 2016; Wang et al., 2018; Mosa et al., 2021).

1.5.5 Peptide toxins

Several toxin peptides isolated from distinct snails and snake venoms exhibit selectivity for blocking for L-VGCCs over other VGCCs (Shroeder et al., 2013).

ω-conotoxin TxVII is a cone snail (*C. textile*) toxin with 26 a.a., from the ω-conotoxin family, sharing a four-loop backbone with six cysteines forming three disulfide bonds (Fainzilber et al., 1996). The negative charges and hydrophobic patches explained the selectivity of TxVII for L-VGCCs over N- and P/Q-type VGCCS, which are blocked by ω-CTX GVIA and ω-Aga IVA, respectively (Kim et al., 1994; Sato et al., 1994; Lew et al., 1995; Nasadi et al., 1995). However, this toxin reversibly inhibits snail L-type currents but not in rats, suggesting a species-specific binding (Sasaki et al., 1999). DW13.3 is from *Filistata hibernalis* (spider) venom with 74 a.a, reversibly blocking $Ca_v1.2$ with higher efficacy than all three Ca_v2 channels (Sutton et al., 1998). A snake peptide toxin, S4C8 from *Aspidelaps scutatus* (shield-nosed cobras) with 63 a.a also blocks L-type currents (Jouber et al., 1988).

Four L-type specific mamba toxins were identified. Calciseptine (CaS) is from *Dendroaspis polyepis polyepis* venom (black mamba) with 60 a.a., blocking $Ca_v1.2$ more than $Ca_v1.3$, while ineffective on $Ca_v1.1$ (de Weille et al., 1991; Yasuda et al., 1993; Garcia et al., 2001). FS2 is also from black mamba with 60 a.a., competitively bind to rat synaptosomal membrane with a higher affinity than CaS (Strydom 1977; Yasuda et al., 1994; Kini et al., 1998a). FS2 and CaS differ in 2 residues and have a similar blocking effect (Spedding et al., 1980; Watanabe et al., 1995). A *Dendroaspis augusticeps* (Green mamba) toxin C10S2C2 was first isolated from the venom (Joubert and Strydom 1978) with 63 a.a. and shown to block L-type currents (Lee et al., 1985). Calcicludine (CaC) is another green mamba venom peptide with 60 a.a, irreversibly inhibiting L-VGCC with an IC_{50} of 90nM and non-altered voltage-dependent biophysical properties (Stotz et al., 2000). CaC reaches its plateau of 60% block at the maximum concentration in a tissue- and species-dependent manner, suggesting a partial pore blockage or channel gating. Interestingly, CaC shares homology with protease inhibitors, including bovine pancreatic trypsin inhibitor (BPTI) (Schweitz et al., 1994; Gilquin et al., 1999). Moreover, CaC shares three prolines and a tryptophan in the N-terminus with ω-conotoxin TxVII (Fainzilber et al., 1996; Kobayashi et al., 2000), FS2, and CaS (Kini et al., 1998b).

1.5.6 Non-classified modulators

In addition to the three classes of compounds and toxin peptides, several small molecules were reported to bind with VGCCs. Besides the prominent L-VGCC antagonists mentioned earlier, there is a group of DHP agonists such as (-) -(S)-Bay K (Schramm et al., 1983), 202-791 (Hof et al., 1985) (Figure 1.8.B), CGP 28392 (Erne et al., 1984), RS 30026 (Patmore et al., 1990), and other compounds that have been studied for their potentiation effect on Ca^{2+} channel activity. A non-dihydropyridine, benzoyl pyrrole derivative FPL 64176 also has an agonistic effect on L-type Ca^{2+} channels. It has a higher potency compared to (-)-Bay K 8644 (McKechnie et al., 1994), and is suspected to act on or near the extracellular face of the L-type channel. FPL was first established to increase current amplitude only after the drug was applied outside the cell, even though the drug was present in the patch pipette throughout the measurement (Rampa and Lacerda, 1991). FPL also slows current activation and inactivation as well as prolonging tail current during whole-cell patch-clamp recordings of smooth muscle cell Ca^{2+} current in a reversible manner (Rampe and Dage RC, 1992). Although FPL imposes a high potentiation, its effects can be blocked by further addition of the DHP agonist (-)-Bay K 8644. In contrast, FPL cannot exert an effect on (-)-Bay K 8644 action. Besides the DHP agonist, potentiation induced by FPL in the contractile responses of smooth muscle cells can be noncompetitively antagonized by the Ca^{2+} antagonists, DHP, PAA, and BZT (Zheng et al., 1991). It was reported that negative allosteric interactions among these three majors Ca^{2+} antagonists and FPL 64176 occur at specific sites or conformations in the Ca^{2+} channel. To understand the mechanism of FPL-induced kinetics change, a group detected the dissociation between effects of FPL on ionic currents and gating currents (McDonough et al., 2005). Inward ionic currents were enhanced ~5-fold for a voltage step from -90mV to +10mV, and there was no discernible effect on the fundamental movements of the gating charge that drive channel gating. It was proposed that FPL affects the coupling of charge movement to the opening and closing of the pore and potentially causes an inactivated state to become conducting without otherwise affecting gating transitions.

Interestingly, FPL is selective for potentiating L-type as it was reported to inhibit N-type neuronal calcium currents (Liu et al., 2003), that both FPL and (+)-202-791 similarly affect the whole-cell L-type currents in sympathetic neurons in PC12 cells but inhibit the majority of the whole-cell current in HEK cells expressing a recombinant N-type Ca^{2+} channel. Besides voltage-gated channels, FPL stimulated both [^{3}H] ryanodine binding and RyR activity at higher than 1μM

Ca^{2+} concentration (Wasserstrom et al., 2002). It was proposed that the primary effect of FPL is to reduce the sensitivity of inactivation to Ca^{2+}.

1.6 Ca^{2+} activity and insulin secretion in pancreatic β cells

1.6.1 Diabetes and pathology

Diabetes mellitus is a chronic progressive disorder associated with the inability to produce or utilize sufficient insulin to maintain a homeostatic blood glucose level. Long-term deficits in proper insulin functions lead to chronic hyperglycemia, facilitate the development of glucose intolerance and insulin resistance, and impair the ability to respond to blood glucose fluctuations (Back et al., 2012; Natarajan et al., 2012). Besides pancreatic dysfunction, diabetic complications resulting from uncontrolled hyperglycemia include neuropathy, nephropathy, retinopathy, and cardiomyopathy (Al Kury et al., 2020).

1.6.1.1 Type I diabetes

Type 1 diabetes mellitus (T1DM or T1D), also known as juvenile, childhood-onset, or insulin-dependent diabetes, is a chronic autoimmune disease that ultimately leads to the selective destruction of pancreatic β-cells. Approximately 1.6 million Americans are diagnosed with T1D (DiMeglio et al., 2018). Unlike the development of T2D, T1D has a strong autoimmune and inflammatory component. Several autoantibodies which direct against β-cells antigens in the pathogenesis of T1D were identified, such as islet cell autoantibodies (ICA) and antibodies to insulin (IAA) (Taplin and Barker 2008). A perplexing association between environmental factors and microbiome, genome, metabolism, and immune systems all contribute to the development of T1D (DiMeglio et al., 2018, and see Rewers et al., 2016 for review).

1.6.1.2 Type II diabetes

90% of diabetic patients have type 2 diabetes mellitus (T2DM or T2D) (Santos-Longhurst 2020). T2DM is a metabolic disorder opposed to T1DM, and it results from insufficient insulin secretion or insulin resistance in the insulin-sensitive tissues (Perry et al., 2014; Frayn et al., 2001; DeFronzo et al., 2009). Simple lifestyles have been suggested to reduce the risks of T2DM,

including a healthy diet, physical activity, and maintaining an appropriate body mass. However, it is clear that genetics plays a role in the pathogenesis of T2D. The role of epigenetics in T2D is an area of intense research.

T2D is fundamentally a condition in which insulin supply does not meet insulin demand. Normally, the β-cell has a broad capacity to compensate for the considerable variations in insulin demand (Seino et al., 2005; Kahn et al., 2006). Plasma NEFA elevation and increased lipolysis have been proposed to correlate with reduced GSIS and progression of obesity and T2DM (Stein et al., 1997). However, T2DM development is a complicated process and not simply explained by insulin secretion defects.

ER stress has become a vital regulator of transcriptional and translational response in T2DM. Proper protein folding in ER is essential for protein function and cell survival, and misfolding is very sensitive to environmental factors (Malhi et al., 2014; Sun et al., 2015). Disruption of protein folding and ER stress initiation have been implicated in various diseases, including Alzheimer's disease (Pereira et al., 2013), chronic kidney disease (Maekawa et al., 2017), hepatocellular carcinoma (HCC) (Shuda et al., 2003), and β cell dysfunction (Eizirik et al., 2008; Berry et al., 2018). VEGF-B (vascular endothelial growth factor B) is upregulated in T2D patients (Hagberg et al., 2012; Mehlem et al., 2016). The most recent study found that VEGF-B can modulate Ca^{2+} and cAMP levels by involving signaling proteins in β-cell dysfunction. (Jia et al., 2021).

1.6.2 Pancreatic islets, β cells, and insulin

The pancreatic islets are endocrine micro-organs localized in the exocrine parenchyma of the pancreas, exposed to the systemic glucose concentration in the blood flow. Pancreatic islets express mainly four endocrine cells: glucagon-releasing α-cells, insulin-secreting β-cells, somatostatin-releasing δ cells, and pancreatic polypeptide (PP)-secreting cells (F cells) (Figure 1.11). Among these four cell types, β-cells play the most important roles, making up 50% of cells in human islets and 75% in mouse islets (Cabrera et al., 2006). A mouse islet is about 60 μm in diameter and carries around 80 β-cells (Adriaenssens et al., 2016), and a human islet is about 130 μm in diameter and carries around 200 β-cells (Hellman and Angervall 2009).

The pancreatic β-cells have an average diameter of 13~18 μm and contain ~10,000 secretory granules with 8~9 fg insulin each, corresponding to an intragranular insulin

concentration of ~199 mM (Huang et al., 1995; Göpel et al., 1999; Olofsson et al., 2002). Insulin is complexed with Zn^{2+} (Zn_2-$insulin_6$), carried by β-cell secretory vesicles, and released in response to glucose stimulation (Rorsman and Ashcroft 2018).

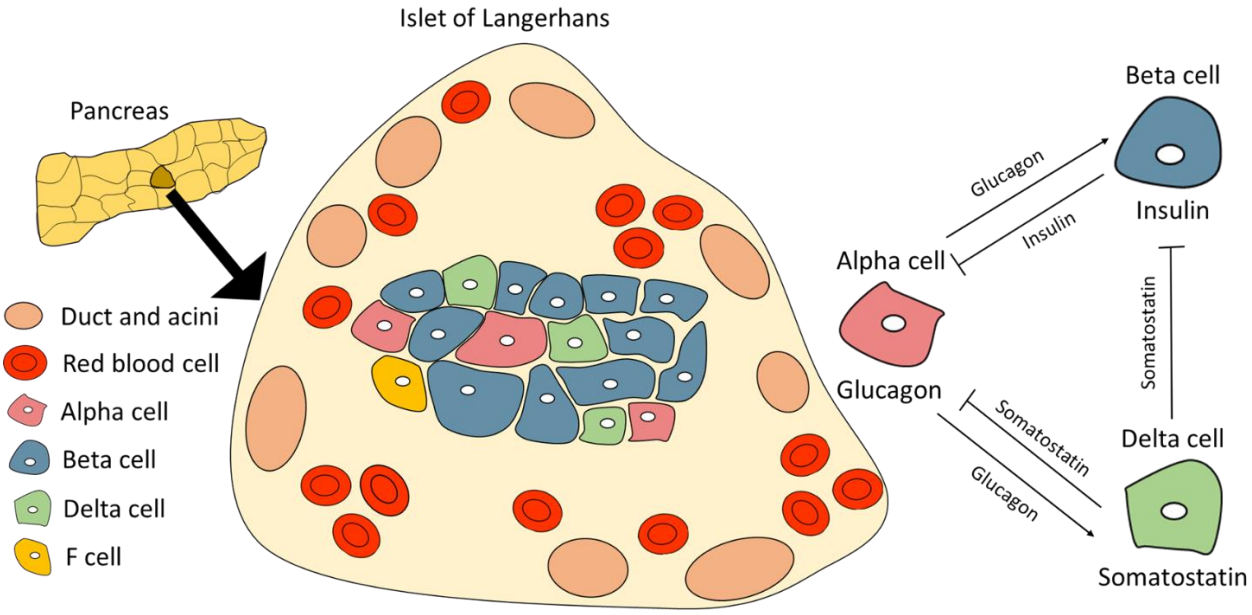

Figure 1.11. Schematic of an islet of Langerhans containing α- β- δ- and F cells. α-cells secret glucagon, stimulating β-cell and δ-cell activity. β-cells secrete insulin, inhibiting α-cells. δ-cells secrete somatostatin, inhibiting α-cells and β-cells. F cells secret polypeptides. The exocrine pancreas contains acinar cells and duct cells (Ref. Ross and Wilson 2021; Encyclopedia Britannica, Inc 2010)

1.6.3 Glucose uptake and metabolism

Various molecules can initiate insulin secretion, including glucose, leucine, stimulative substances for endogenous nutrient metabolism, and antidiabetic drugs. In addition, the effect of these secretagogues can be amplified by potentiators that have a little direct stimulatory effect. These potentiators require a threshold level of glucose, and some examples include amino acids, free fatty acids, incretin hormones such as glucagon-like peptide-1, and neurotransmitters (Jensen et al., 2008). Incretin hormones are released from the small intestines as glucose is absorbed into the bloodstream after a meal, establishing synergistic effects with initiators when plasma glucose increases (Vollmer et al., 2008).

Glucose-stimulated insulin secretion (GSIS) is the primary mechanism to prevent hyperglycemia. Impairment or loss of GSIS is the result of β-cell failure in type-2 diabetes (T2D).

GSIS is also proposed to follow a biphasic time course: Steep plasma glucose increase leads to initial transient response, referred to as the first-phase secretion, followed by a slower and gradual secretion upregulation referred to as the second phase release (Nesher and Cerasi 2002).

1.6.3.1 Glucose uptake

Facilitated diffusion glucose transporters (GLUTs; encoded by the *SLC2A* genes) transport glucose into the β-cells (Figure 1.12). GLUT2 (*SLC2A2*) is required in rodent islet while it is dispensable in human β cells since all low K_m glucose transporters GLUT1/2/3 (*SLC2A1/2/3*) are expressed. In diabetic rodents, significantly reduced GLUT2 is associated with impaired GSIS (Thoren et al., 1990; Orci et al., 1990). GLUT1 has a lower affinity than GLUT2 and constitutes the primary glucose transporters in human β-cells (Heimberg et al., 1995; McCulloch et al., 2011), supporting the observation of higher glucose sensitivity in human islets than mouse islets. GLUT2 loss-of-function mutations cause transient neonatal diabetes mellitus, suggesting an essential role of a functional GLU2 and a compensatory role of other protein expressions during development (Sansbury et al., 2012). Interestingly, Na^+-dependent glucose transporters SGLT (encoded by *SLC5A* genes) were also found in human β-cells but at much lower levels than GLUT1. SGLT transporters are not expressed in mouse islets (Benner et al., 2014; Blodgett et al., 2015). All three GLUT transporters efficiently take up glucose. Thus, the rate-limiting step in GSIS is not glucose uptake but rather phosphorylation of glucose by glucokinase.

1.6.3.2 Glucose metabolism

Once the glucose is successfully transported into the β-cells, glucokinase (GCK) catalyzes the phosphorylation of glucose and initiates glucose metabolism (Bonner et al., 2015) (Figure 1.12). GLUT2 and GCK accelerate glucose metabolism in response to glucose concentration (Ashcroft et al., 1970). In β-cells, the predominant fate of glucose is metabolism via the Krebs cycle and glycolysis (Schuit et al., 1997). Upregulating β-cell glucose metabolism results in increased glycolytic ATP production, mitochondrial glucose oxidation, and active shuttling of reducing equivalents to the mitochondrial electron transport chain (ETC) from the cytosol. The close coupling between glycolysis and mitochondrial oxidation supports accelerated glycolysis in the presence of lowered ATP (Jensen et al., 2008). Mitochondrial calcium signaling is crucial for

pancreatic β-cell function in the metabolism-secretion coupling, including modulating mitochondrial structure, function, and signal transduction (See Weiser et al., 2021 for review).

1.6.4 K_{ATP} modulation in GSIS

Glucose metabolism leads to increased ATP/ADP ratio and inhibition of ATP-sensitive K^+ (K_{ATP}) channels. This process leads to the later stages of GSIS, including depolarizing plasma membrane, activating VGCCs and Ca^{2+} influx, and stimulating insulin granule exocytosis (Figure 1.12).

1.6.4.1 K_{ATP} channel-dependent pathway

The K_{ATP} channel contains four binding sites for ATP, with the occupation of only one binding site by ATP required for channel inhibition (Markworth et al., 2000). Identifying K_{ATP} channel subunits, sulfonylurea receptor 1 (SUR1), and inward rectifying the K^+ channel (Kir6.2) has provided better insights into understanding K_{ATP} channel involvement in GSIS. K_{ATP} channel is an octameric complex of four pore-forming Kir6.2s and four regulatory SUR1 subunits (Inagaki et al., 1995). Kir6.2 is inhibited by ATP/ADP binding while SUR1 regulates the activity of Kir6.2 pore, including sensitivity to sulfonylurea inhibition, K^+ channel opener diazoxide, and ADP stimulation. K_{ATP} channel requires both subunits to correctly traffic to the plasma membrane, and each Kir6.2 subunit requires a SUR1 partner to traffic and vice versa (Zerangue et al., 1999).

Plenty of evidence has shown that GSIS depends on the KATP channel pathway, but this mechanism does not fully describe all the observations within the β-cell activity, including the biphasic time course. First phase secretion is explained by the K_{ATP} channel-dependent pathway, releasing a low level of granules from a readily releasable pool (RRP) (Ashcroft et al., 1984; Cook et al., 1984). Second phase secretion is better supported by a K_{ATP} channel-independent pathway including amplifying signals, and both readily releasable granules and newly recruited granules from the intracellular storage pool are secreted in this phase (Henquin et al., 2003).

1.6.4.2 K_{ATP} channel-independent pathway

Experiments that demonstrated insulin secretion while K_{ATP} channels were maintained in the open state with diazoxide challenged the obligate role of the K_{ATP} channel (Gembal et al., 1992). Interestingly, islets from SUR1 knockout mice either have normal glucose homeostasis (Shiota et al., 2002) or increased insulin secretion in response to 15mM glucose (Nenquin et al., 2004). On the other hand, homozygous Kir6.2 knockout mice showed reduced GSIS, whereas heterozygous mice exhibited increased insulin secretion (Remedi et al., 2006). Moreover, the K_{ATP} channel has been shown to interact with numerous proteins, such as actin (Brady et al., 1996), EPAC2 (exchange protein directly activated by cAMP; Shibasaki et al., 2004), 14-3-3 proteins (Heusser et al., 2006), and syntaxin (Ng et al., 2007). Altogether these results suggest that insulin secretion may proceed along with an ATP-independent pathway.

1.6.4.3 K_{ATP} modulation

One important lipid regulator for the K_{ATP} channel is phosphatidylinositol 4,5-bisphosphate (PIP_2), stimulating channel opening and reducing its ATP sensitivity (Shyng et al., 1998). Purinergic P2Y receptor-mediated activation of phospholipase C decreased the PIP_2 in the plasma membrane, leading to decreased whole-cell K_{ATP} currents. PIP_2 is proposed to bind closely to and modulate the ATP binding site. PIP_2 binding stabilizes the open state of the K_{ATP} channel, increasing the open probability and reducing sensitivity to block by ATP (Nichols et al., 2006). It is also believed that the rundown of channel current occurring upon membrane rupture during patch-clamp recording is explained by PIP_2 hydrolysis (Suh and Hille 2008; Harraz et al., 2020).

Many electrophysiological studies of the K_{ATP} channel in conjunction with membrane potential measurements agree that glucose and sulfonylurea drugs such as tolbutamide inhibit K_{ATP} channel activity at concentrations below those required to stimulate insulin secretion. Glucose-induced block of the K_{ATP} channel is also in line with glucose-induced intracellular ATP increase. K_{ATP} channel block leads to membrane depolarization and stimulates action potentials (APs) related to insulin secretion. K_{ATP} channel activity is enhanced by activation of plasmalemma (PMCA) and Sarco/endoplasmic reticulum (sER) Ca^{2+}-ATPases (SERCA), lowering the intracellular ATP concentration and influencing the burst duration (Gandasi et al., 2014).

Figure 1.12. Ion channels involved in glucose-stimulated insulin secretion in human β-cells and the corresponding electrical activity in the current-clamp recording. GLUT1 and GLUT2 (green) take up the extracellular glucose, inducing the mitochondrial glucose metabolism, producing ATP, increasing ATP/ADP ratio, and closing K_{ATP} channels (Kir6.2 and SUR1). Inwardly rectifying Kir5.1 and 7.1 channels have a small contribution to resting conductance. K_{ATP} channel closure leads to membrane resistance increase, allowing T-type Ca_vs to open spontaneously, inducing ① the initial depolarization. Further depolarization activates L-type Ca_vs (purple) and Na_v (grey), leading to the ② upstroke of the action potential. ③ The peak of the action potential, P/Q Ca_vs are open, and Ca^{2+} influx triggers insulin exocytosis. BK (large Ca^{2+}-activated high-conductance K^+) channels are activated and explain ④ action potential repolarization. Interspike membrane potential is regulated by TALK-1/TASK-1, SK (small Ca^{2+}-activated high-conductance K^+) channels, and delayed rectifying voltage-gated K^+ channels. SK channels mediate ⑤ the afterhyperpolarization (AHP). The numbers 1-10 highlight the different phases of β-cell electrical activity: ⑥ the plateau/ interspike potential; ⑦ the progressive reduction of actional potential amplitude and potential during electric activity; ⑧ the silent interval between two bursts of action potentials that eventually results in the initiation of a new burst of action potentials and insulin secretion at high glucose concentration; ⑨ burst termination. Glucose-induced insulin secretion is more significant at high glucose than at low glucose despite the reduction of action potential magnitude because glucose exerts an amplifying effect on insulin secretion in addition to triggering electrical activity.

Figure 1.12 continued

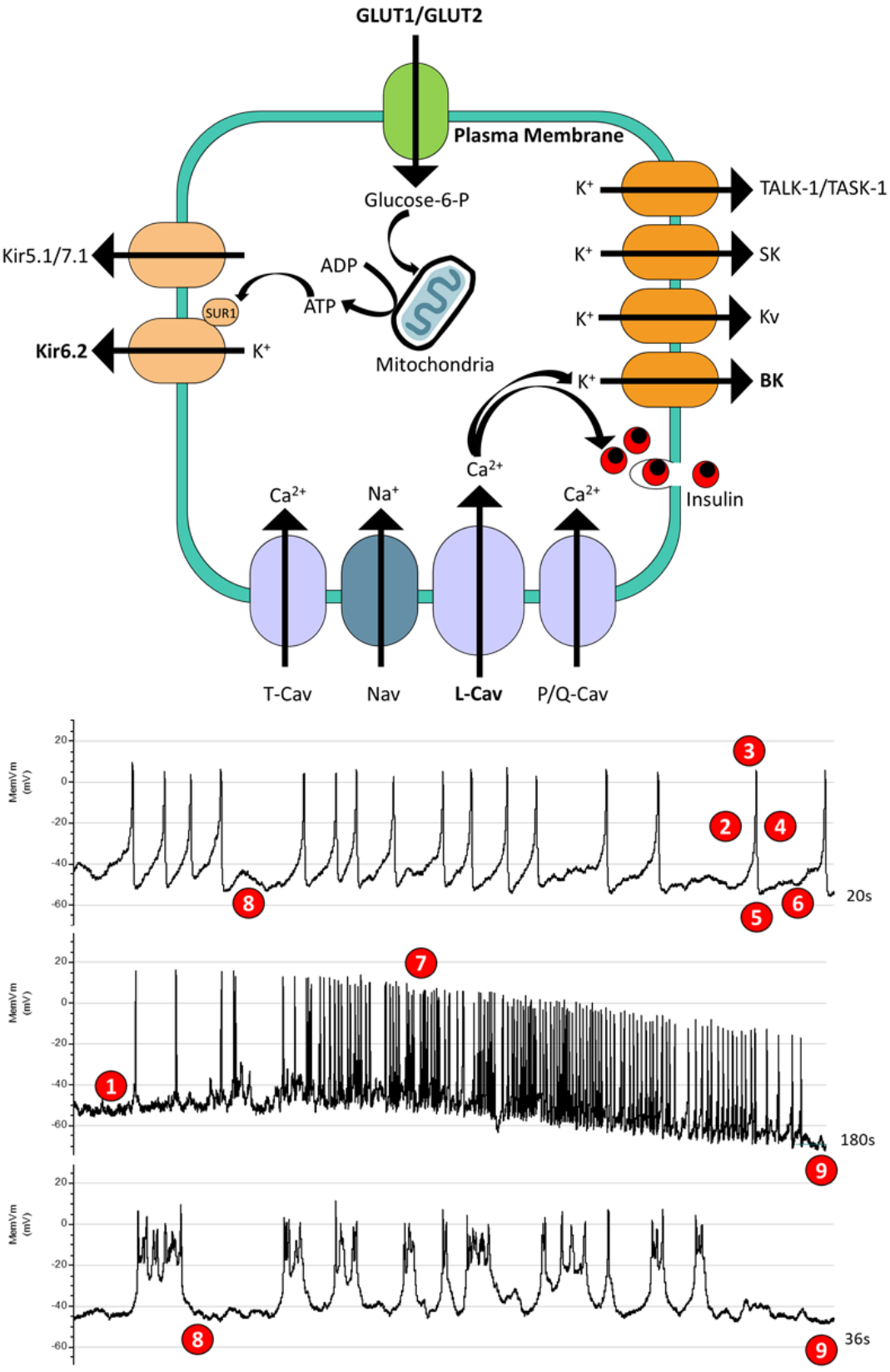

1.6.5 L-VGCC modulation in GSIS

Inward currents elicited by either K_{ATP} or other background channels depolarize the membrane above a threshold level and initiate regenerative bursts of APs. A variety of voltage-dependent currents are shown to contribute to APs, varying among species and depending on experimental methodology, including voltage-gated Ca^{2+} channels, voltage-gated Na^{+} channels, voltage-gated K^{+} channels, large-conductance Ca^{2+}-activated K^{+} (BK) channels, small-conductance Ca^{2+}-activated K^{+} (SK) channels, and hyperpolarization-activated cation channels (HCN). Voltage-gated calcium channels (VGCCs) are the main channels conducting Ca^{2+} entry, attributing to the increase of cytoplasmic Ca^{2+} concentration (Jacobson and Philipson 2007).

In mouse β-cells, L-type VGCCs are predominately expressed along with a smaller amount of N-type and P/Q-type VGCCs. As for human β-cells, L, P/Q, and T-type VGCCs were found but not N-type. Moreover, the L-VGCC subtype $Ca_v1.2$ has a higher transcript level than $Ca_v1.3$ and $Ca_v1.1$. VGCC subtype-selective inhibitors and knockouts suggest that $Ca_v1.2$ is the principal channel in mouse β-cells and essential for first-phase insulin secretion, possibly due to the direct interaction with release-competent secretory granules (Schulla et al., 2003). In human β-cells, $Ca_v1.3$ transcript is more prevalent than $Ca_v1.2$ (See section 1.7.3 Braun et al., 2008; Reinbothe et al., 2012).

Interestingly, glucose metabolism regulates L-VGCCs. Glucose and glucose metabolite glyceraldehyde increase current and activity in β-cells and RINm4F cells by a Ca^{2+}-dependent PKC (Velasco et al., 1988; Smith et al., 1989). This process could be reversed by mannoheptulose (glucose phosphorylation blocker) and oligomycin (mitochondrial ATP production inhibitors) (Smith et al., 1989). L-VGCC activity is also regulated by protein phosphorylation such as PKA and PKC. Elevated cAMP induced by forskolin almost doubles Ca^{2+} current, and it is amplified by okadaic acid, which inhibits serine-threonine protein phosphatase (PP) type 1, 2A, and 3 (Ammälä et al., 1993, 1994), suggesting the activation of L-VGCCs by PKA. IP_6, the dominant inositol phosphate in insulin-secreting cells, inhibits PP1, PP2A, and PP3 and increases the Ca^{2+} current (Larsson et al., 1997). The PKC activator, PMA (Phorbol 12-myristate 13-acetate), blocks the okadaic acid-induced Ca_v channel activity, suggesting that these PPs dephosphorylate at PKA sites but not PKC sites in mouse pancreatic β-cells. This observation was drastically more intense in RINm5F cells than primary mouse β-cells (Ammälä et al., 1994; Haby et al., 1994).

L-VGCC auxiliary subunits were also found to associate with β-cell current activity. Interestingly, different from the results in a heterozygous expression system, $Ca_v\beta_3$ is not required for expression of β-cell Ca_v channels but forms a $Ca_v\beta_3$ subunit-intracellular Ca^{2+} store network, and there was no compensatory increase of expression of other β subunits (Berggren et al., 2004). $Ca_v\beta_3$-knockouts do not affect the gating nor activity of Ca_v channels. Disruption of $Ca_v\alpha_2\delta$ expression in β-cells reduces Ca^{2+} current amplitude in half and substantially reduces insulin secretion (Mastrolia et al., 2017). This result is consistent with the role of $Ca_v\alpha_2\delta$ in neurons (Hoppa et al., 2012) and suggests that $Ca_v\alpha_2\delta$ subunits are critical for coupling VGCC to insulin secretion.

1.6.6 β-cell electric activity

1.6.6.1 modulators of β-cell electric activity

As mentioned earlier, a variety of GSIS modulators have been identified. Except for initiators, sulfonylureas, and non-esterified fatty acids (NEFA, also called free fatty acids FFA), no modulators can initiate insulin secretion directly but amplify β-cell electrical activity and insulin secretion when plasma glucose concentration increases. Modulators like hormones and neurotransmitters have to interact with intracellular or membrane receptors to initiate the regulatory pathway.

Ionotropic and metabotropic receptors were identified in different signaling pathways. Ionotropic receptors contain ion channels to regulate ion flux, while metabotropic receptors comprise mostly G protein-coupled receptors (GPCR), indirectly regulating ion flux by activating G proteins or second messengers like Ca^{2+}. Among the hormones and neurotransmitters, several insulin potentiators were identified, such as acetylcholine (Ach), glucagon-like peptide 1 (GLP-1), gastric inhibitory peptide (GIP), and opioids (Irwin et al., 2013). Inhibitory insulin regulators include paracrine hormone somatostatin, the neurotransmitter epinephrine, and the peptides galanin, ghrelin, and leptin. The potentiators also reduce the hyperpolarizing background K_{ATP} conductance and activate a depolarizing TRPM channel (TRPM2 or TRPM4) current. On an additional note, nicotinic acid dinucleotide phosphate (NAADP) activates TRPM2 channels and increases glucose response and potentially background current (Masgrau et al., 2003; Sumoza-Toledo et al., 2011; Yoshida et al., 2014).

Besides the GSIS modulators mentioned above, various autocrine regulators are found in the β-cell secretory granules and are co-released with insulin in response to glucose, modulating β-cell electrical activity. These regulators include islet amyloid polypeptide (IAPP or amylin), ATP/ADP, zinc, the neurotransmitter GABA, glutamate, and glycine (Henquin et al., 2021).

1.6.6.2 β-cell action potential upstrokes

The measured resting membrane potentials for β-cells in humans at -65mV and -75mV for mouse β-cells due to high resting K_{ATP} channel activity when cytoplasmic ATP/ADP ratio is low and minor effects of Kir5.1 and Kir7.1 (Riz et al., 2015). -55mV is the approximate threshold target to open VGCCs in mouse β-cells (Figure 1.12) (Göpel et al., 1999; Barnett et al., 1995; Braun et al., 2009).

The initial depolarization and upstroke of the APs are associated with regenerative activation of L-VGCCs, as assessed by studies with Ca^{2+} channel antagonists. Inorganic Ca^{2+} channel blockers (such as Co^{2+}) block VGCCs, hyperpolarizing the membrane potentials and suppressing the electrical activity (Ribalet et al., 1979). However, sustained blocking results in paradoxical membrane depolarization, correlating with resting β-cell K^+ conductance reduction and K_{ATP} channel inhibition (Göpel et al., 2004). Organic L-VGCC blockers like verapamil and nifedipine transiently suppress the electric activity but do not diminish the low-amplitude action potential activity (Vasseur et al., 1987).

Voltage-gated Na^+ channels contribute to action potential firing in a smaller proportion of β-cells by spreading depolarization to neighboring cells lacking Na^+ channels via gap junctions (Rocheleau et al., 2006; Zhang et al., 2014). Other L-VGCC-independent action potentials imply the opening of P/Q- and N-type Ca^{2+} channels at -20mV and above.

1.6.6.3 β-cell action potential repolarization

Rapid CDI in VGCCs underlies action potential repolarization, along with VDI of Na^+ channels and activation of delayed rectifying $K_v2.1$ and BK channels (Figure 1.12) (Houamed et al., 2010). $K_v2.1$ channels only contribute to the late phase of repolarization because of their slow opening, with maximal activation occurring after membrane potential returns to the plateau (Smith et al., 1990; Jacobson et al., 2007; Houamed et al., 2010). BK channels, the large-conductance

Ca^{2+} -activated K^+ channels, are activated during the upstroke of the action potential, and blocking BK channels increases action potential amplitude (Henquin et al., 1990; Houamed et al., 2010). $K_v2.1$ and BK channels together modulate the AP downstroke velocity.

1.6.6.4 β-cell action potential plateau

Following the action potential repolarization, the membrane potential returns to a level around -50 ~ -40 mV, depending upon species (Figure 1.12). This plateau potential is potentially influenced by delayed rectifying K^+ channels, two-pore K^+ channels, and small-conductance (SK) Ca^{2+} -activated K^+ channels. $K_v2.1$ and $K_v11.1/11.2$ have slow activation and deactivation, maintaining K^+ conductance after repolarization, contributing to the interval of successive action potentials (Ashcroft et al., 1989; Kang et al., 2006; Düfer et al., 2009). These delayed rectifying K^+ channels also help reactivate VGCCs (Rorsman et al., 2011). The outwardly rectifying two-pore K^+ channels TASK-1 and TALK-1 stabilize membrane potentials when the membrane potential is above -40mV in a voltage-independent manner (Vierra et al., 2015; Dadi et al., 2015). SK3 and SK4 channels are activated by Ca^{2+} accumulation during action potential firing, underlying the brief after-hyperpolarization, and regulating AP frequency.

1.6.6.5 β-cell action potential bursts

Apamin, a blocker of SK (SK1-3) channels, stimulates action potential firing in both human and mouse β-cells and reduces actional potential amplitudes (Jacobson et al., 2010). Another SK channel blocker, NS8693, depolarizes the membrane potential by 10mV, increasing the firing frequency and insulin secretion in human β-cells in the presence of 10mM glucose (Jacobson et al., 2010). Blocking the TASK-1 channel is also found to increase action potential firing (Dadi et al., 2015; Vierra et al., 2015). Compared to mouse β-cells, human β-cells tend to have more negative action potentials with shorter silent intervals lacking well-defined plateau potentials.

Often time, a progressive decrease in both action potential amplitude and frequency are recorded during experiments, and cumulative VDI of Na^+ channels and VDI/CDI of Ca^{2+} channels can explain this unique observation (Plant et al., 1988; Rorsman et al., 2011; Satin et al., 1989; Zhou et al., 1995).

1.6.6.6 β-cell action potential burst termination

Termination of the continuous firing is associated with the activation of K_{slow} (K_{ATP} and SK3/4) channels. Ca^{2+} influx activates K_{slow} by stimulating Ca^{2+} -ATPases SERCA, utilizing ATP, reducing ATP/ADP ratio in the cytoplasm, terminating the bursts, and repolarizing the membrane potential to -70mV (Detimary et al., 1998; Tarasov et al., 2012). Increased K_{ATP} channel activity during repolarization and the regenerative closure of VGCCs after dropping below the threshold accounts for the rapid final repolarization to the interburst membrane potential (Rorsman et al., 2011).

Interestingly, a long silent plateau potential below the threshold is often observed between two intense bursts of action potentials. During this period, intracellular Ca^{2+} is reduced, and ATP/ADP ratio keeps climbing up, resulting in a time-dependent decrease in K_{slow} activity. Reactivation of voltage-gated Na^{+} and Ca^{2+} channels initiates a pacemaker depolarization and induces a new burst of action potentials. In human β-cells, T-type VGCC is also activated when SK current is sufficiently reduced (Zhou et al., 1995).

Fascinatingly, this termination is less likely to be found when glucose concentration reaches around 20~30mM. Instead, continuous action potential firing exists to replace the oscillatory electrical activity in the presence of low 10mM glucose (Barnett et al., 1995). This high excitability is proposed to be led by the increased metabolic rate of β-cells at higher glucose levels and ATP production. β-cells have a higher capacity to buffer ATP/ADP with a more stable ratio, and reactivation of the K_{ATP} channel is limited to permanently depolarize β-cells (Henquin et al., 1984; Sánchez-Andrés et al., 1995). In human β-cell depolarization, the T-type Ca^{2+} channel and the TTX (tetrodotoxin) -sensitive Na^{+} channel stay in VDI, leading to a reduced action potential amplitude in high glucose conditions compared to low glucose. Action potential peak amplitudes correlate with the activation of voltage-gated P/Q type-Ca^{2+} channels, diminishing when the membrane potential goes more negative. Different VGCCs activated at different membrane potentials dominate the GSIS in the presence of different concentrations of glucose (Braun et al., 2008).

1.6.7 Insulin secretion

Insulin secretion from the secretory vesicles is a highly regulated process and can be explained by the SNARE (Soluble NSF attachment protein (SNAP) receptor) proteins. (vesicle) v-SNAREs and (target) t-SNAREs are the essential proteins on vesicular, granular, and plasma membranes involved in this process (Südhof et al., 2012), including tethering, docking, and assembly of the loose SNARE complex, formation of the tight ternary SNARE complex, fusing into the plasma membrane, opening the pore and delivering insulin into the extracellular environment with an expanded fusion pore.

Tethering is regulated by VGCCs and active zone proteins munc18, munc13, and RIM. SNARE complex is formed by SNAP-25 and t-SNARE protein syntaxin-1 in the plasma membrane interacting with v-SNARE protein VAMP2 in the secretory vesicle membrane. Syntaxin-1 forms one helix, SNAP-25 forms two helices, and VAMP-2 forms the last helix of the SNARE complex, stabilized by complexin. The fusion pore is opened upon Ca^{2+} binding to synaptotagmin, displacing complexin and completing zippering. These fusion pores are further expanded to release the cargo from a dense core vesicle by disassembling the *cis*-SNARE complex with the help of NSF/SNAP ATPases and recycled (Südhof et al., 2009, 2012, 2013). Additionally, the cytomatrix active zone (CAZ) protein piccolo (PCLO, also known as aczonin) binds to the cAMP sensor Epac2 (cAMP-GEFII) and RIM2, which mediates the stimulatory effect of cAMP on exocytosis in a Ca^{2+} -dependent manner. Downregulation of PCLO in mouse islets inhibits insulin secretion (Fujimoto et al., 2002).

1.6.8 Intracellular Ca^{2+} homeostasis

Besides the VGCCs on the extracellular membrane of β-cells, multiple ion channels also reside on the intracellular organelle membranes such as secretory vesicles, lysosomes, and endoplasmic reticulum (ER). Two ligand-gated Ca^{2+} release channels, the Ryanodine receptor (RyR) and $InsP_3$ receptor (IP_3R), are localized in ER and play essential roles in regulating intracellular Ca^{2+} homeostasis by mobilizing Ca^{2+} from intracellular stores (Gilon et al., 2002). A variety of stimuli can activate RyR and IP_3R, including neurotransmitters, hormones, metabolic fuels, and Ca^{2+}, and release Ca^{2+} into the cytosolic compartment and induce complex dynamic changes. This Ca^{2+} -induced Ca^{2+} release (CICR) has been shown to mediate the effects of GLP-1

on β-cell Ca^{2+} concentrations (Kang et al., 2003; Kanai et al., 2004). The ER Ca^{2+} pump inhibitor thapsigargin can deplete the ER Ca^{2+} pool, disturbing the electrical bursting in β-cells and Ca^{2+} oscillations (Beauvois et al., 2006). Multiple studies proposed that the complex dynamic changes in Ca^{2+} concentrations modulate both exocytotic proteins and intracellular Ca^{2+} -sensitive proteins to regulate cellular events (Yang et al., 2014).

1.6.8.1 IP_3 receptor in β-cells

All three IP_3R subtypes ($IP_3R1/2/3$) can be found in the β-cell ER membrane, opening pores in response to activation of phospholipase C (PLC)-linked GPCRs such as muscarinic M3 receptors and purinergic P2Y receptors. PIP_2 does not only activate K_{ATP} channel pore opening or inhibit TRP channels, but also mediates GPCR coupling (Yen et al., 2018). Activation of Gs or Gi-coupled receptor results in an increase or decrease in the cAMP level. G_q activates PLC and initiates the hydrolysis of receptor-triggered PIP_2 to generate diacylglycerol (DAG) and IP_3. IP_3 is a second messenger and undergoes extensive metabolism. IP_3 can either be directly hydrolyzed or be first phosphorylated to generate D-myo-inositol 1, 3, 4, 5-tetrakisphosphate (IP_4), or dephosphorylated to D-myo-inositol bisphosphates (IP_2) and D-myo-inositol monophosphates (IP_1). Synthesis and hydrolysis of PIP_2 induced by IP_3-induced ER Ca^{2+} release support a buffering of global plasma membrane PIP_2 pool (Gamper and Shapiro 2007; Trinquet et al., 2011).

Glucose induces CICR and increases IP_3 levels efficiently. Insulin from GSIS is co-released with ATP, which activates autocrine P2Y receptors, potentially explaining the IP_3 level increase (Barker et al., 2013). Ach effects are partly mediated by elevation of IP_3, stimulating ER Ca^{2+} release via binding to IP_3R (de Sevilla et al., 2008).

IP_3-induced Ca^{2+} release can be significantly increased in $Ca_v\beta_3$ knockout β-cells and is associated with an increase in the frequency of glucose-induced Ca^{2+} oscillations, creating more efficient glucose homeostasis (Berggren et al., 2004). It was speculated that $Ca_v\beta_3$ slows the IP_3-mediated Ca^{2+} mobilization from intracellular stores by reversibly interacting with the IP_3 receptor (Yang and Berggren 2006).

1.6.8.2 RyR2 in β-cells

All three subtypes of RyRs have been reported to be expressed in human β-cells (Mitchell et al., 2003). RyR expression level in mouse β-cells is low (Benner et al., 2014), but in somatostatin-secreting δ cells, RyR3 has a high expression (Zhang et al., 2007). Paracrine action of somatostatin is dependent on RyR activity in mouse islets and inhibits insulin secretion (Zhang et al., 2007; e Drigo et al., 2019). Interestingly, RyR2 is found to be prominent in human islets without other subtypes expressed (Bruton et al., 2002; Johnson et al., 2004). Activation of RyR2 induces insulin secretion at 3mM glucose but not in higher glucose concentrations (Kanatsuka et al., 1989). RyRs can be activated by glucose-induced Ca^{2+} influx, caffeine, ATP, fructose 1,6-diphosphate, long-chain acyl CoA, and cADPR (cyclic ADP-ribose) (Gilon et al., 2002). Once activated, RyRs undergo a rapid conformational switch from an impermeable state to a highly permeable pore, allowing rapid Ca^{2+} release into the cytoplasm, regulating insulin secretion, and interacts with Ca^{2+}-sensitive proteins (Yang et al., 2014). Altogether the expression of RyR is slightly lower than that of IP_3R in β-cells, and their roles are not fully understood yet. RyR expression or function decreases in multiple diabetic animal models and patients, suggesting a potential role in the pathophysiology of diabetes (Islam 2002).

1.6.8.3 IRBIT in β-cells

IRBIT (IP_3R binding protein released with inositol 1,4,5-trisphosphate, also called AHCYL1 or DCAL) was first identified as a binding protein of IP_3R and served as an inhibitor (Ando et al., 2003). IRBIT competes with IP_3 for the common binding site on IP_3R and suppresses IP_3R activation (Ando et al., 2006). IRBIT activity is regulated in the serine-rich region, and phosphorylation of S68 is required for binding to binding to IP_3R. Protein phosphatases (such as PP1) dephosphorylate IRBIT and reduce its affinity to IP_3R (Ando et al., 2006; Devogelaere et al., 2007). Two motifs in IRBIT, PEST, and PDZ, were identified to regulate the binding of IRBIT to IP_3R by *in-silico* analysis and pull-down assays (Devogelaere et al., 2006). Splicing variation of IRBIT long- and short- forms affects protein stability and target selectivity (Kawaai et al., 2017).

IRBIT was reported to bind to and regulate the Na^+/HCO_3^- cotransporter NBCe1-B (Shirakabe et al., 2006), the Na^+/H^+ exchanger NHE3 (He et al., 2008), the Cl^- channel CFTR (cystic fibrosis transmembrane conductance regulator) (Yang et al., 2009), and the

Cl^-/HCO_3^- exchanger Slc26a6 (Park et al., 2013). The physiological and pathological roles of IRBIT have been examined in renal collecting tubule epithelium, zebrafish embryonic development, and tumors (Ando et al., 2014), but the role of IRBIT in pancreatic β-cells has not been reported.

1.6.8.4 Store-operated Ca^{2+} entry

The deficiency of ER Ca^{2+} levels regulated by SERCA inhibitors induces Ca^{2+} entry and depolarizes the membrane potentials of β cells (Gilon et al., 1992). Store-operated calcium entry (SOCE) is a process activated in response to this depletion following the stimulation of plasma membrane receptors that couple to PIP_2 hydrolysis and IP_3/DAG generation. Stromal interaction molecule 1 (STIM1) acts as a calcium sensor enabled by an intraluminal EF-hand domain, and when active IP_3R generates a low calcium microenvironment (Sampieri et al., 2018), it interacts with Ora1 in the plasma membrane to form a Ca^{2+} permeable pore. TRPC channels are also thought to contribute to SOCE activity in β-cells (Islam 2010; Prole and Taylor 2019). The SOCE is almost universally associated with IP_3-evoked Ca^{2+} release. Interestingly, RyR-induced Ca^{2+} entry through TRP-like channels does not involve Ca^{2+} store depletion (Gustafsson et al., 2004).

Additionally, two intracellular messengers, cADPR (cyclic ADP ribose) and NAADP (nicotinic acid adenine dinucleotide phosphate), are formed from β-NAD^+ and $NADP^+$ by several ADP ribosyl cyclases such as CD38 (Michell et al., 2003). TRPM2 activation induces cADPR to release Ca^{2+} from ER and triggers Ca^{2+} entry, while NAADP releases Ca^{2+} from acidic Ca^{2+} stores like lysosomes and insulin secretory vesicles (Michell et al., 2003). Activation of the CD38 /cADPR /NAADP pathways was shown to reduce apoptosis in β-cells (Johnson et al., 2006).

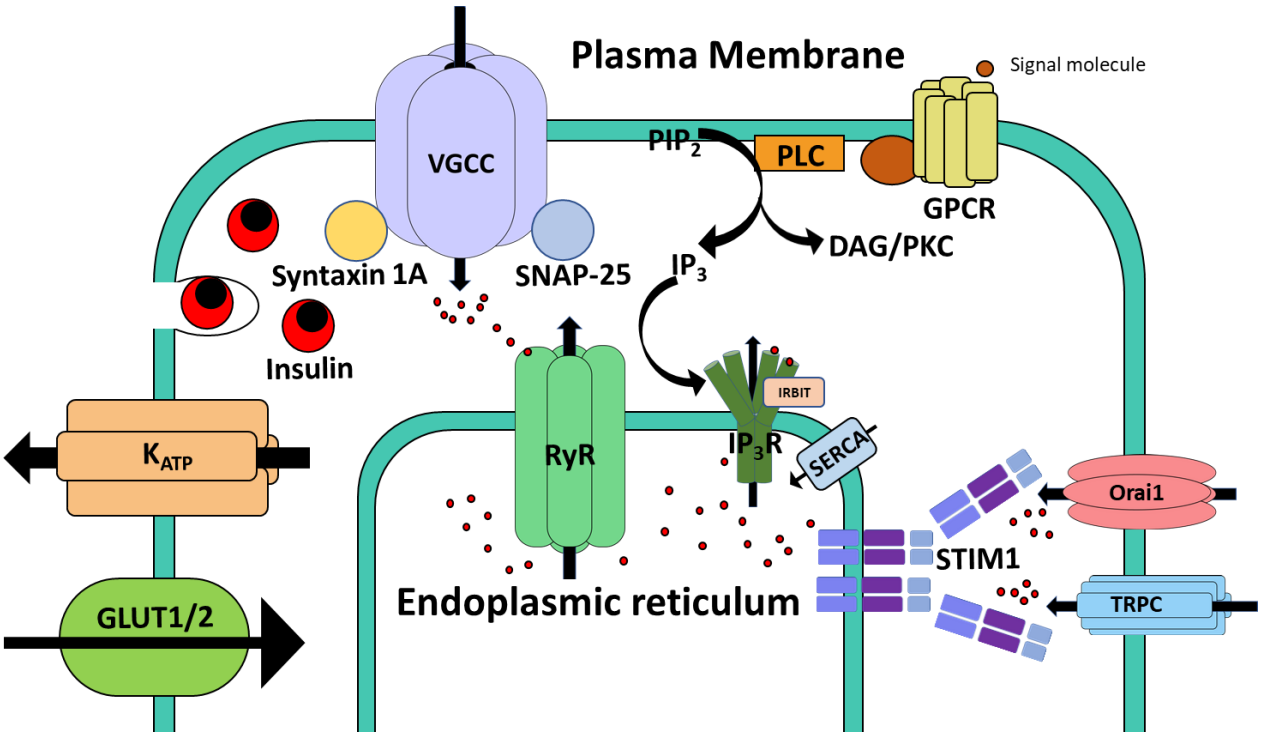

Figure 1.13. Ca^{2+} homeostasis in pancreatic β-cell physiology. L-VGCCs are involved in insulin secretion by interacting with syntaxin 1A and SNAP-25. The Ca^{2+} store in the endoplasmic reticulum is regulated by RyRs and IP_3Rs in response to intracellular Ca^{2+} concentration, resulting in calcium-induced calcium release (CICR). IRBIT inhibits to IP_3Rs. Store-operated calcium entry (SOCE) is activated upon depletion of Ca^{2+} stores, and STIM1 interacts with Ora1 and/or TRPC to induce Ca^{2+} entry. GPCR pathway activates PLC, hydrolyzing PIP_2 into DAG and IP_3, which activates IP_3R and release Ca^{2+} from ER.

1.7 Physiological and Clinical significances of L-VGCCs $Ca_v1.2$ and $Ca_v1.3$

The previous sections have introduced the biophysiological and pharmacological properties of L-VGCCs, and this section will summarize the roles of L-VGCC subtype $Ca_v1.2$ and $Ca_v1.3$ in human diseases associated with genetic Ca^{2+} channel defects (channelopathies), gain- and loss-of-functions. Spontaneous gain-of-function in $Ca_v1.2$ (*CACNA1C* gene) leads to Timothy syndrome (see section 1.7.2.1; Splawki et al., 2004, 2005; Calorio et al., 2019), and homozygous deletion of $Ca_v1.2$ in mice is embryonically lethal due to malformation of the cardiovascular system (Seisenberger et al., 2000). SANDD (sinoatrial node dysfunction and deafness) syndrome is the only channelopathy currently associated with $Ca_v1.3$ channels (Striessnig et al., 2010, Baig et al., 2011). $Ca_v1.3$ is co-expressed with $Ca_v1.2$ in many neuronal and endocrine tissues (Fig 1.14).

Existing L-VGCC blockers inhibit both of the isoforms with no selectivity, and their physiological roles could not be pharmacologically separated and studied.

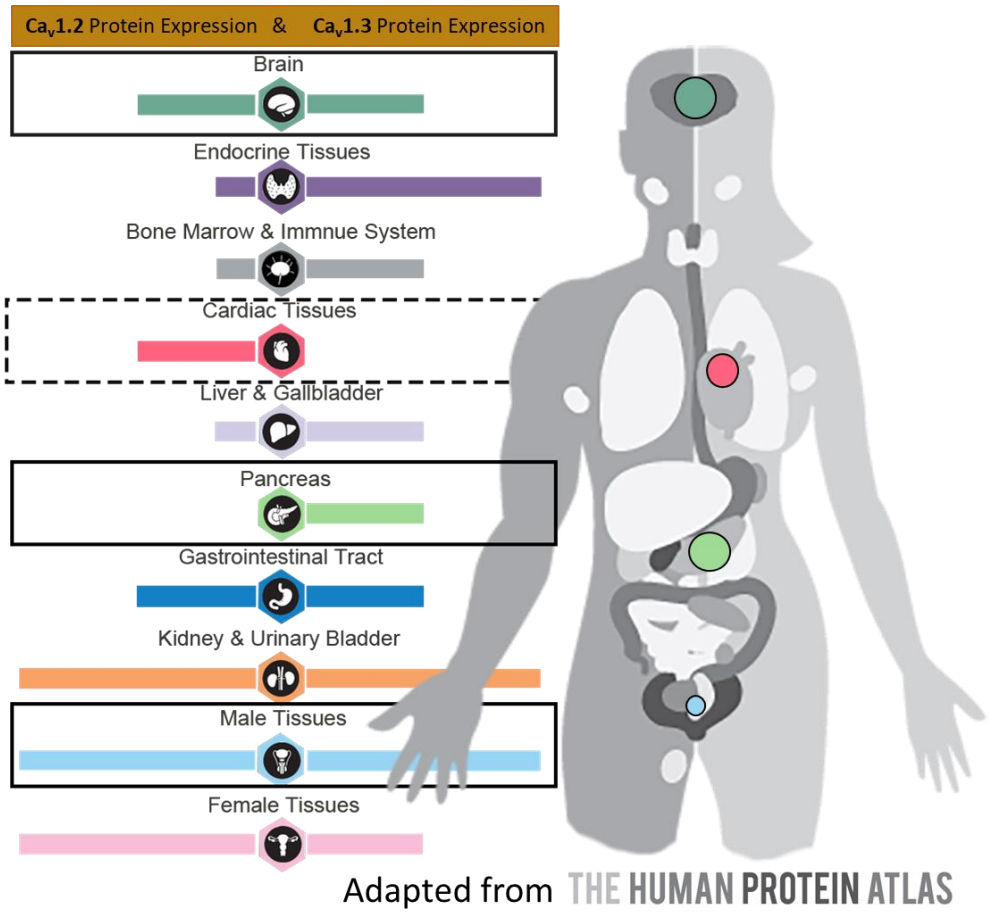

Figure 1.14. Relative distribution of $Ca_v1.2$ and $Ca_v1.3$ in different significant organs. Dashed box indicates the predominant expression of $Ca_v1.2$ in cardiac tissues associated with hypertension treatment. The Solid boxes indicate the clinical significance of $Ca_v1.3$ associated with Parkinson's disease, type-1 diabetes, and prostate cancer.

1.7.1 Physiological significance of $Ca_v1.2$ and $Ca_v1.3$

Even though both $Ca_v1.2$ and $Ca_v1.3$ are expressed together in many tissues, they display divergent involvement in various cellular processes. Genetically modified mice have revealed (Platzer et al., 2000; Sinegger-Brauns et al., 2004) their distinct subtype-specific regulation of mood behavior, pancreatic beta-cell activity, and cardiovascular functions. $Ca_v1.3$ is found to serve pacemaker functions in neurons (Olson et al., 2005), the sinoatrial node (Mangoni et al., 2003), and in chromaffin cells (Macrcantoni et al., 2007, & 2010; Hasreiter et al., 2014).

1.7.1.1 L-VGCCs regulate cell survival and endo/exocytosis

A fast and irreversible decrease in intracellular Ca^{2+} is associated with an apoptotic process and survival-promoting activity (Galli et al., 1995). Two transcription factors, MEF2 (Mao et al., 1999) and C/EBPβ (CCAAT enhancer-binding proteins) (Marshall et al., 2003), were identified to promote neuronal cell survival.

In select cells and synapses, L-VGCCs also regulate exocytosis. L-VGCCs activation induces Ca^{2+}/CaM-dependent protein kinase, and GTP-binding protein inhibition, which is involved in β cell exocytosis (Ashcroft et al., 1994). In INS-1 cells, $Ca_v1.3$ has been preferentially linked to glucose-triggered calcium oscillations (Liu et al., 2004). In *Xenopus* nerve-muscle synapses, varicosities possess L-VGCCs that are activated more rapidly than N-type channels, contributing significantly to evoked exocytosis of Ach (Sand et al., 2001). Expression of $Ca_v1.2$ II-III loop competitively disrupts the spatial coupling with secretory apparatus, and the depolarization evoked exocytosis in *Xenopus* Oocytes (Wiser et al., 1999). L-VGCCs carry almost half of the whole-cell Ca^{2+} current and are responsible for rat chromaffin cells (RCC) exocytosis (Carabelli et al., 2003, 2007), while RCC endocytosis is attenuated when L-VGCCs are blocked (Rosa et al., 2007, 2010, 2012).

1.7.1.2 $Ca_v1.3$ is required for hearing

Both isoforms $Ca_v1.2$ and $Ca_v1.3$ have been detected by PCR in cochlea hair cells (Green et al., 1996), and hair cells of the chick basilar papilla predominantly express $Ca_v1.3$ (Kollmar et al., 1997), suggesting their roles for afferent synaptic transmission. To examine their physiological role and significance as a potential drug target, Striessnig's lab generated $Ca_v1.3$ deficient mice ($\alpha1D^{-/-}$) that turned out to be deaf due to lacking L-VGCC currents in cochlear inner hair cells (IHC) and degeneration of outer and inner hair cells (Platzer et al., 2000).

1.7.1.3 $Ca_v1.3$ regulates cardiac pacemaking

The heart rhythm is controlled by the spontaneous activity of pacemaker cells in the sino-atrial node (SAN), and this activity in SAN cells is due to a slow diastolic depolarization driving the membrane voltage from the end of an AP to the threshold of a new AP (Zipes et al., 1980). $Ca_v1.3$ exhibits negative activation thresholds essential for normal auditory function and controls

cardiac pacemaker activity. Loss of $Ca_v1.3$ in $\alpha1D^{-/-}$ mice leads to SAN dysfunction (such as bradycardia and arrhythmia) in electrocardiogram recordings (Platzer et al., 2000). Later studies showed that the inactivation of $Ca_v1.3$ slows pacemaker activity and promotes spontaneous arrhythmia in SAN pacemaker cells (Mangoni et al., 2003). Both studies indicated the link between pacemaker activity alterations and activation at a negative membrane potential. The voltage range from -60 to -40 mV for IHCs and SAN cell operation also supports $Ca_v1.3$ channel gating (Koschak et al., 2001; Xu and Lipscombe et al., 2001; Lipscombe et al., 2004).

1.7.1.4 $Ca_v1.3$ regulates adrenal chromaffin cell pacemaking

Both $Ca_v1.2$ and $Ca_v1.3$ are highly expressed in chromaffin cells of the adrenal medulla (García-Palomero et al., 2000; Baldelli et al., 2004; Pérez-Alvarez et al., 2010; Segura-Chama et al., 2012), where they regulate cell excitability, catecholamine secretion, and vesicle retrieval. $Ca_v1.3$ exhibits weak or strong CDI depending on the alternative splicing of its carboxy tail (Lieb et al., 2012). Multiple studies eliminated the contribution of CDI to the total inactivation in the chromaffin cells, because of the low calcium concentration and the physiological range of membrane potential for pacemaker activity. $Ca_v1.3$ carries most of the pacemaker's current that sustains chromaffin cell's spontaneous activity (Marcantoni et al., 2009, 2010; Vandael et al., 2010; Mahapatra et al., 2012). $Ca_v1.3$ drives sufficient SK current that helps with adapting the firing rate to a sustainable frequency during prolonged depolarizations (spike-frequency adaptations, SFA) (Vandael et al., 2012). Besides SK channels, $Ca_v1.3$ is tightly coupled to BK channels, playing a pivotal role in controlling action potential shaping (Marcantoni et al., 2010; Vandael et al., 2010). All three channels support catecholamine secretion sensitivity to L-VGCC currents in rat and mouse chromaffin cells (Kim et al., 1995; Engisch et al., 1996; Nagayama et al., 1999; Lukyanetz et al., 1999; Carabelli et al., 2003; Akiyama et al., 2004; Marcantoni et al., 2009), helping chromaffin cells optimally adapt under stimulus to switch from regular to stress conditions (Vandael et al., 2012).

Another interesting finding showed atypical voltage-dependence and kinetics of calcium recording due to deficient expression of a splice variant of $Ca_v1.3$ (short-form $Ca_v1.3_{42A}$) in spontaneously hypertensive (SHR) and normotensive Wistar-Kyoto (WKY) rat chromaffin cells. This observation relates to the functional and behavioral alterations in SHR/WKY rats, such as their susceptibility to developing hypertension (Segura-Chama et al., 2012).

1.7.2 $Ca_v1.2$ and $Ca_v1.3$ in Neuronal and psychiatric regulation

Both $Ca_v1.2$ and $Ca_v1.3$ regulate memory and learning. $Ca_v1.2$ mediates long-term potentiation (LTP), spatial learning, and memory in the hippocampus (Moosmang et al., 2005). $Ca_v1.3$ mediates LTP in the amygdala, participates in the consolidation of fear memory (Gamelli et al., 2009), contributes to neuronal plasticity (Murphy et al., 1991; Deisseroth et al., 1998; Hardingham et al., 1998; Tao et al., 1998; Graef et al., 1999; Rajadhyaksha et al., 1999), and is required for correct hippocampal neurogenesis and cognitive functions (Marschallinger et al., 2015).

Different VGCC subtypes participate in distinct neuronal functions. Low threshold channels likely play a role in dendritic integration while high-threshold channels are involved in somatic Ca^{2+}-dependent process (Christie et al., 1997). L-VGCCs and NMDA receptors can mobilize calmodulin, initiating the transcription factor CREB phosphorylation that is essential for forming long-term memory in several animal species (Deisseroth et al., 1998).

Neuronal plasticity is attributed to L-VGCCs in coupling synaptic excitation to activation of transcriptional events (Murphy et al., 1991). During the aging process, L-VGCCs facilitate long-term depression (LTD) during low rates of synaptic activity but impair LTD during higher levels of synaptic activation via an increased level of Ca^{2+}-dependent K^+-mediated afterhyperpolarization (AHP) (Norris et al., 1998). L-VGCCs induce long-term potentiation (LTP) in the thalamo-amygdala by paring presynaptic activity with either APs or continuous depolarization in the postsynaptic cell, a leading mechanism to explain fear conditioning, a prominent model of emotional memory (Weisskopf et al., 1999).

1.7.2.1 $Ca_v1.2$ channelopathies causing autism

The earliest neurological and psychiatric involvement of $Ca_v1.2$ could be traced back to the study investigating the genetics of Timothy Syndrome (TS; Splawski et al., 2004). TS brings the suffering of cardiac arrhythmia, immune deficiency, hypoglycemia, and syndactyly and cognitive impairment to children, who might have difficulties in language, motor skills and symptoms of autism spectrum disorders (ASD). The missense TS mutation is shown to locate in the intracellular end of IS6 of $Ca_v1.2$ subunit at G406R, exon 8A of the alternative splicing, while TS2 locates at G402S in exon 8, which leads to more severe phenotypic alterations in affected

patients (Splawski et al., 2005). The G406R change leads to a gain of function, attenuating the VDI of $Ca_v1.2$ while accelerating CDI (Barrett and Tsien, 2008; Dick et al., 2016). To study the physiological consequences of TS mutant in $Ca_v1.2$, Dolmetsch's lab generated induced pluripotent stem cells (iPSCs) (Pasca et al., 2011). They reported wider APs, increased intracellular Ca^{2+} levels, dysregulation of ASD-associated genes, and upregulation of tyrosine hydroxylase (TH), leading to higher production of neurotransmitters norepinephrine and dopamine, which were widely accepted to play critical roles in many psychiatric diseases (Hirschfeld 2000; Howes and Kapur 2009; Berger et al., 2014). More findings have shown the association between TS mutation models and various autism-related endophenotypes (Krey et al., 2013; Pasca et al., 2011; Bader et al., 2011), such as defects in connectivity of different cortical areas in ASD (Batterfeld et al., 2011).

Additional Genome-wide analysis (GWA) studies have spotted the association between $Ca_v1.2$ gene alterations and the pathology of several psychiatric diseases (Bhat et al., 2012). Vulnerability factors of bipolar disorder have been identified as the *CACNA1C* gene (Moskvina et al., 2009) or a specific *CACNA1C* single nucleotide polymorphism (SNP) variant (rs1006737) (Ferreira et al., 2008; Keers et al., 2009; Sklar et al., 2008). GWAS has detected a shared effect of these SNP variants on bipolar disorder, attention deficit-hyperactivity disorder (ADHD), ASDs, schizophrenia, and major depression (Cross-Disorder Group of the Psychiatric Genomics Consortium, Genetic Risk Outcome of Psychosis [GROUP] Consortium 2013). $Ca_v\beta_2$ subunit, encoded as *CACNB2* gene, was found to interact with an SNP variant in all five psychiatric disorders. Interestingly, the cardiac disease Brugada syndrome has been identified as mutations in *CACNA1C* and *CACNB2*, characterized by an ST-segment elevation in the right precordial electrocardiogram and sudden cardiac death (Antzelevitch et al., 2007; Napolitano and Antzelevitch, 2011). *CACNA1C* risk allele rs1006737 are associated with emotional alterations and cognitive deficits in humans (Zhang et al., 2020) and mice (Berger et al., 2014). Multiple proposals of molecular pathways suggest that mistuned Ca^{2+}-mediated excitation-transcription signals bring more support for new hallmarks on Timothy syndrome (Marcantoni et al., 2020).

1.7.2.2 $Ca_v1.3$ in the early onset of Parkinson's Disease

Neuronal calcium signaling has been indicated with solid evidence to be abnormal in multiple neurodegenerative disorders, including Alzheimer's disease (AD), Parkinson's disease (PD), amyotrophic lateral sclerosis (ALS), Huntington's disease (HD), and spinocerebellar ataxias

(SCAs), which present an enormous medical, social financial and scientific problem (Bezoprozvanny et al., 2009). Intense research has been devoted to study the cause of these disorders, but only marginal clinical progress has been made, and most of them remain incurable.

Parkinson's disease is a progressive hypokinetic neurodegenerative disorder characterized by bradykinesia, rigidity, akinesia, abnormal posture, and resting tremor and is the most prevalent movement disorder. The risk of PD increases with aging, affecting 1% of people over 60 years of age, rising to 2~4% for those aged over 80 years (Lees et al., 2009). PD results from selective dopaminergic neuron loss in substantia nigra pars compacta (SNc). Mitochondria are a crucial locus in PD pathogenesis as most of the genes implicated in familial PD (e.g., *PINK1*, *DJ-1*, *LRRK2*, and *Parkin*) encode proteins associated with mitochondrial function (Abou-Sleiman et al., 2006). The most popular idea exploring the cause of PD includes the dopamine (DA) hypothesis, claiming that DA acts as a natural toxin and goes through the oxidation process from cytosolic DA to 6-hydroxy-DA. Other metabolites also damage mitochondria and cause SNc neuron death (Sulzer et al., 2007). The most commonly prescribed PD medication, levodopa (L-dopa), is converted to DA increasing the cytosolic level of DA and synaptic vesicles of remaining SNc neurons. A 'multi-hit' hypothesis of PD has risen, stating that SNc neurons in PD are subjected to a combined effect of DA-related oxidative stress and an additional 'factor X', which includes interactions of cytosolic DA with α-synuclein, inflammation, and mitochondrial dysfunction (Sulzer et al., 2007).

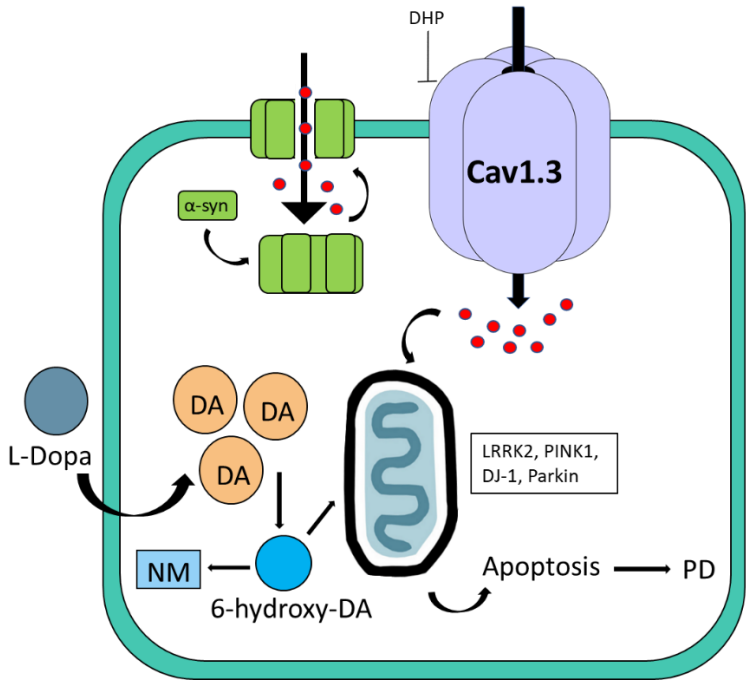

Figure 1.15. Simplified model of Ca^{2+} dysregulation in Parkinson's Disease. L-VGCC $Ca_v1.3$ mediates continuous Ca^{2+} influx to SNc neurons. α-synuclein forms aggregates, potentially forming Ca^{2+}-permeable channels in the plasma membrane. Elevated cytosolic Ca^{2+} is transported into mitochondria. Dopamine (DA) is oxidized to 6-hydroxy-DA, causing damage to proteins and mitochondria by oxidative stress. Accumulation of oxidative stress leads to lysosome neuromelanin (NM). Several mitochondria-related genes (e.g., *LRRK2, PINK2, DJ-1, Parkin*) are highlighted. Both Ca^{2+} overload and DA-mediated oxidative stress lead to the apoptotic process of SNc neurons in PD. L-dopa, the clinically used treatment for PD, is converted to DA, loaded to synaptic vesicles, and temporarily alleviates PD symptoms (Liss and Striessnig 2019).

During the early stages of PD, an increased level of $Ca_v1.3$ subtype expression has been observed in the cerebral cortex before the appearance of pathological changes, supporting the idea that disturbed calcium homeostasis is an early feature of PD progression and not just a compensatory consequence to the neurodegenerative process (Hurley et al., 2013). In contrast to most other neurons, which rely exclusively on monovalent cation channels to drive pacemaking, $Ca_v1.3$ drives spontaneous pacemaking activity in 2-4 Hz range in the absence of synaptic input in SNc dopaminergic neurons (Fujimura and Matsuda, 1989; Chan et al., 2007; Khaliq and Bean, 2010; Surmeier et al., 2011; Goldberg et al., 2012). Compared to monovalent cations, calcium used for pacemaking consumes more energy to maintain a non-toxic intracellular calcium concentration, necessitating efficient mitochondrial function (Surmeier et al., 2011). Continuous calcium influx

through $Ca_v1.3$ renders SNc neurons vulnerable to stressors due to excessive metabolic overloads. The reliance of SNc neurons on $Ca_v1.3$ to control pacemaking increases with age, the significant PD risk factor. Isradipine, the L-VGCC DHP inhibitor, was shown to restore Ca^{2+}-independent 'juvenile' pacemaking activity in SNc neurons, protecting the SNc neurons in animal models of PD (Chan et al., 2007). Susceptibility to degeneration varies in neuron degeneration in pacemaking neuron regions, which coincide with the level of calcium-binding proteins, which can dampen the potentially toxic oscillations of Ca^{2+} concentrations (Yamada et al., 1990; German et al., 1992; Damier et al., 1999). Computer modeling of SN dopaminergic electric activity concluded that the voltage dependence of $Ca_v1.3$ activation and inactivation strongly support its role as the pacemaking current (Putzier et al., 2009). Altered CaM concentrations may also be linked to PD because of the tight connections to $Ca_v1.3$ C-terminus (Sang et al., 2021).

Interestingly, a few retrospective epidemiological studies showed a significantly diminished risk of developing PD in patients treated for hypertension with Ca^{2+}-channel antagonists (Becker et al., 2008; Ritz et al., 2010; Marras et al., 2012; Pasternak et al., 2012). These studies suggest a pathogenic role of $Ca_v1.3$ in PD, and $Ca_v1.3$ may therefore be an important therapeutic target for protecting dopaminergic neurons from neurodegeneration. L-VGCCs were found to mediate mitochondrial oxidant stress in DA neurons, attenuated by DJ-1 (or PARK7), a defective gene in the early onset of Parkinson's disease (Guzman et al., 2009 & 2010). Chronic treatment of isradipine administered systemically to mice at a close-to-patient dose diminished cytosolic Ca^{2+} oscillations in SNc DA neurons without altering autonomous spiking or L-VGCC expression (Ortner et al., 2017). Similar to $Ca_v1.3$ knockouts, isradipine treatment lowered mitochondrial oxidant stress, reduced the mitophagy basal rate, and normalized the mitochondrial mass (Guzman et al., 2018).

Targeting L-VGCCs is based on the solid rationale provided by human epidemiological and preclinical *in vitro* studies, and the ongoing clinical trials support a protective role of DHPs in PD. Unfortunately, the STEADY-PD phase III trial results came out negative because long-term treatment with immediate-release isradipine did not slow the early progression of PD (Parkinson Study Group STEADY-PD Investigators, 2020). Though this result was disappointing, the study may have been confounded by the use of isradipine, which potently blocks $Ca_v1.2$, particularly in the cardiovascular system. Thus, $Ca_v1.3$-specific blockers are needed to realize the full potential of $Ca_v1.3$ inhibition in PD treatment.

1.7.2.3 $Ca_v1.3$ in Substance abuse and Psychiatric disorders

Substance abuse disorder and related psychiatric disorders are significant sources of mortality and morbidity in the United States and globally (Peacock et a., 2018). In addition to the widespread abuse of opiates, stimulant drugs such as cocaine and amphetamines contribute significantly to morbidity and increased utilization of health care services. In the United States, approximately 5.5 million people regularly use cocaine, and another 2 million regularly use methamphetamine (Substance Abuse and Mental Health Services Administration 2020). Efforts to understand drug addiction have focused on the reward pathway of the ventral tegmental area-nucleus accumbens (VTA-NAc) brain region, where the major neurotransmitter is dopamine (Nestler et al., 2005). However, not all addictive substances strongly release dopamine into the NAc (Nutt et al., 2015), and therapeutic interventions based on directly regulating dopamine release and activity have not successfully treated and prevented substance abuse (Lingford-Hughes et al., 2012). It is likely that pathways mediating addiction are diverse and may be distinct for different drugs of abuse (Nutt et al., 2015). Currently, there are FDA-approved drugs to treat alcohol addiction (Antabuse^{TM}, Acamprosate^{TM}), opioid addiction (full or partial μ-opiate receptor agonists or antagonists), and nicotine addiction (Varenicline^{TM}). Currently, there are no FDA-approved drugs for the treatment of patients with stimulant use disorder. Although non-pharmacological interventions have shown some efficacy in reducing the use of stimulant drugs of abuse such as cocaine, amphetamine, or methamphetamine, these are inadequate for many patients. Accordingly, there is an urgent need to validate strategies and drug development to treat stimulant use disorder.

Numerous studies reveal that L-VGCC $Ca_v1.3$ is a promising target for treating addiction to stimulants such as cocaine and amphetamines. $Ca_v1.3$ is required for upregulation of dopamine D2L receptors and sensitization to amphetamine (Giordano et al., 2006) and recruitment of D2L receptors in the striatum upon cocaine withdrawal (Schierberl et al., 2012). $Ca_v1.3$ protein is upregulated as assessed by western blot, along with $Ca_v1.2$, in the limbic forebrain and frontal cortex of mice dependent on cocaine, methamphetamine, or morphine, and the non-selective L-type channel blocker nifedipine reduced the rewarding effect of these drugs of abuse (Shibasaki et al., 2010). $Ca_v1.3$, along with $Ca_v1.2$, regulates the activity of dopaminergic (DA) neurons in the VTA of mice (Liu et al., 2014) and the non-selective L-type channel blocker isradipine reduced cocaine-seeking behavior in rats (Addy et al., 2018). A study comparing WT and transgenic mice

expressing drug-insensitive $Ca_v1.2$ found that activation of $Ca_v1.3$ in the VTA mediated cocaine-related behaviors by enhancing phosphorylation of GluA1 AMPA receptors in the NAc via up-regulation of CamKIIα (Martinez-Rivera et al., 2017). The same conclusion was supported in WT mice using acute knockdown of $Ca_v1.3$ with shRNA. Further, SNPs in *CACNA1D*, the gene encoding $Ca_v1.3$, are associated with cocaine dependence in humans (Martinez-Rivera et al., 2017). These SNPs occur in introns, so they likely affect $Ca_v1.3$ expression levels. Thus, there is strong evidence that Ca^{2+} influx via $Ca_v1.3$ activity in DA neurons of the VTA is a critical step in developing dependence on stimulant drugs and that inhibition of $Ca_v1.3$ is a viable strategy to treat stimulant use disorder.

1.7.2.4 $Ca_v1.2$ upregulation in alcohol abuse

The critical roles of Cav1.2 and Cav1.3 in the hippocampus regulating glutamatergic neurotransmission underlying multiple physiological significances have been introduced in the earlier sections. Their overexpression has also been implicated in neuroexcitatory cell death associated with chronic alcoholism. Alcohol dependence develops through excessive drinking and abstinence cycles, accompanied by altered neurotransmitters, hormones, and ion channel adaptation. Upregulation of Cav1.2 gene expression has been reported in the hippocampus after chronic alcohol exposure in rats, further underlining the importance of central L-VGCCs in some aspects of schizophrenia (Uhrig et al., 2016). Acute alcohol increases neuronal activity in the rat central amygdala, and blockade of central amygdala L-VGCC reduces alcohol intake. This study also proposed that alcohol dependence disrupts the L-VGCC-based mechanism and gets mediated by corticotropin-releasing factor 1 receptors (CRF_1s) to escalate alcohol intake (Varodayan et al., 2017). A recent study suggests that calcium signaling in the subregions of the hippocampus is differentially affected by ethanol consumption, potentially contributing to eventual calcium-mediated apoptosis (Kokaska et al., 2020).

1.7.3 $Ca_v1.2$ and $Ca_v1.3$ in Pancreatic β-cell physiology and pathophysiology

mRNA for $Ca_v1.2$ and $Ca_v1.3$ is present in all primary β-cells and insulin-secreting cell lines, including β-cell/islet from humans, rats, mice, HIT-15T in hamster cells, INS-1/RINm5F in rat cells, and MIN5/βTC-3 in mouse cells. Moreover, L-type currents were whole-cell patch-clamp (Yang and Berggren 2006).

The insulinotropic effects regulated by Ca_vs have been shown in many critical ways, including stimulating secretory granule trafficking and triggering insulin exocytosis, along with maintaining β-cell mass and function. Ca_v1 channel is believed to play the predominant role over other Ca_v channel types in Ca^{2+}-triggered insulin exocytosis (Yang and Berggren 2005). Down-regulation of Ca_v channel density or activity reduces insulin secretion and leads to glucose intolerance (Iwashima et al., 1993; Roe et al., 1996; Sharp et al., 1996; Bito et al., 2013). Islets from $Ca_v1.2$ knockout mice show a significant decrease in first-phase insulin secretion (Schulla et al., 2003), which plays the leading role in overall insulin release from pancreatic β cells (Sinnegger-Braus et al., 2004). On the other hand, one $Ca_v1.3$-knockout mouse line induced hypoinsulinemia and impaired glucose tolerance, which are associated with a deficit in postnatal β cell generation and proliferation (Namkung et al., 2001). In the parallel study of human pancreatic β cells, reduction in $Ca_v1.3$ transcripts was strongly associated with T2D and reduced insulin secretion (Reinbothe et al., 2013). L-VGCC complexes with the exocytotic machinery and forms a functional molecular network, serving to fine-tune the β-cell Ca_v1 function and insulin exocytosis (Figure 1.13).

1.7.3.1 L-VGCCs in Type I diabetes

The progressive and selective destruction of pancreatic β-cells in genetically predisposed individuals is hallmark T1D, and β-cell apoptosis leads to progressive loss of pancreatic β-cells. T1D serum hyperactivates β cell Ca_v1 channels, leading to an increased level of cytosolic free Ca^{2+} concentration and β cell apoptosis (Yang and Berggren 2006, Junti-Berggren et al., 1993, 2004). Coxsackievirus B4, an enterovirus, has been involved in the pathogenesis of T1D by inducing antibodies against $Ca_v1.3$ (Bason et al., 2013). T1D serum hyperactivates both $Ca_v1.2$ and $Ca_v1.3$ by increasing their conductance and numbers (Yang et al., 2015). These findings suggest that $Ca_v1.3$-specific inhibitors be useful for treating the early onset of T1D.

1.7.3.2 L-VGCCs in Type II diabetes

Previous studies explored the roles of L-VGCCs in regulating insulin secretion in insulinoma INS-1 832/13 cells. For $Ca_v1.2$, in rat β-cells, the mRNA level of $Ca_v1.3$ is 2.5 higher than that of $Ca_v1.2$ (Iwashima et al., 1993). Another study showed that the mRNA level of $Ca_v1.2$ exceeded that of $Ca_v1.3$ and $Ca_v2.3$ two-fold, and $Ca_v1.3$ knockdown did not affect glucose-stimulated insulin secretion while $Ca_v1.2$ knockdown diminished GSIS using the siRNA method (Nitert et al., 2008). Mouse β-cells without $Ca_v1.2$ displayed reduced Ca_v currents by 45% and first-phase insulin secretion by 80%, developed glucose intolerance, and were not affected by Ca_v1 channel blockers (Schulla et al., 2003). Immunoreactivity of $Ca_v1.3$ was not found in mouse pancreatic β-cells (Barg et al., 2001). The involvement of $Ca_v1.3$ in mouse pancreatic β-cells has been observed in interaction with syntaxin 1 and β-cell generation (Yang et al., 1999; Namkung et al., 2001). Interestingly, $Ca_v1.3$-knockout mice show overexpression of $Ca_v1.2$ in a compensatory mechanism, shifting the current-voltage relationship by +10mV (Namkung et al., 2001). In the presence of 3mM glucose, $Ca_v1.3$-knockout mouse islets showed reduced insulin secretion but were not different from the controls in the presence of 6mM or higher concentrations of glucose. Another group also concluded that the $Ca_v1.3$ plays a vital role in human glucose-induced insulin secretion. *CACNA1D* mRNA expression is 60-fold that of *CACNA1C* mRNA in FACS-enriched human β-cells and decreases in T2D patients. In addition, *in vitro* insulin secretion results in INS-1 832/13 cells were in line with this finding. Phenotype and genotype association was also drawn between three SNPs and reduced mRNA expression in $Ca_v1.2$ (Reinbothe et al., 2012). RRP is absent in T2MD donors and INS-1 cells cultured in fatty acids that mimic a diabetic state. Moreover, the proximity of the recruitment of $Ca_v1.2$ to insulin granules is required for rapid insulin secretion with high probability and minimal latency (Gandasi et al., 2017).

All these results support a compensatory overexpression of $Ca_v1.2$ upon the loss of $Ca_v1.3$-conducted Ca_v currents to maintain insulin secretion capacity. It was also discovered that $Ca_v1.3$ is likely to play a leading role in basal insulin secretion and stimulus-secretion coupling at a lower range of glucose concentrations (Namkung et al., 2001; Pan et al., 2016).

1.7.3.3 II-III loop of L-VGCCs in β-cells

A His_6-fused $Ca_v1.2$ peptide corresponding to the $Ca_v1.2$ II-III loop effectively pulled down syntaxin 1A, SNAP-25, and synaptotagmin (p65) in β-cells (Wiser et al., 1999; Ji et al., 2002). This interaction alters the voltage-dependence of $Ca_v1.2$ and reduces the current amplitude in $Ca_v1.2$ currents in *Xenopus* oocytes, and can be partially reversed in the presence of synaptotagmin. $Ca_v1.2$ II-III loop peptide interrupts this association and completely blocks depolarization-evoked exocytosis without significant influence on calcium influx but prevents granule-localized Ca^{2+} influx (Barg et al., 2002; Wiser et al., 1999; Jacobo et al., 2009; Yasuda et al., 2010; Gandasi et al., 2017). Another study overexpressed syntaxin 1A/3 and observed markedly decreased Ca_v1 channel activity and Ca^{2+}-dependent insulin secretion (Kang et al., 2002; Xie et al., 2016).

1.7.4 L-VGCCs in cancer

The ONCOMINE (multi-biomarker targeted next-generating sequencing assays designed for cancer research, www.oncomine.org), a web-based microarray database, was used to perform a systematic analysis by comparing mRNA expression of every VGCCs across 21 different types of cancer to that in normal tissue (Wang et al., 2015). They found high expression of *CACNA1C* ($Ca_v1.2$) in most cancer types, including colorectal, gastric, pancreas, brain, breast, uterus, skin, and prostate cancers and leukemia. High expression of *CACNA1D* ($Ca_v1.3$) is also found in several cancer types, including prostate and breast cancer. *In silico* analysis suggest that $Ca_v1.3$ might play a role in cancer progression.

1.7.4.1 $Ca_v1.3$ mutation in aldosterone-producing adenomas and primary aldosteronism

It was universally believed that the predominant $Ca_v1.2$ distribution in the cardiovascular system accounts for the efficacy of calcium channel blockers in hypertension. However, severe hypertension caused by the salt-retaining hormone aldosterone, which is constitutively produced by adrenal aldosterone-producing adenomas(APAs; Rossi et al., 2006), offers another mechanism KCNJ5 (potassium channel gene) mutations result in cell depolarization and Ca^{2+} influx and cause ~40% of these adenomas (Choi et al., 2011). One lab identified five somatic mutations, 4 altering Gly403 and one altering Ile770, in the S6 segments of *CACN1D* ($Ca_v1.3$) without mutated KCNJ5.

These alterations cause channels to activate at more negative potentials and impair channel inactivation (Scholl et al., 2013). This result argues that increased Ca^{2+} influx is a sufficient stimulus for aldosterone production and cell proliferation in adrenal glomerulosa (Spät and Hunyady 2004). These findings implied that the somatic $Ca_v1.3$ mutations are involved in the increased Ca^{2+} influx in APAs and primary aldosteronism.

1.7.4.2 Overexpression of $Ca_v1.3$ in prostate cancer

L-VGCC blockers were used in multiple epidemiological studies to assess the risk of prostate cancer incidence. Several studies examined the expression profiles of different L-VGCC genes in prostate cancers and their functional roles in androgen receptor (AR) transactivation and cancer cell growth. Overexpression of $Ca_v1.3$ was found in cancer tissues relative to non-cancer tissues by analyzing the published complementary deoxyribonucleic acid microarray data sets in the ONCOMINE database (Chen et al., 2014). Blocking L-VGCCs or knocking down *CACNA1D* gene ($Ca_v1.3$) expression significantly repressed androgen-stimulated Ca^{2+} influx, AR transactivation, and prostate cancer cell growth. An ongoing study (McKerr et al., 2018~2021) investigates the expression, function, and localization of $Ca_v1.3$ during prostate cancer progression and hormone therapy and the effects of nifedipine. Nifedipine-block of $Ca_v1.3$ in Enzalutamide (ENZ; an AR antagonist)-treated LNCaP cells (androgen-sensitive human prostate adenocarcinoma cells) appeared to increase apoptosis compared to ENZ treatment alone. Interestingly, $Ca_v1.3$ plasma membrane localization and functional expression in the prostate cancer subpopulation were promoted by ENZ treatment.

A systematic review and meta-analysis explored the impact of calcium channel blockers (CCBs) on prostate cancer (PCa), and they showed a tendency to increase the overall risk of PCa, and a cumulative duration also showed a positive correlation (Yang et al., 2020).

1.7.4.3 Overexpression of $Ca_v1.3$ in endometrial cancer

L-VGCC inhibitor nifedipine inhibits the proliferation, apoptosis, and migration of endometrial carcinoma (EC) cells *in vitro*, and the expression of $Ca_v1.3$ was regulated by E2 (predominant biological effects of estradiol, exerted via its interaction with intracellular estrogen receptors, ER) (Bao et al., 2012). Higher expression of $Ca_v1.3$ is found in atypical hyperplasia and

endometrial carcinoma tissues than benign endometrial tissues. $Ca_v1.3$ controls the migration and the proliferation of endometrial cancer cells via the regulation of estrogen-stimulated phosphorylation of ERK1/2 and CREB and Ca^{2+} influx (Hao et al., 2015).

1.7.4.4 Overexpression of $Ca_v1.3$ in colon cancer

$Ca_v1.3$ regulates postprandial depolarization when luminal Ca^{2+} increases during digestion (Kellett et al., 2011). Apical expression of $Ca_v1.3$ contributes to intestinal epithelial Ca^{2+} reabsorption independent of the TRPV6 pathway (Kellett et al., 2011). Stabilizing TRPV5 channel activity in human and mouse colons supports Ca^{2+} reabsorption accompanied by NCX1 Na^+/Ca^{2+} exchanger upregulation (Radhakrishnan et al., 2017). $Ca_v1.3$ is overexpressed in colorectal cancer biopsies compared to normal tissues. Blocking of NCX1/3 increased the cytosolic Ca^{2+} concentration and colon cancer cell migration. (Fourbon et al., 2017).

1.7.5 Summary of $Ca_v1.2$ and $Ca_v1.3$ relevance

$Ca_v1.2$ and $Ca_v1.3$ have been shown to regulate a variety of important cellular processes in the human body, such as development stages, cardiac systems, neuronal and psychiatric systems, and pancreatic β-cell function. These two subtypes are co-expressed in numerous tissues but play divergent roles. $Ca_v1.2$ has been extensively studied, especially in cardiac tissues, but the physiological and clinical significances of $Ca_v1.3$ were not fully understood compared to $Ca_v1.2$. Table 1.5 summarized the physiological and clinical significances of $Ca_v1.2$ and $Ca_v1.3$ that were discussed in Section 1.7.

Table 1.5. Summary of $Ca_v1.2$ and $Ca_v1.3$ significances

$Ca_v1.2$	$Ca_v1.3$	Significances	
	required for	Hearing	Physiological
	regulates	Cardiac pacemaking	
	regulates	Chromaffin cell pacemaking	
channelopathies		Timothy Syndrome (and autism)	Neuronal and psychiatric
	dysfunction	Early onset of Parkinson's Disease	
	upregulation	Substance abuse and Psychiatric disorders	
upregulation		Alcohol Abuse	
regulates	regulates	Pancreatic β-cell function	Diabetes
	dysfunction	Early onset of Type-1 diabetes	
	mutation	Aldosterone-producing adenomas	Cancer
	overexpression	Prostate cancer	
	overexpression	Endometrial cancer	
	overexpression	Colon cancer	

1.8 Summary of introduction

Calcium channels are ubiquitous in our bodies and regulate the Ca^{2+} to mediate various cellular processes. Two major calcium channels, voltage-gated and ligand-gated calcium channels, regulate the Ca^{2+} homeostasis.

Voltage-gated calcium channels sense the membrane potential change and allow the Ca^{2+} influx. L-type VGCCs have long-lasting Ca^{2+} current activities. L-VGCCs are comprised of a pore-forming α_1 subunit, auxiliary β, $\alpha_2\delta$, and γ subunits. Four α_1 subunits were identified and four L-type VGCC subtypes ($Ca_v1.1$-$Ca_v1.4$) were isolated. L-VGCCs exhibit unique Ca^{2+} current behaviors controlled by gating and can be observed with electrophysiology. These channels can also be pharmacologically studied using small molecules such as dihydropyridines. However, these calcium channel blockers were developed to target $Ca_v1.2$ and treat cardiac diseases, and the role of $Ca_v1.3$ is less well-studied due to lacking selective tools. A variety of studies implicated the crucial involvement of $Ca_v1.3$ in different cellular processes, especially the neuronal pacemaking activity in the early onset of Parkinson's Disease. Developing selective $Ca_v1.3$ antagonists will be a promising strategy to improve the treatment of $Ca_v1.3$-related neuronal diseases.

Ligand-gated calcium channels on ER, such as RyR and IP_3R, regulate intracellular Ca^{2+} activity. Nonetheless, the role of RyR2 in pancreatic β-cells has not been fully understood. IRBIT, the inhibitory IP_3R binding protein, is a novel target to study intracellular Ca^{2+} mediation and insulin secretion in pancreatic β-cells. Electrophysiological characterization of RyR2 and IRBIT knock-out β-cells will provide comprehensive information on their roles in CICR and GSIS.

CHAPTER 2. MATERIALS AND METHODS

2.1 Cell Culture

2.1.1 tsA-201 cells

tsA-201 is a transformed human embryonic kidney (HEK-293) cell line stably expressing an SV40 (simian virus 40) temperature-sensitive T antigen (Grahan et al., 1977; Heinzel et al., 1988). The production of high levels of recombinant proteins has extended their use in protein-binding studies, whole-cell patch-clamp recordings, and transfection studies. They were cultured in Dulbecco's Modified Eagle's medium (D-MEM/F-12; Gibco, Life Technologies Limited, Paisley, UK) supplemented with 10% Fetal Bovine Serum (FBS, R&D systems, Minneapolis, MN, US, Catalog: S11150), 100 units/mL penicillin (Sigma-Aldrich), and 100μg/mL streptomycin (Sigma-Aldrich) and were maintained at 37°C in 5% CO_2.

2.1.2 INS-1 cells

INS-1 is a rat insulin-secreting β-cell derived cell line and a useful model for insulin secretion regulation and pancreatic islet beta-cell function studies (Asfari et al., 1992). They were cultured in RPMI-1640 medium (Gibco, Grand Island, NY, catalog number: 11875101) containing 11.1mM glucose supplemented with 10mM HEPES, 10% Fetal Bovine Serum (Hyclone, Logan, UT, Catalog number: SH30071.03), 11mg/mL sodium pyruvate, 100 units/mL penicillin, 100 μg/mL streptomycin and 50 μM β-mercaptoethanol. Cells were maintained at 37 °C and 5% CO_2.

INS-1 cells stably expressing the intracellular II-II loop of $Ca_v1.2$ or $Ca_v1.3$ were established as previously described (Liu et al., 2006). These two cell lines are named $Ca_v1.2$/II-III cells or $Ca_v1.3$/II-III cells. INS-1 cells stably expressing the C-terminal tails of $Ca_v1.2$ or $Ca_v1.3$ were made (Guerra, 2011), and these two cell lines are named CCTS ($Ca_v1.2$/C-terminal tails, 1568D - 2750L) and DTCS ($Ca_v1.3$/C-terminal tails, 1627D - 2662L). These stable cell lines were maintained in RPMI-1640 medium supplemented with 200 μg/mL G-418. All cell culture reagents were purchased from Sigma-Aldrich (St. Louis, MO) unless otherwise stated. RyR2 and IRBIT knockout cells were created using CRISPR-Cas9 and cultured in the same RPMI-1640 medium mentioned above (Harvey et al., Unpublished).

2.2 Transient transfection of tsA-201 and INS-1 cells

2.2.1 Transfection for electrophysiology

tsA-201 cells were carried in a 10cm culture dish with over 80% confluence, washed (with phosphate-buffered saline, PBS; 138Mm NaCl, 2.7mM KCl, pH7.4), and carried into either 35mm culture dish or 6-well plate (Corning) for transfection using 1mL Trypsin or TrypLE once they reached over 80% confluence, using either Lipofectamine 2000 (Invitrogen, Life Technology, Carlsbad, CA), polyethyleneimine (PEI; Boussif et al., 1995, Longo et al., 2014), or electroporation (Bio-Rad, GenePulser Xcell^{TM}, CE Module). tsA-201 cells were transfected with the 4 μg of plasmids encoding the α_1, β, $\alpha_2\delta_1$ subunit (in the plasmid vector pCDNA3.1; Invitrogen, Carlsbad, CA) and green fluorescent protein (pEGFPN1 or GFP-fusion proteins; BD Biosciences Clontech, Palo Alto, CA) at a weight ratio of 1.2: 0.8:1.2:0.8 (Hockerman et al., 1995) using either Lipofectamine 2000 or electroporation for electrophysiology experiments:

Lipofectamine 2000/ PEI: 1. 10 minutes before performing transfection, 250μL Opti-MEM or other reduced serum media (Gibco, a modification of Eagle's Minimum Essential Medium) was added to each two 1.5mL centrifuge tubes. 2. 10μL Lipofectamine 2000 or PEI was added to tube 1 and 4μg of DNA into tube 2. Tube 2 mixture was added to tube 1, mix, and sit for 5 minutes. 3. Cell medium was removed from the 35mm plate and replaced with either 1mL Opti-MEM or fresh DMEM/F-12. 4. DNA complexes were added to the 35mm plate from the side, slightly rocked, and stored overnight at 28 °C and 5% CO_2. 5. On the next day, the media was removed and resuspended the 35mm plate in 1mL new media, passaged into new 35mm plates for electrophysiological experiments.

Electroporation: 1. 35mm plate was resuspended by adding 200μL Opti-MEM. 2. Cell suspension was transferred into a 4mm gap sterile electroporation cuvette. 3. 4μg of DNA was added into the cuvette and flick to mix. 4. Cuvette was placed into GenePulser Xcell^{TM}, pulsed at the voltage of 190V, and the capacitance of 975μF. 5. The suspension was transferred into either a 35mm plate or 6-well plate and stored overnight at 28 °C and 5% CO_2. 6. The next day, cells were resuspended and split in the same way as step 5 in the lipofectamine 2000 method.

LipoJet^{TM}: INS-1 cells and INS-1 knockouts, RyR2 knockouts, and IRBIT knock-outs were carried in a 10cm culture dish with over 70% confluence and transfected using LipoJet^{TM}. 1. The medium was switched to 10mL fresh RPMI-1640 and split into a 12-well plate. 2. 1 μg of DNA

(LYN11-FRB-CFP and Pseudojanin (PJ) or PJ-DEAD (Hammond et al., 2012)) was diluted into 200uL of Opti-MEM. 3. 1μL Diluted LipoJet™ (1:1 ratio; SignaGen® Laboratories, catalog #: SL100468) was distributed into another 100 μL LipoJet Transfection Buffer(5x), and the plate was centrifuged down at x 500g for 30 seconds. 4. The mixture was incubated at room temperature for 15~20minutes and mixture was gently added to well from the side. 5. The mixture was gently rocked and incubated overnight at 37 °C and 5% CO_2 6. The next day, the media was removed and resuspended the 35mm plate in 1mL new media, passaged into new 35mm plates for electrophysiological experiments.

2.2.2 Transfection for protein assays

tsA-201 cells were carried in a 10cm culture dish with over 80% confluence and ready for transfection using PEI. 1. The medium was switched to 10mL fresh DMEM/F-12. 2. 12μg of DNA (Ca_v1 II-III loop with FLAG tag and β subunit, weight ratio 1:1) was diluted into 500μL of Opti-MEM. 3. Diluted 36μL PEI (1:3 ratio) into another 500μL of Opti-MEM. 4. The mixture was incubated at room temperature for 15~20minutes and gently added to 10cm culture dish from the side. 5. The mixture was gently rocked and incubated overnight at 37 °C and 5% CO_2 6. On the following day, the mixture was collected, and the cell lysates were extracted for protein assays.

INS-1 cells with stably expressed C-terminal of $Ca_v1.2$ or $Ca_v1.3$ were carried in a 10cm culture dish with over 70% confluence and transfected using polyethyleneimine (PEI). 1. The medium was switched to 10mL fresh RPMI-1640. 2. 10μg of DNA (Ca_v1 II-III loop with FLAG tag) was diluted into 500uL of Opti-MEM. 3. 30μL PEI (1:3 ratio) was diluted into another 500 μL of Opti-MEM or diluted LipoJet™ (1:2 ratio; SignaGen® Laboratories, catalog #: SL100468) into another 100 μL LipoJet Transfection Buffer(5x) and plate (6-well or 12-well, balanced) was centrifuged down at x500g for 30 seconds. 4. The mixture was incubated at room temperature for 15~20minutes and mixture was gently added to 10 cm culture dish from the side. 5. The mixture was gently rocked and incubated overnight at 37 °C and 5% CO_2 6. On the following day, cell lysates were collected for protein assays.

2.3 Plasmid and molecular cloning

$Ca_v1\alpha_1$ transmembrane subunit: Rat $Ca_v1.3_{42}$ (in pcDNA6, accession #: AF370010), $Ca_v1.3/LL_{(42a)}$: the longer version of $Ca_v1.3$ with three cloning errors (accession #: AF370009, Xu and Lipscombe, 2001), $Ca_v1.3$/fLL: the same $Ca_v1.3$ construct with the three errors fixed by S244G, V1104A and A2123V substitutions (Huang et al., 2013) was a gift from Dr. Tuk-Wash Soong, University of Singapore. $Ca_v1.2$ (in pcDNA3, accession #: M67515) (Snutch et al., 1991) was a gift from Dr. Terrance Snutch, University of British Columbia.

Ca_v auxiliary subunits: rat $Ca_v\beta_3$ (Castellano et al., 1993, accession #: M88751), rat $Ca_v\beta_{1B}$ (Pragnell et al., 1991), rat $Ca_v\beta_{2A}$ (Wyatt et al., 1998, accession #: NM053851), rat $Ca_v\beta_4$ (Brodbeck et al., 2001; accession #L02315) and rat $\alpha_2\delta$-1 (Ellis et al., 1988; accession #: AF286488)

$Ca_v1.3$+ (Cav1.3/1.2 chimera) was constructed (Wang, 2015) by removing the fragment containing the IIIS5-IIIP region of Cav1.3 from Cav1.3/LL/pSPORT6 by double digestion using BamHI and BstBI and ligating the IIIS5-IIIP region of $Ca_v1.2$ (1.2/IIIS5-IIIP, 1058-1118) made by GenScript (Nanjing, People's Republic of China) using BamHI and BstBI. The final version in $Ca_v1.3_{42}$ pcDNA6 was created by ligation of the BamH1/EcoRV fragment containing the chimeric region from pSPORT6. All mutant constructs were verified by DNA sequencing and restriction digest analysis.

$Ca_v1.2$/DHPi was created (Hockerman et al., 2000) by mutating T1039 to Y and Q1043 to M using splice overlap extension (Horton et al., 1989). The mutant DNA fragment with 600 base pairs cut with SpeI and BglII was inserted in a four-way ligation into the full-length subunit construct in the expression vector Zem 229 (Dr. Eileen Mulvihill, University of Washington, Seattle, WA) using 900-bp BglII//DraIII fragment and the 2720bp DraIII/DraIII fragment. $Ca_v1.3$/DHPi was created (Liu et al., 2003) by introducing two corresponding amino acid changes at T1033Y (ACG changed to TAC) and Q1037M (CAG changed to ATG) in a similar minor to $Ca_v1.2$/DHPi. These two mutants were subcloned into the EGFP vector and fused in-frame to the C-terminal tail of each channel. $Ca_v1.2$/DHPi and $Ca_v1.3$/DHPi were made into express stably in INS-1 cells followed by transfection, G418 selection, colony screening by RT-PCR with either mutant IIIS5 domain primers or GFP primers. Western blot was used to detect the transfected INS-1 clone by anti-GFP antibodies, and a whole-cell patch clamp was used to determine the loss of DHP sensitivity.

$Ca_v1.2$/II-III and $Ca_v1.3$/II-III were previously prepared (Liu et al., 2003). Cav1.2 or Cav1.3 C-terminally fused to GFP in the pcDNA3 vector was constructed first by digesting Cav1.2/GFP in the pzem229 vector or Cav1.3/GFP in the pTRE vector with KpnI and NotI. Cav1.2/GFP or Cav1.3/GFP was then subcloned into the pcDNA3 vector using the KpnI and NotI sites (Guerra, 2011). The INS-1 with stably expressed C-terminal tails were made in the comparable transfection and selection process and named INS-1 CCTs ($Ca_v1.2$/overexpression of C-terminal tails) and DCTs ($Ca_v1.3$/overexpression of C-terminal tails).

2.3.1 Mutagenesis on Ca_v1 for $Ca_v1.2$ and $Ca_v1.3$ differentiation

Site-directed mutagenesis of Ca_v1 to differentiate the DHP binding affinity was used to create the mutants listed below with paired forward primer and reverse primer using oligonucleotide-directed mutagenesis, as described previously (Dilmac et al., 2003). The PCR products were transformed into DH5α *Escherichia coli* cells. The purified plasmids were screened by digestion with either input restriction enzyme or PCR amplification and further confirmed DNA sequencing.

Two additional mutants designed for FPL 64176 potentiation difference were made by obtaining the synthesized 500-bp fragment from GenScript (Piscataway, NJ, USA) with four ($Ca_v1.3$/QDNS) and five mutations ($Ca_v1.3$/FQDNS) with designed restriction enzymes BamHI and BstBI at the two ends, similar to the process of generating $Ca_v1.3$+.

Table 2.1. Primers of site-directed mutagenesis of Ca_v1

	Forward Primer 5'-3'	Reverse Primer 5'-3'
1.3/MV	CCA TCG GCA ACA TCG TGA TCG TCA CGA CCC TGC TCC AGT TCA TGT TTG C	GGA GCA GGG TCG TGA CGA TCA CGA TCA CGA TGT TGC CGA TGG TTC GGA TGG C
1.2/VM	CCA TTG GAA ACA TTA TGA TTG TCA CCA CTC TGC TGC AGT TCA TGT TCG C	GCA GCA GAG TGG TGA CAA TCA TAA TGT TTC CAA TGG TCC GGA TGG CC
1.3/PEEP (1)	GGC CAA AAG TAA CGA AGA GGA GTG CAG GGG GCT TTT CAT CC	CCC CCT GCA CTC CTC TTC GTT ACT TTT GGC CTC ATC TGT GC
1.3/PEEP (2)	CCC GTG GTC CGT CCT AGG ATC TGG CAA AAC AGT GAT TTC AAT TTC G	GAA ATC ACT GTT TTG CCA GAT CCT AGG ACG GAC CAC GGG ACT GTC G
1.3/N6	CCG TTG CAC AGA TTC TTC GAA ACA GAC CGA AGC GGA GTG CAG GGG GCT TTT CAT CC	GCC CCC TGC ACT CCG CTT CGG TCT GTT TCG AAG AAT CTG TGC AAC GGT AGA ACT TCC CC
1.3/SA	CGA CAA TGT CCT TGC GGC AAT GAT GGC GCT CTT CAC GGT CTC GAC TTT TGA GG	CCG TGA AGA GCG CCA TCA TTG CCG CAA GGA CAT TGT CGA AAT TGA AAT CAC TG
1.3+V	CCA TTG GAA ACA TTA TGA TTG TCA CCA CTC TGC TGC AGT TCA TGT TCG C	GCA GCA GAG TGG TGA CAA TCA TAA TGT TTC CAA TGG TCC GGA TGG CC
1.3/FL	GCT GTT CAA GGG GAA GCT TTA CCG TTG CAC AGA TGA GGC CAA AAG TAA CCC	CCT CAT CTG TGC AAC GGT AAA GCT TCC CCT TGA ACA GCT GGA CC
1.3/VI	CTA CAT CAT CAT CAT TGC CTT CTT CAT GAT GAA TAT CTT CG	CAT CAT GAA GAA GGC AAT GAT GAT GAT GTA GAT AAT GAA GAA GAT GG

$Ca_v1.3$/QDNS includes the sequence as below: 5'-
CCGCGCCTGCAGGAACTACTTCAATTTGCTGGACATGCTGGTCGTTGGGGTGTCTCT
GGTGTCATTTGGGATTCAATCCAGTGCCATCTCGGTTGTGAAGATTCTGAGGGTCTT
AAGGGTCTTGAGGCCTCTCAGAGCAATCAACAGAGCAAAAGGACTTAAGCACGTGG
TCCAGTGTGTCTTTGTGGCCATCCGAACCATCGGCAACATCATGATCGTCACGACCC
TGCTCCAGTTCATGTTTGCTTGCATTGGGGTCCAGCTGTTCAAGGGGAAGTTCTACC
GTTGCACAGATGAGGCCAAAAGTAACCCCGAGGAGTGCAGGGGGCTTTTCATCCTTT
ATAAGGACGGCGATGTCGACAGTCCCGTGGTCCGTGAGAGGATCTGGGAAAACAGT
AAGTTCGATTTCGACAATGTCCTTGCGGCTATGATGGCGCTCTTCACGGTCTCGACTT
TTGAGGGCTGGCCCGCGTTGCTGTACAAAGCTATCGATCCGCGC-3'
$Ca_v1.3$/FQDNS includes the sequence as below: 5'-
CCGCGCCTGCAGGAACTACTTCAATTTGCTGGACATGCTGGTCGTTGGGGTGTCTCT
GGTGTCATTTGGGATTCAATCCAGTGCCATCTCGGTTGTGAAGATTCTGAGGGTCTT
AAGGGTCTTGAGGCCTCTCAGAGCAATCAACAGAGCAAAAGGACTTAAGCACGTGG
TCCAGTGTGTCTTTGTGGCCATCCGAACCATCGGCAACATCATGATCGTCACGACCC
TGCTCCAGTTCATGTTTGCTTGCATTGGGGTCCAGCTGTTCAAGGGGAAGCTCTACC
GTTGCACAGATGAGGCCAAAAGTAACCCCGAGGAGTGCAGGGGGCTTTTCATCCTTT
ATAAGGACGGCGATGTCGACAGTCCCGTGGTCCGTGAGAGGATCTGGGAAAACAGT
AAGTTCGATTTCGACAATGTCCTTGCGGCTATGATGGCGCTCTTCACGGTCTCGACTT
TTGAGGGCTGGCCCGCGTTGCTGTACAAAGCTATCGATCCGCGC-3'

2.3.2 Generating truncations of $Ca_v1.3$ II-III loop

Intracellular II-III loop of $Ca_v1.3$ in the pEGFP-N1 vector was truncated into three regions: N-terminal region with 59 amino acids from 640 to 820 (NT59), the overlapping region with 68 amino acids from 740 to 945 (OL68), and C-terminal region with 56 amino acids from 880 to 1040 (CT56) using site-directed primers listed as below. The PCR products were transformed into DH5α *Escherichia coli* cells. The purified plasmids were screened by digestion with either input restriction enzyme or PCR amplification and further confirmed DNA sequencing. D23/pEGFP-N1($Ca_v1.3$ intracellular II-III loop) was digested with restriction enzymes EcoRI and BamHI (sites 640 and 850) to generate template vectors for amplified inserts. NT59 and OL68 were digested with AfeI, while CT56 was digested with MfeI to confirm the successful ligation.

Table 2.2. Primers of truncations of $Ca_v1.3$ II-III loop

	Forward Primer 5'-3'	Reverse Primer 5'-3'
NT59	CCC CCC GAA TTC GCC ACC ATG GAC AAT TTG GCT GAT GC	CCC CCC GGA TCC TCC TCT TCT CTA TAG TCA TCA ATT GTA ACC TTG TTG TCA CTG TTG GC
OL68	CCC CCC GAA TTC GCC ACC ATG GAA AAA AAG AAC AAA CC	CCC CCC GAA TCC GCC ATG TTC AAC TCC GAG
CT56	CCC CCC GAA TTC GCC ACC ATG GAA GAG GAG GAG GAT G	CCC CCC GGA TCC GCG TGG TGG TTG ATG AG

2.4 Electrophysiology recordings

2.4.1 Voltage-gated calcium channel and INS-1 cell preparation

Either INS-1 cells or tsA-201 cells were plated in plastic 35-mm tissue culture dishes (Corning) from 30~60% with single-cell distribution (50 μL from a transfected plate at 80% confluence, which could be flexible depending on transfection situation) in the previous day. tsA-201 cells were transfected as described in section 2.2.2, and the transfection was evaluated on the day of electrophysiology recordings by visualizing green fluorescent protein (GFP) fluorescence 18~24 hours post-transfection. INS-1 cells used for perforated current-clamp recordings were cultured in a complete RPMI medium containing low glucose (2.5mM) for more than 18 hours before experiments.

2.4.2 Conventional whole-cell recordings

Whole-cell patch-clamp recordings were performed at room temperature using an Axopatch 200B amplifier (Molecular Devices, Sunnyvale, CA). Data were sampled at a frequency of 10k Hz and filtered at 1kHz (six-pole Bessel filter, -3dB**)**. Patch pipettes were pulled by the flaming/brown micropipette puller (Sutter instrument model P-87, Novato, CA) using borosilicate glass (VMR, West Chester, PA) to an inside diameter of approximately 3~5 mm and fire-polished using the microforge (Narishige MF-830, JP) to achieve resistance values of 2 to 4 mΩ. Barium

ions (Ba^{2+}) were used as the charge carriers for voltage-gated calcium channel conducted currents, and the $Ca_v1.2$ and $Ca_v1.3$-mediated barium currents (IBa^{2+}) were evoked by stepping voltage to 0mV and -10mV for 100ms from holding potential at -70mV and -80mV, respectively, using pClamp 10.7-11.2 software (Molecular Devices). A simplified illustration of the electrophysiology setup is shown in figure 2.1.

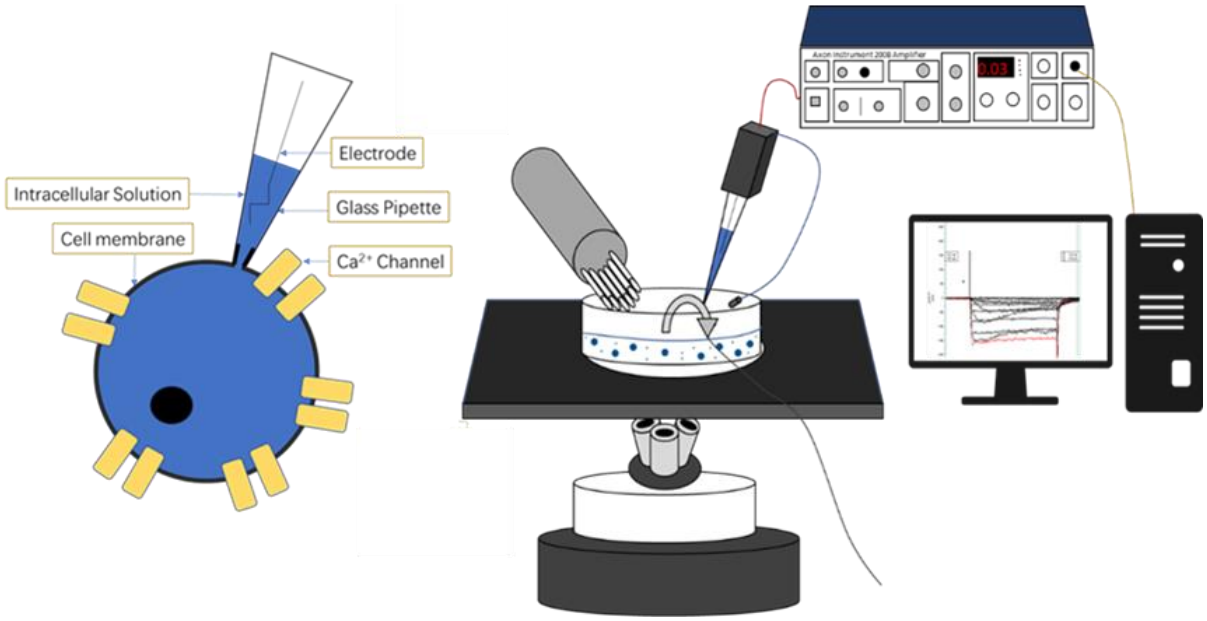

Figure 2.1. Simplified illustration of electrophysiology setup. On the right, the 35 mm cell culture dish is placed on the platform of the inverted microscope (Olympus) preinstalled with a mercury lamp and corresponding filters to detect fluorescence signals upon transfections. The perfusion system (Gray cylinder with glass pipettes attached) is located on the top left of the plate and an automated aspirator on the side of the plate to maintain an even liquid level of the plate. Patching pipette (loaded with blue extracellular solution) movement is controlled by an ultraprecise micromanipulator (Burleigh PCS-5000 and PCS-PC60, Thorlabs, Inc., Newton, NJ) and positioned on the top right, connecting to the Axopatch 200B amplifier, which sends signals to the computer via USB. A close-up illustration on the left shows when the pipette breaks open the cell membrane and form a closed circuit under a whole-cell patch-clamp.

2.4.2.1 Whole-cell patch-clamp solution sets

A variety of solution sets were prepared for different cell lines and calcium channels. They are listed below and will also be explained in upcoming sections.

Standard solution sets could be applied to all existing cells and are Tris-barium-based. Extracellular solution contained (in nM):150 Tris, 10 $BaCl_2$ and 4 $MgCl_2$. Intracellular solution contained (in nM): 130 N-methyl-D-glucamine (NMDG), 10 EGTA (ethylene glycol-bis(β-aminoethyl ether)-N,N,N′,N′-tetraacetic acid), 60 HEPES, 20 ATP and 1 $MgCl_2$. The pH of both solutions was adjusted to 7.3 with methanesulfonic acid, and the osmolality was corrected by adding distilled and deionized water to 290~300 mOsm.

For experiments conducted for testing VGCC antagonism, we adapted a high sodium solution set (Kang et al., 2013). The extracellular solution contained (in mM): 140 NaCl, 1 $MgCl_2$, 10 $BaCl_2$, 10 HEPES, 10 dextrose, 10 sucrose, and 20 CsCl at pH 7.4 and with an osmolality of ~350mOsm or lower after adjustment. The intracellular solution contained (in mM) 180 N-methyl-D-glucosamine (NMDG), 40 HEPES, 4 $MgCl_2$, 12 phosphocreatine, 0.1 leupeptin, 2 Na_2ATP, 0.5 Na_3GTP, 5 BAPTA, pH 7.2~7.3 and an osmolality of ~320mOsm after adjustment.

In some mutant $Ca_v1.3$ channels, large outward currents were observed in response to depolarization, particularly in the presence of FPL 64176. The NMDG-balanced solution was made based on existing standard Tris-barium solution sets. The extracellular solution contained (in mM): 130 NMDG, 20 Tris, 10 $BaCl_2$, 2 $MgCl_2$. The intracellular solution was not altered from above. The pH of the extracellular solution was adjusted to ~7.3, and the osmolality was adjusted to 285~300mOsm, regarding the existing intracellular solution.

Experiments with recombinant $Ca_v1.2$ and $Ca_v1.3$ channels were also performed in solutions containing Ca^{2+} rather than Ba^{2+}. The extracellular solution contained (mM): 140 NaCl, 1 $MgCl_2$, 10 $CaCl_2$, 10 HEPES, 10 dextrose, 10 sucrose, and 20 CsCl at pH 7.4 and with an osmolality of ~350mOsm or lower after adjustment with deionized water.

2.4.2.2 Whole-cell patch-clamp pharmacological reagents

The L-VGCC modulators: nifedipine, nicardipine, isradipine, diltiazem, amlodipine, azelnidipine, verapamil, and the agonist FPL 64176 were purchased from Sigma-Aldrich and RBI

(Sigma/RBI, Natick, MA) and dissolved in dimethyl sulfoxide (DMSO) to make a stock solution based on the suggested solubilities and likely ranging from 1:500 to 1:20,000 for dilution.

The peptide toxin calcicludine (Alomone Lab/ Peptide Institute, INC.) was dissolved in distilled water to make a 10μM stock solution. The synthesized calcicludine peptides Cyc-23, Cyc-24, and amlodipine-linked calcicludine peptides were dissolved in the bath saline solution to make a 10μM stock solution. The truncated peptides in $Ca_v1.3$/II-III were dissolved in the standard extracellular solution set at 5mM stock solution and diluted in the same bath solution for back-filling the pipettes during whole-cell patch-clamp recordings.

The stock solutions were diluted to the desired working concentrations in extracellular solution, then perfused on cells attached to the bottom of 35 mm cell culture dishes using RSC160 perfusion system (BioLogic, Climax, France at the rate of 0.5 mL/minute.

2.4.2.3 Whole-cell patch-clamp pulse protocols

Once the pipette loaded with intracellular solution reached close enough to the targeted cell, which is expected to be adhesive to the plate and display a spindle shape, the ultraprecise micromanipulator was moved diagonally to gently touch the cell with a tiny increase in resistance in the square wave of membrane test. A suction pulse was applied through the pipette pressure tubing from the mouth pipette, waiting for the seal resistance to reach 1 GΩ.

Upon going whole-cell, a current-voltage relationship was typically recorded below, followed by either voltage-clamp during perfusion, steady-state inactivation, or other frequency-dependent protocols, which will be described below.

Current-voltage relationship: IV-curve can provide the voltage range of activation and equilibrium potential. Depolarizing voltage steps with increments of 10 mV are applied from -60 to +50 mV every 2 seconds from a holding potential at -80mV. Most channels stay closed at hyperpolarized potentials from -40 mV but start to open when the potential is stepped to more positive values. All channels will practically open when steps more positive than 0mV, with a constant conductance, and current amplitude is only altered by the driving force of permeant ions in a linear relationship (Molleman, 2002). Voltage-dependent leak currents were subtracted using an on-line P/-4 subtraction paradigm.

Current density: This value (pA/pF) is obtained using the peak current amplitude divided by cell capacitance recorded during the membrane test.

Voltage-dependent activation: Tail current amplitudes from current elicited during curve protocols were plotted against test voltage with the equation. The activation curve (percentage of maximum conductance versus membrane voltage) can be obtained from the IV-curve tail current. The maximum conductance of a population of ion channels often coincides with the linear part of the I/V relation.

Voltage-dependent inactivation: The steady-state inactivation protocol uses 10-second conditioning pulses from −80 to +20 mV in 10-mV increments from a holding potential of −90 mV, followed by a 100-millisecond test pulse to +10 mV.

Dose-response protocol: Dose-response curves can be obtained by fitting the varying current amplitudes held at a constant potential in response to increasing concentrations of indicated drugs. Channels were activated with 100-millisecond steps to +10mV at a frequency of 0.033Hz from a holding potential of -80mV. Alternate increasing concentration will be applied when two previous sweeps overlap, and one stable value at each concentration will be used to generate the fit for affinity measurements.

Frequency-dependent dose-response protocol: Whole-cell currents were measured using 100-ms depolarizations to +10 mV from a holding potential of -60 mV in the absence or presence of the indicated drug concentrations at 0.05Hz. In cells to which the drug was applied, the block was allowed to reach equilibrium for several minutes at 0.05-Hz stimulation. The stimulation frequency was then increased to 1 Hz for 20 pulses (Dilmac et al., 2004).

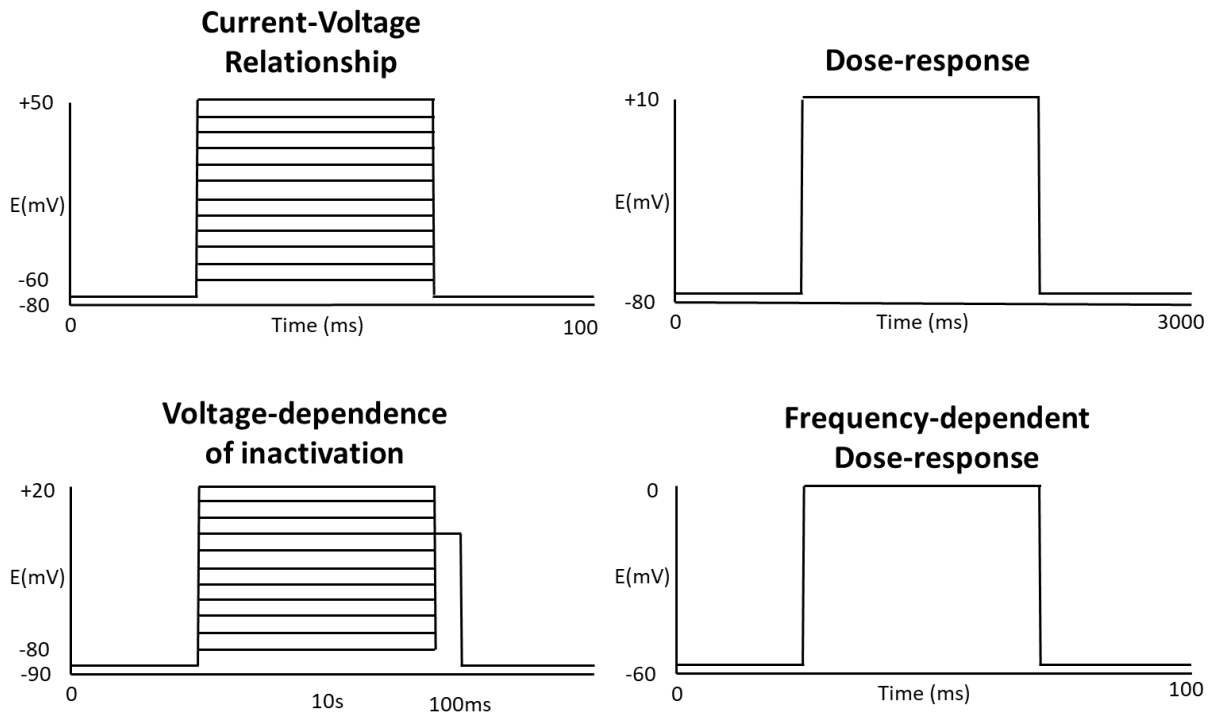

Figure 2.2. Waveforms of electrophysiological pulse protocols mentioned above.

2.4.3 Perforated whole-cell recordings

Similar to the set-up of whole-cell patch-clamp, perforated-patch clamp experiments were also performed at room temperature using an Axopatch 200B amplifier and filtered at 1 kHz (six-pole Bessel filter, -3dB). Patch pipettes were pulled by the flaming/brown micropipette puller (Sutter instrument model P-87, Novato, CA) using borosilicate glass (VMR, West Chester, PA) and fire-polished using the microforge (Narishige MF-830, JP) to achieve resistance values of 3 to 6 mΩ, which were relatively bigger than that of whole-cell patch-clamp experiments for a larger contacting surface area.

2.4.3.1 Perforated patch-clamp solution sets

Extracellular solution contained: 138 mM NaCl, 5.6 mM KCl, 2.5 mM D-glucose, 10 mM HEPES, 1.2 mM $MgCl_2$, 2.6mM $CaCl_2$. Intracellular solution contained: 90 mM K_2SO_4, 10 mM NaCl, 1 mM $MgCl_2$, 1.1 mM EGTA, 0.1 mM $CaCl_2$, 5 mM HEPES, 0.3 mM ATP, 0.2 mM GTP. The pH of both solutions was adjusted 7.4 with NaOH, and the osmolality was adjusted to ~230mOsm for intracellular solution and ~280mOsm for extracellular solution.

2.4.3.2 Perforated patch-clamp pharmacological reagents

Amphotericin B, an antifungal drug, was used to create holes in the membranes of a very distinct size, permeable to ions but not larger molecules. To avoid the drug disturbance before giga-seal is formed, we front-filled the pipette with a standard intracellular solution and back-filled with the freshly made intracellular solution containing the perforating drug. Amphotericin B (Sigma-Aldrich) was distributed into 1.5mL brown centrifuge tubes with minimal amount, dissolved in DMSO (~3mg/100μL) to make the 30 mg/mL stock solution with the help of sonicator (Branson 3200, Danbury, CT) for 15 minutes until all visible particles were removed. It was stored at -20℃, away from the light before further diluted in the intracellular solution to maintain a concentration of 50~60 μg/mL. Sucrose was used to elevate the osmolality of the front-filled intracellular solution so that amphotericin B can diffuse before the giga-seal formation in the difference of ~15mOsm between two solutions. The amphotericin preparation was adapted from earlier research (Rae et al., 1991).

Diazoxide (Sigma-Aldrich), the K_{ATP} channel activator (Trube et al., 1986), was diluted in DMSO to make 40mM stock solutions. It was applied to maximally open K_{ATP} channels and establish a stable resting membrane potential at a final concentration of 300 μM, assuring the exclusive effects of glucose-induced action potentials. Once the current clamp recordings show the stabilized membrane potentials, perfusion of diazoxide was stopped, and the extracellular solution was applied to wash out diazoxide before the addition of other modulators.

Glucose (Sigma-Aldrich) was prepared in deionized water to make 1 M fresh weekly. 18mM glucose in extracellular solution was used to depolarize the INS-1 cells.

Apamin (Alomone Labs), an SK channel inhibitor (Jacobson et al., 2010), was prepared in DMSO to make 200 μM stock solutions. 1μM apamin was added into a second perfusion line of 18mM glucose-treated extracellular solution when action potentials are stabilized.

2.4.3.3 Perforated patch-clamp pulse protocols

Once the pipette attached the cell, the access resistance (R_a) was monitored in cell mode of membrane test while the diffusion of amphotericin B and perforation of the cell membranes happened. Current clamp recordings were initiated after R_a reached less than 50MΩ. This could require up to 15 minutes after sealing the pipette to the cell membrane. Once the adequate access and typical whole-cell current response appear, the membrane potential can be measured by switching the amplifier to the current clamp (zero current injection mode). The membrane potential of INS-1 was measured using gap-free recording at a sampling frequency of 1kHz in *I*=0 current-clamp mode. 300 μM diazoxide, The K_{ATP} channel activator, was perfused to fully hyperpolarize the membrane potential once the recording starts. This perfusion was stopped once the membrane potential was stabilized and a standard extracellular solution without any additional drug was applied to wash out diazoxide. When the resting membrane potential remained steady (~60-65 mV), action potentials were stimulated by applying 18 mM glucose to the cell via extracellular perfusion. Current injections (100nA) were sometimes used to stimulate action potentials to assess cell viability if the cell did not respond to glucose.

2.5 Western Blot

2.5.1 Protein lysates collection

Transfected tsA-201 cells or INS-1 cells in either 6-well or 10cm dish were lysed following the standard lysis protocol. Iced cells were collected and lysed in 10mM Tris, 10mM EDTA, 10mM EGTA, 150mM NaCl and 1% Triton X-100 with protease inhibitor cocktail. Protein concentration was measured using Bradford protein assay, which was based on the ability of Coomassie blue to bind directly with protein molecules (*Western Blot Sample Preparation | Abcam*, 2021).

2.5.2 Co-immunoprecipitation

10~50 μg cell lysate protein was incubated with either affinity resin or antibody with corresponding magnetic beads in binding buffers: 20mM Na_2HPO_4 and 0.15M NaCl. Anti-DYKDDDK G1 affinity (mouse monoclonal antibody against FLAG tag, clone G1) resin

(GenScript, Piscataway, NJ, Cat. No. L00432) was preferably used in our experiments. Protein A MagBeads (GenScript, Cat. No. L00273) and Protein G MagBeads (GenScript, Cat. No. L00274) were used to bind with anti-DYKDDDK (in Table 2.3) antibodies in different species during experiment optimization.

The protein sample for co-immunoprecipitation was later eluted in 0.1M glycine and neutralized in 1M Tris.

2.5.3 Electrophoresis and immunoblotting

50μg of each protein sample after anti-FLAG beads elution were mixed with 5X protein-dye (BioLegend, San Diego, CA) and 1% β-mercaptoethanol (BME; Sigma-Aldrich), boiled and loaded and separated by SDS- polyacrylamide gel electrophoresis (SDS-PAGE) at 150~190mV for 40~60 minutes in running buffer diluted from 10X stock solution containing (in 1L ddH_2O): 30.3g Tris Base, 114.2g Glycine, 1% SDS. Proteins were transferred to PVDF membranes at 100mV for 30 minutes in transfer buffer containing: (in 2L ddH_2O): 30.3g Tris Base, 114.2g Glycine, 10% methanol. PVDF membrane was later blocked in 5% non-fat milk in tris-buffered saline containing 0.1% Tween-20 (TBST) for 30 minutes at room temperature. Primary antibodies were applied, and the membrane was incubated at 4℃ overnight (See Table 2.3 for details on primary antibodies). The membrane was washed the next day with TBST three times (one fast wash and two slow washes), incubated with HRP-conjugated secondary antibodies (1:10,000, BioRad Laboratories). The membranes were washed with TBST as described previously to reduce the excessive secondary antibodies. Enhanced chemiluminescence (ECL; Amersham Bioscience, Piscataway, NJ) was applied and incubated for 5 minutes before imaging on the Sapphire Biomolecular Imager (Azure Biosystems, Dublin, CA) using Sapphire Capture software.

Table 2.3. Primary antibodies information

Target	Manufacturer	Species	Dilution	Population
CACNB3 ($Ca_v\beta_3$)	Alomone Labs	Rabbit	1:200	Polyclonal
CACNB3 ($Ca_v\beta_3$)	Sigma-Aldrich	Mouse	1:500	Polyclonal
DYKDDDDK peptide (FLAG)	GenScript	Rabbit	1:20,000	Polyclonal
DYKDDDDK peptide (FLAG)	ThermoFischer	Mouse	1:1000	Monoclonal

2.6 Homology Models

Homology models of $Ca_v1.2$ and $Ca_v1.3$ were generated using SWISS-MODEL (Guex et al., 2009; Benkert et al., 2010; Bertoni et al., 2017; Bienert et al., 2016; Waterhouse et al., 2018). Both models were based on the cryo-EM structure of $Ca_v1.1$ (PDB-code: 5gjw; Wu et al., 2016). $Ca_v1.2$ and $Ca_v1.3$ share amino acid sequence identity of 72% and 71% with $Ca_v1.1$, respectively.

2.7 Data analysis

Electrophysiology data were analyzed using Clampfit 10.6, 10.7, and 11.2 (Axon Instruments), Windows Excel 2016-2020 (Microsoft), SigmaPlot 11 and 13 (Systat Software, San Jose, CA), and GraphPad Prism 6.1, 7.04, and 9.1 (GraphPad Software, La Jolla, CA).

Characterization of L-VGCC physiological and pharmacological values including $V_{1/2}$ activation, $V_{1/2}$ inactivation, IC_{50}, EC_{50} was determined using either GraphPad or SigmaPlot in the exact regression fit and same correction. Current clamp analysis was mainly generated in Clampfit.

2.7.1 Voltage-dependence of activation and inactivation

$V_{1/2}$ activation values were determined by plotting normalized tail-current amplitudes versus the corresponding 100-millisecond depolarizing voltage steps from −50 to +60 mV, in 10 mV-increments, from a holding potential of −80 mV. The data were fit to the Boltzmann equation, $I = 1/(1 + exp((V_{1/2} - V)/k))$, where k is a slope factor.

$V_{1/2}$ inactivation was determined by plotting the normalized test pulse amplitude versus the conditioning pulse potential and fitting the data to the Boltzmann equation $I = 1/(1 + exp(-(V - V_{1/2})/k))$, where k is a slope factor.

When fitting equations to the data for voltage-dependence of activation and inactivation, we set curves to start at 0 or 1, respectively, and force the curves to plateau at 1 or 0, respectively. Slopes were allowed to vary. The time course of channel deactivation was determined by fitting tail-current decay to either a single or double exponential function.

2.7.2 IC_{50} and EC_{50}

$LogIC_{50}$ values for nifedipine block were determined by fitting the fraction of current blocked at each drug concentration to the equation: Fraction Blocked = a − (a/ (1 + ([nifedipine] / IC_{50}) ^{b})), where a = maximum fraction blocked, b = slope. When fitting equations to the nifedipine dose-response data ($logIC_{50}$), we set the minimum at zero and let the slope and maximal block vary.

$LogEC_{50}$ values for FPL potentiation were determined by normalizing the increase in current with each concentration of FPL to the increase in current observed with 10 μM FPL. This reflects the experimental observation that the current block is often incomplete even at maximally effective concentrations. When fitting equations to the FPL 64176 dose-response data ($logEC_{50}$), we set the minimum at zero and the maximum at 1 (maximal current stimulation) but allowed the slope to vary. The range of *N* values for dose-response curves represents the number of data points for each drug concentration.

The number of separate experiments performed (i.e., cells clamped) to obtain a given dose-response curve is equal to or greater than the highest number of replicates indicated for any single drug concentration. The basis of the $logIC_{50}$ and $logEC_{50}$ values ± S.E. of the fit shown in Table 3.1 is the fit of all the data for a given channel construct.

2.7.3 Analysis in the kinetics of tail currents

Kinetics of tail current decay of $Ca_v1.2$ and $Ca_v1.3$ at a holding voltage of -80mV in the absence and presence of FPL were analyzed in either GraphPad or SigmaPlot. A 25-millisecond duration starting from the tail current peak was framed for analysis in a one-phase association in GraphPad or Exponential rise to the maximum in SigmaPlot. The fractional change was normalized for each data point to the full distance between the peak to the most positive current amplitude within this 25-millisecond window ranging from 0 to 1. Plateau (Frac. Fast in Table 3.2) was obtained from the fit f=a*(1-exp(-b*x)) with two parameters, along with τ values which are 1/b. R10 values were obtained by measuring the fraction of the tail current remaining 10 milliseconds after reaching a peak.

2.7.4 Analysis in current-clamp

All the current clamp measurements in the perforated whole-cell patch-clamp were obtained from Clampfit 10.6, 10.7, and 11.2. Action potential frequencies were calculated by picking a stable period preferentially longer than 10 seconds and analyzing the in the event detection with pre-set thresholds. Half-width and action potential amplitude were also obtained in the same set-up. Action potential hyperpolarization amplitude was calculated by subtracting the negative peak current from the previous plateau.

2.7.5 Comparison tests

Comparisons of two independent means were made with Student's unpaired *t*-test with different distribution assumptions. Comparisons of three or more independent means with one single treatment were made using a one-way analysis of variance (one-way ANOVA). Comparisons of multiple independent means with individual groups were made with multiple Student's unpaired *t*-tests throughout the columns with different distribution assumptions. $P < 0.05$ was considered significant. Data shown are means ± S.E. Lines are fits of the equations indicated for each type of experiment to the data.

CHAPTER 3. DIFFERENTIATION OF CAV1.2 AND CAV1.3 IN RESPONSE TO CHANNEL MODULATORS

3.1 Introduction

3.1.1 $Ca_v1.3$ involvement in $Ca_v1.2$-nonrelated disease

The development of L-VGCC modulators has been based on treating cardiovascular diseases such as hypertension and angina pectoris. L-type voltage-gated calcium channel (L-VGCC) inhibitors were established to antagonize the involvement of $Ca_v1.2$, a subtype predominant in vascular smooth muscle, to induce vasodilation (Catterall, 2000). Nonetheless, another closely related L-VGCC subtype $Ca_v1.3$, highly expressed in SA and AV nodal tissue (Platzer et al., 2000), is probably an essential target for suppressing supraventricular arrhythmias. Three main chemical classes of L-VGCC blockers, dihydropyridines (DHPs), phenylalkylamines (PAAs), and benzothiazepines (BTZs) (Hockerman et al., 1997), are currently in clinical use but have no high degree of discrimination between $Ca_v1.2$ and $Ca_v1.3$. Besides the cardiovascular system, $Ca_v1.2$ and $Ca_v1.3$ are expressed in various types of neurons (Hell et al., 1993) and endocrine cells (Seino et al., 1992), where they are thought to play distinct roles in cellular regulation. One example of a neurological role for $Ca_v1.3$ is the mediation of cortical excitability and Ca^{2+} oscillation in dopaminergic neurons of substantia nigra that may lead to Ca^{2+} overload and contribute to the selective loss of affected neurons in the early-onset stage of Parkinson's disease (Guzman et al., 2009, 2010; Surmeier and Schumacker, 2013). $Ca_v1.3$ is required for upregulation of dopamine D2L receptors and sensitization to amphetamine (Giordano et al., 2006) and recruitment of D2L receptors in the striatum upon cocaine withdrawal (Schierberl et al., 2012) by regulating the DA activity in the ventral tegmental area-nucleus accumbents (VTA) brain region (Nestler et al., 2005). Non-selective DHPs were found to reduce cocaine-seeking behaviors in rats (Addy et al., 2018). On the other hand, $Ca_v1.2$ is involved in alcohol-seeking and relapse behavior (Uhrig et al., 2016). As for endocrinal pathways, $Ca_v1.3$ is activated by autoantibodies, which have been detected in serum collected from type-1 diabetes patients (Juntti-Berggren et al., 1993; Bason et al., 2013). $Ca_v1.3$ is also considered a potential therapeutic target for ischemic stroke (Busquet et al., 2008) and prostate cancer (Chen et al., 2014). These observations have driven the search for selective inhibitors of $Ca_v1.3$ as potential therapeutics for neurological and endocrinal diseases.

3.1.2 Development of $Ca_v1.3$ selective inhibitors

Given the novel direction of targeting $Ca_v1.3$ as therapeutic targets, several efforts have been devoted to developing L-VGCC subtype-selective inhibitors. One study examined dozens of derivatives of DHP scaffold, but only a modest degree of selectivity (at most 1.34) for $Ca_v1.3$ over $Ca_v1.2$ (Chang et al., 2010) was reported. Later, another study examining 5-unsubstituted DHPs reported compounds with better but not good enough $Ca_v1.3$ selectivity (at most 2.94 in cardiovascular tissues and no selectivity in neuronal tissues) (Tenti et al., 2014). A screen of over 60,000 compounds identified a class of compounds, pyrimidine-2,4,6-triones, as moderately selective inhibitors of $Ca_v1.3$ over $Ca_v1.2$ (Kang et al., 2012, 2013). Other labs, however, failed to reproduce this selectivity. One follow-up study concluded that the lead pyrimidine-2,4,6-trione (compound 8) was dependent on the subtype of the auxiliary β subunit expressed with $Ca_v1.3$ (Huang et al., 2014), and another lab concluded that compound 8 was an activator of L-type channels (Ortner et al., 2014).

The mixed results reported in studies using derivatives of DHPs or screens of chemical libraries suggest the need for more insight into differences between $Ca_v1.2$ and $Ca_v1.3$ that might be exploited in selective-drug development. The molecular pharmacology of $Ca_v1.2$ is well studied. The molecular determinants of $Ca_v1.2$ modulation by DHPs (Hockerman et al., 1997c; Sinnegger et al., 1997; Yamaguchi et al., 2003; Lin et al., 2011), PAAs (Hockerman et al., 1995, 1997a; Dilmac et al., 2004), and BTZs (Hering et al., 1996; Hockerman et al., 2000; Dilmac et al., 2003) have been identified. Even though there have not been cryoEM structures of $Ca_v1.2$ and $Ca_v1.3$ solved, the homology models of the binding sites have been developed (Cosconati et al., 2007; Cheng et al., 2009; Tikhonov and Zohorov, 2009). However, the molecular pharmacology of $Ca_v1.3$ has not been extensively studied so far. One reason for this disparity might be from the highly conserved domains between $Ca_v1.2$ and $Ca_v1.3$ for drug block, leading to the perception that the drug binding sites in both channels are identical. Even though $Ca_v1.3$ has been reported to be less sensitive to block by some DHPs than $Ca_v1.2$ (Xu and Lipscombe, 2001; Huang et al., 2013), the molecular determinants that mediate this difference in DHP affinity are not known.

3.1.3 Differentiation of subtype pharmacology

The transmembrane domains of $Ca_v1.2$ and $Ca_v1.3$ contributing to drug binding are highly conserved or nearly identical but with two subtle differences in two regions: IIIS5 and IIIS6, along with the extracellular/ pore IIIS5-3P loop, a highly divergent region, connecting these two domains. The IIIS5-3P domain contains two amino acid residues critical for the DHP block of $Ca_v1.2$ (Yamaguchi et al., 2000, 2003), but they are conserved between $Ca_v1.2$ and $Ca_v1.3$. However, another cluster of amino acids closer to IIIS5 and not conserved between $Ca_v1.2$ and $Ca_v1.3$ is reported to influence DHP binding affinity (Wang et al., 2007). Therefore, we examined if substituting these critical divergent amino acids from $Ca_v1.2$ into $Ca_v1.3$ could reduce the IC_{50} for nifedipine (1,4-dihydro-2,6-dimethyl-4-(2-nitrophenyl)-3,5-pyridine carboxylic acid dimethyl ester) and EC_{50} for a non-dihydropyridine L-VGCC agonist FPL 64176 compared with wild-type $Ca_v1.3$.

3.2 Structurally distinct dihydropyridines (DHP) differentially block $Ca_v1.2$ and $Ca_v1.3$

To understand the pharmacological differences between $Ca_v1.2$ and $Ca_v1.3$, we tested the universal L-VGCC antagonists, including the structurally distinct dihydropyridines (DHP) listed below: nifedipine, amlodipine, isradipine, and azelnidipine (Figure 3.1.A). Two concentrations of DHPs were tested on $Ca_v1.2$ and $Ca_v1.3$, ranging from 0.05 to 10μM. Each DHP we tested was more potent on $Ca_v1.2$ over $Ca_v1.3$ but not selective enough to differentiate these two subtypes (Figure 3.1.B). We chose nifedipine for the subsequent experiments since it does not have chirality like most of DHPs and was the most compact and symmetrical compound among all we tested. At 1μM, it blocks 80 percent of $Ca_v1.2$ and 70 percent of $Ca_v1.3$, and at a lower concentration, it shows more clear pharmacological differences.

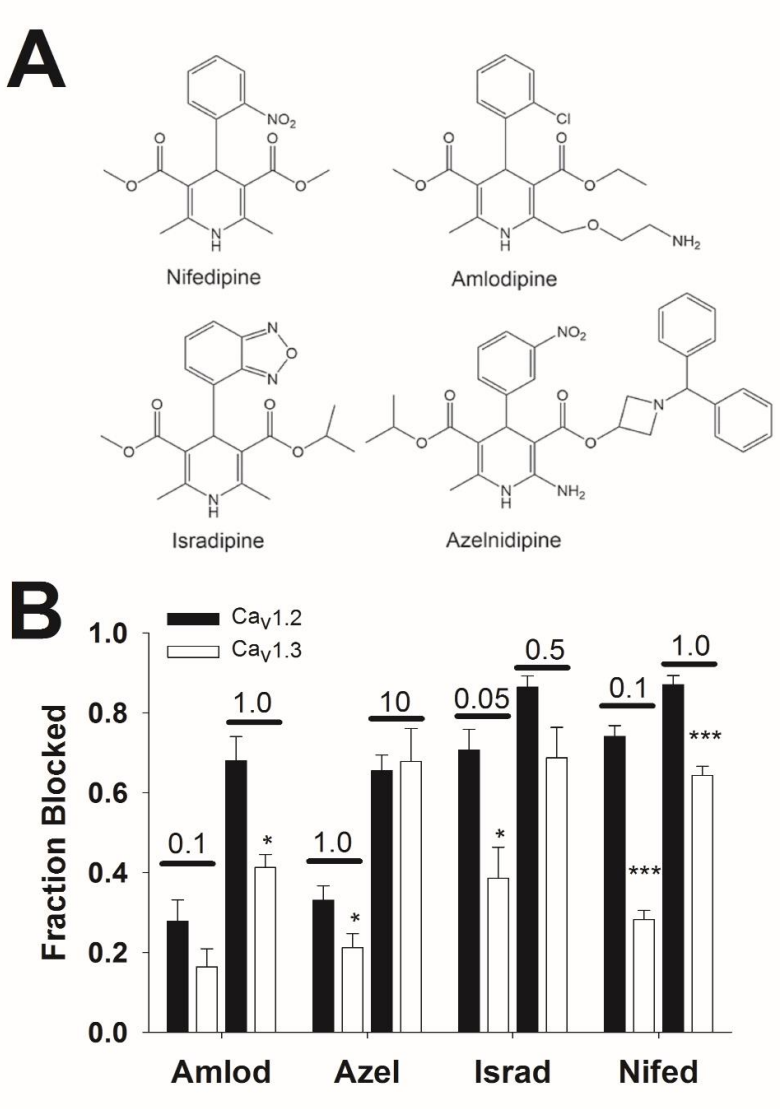

Figure 3.1. Differential block of $Ca_v1.2$ and $Ca_v1.3$ by structurally distinct dihydropyridines. (**A**) Chemical structures of nifedipine, amlodipine, isradipine, and azelnidipine. (**B**) Two concentrations (0.1 and 1.0μM for amlodipine, azelnidipine, and nifedipine, and 0.05 and 0.5 μM for isradipine) of the mentioned nifedipines in (A) were applied to block $Ca_v1.2$ and $Ca_v1.3$. Note that each drug is more significantly potent in blocking $Ca_v1.2$ compared to $Ca_v1.3$. Nifedipine (100nM: P <0.001, N=4; 1μM: P<0.001, N=4), Amlodipine (1 μM: P <0.05, N=4), Azelnidipine (1 μM: P<0.05, N=5), and Isradipine (50nM: P<0.01, N=5) all showed statistical significance between $Ca_v1.2$ and $Ca_v1.3$ using non-paired t-test.

3.3 Characterization of $Ca_v1.2$ and $Ca_v1.3$ gating and pharmacological properties

Biophysical and pharmacological properties were assessed by characterizing Ba^{2+} current conducted by $Ca_v1.2$ or $Ca_v1.3$ co-expressed with the β_3 and $\alpha_2\delta_1$ subunits in tsA201 cells. We measured their voltage-dependence of activation (Figure 3.2.A), inactivation (Figure 3.2.B), and dose-response curves treated with nifedipine (Figure 3.2.C). Voltage-dependence of activation was recorded as described in Chapter 2, and an IV curve was generated from a holding potential of -80 mV by stepping to voltages from -50 mV to +60 mV in 10 mV increments. We applied the peak tail currents to the Boltzmann distribution to generate a Boltzmann-type activation curve [i.e., open probability (P_{open}) -V curve]. $V_{1/2}$ activation for $Ca_v1.2$ and $Ca_v1.3$ are -20 ± 0.5 mV and -30 ± 1.5 mV, respectively. Voltage-dependent inactivation was recorded from a holding potential of -90 mV with conditioning voltage steps from -80mV to 20mV by 10mV every 60 seconds with a 100ms test pulse to -10mV. The same Boltzmann distribution was applied, and $V_{1/2}$ inactivation for $Ca_v1.2$ and $Ca_v1.3$ are as -41 ± 0.6 mV and -36 ± 1.3 mV, respectively. Dose-response curves were generated with an extracellular perfusion system and multiple concentrations of nifedipine through capillaries and observed with an inverted epi-fluorescence microscope. Both L-VGCCs were activated with 100-millisecond steps to +10mV at a frequency of 0.033 Hz from a holding potential of -80mV. The baseline was established when more than two traces were superimposed after perfusion of extracellular solution without any addition of compounds. Increasing concentrations of nifedipine were applied, and unstable cells were eliminated. Currents were normalized by the difference between baseline and specific concentration divided by baseline to generate block fraction. $Ca_v1.2$ was blocked more potently by nifedipine than $Ca_v1.3$ with IC_{50} values of 22 ± 2 nM for $Ca_v1.2$ and 289 ± 30nM for $Ca_v1.3$. We also tested the truncated splice variant $Ca_v1.3_{42a}$ (Xu and Lipscombe, 2001) without a long C-terminal tail, which was less sensitive to nifedipine than the full-length $Ca_v1.3_{42a}$ variant (Huang et al., 2013). We chose to use the full-length $Ca_v1.3_{42a}$ variant over the truncated version as it is more structurally similar to the $Ca_v1.2$ variant used in this study. The IC_{50} for $Ca_v1.3_{42a}$ was 436 ± 24 nM.

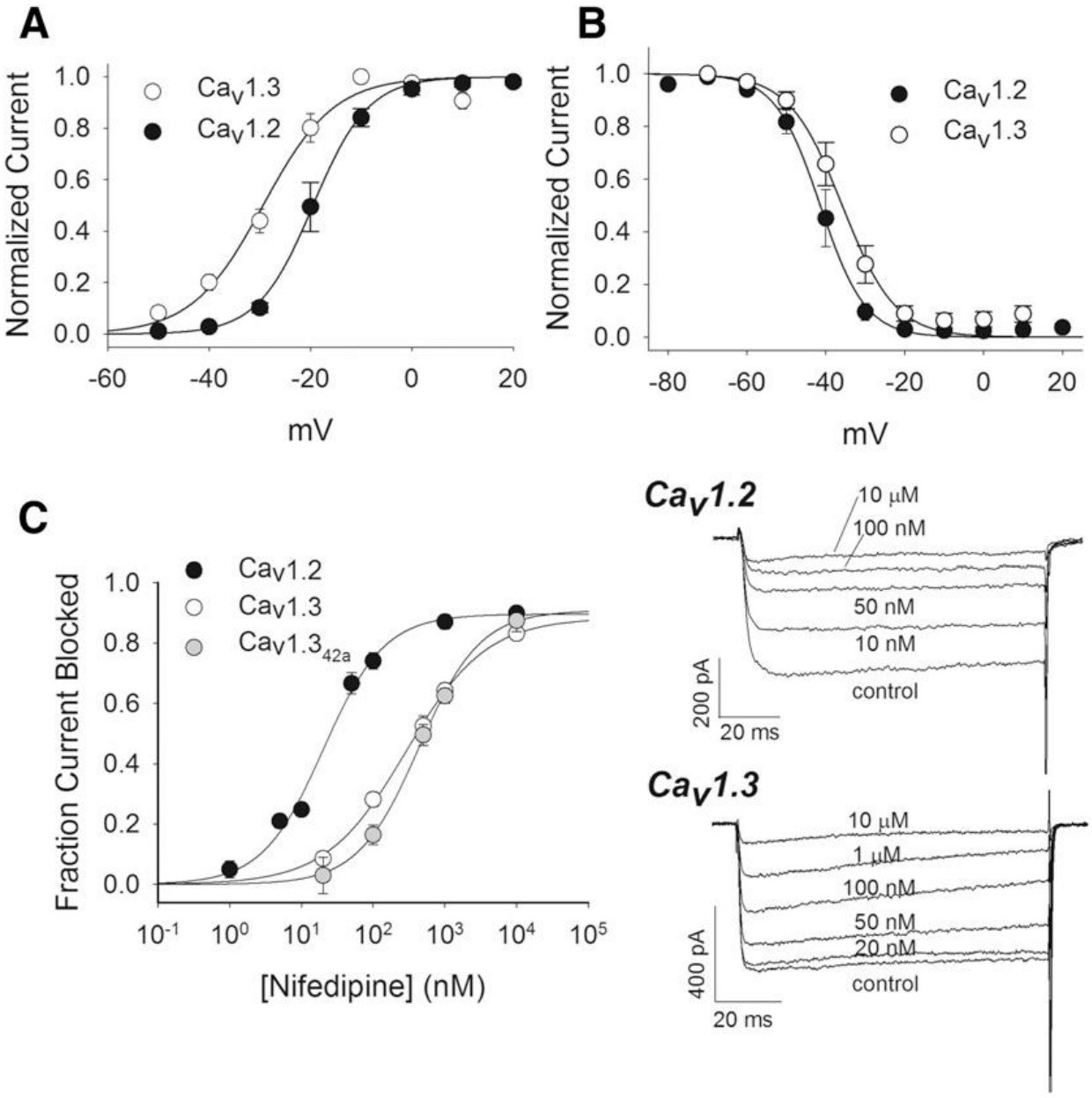

Figure 3.2. Characterization of $Ca_v1.2$ and $Ca_v1.3$ electrophysiological properties and nifedipine block. (**A**) Determination of the voltage-dependence of activation in $Ca_v1.2$ and $Ca_v1.3$. $V_{1/2}$ activation values were -20 ± 0.5 mV for $Ca_v1.2$ (N = 6) and -30 ± 1.5 mV for $Ca_v1.3$ (N = 9) ($P < 0.001$). (**B**) Determination of the voltage-dependence of inactivation in $Ca_v1.2$ and $Ca_v1.3$. $V_{1/2}$ inactivation values were -41 ± 0.6 mV for $Ca_v1.2$ (N = 6) and -36 ± 1.3 mV (N = 5) for $Ca_v1.3$ ($P < 0.01$). (**C**) Determination of potency of nifedipine block of $Ca_v1.2$ and $Ca_v1.3$. The IC_{50} values of nifedipine block were 22 ± 2nM (N = 3–12) for $Ca_v1.2$ and 289 ± 30nM (N = 7) for $Ca_v1.3$ ($P < 0.001$). Example traces from experiments are shown at right. The IC_{50} for nifedipine block of $Ca_v1.3_{42a}$, a truncated splice variant, was 436 ± 24nM (N = 5 to 6), statistically significantly greater than that of $Ca_v1.3$ ($P < 0.01$).

3.4 Homology models and DHP binding pocket

Thinking about the substantial biophysical and pharmacological differences between these two subtypes and the fact that they share a 75% homology overall and over 90% homology within the transmembrane domains, we hypothesized that the DHP sensitivity difference between $Ca_v1.2$ and $Ca_v1.3$ comes from the most divergent region. Since there are no high-resolution structures of $Ca_v1.2$ and $Ca_v1.3$ co-crystallized with DHP available, we collaborated with Dr. Markus A. Lill and built two 3D models based on the high-resolution CryoEM structure of rabbit $Ca_v1.1$ (Wu et al., 2016) (Figure 3.3.A). Based on the findings of three classes of drugs, PAAs, BTZs, and DHPs binding to L-VGCCs in IIIS5, IIIS6, and IVS6 transmembrane regions (Hockerman et al., 1997), our 3D models provide a better perspective of the DHP binding pocket (Figure 3.3.B).

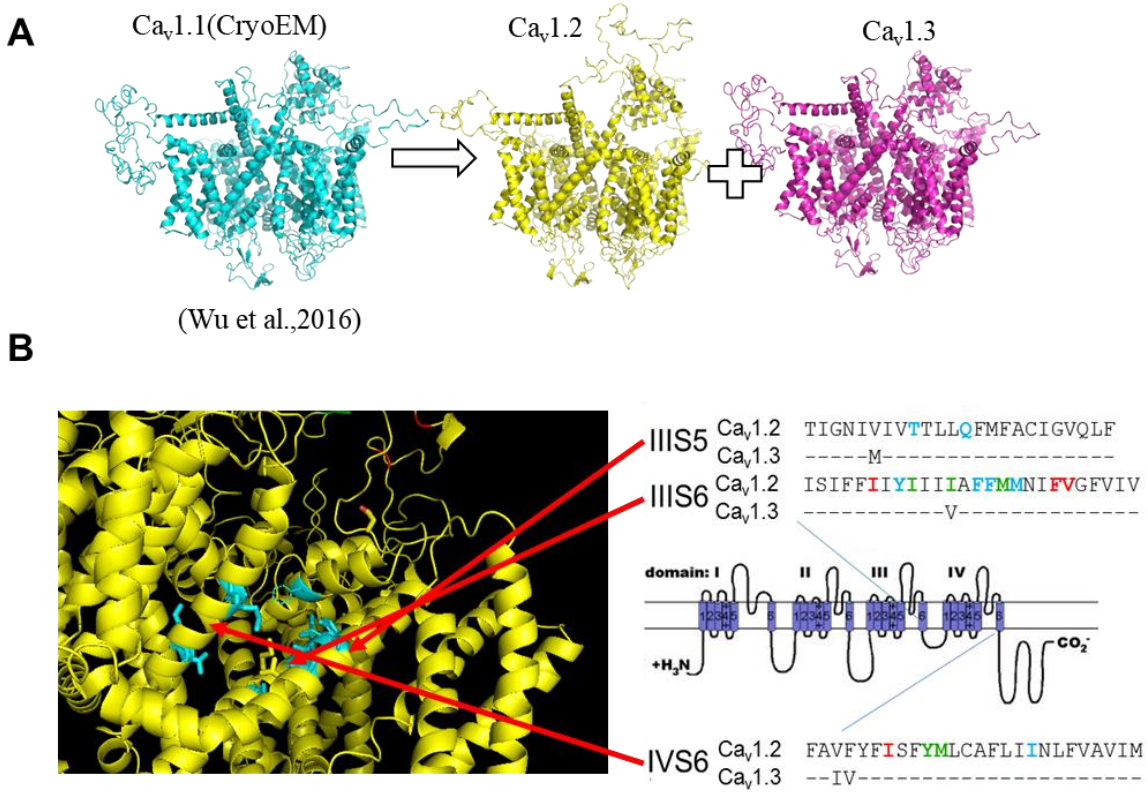

Figure 3.3. 3D models of $Ca_v1.2$ and $Ca_v1.3$ and DHP binding pocket. (**A**) We built the 3D models of $Ca_v1.2$ (yellow) and $Ca_v1.3$ (purple) based on Cryo-EM $Ca_v1.1$ (cyan). (**B**) Topology of DHP binding pocket in the 3D model of $Ca_v1.2$ and sequence alignments of $Ca_v1.2$ and $Ca_v1.3$. Shaded cylinders represent transmembrane segments (1-6) organized into four homologous domains (I-IV). The C- and N- terminal domains are intracellular. The critical amino acids in the binding pocket with three classes of the drug: phenylalkylamines, benzothiazepines, and dihydropyridines, are color-coded in red, green, and blue. Dashes represent identity between these two subtypes.

3.5 Molecular determinants in IIIS5 transmembrane in response to Nifedipine

3.5.1 Generation of DHP insensitive mutants

Transmembrane IIIS5 is a critical component of the DHP binding pocket in $Ca_v1.2$ (Mitterdorfer et al., 1996, Hockerman et al., 1997). The mutations of T1039 and Q1043 in Cav1.2 to tyrosine and methionine result in a DHP-insensitive voltage-gated Ca^{2+} channel, Cav1.2/DHPi, markedly less sensitive to DHPs but normally sensitive to diltiazem (Hockerman et al., 2000; Lin et al., 2011). Corresponding mutations were made on $Ca_v1.3$ by switching the same threonine and glutamine to tyrosine and tyrosine (Figure 3.4.A), and $Ca_v1.3$/DHPi was generated, which also lost DHP sensitivity as expected (Wang et al., 2018). However, due to the insolubility of nifedipine over 200μM (Ran et al., 2002) and the very low sensitivity of $Ca_v1.3$/DHPi to nifedipine block, we were unable to determine the maximum nifedipine block. Instead, we assumed the maximal nifedipine block of $Ca_v1.3$/DHPi to be 90% at the highest concentration, and by applying the inhibition fit, we estimated the IC_{50} of nifedipine block of $Ca_v1.3$/DHPi to be ~93μM, compared to IC_{50} of $Ca_v1.3$ at 289nM (Figure 3.4.B). We also measured the potency of diltiazem in blocking of $Ca_v1.3$/DHPi and wild-type $Ca_v1.3$. The sensitivity of $Ca_v1.3$/DHPi was not altered compared to $Ca_v1.3$ (Figure 3.5).

3.5.2 Significant amino acids in IIIS5 to differentiate $Ca_v1.2$ and $Ca_v1.3$

Considering the important role of the transmembrane IIIS5 domain contributing to DHP binding, we would like to explore the single amino acids not conserved between $Ca_v1.2$ and $Ca_v1.3$. The only difference is $Ca_v1.3$/M1030 and $Ca_v1.2$/V1036 (Figure 3.4.A). We constructed the mutant channel $Ca_v1.3$/MV using the site-directed mutagenesis mentioned in Chapter 2 to determine whether this conservative change could contribute to the nifedipine potency difference between $Ca_v1.2$ and $Ca_v1.3$. We first measured its biophysical characteristics and reported its $V_{1/2}$ activation as -26 ± 1.1 mV (N = 23) and $V_{1/2}$ inactivation as -35 ± 0.5 mV (N = 6) (Table 3.1). The voltage-dependent inactivation for this mutant is not very different from $Ca_v1.3$ at -36 mV, but the voltage-dependent activation shifts to a more positive voltage from -30mV of $Ca_v1.3$ ($P < 0.05$). Then we measured the pharmacological property of this mutant, and it generated a nifedipine IC_{50} of 89 ± 7nM, shifting from 289nM of $Ca_v1.3$ ($P < 0.001$) by ~3 fold. We were curious whether the reciprocal change of $Ca_v1.2$/VM would generate a similar shift in $Ca_v1.2$. The additional mutant

$Ca_v1.2$/VM was found to increase the IC_{50} of the nifedipine block of $Ca_v1.2$ from 22nM to 39nM ($P < 0.01$) (Figure 3.4.D, Table 3.1). Additionally, the $V_{1/2}$ activation and inactivation for this mutant were reported as -24 ± 1.0mV (N=8) and -38 ± 0.5mV (N=6). They are both close to the measurements of $Ca_v1.2$ but with a more negative activation and more positive inactivation. From the findings, we were certain that this $Ca_v1.3$/M1030 to $Ca_v1.2$/V1036 switch contributes to differentiating the nifedipine potency between subtypes and moderately changed voltage-dependent activation. Our model of $Ca_v1.3$, colored in purple, includes the IIIS5 helix at the bottom and IVS6 helix at the top with the 3P helix to the right, with valine of $Ca_v1.2$ shown at the mutation in yellow. Methionine could potentially decrease the accessibility of nifedipine to the Q1037 and F1106 residues (Figure 3.4.F).

Figure 3.4. Significant amino acids in transmembrane IIIS5 contributing to Nifedipine block. (**A**) Topological representation of L-VGCCs with transmembrane IIIS5 sequence alignment of $Ca_v1.2$, $Ca_v1.3$, and mutant $Ca_v1.3$/DHPi. The $Ca_v1.3$/M1030 and $Ca_v1.2$/V1036 are colored in red. $Ca_v1.3$/T1033, $Ca_v1.3$/Q1037, and $Ca_v1.2$/T1039, $Ca_v1.2$/Q1043 are underlined, mutated to tyrosine and methionine for generation of $Ca_v1.2$/DHPi and $Ca_v1.3$/DHPi. (**B**) Dose-response curve for nifedipine block of $Ca_v1.3$/DHPi and $Ca_v1.3$. The IC_{50} for $Ca_v1.3$/DHPi was estimated at ~93μM. (**C**) Dose response curve for nifedipine block of $Ca_v1.3$/MV and $Ca_v1.3$. The IC_{50} value was 89 ± 7nM (N = 5~7), less than IC_{50} of nifedipine block of $Ca_v1.3$ ($P < 0.001$). (**D**) Dose response curve for nifedipine block of $Ca_v1.2$/VM and $Ca_v1.2$. The IC_{50} value was 39 ± 5nM (N = 4~6), greater than the IC_{50} of nifedipine block of $Ca_v1.2$ ($P < 0.05$). (**E**) Voltage-dependent activation of $Ca_v1.2$/VM and $Ca_v1.2$. The $V_{1/2}$ activation for $Ca_v1.2$/VM was -24 ± 1mV (N = 8), more negative than that of $Ca_v1.2$ ($P < 0.05$). (F) Homology models of $Ca_v1.2$ (yellow) and $Ca_v1.3$ (purple). This view indicates the DHP binding pocket of $Ca_v1.3$ and includes the $Ca_v1.2$/V1036 superimposed with $Ca_v1.3$/M1030. The frame includes the IIIS5 helix (bottom), IVS6 helix (top), and the 3P helix (right) with Q1037 and F1106, the significant amino acids in DHP binding.

Figure 3.4 continued

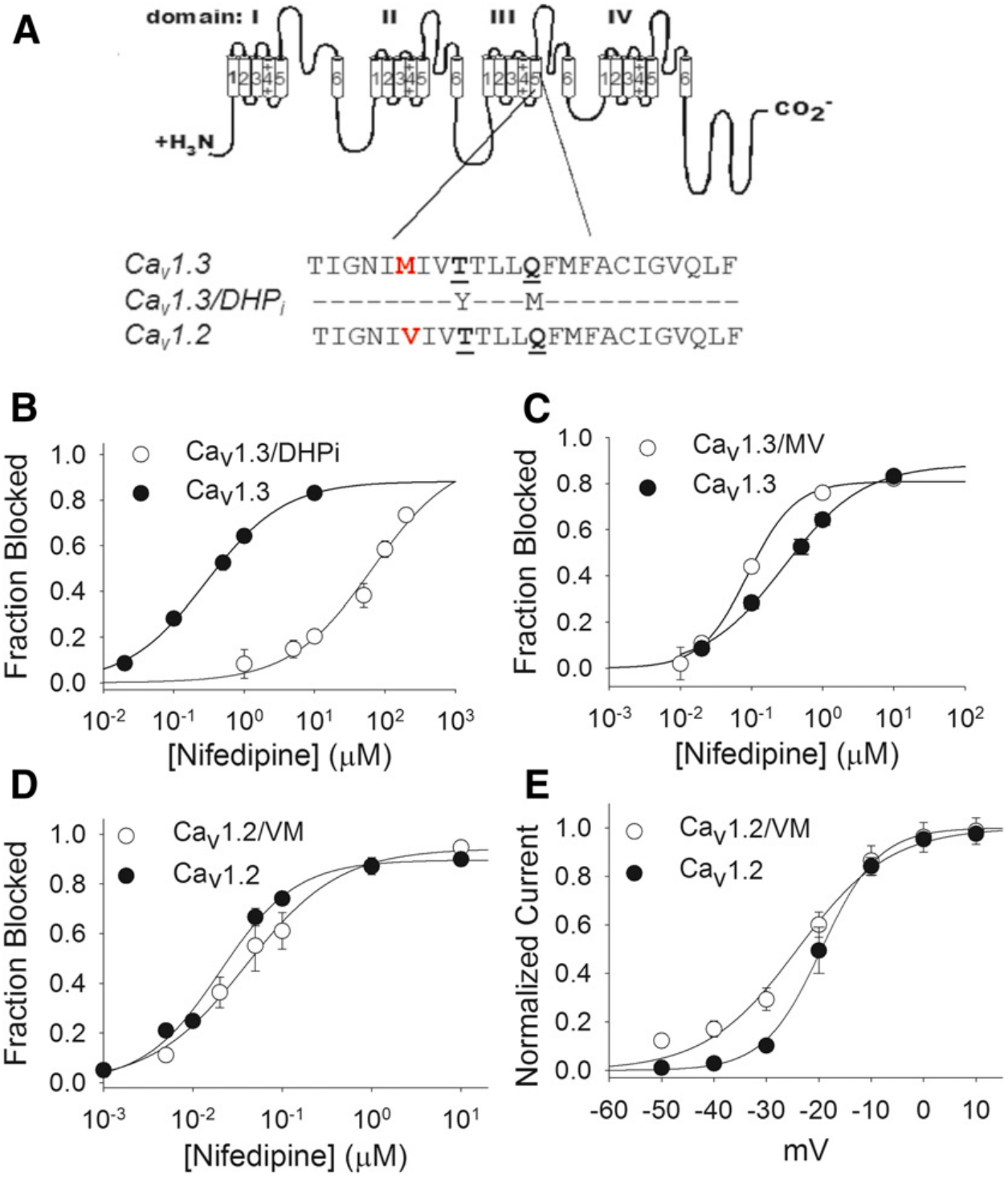

Figure 3.4 continued

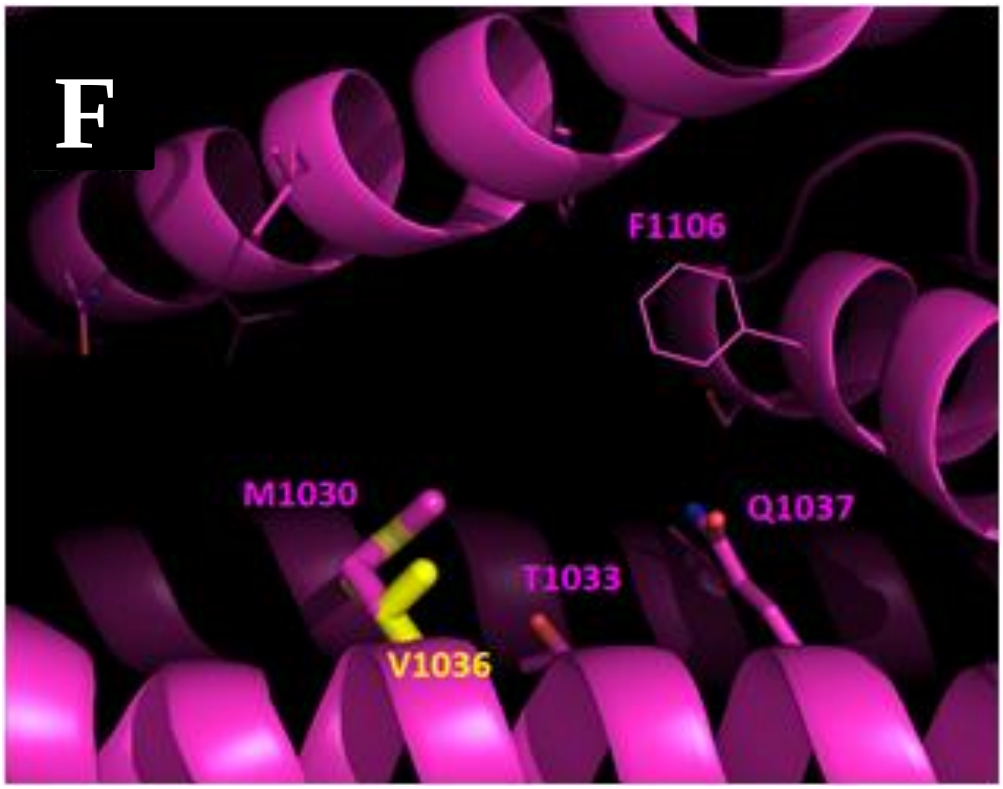

3.6 Molecular determinants in the extracellular IIIS5-3P loop in response to Nifedipine

3.6.1 Generation of chimeric $Ca_v1.3$ with $Ca_v1.2$ IIIS5-3P loop

IIIS5-3P loop is an area of relatively high amino acid sequence divergence between $Ca_v1.2$ and $Ca_v1.3$ compared to transmembrane IIIS5 (Figure 3.6.A). Furthermore, some determinants of DHP potency and affinity have been identified in this region, as mentioned in chapter 1 and figure 3.3. Therefore, we believe that this extracellular loop might exhibit some molecular determinants to differentiate these two subtypes.

We created a chimeric channel and named it $Ca_v1.3+$, which incorporates the $Ca_v1.2$ IIIS5-3P loop into the $Ca_v1.3$ backbone. The method was mentioned in section 2.3. The voltage-dependence of activation and inactivation were examined and essentially unchanged in $Ca_v1.3+$ compared with $Ca_v1.3$ (Table 3.1). Excitingly, the IC50 for the nifedipine block of $Ca_v1.3+$ was reported as 101 ± 4nM, reduced compared with that for $Ca_v1.3$ ($P < 0.001$) (Figure 3.6.B). Like $Ca_v1.3$/DHPi, we were also curious about another drug class interacting with this mutant. We applied four increasing

concentrations of diltiazem, 10, 50, 100, and 500 μM onto $Ca_v1.3$, $Ca_v1.3$/DHPi, and $Ca_v1.3$+, and there were no significant differences among the three classes of channels (Figure 3.5). Thus, the IIIS5-3P loop is not critical for diltiazem block but contributes to the difference in nifedipine potency between $Ca_v1.2$ and $Ca_v1.3$.

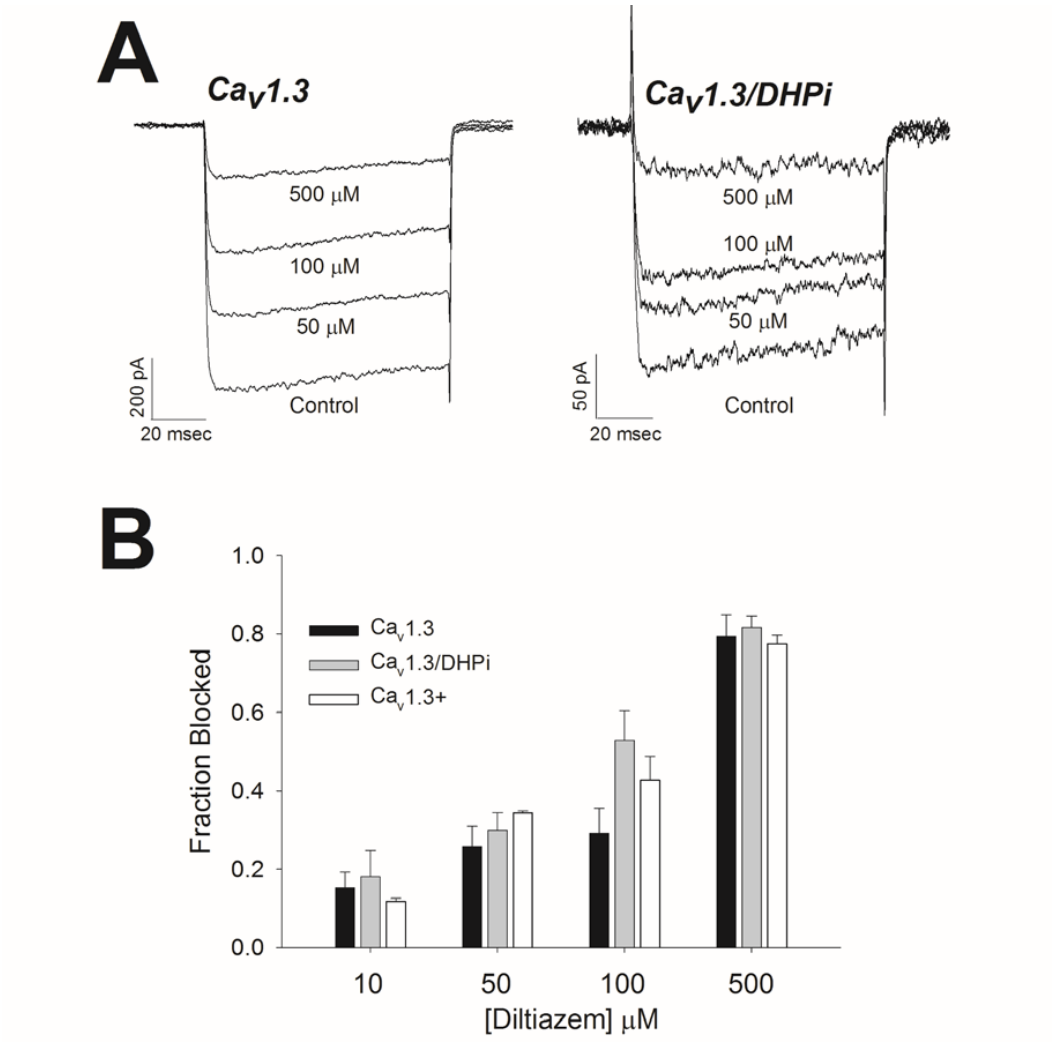

Figure 3.5. Diltiazem (benzothiazepine) block of $Ca_v1.3$, $Ca_v1.3$+ and $Ca_v1.3$/DHPi. (**A**) Example current traces show dose-dependent block in $Ca_v1.3$ and $Ca_v1.3$/DHPi by diltiazem at 50, 100, and 500 μM. (**B**) Fractional block by 10, 50, 100, and 500 μM diltiazem in $Ca_v1.3$, $Ca_v1.3$/DHPi, and $Ca_v1.3$+. There was no significant difference in the fraction of the current blocked in each of the three-channel constructs at any diltiazem concentrations. (one-way ANOVA, N=3~7)

3.6.2 Significant amino acids in III5-3P loop to differentiate $Ca_v1.2$ and $Ca_v1.3$

Given the increased potency of the nifedipine block of $Ca_v1.3+$, we aligned the sequences of subtypes at the IIIS5-IIIP loop and tried to identify the amino acid which might account for it (Figure 3.6.A). This extracellular domain extends from the C-terminal end of transmembrane IIIS5 and includes the ion selectivity filter. $Ca_v1.2$/E1118 and $Ca_v1.3$/E1112 were shown to allow simultaneous interactions with multiple Ca^{2+} ions moving single-file within the pore over more plentiful ions such as Na^+ and K^+ (Yang et al., 1993). IIIS5-3P loop includes conserved $Ca_v1.2$/F1112 and S1115 and $Ca_v1.3$/F1106 and S1109, contributing to DHP binding and Ca^{2+} channel agonist activity (Yamaguchi et al., 2000, 2003). The only divergence between $Ca_v1.2$ and $Ca_v1.3$ in this region is $Ca_v1.3$/S1100 to $Ca_v1.2$/A1106. The mutant $Ca_v1.3$/SA had a $V_{1/2}$ activation not different from $Ca_v1.3$, but a markedly left-shifted $V_{1/2}$ inactivation at -49mV ± 0.8 (Table 3.1). The IC_{50} for the nifedipine block of $Ca_v1.3$/SA was reported as 99 ± 24nM, not statistically different from $Ca_v1.3+$ at 101nM (Figure 3.6.B). Thus, this serine to alanine switch reproduced the DHP sensitivity increase of $Ca_v1.3+$. Our 3D model shows that $Ca_v1.3$/S1100 potentially forms a hydrogen bonding with $Ca_v1.3$/N1094 (Figure 3.7), while $Ca_v1.2$/A1106 and $Ca_v1.2$/D1100 do not. A potential hydrogen bond was also spotted in Cryo-EM $Ca_v1.1$ between $Ca_v1.1$/S1102 and $Ca_v1.1$/H996 and facilitated by D998. These potential hydrogen bonds might explain the lower DHP binding affinity in $Ca_v1.1$ and $Ca_v1.3$ compared to $Ca_v1.2$.

3.6.3 Additional mutants with lower potency

The conserved proline residues at $Ca_v1.2$/P1087 and $Ca_v1.3$/P1081 are located in the first half of the IIIS5-3P domain, while two other proline residues occupy distinct positions within the IIIS5-3P domain: $Ca_v1.3$/P1064 and $Ca_v1.2$/P1091. We reasoned that this proline configuration difference could contribute to DHP affinity by controlling the conformation of the 3P helix. IIIS5-3P loop. We made a mutant $Ca_v1.3$/PEEP by switching the $Ca_v1.3$/P1063 to E and $Ca_v1.3$/E1085 to P, which would mimic the proline configuration of the $Ca_v1.2$ IIIS5-3P loop. This mutant generated a voltage-dependent activation at -27mV, 3mV more positive than $Ca_v1.3$. It generated voltage-dependent inactivation at -36mV, which was not different from the wild-type. We reported the IC_{50} for the nifedipine block of $Ca_v1.3$/PEEP to be 188 ± 28nM, which was not significantly different from IC_{50} for the block of $Ca_v1.3$ at 289nM (Figure 3.6.C). This mutant also produced a

decreased efficacy of nifedipine as the fractional block only reached 60 percent at maximally effective concentrations of nifedipine. The dose-response curve for the nifedipine block of $Ca_v1.3$/PEEP generated a slower Hill slope constant at 0.43 ± 0.02, which was shallower than that of $Ca_v1.3$ ($P < 0.001$).

Besides mimicking proline configuration, we were also interested in the proximal region of this IIIS5- 3P loop, which contains more divergent amino acids than the other parts of the loop. Three negatively charged residues in $Ca_v1.2$ were reported to affect DHP binding affinity: $Ca_v1.2$/D1063. $Ca_v1.2$/E1069 and $Ca_v1.2$/E1071 (Wang et al., 2007). $Ca_v1.3$/D1057 and $Ca_v1.3$/E1065 were conserved in $Ca_v1.3$. $Ca_v1.3$/P1063, which we made a mutation previously based on the assumption of proline configuration corresponds to the position of $Ca_v1.2$ E1071. Therefore, we came up with the idea to insert six amino acids $Ca_v1.2$/SSKQTEA from 1064 to 1070 (shown in the red box on Figure 3.6.A) into the corresponding positions of $Ca_v1.3$/EAKSNPE from 1058 to 1064. The mutant $Ca_v1.3$/N6 formed functional channels, but the mutation causes an outward current in the presence of 180 mM NMDG in the extracellular solution and the absence of NMDG in the intracellular solution. Hence, we used an NMDG-balanced solution (see Chapter 2) to measure the electric activities of $Ca_v1.3$/N6, which restored inward Ba^{2+} current. We reported the voltage-dependent activation of $Ca_v1.3$/N6 under a new solution set as -17 ± 0.8mV, which was 13mV more positive than $Ca_v1.3$. The voltage-dependent inactivation of this mutant fell at -34 ± 0.6mV, which was not significantly different from the wild-type. The IC_{50} for the nifedipine block of $Ca_v1.3$/N6 was 116 ± 53nM, which was lower than that of $Ca_v1.3$/PEEP and $Ca_v1.3$ ($P < 0.05$), closer to that of $Ca_v1.3$+ and $Ca_v1.3$/SA, but it also flattened the dose-response curve like $Ca_v1.3$/PEEP (Figure 3.6.D). We reported the Hill slope constant of the dose-response curve as 0.52 ± 0.1, which was also less than that of $Ca_v1.3$. Even though $Ca_v1.3$/SA almost reproduced the shift of DHP sensitivity of $Ca_v1.3$+, the divergent amino acids in the proximal region of the IIIS5-3P loop might play supportive roles in DHP binding affinity and ion selectivity of the pore.

Interestingly, the mutation sites were close to binding sites of $Ca_v\alpha2\delta$-1 (Bourdin et al., 2017; Briot et al., 2018) (Figure 3.8). Additionally, $Ca_v\alpha2\delta$-1 modulates voltage-sensing domain activations and Ca^{2+} influx (Savalli et al., 2016). The mutations in $Ca_v1.3$/PEEP and $Ca_v1.3$/N6 may interfere with the interaction between $Ca_v1.3$ and $Ca_v\alpha_2\delta$-1 and change the channel gating, cation permeability, and DHP efficacy.

Figure 3.6. Significant amino acids in extracellular IIIS5-3P loop in response to Nifedipine block. (**A**) Topological representation of the L-VGCC with sequence alignments of $Ca_v1.2$ (a.a 1058-1118) and $Ca_v1.3$ (a.a 1052-1112) at IIIS5-3P helix loop. Twenty-four out of sixty amino acids in $Ca_v1.3$ are not conserved in $Ca_v1.2$. Dashes indicate identical amino acids. Asterisks at the proximal and distal regions indicate amino acid residues previously reported to affect dihydropyridine modulation of $Ca_v1.2$. $Ca_v1.2$/E1118 and $Ca_v1.3$/E1112 at the ends were glutamates associated with the Ca^{2+} selectivity filter. (**B**) Dose-response curve for nifedipine block of $Ca_v1.3$+, $Ca_v1.3$/SA and $Ca_v1.3$. The $Ca_v1.3$+ mutant incorporated the IIIS3-3P loop of $Ca_v1.2$ into the corresponding segment of $Ca_v1.3$. The $Ca_v1.3$/SA mutant included the $Ca_v1.3$/S1100 to A single switch. Both $Ca_v1.3$/SA (gray circles) and $Ca_v1.3$+ (black circles) are more sensitive to nifedipine than $Ca_v1.3$ (white circles) ($P < 0.01$; $P < 0.001$, respectively). IC_{50} for nifedipine block of $Ca_v1.3$+ is 101 ± 4nM (N = 6~8). IC_{50} for nifedipine block of $Ca_v1.3$/SA is 99 ± 24nM (N = 4~5). (**C**) Dose-response curve for nifedipine block of $Ca_v1.3$/PEEP and $Ca_v1.3$. $Ca_v1.3$/PEEP mutant included the $Ca_v1.3$/P1063 to E and $Ca_v1.3$/E1085 to P double mutations. The IC_{50} for the nifedipine block of $Ca_v1.3$/PEEP (black circles) is 188 ± 28nM (N = 3~7), not different from that of $Ca_v1.3$ (white circles). The Hill slope constant was 0.43 ± 0.02, shallower than that of $Ca_v1.3$ at 0.78 ± 0.04 ($P < 0.001$). (**D**) Dose-response curve for nifedipine block of $Ca_v1.3$/N6 and $Ca_v1.3$. $Ca_v1.3$/N6 incorporated the six amino acids in $Ca_v1.2$ framed in the red box shown in (A) into $Ca_v1.3$. The IC_{50} for nifedipine block of $Ca_v1.3$/N6 was 116 ± 53 nM (N = 5~9), lower than that of $Ca_v1.3$ ($P < 0.05$). The Hill slope constant was reported to be 0.52 ± 0.10, shallower than that for $Ca_v1.3$ at 0.78 ± 0.04 ($P < 0.05$) (**E**) Dose-response curve for nifedipine block of $Ca_v1.3$+V, $Ca_v1.2$ and $Ca_v1.3$. $Ca_v1.3$+V was made from $Ca_v1.3$+V with $Ca_v1.3$/MV mutation at IIIS5 transmembrane. The IC_{50} for the nifedipine block of $Ca_v1.3$+V was reported to be 42 ± 5 nM (N = 4~10), which was much lower than that for $Ca_v1.3$ at 289nM ($P < 0.001$) and closer to $Ca_v1.2$.

Figure 3.6 Continued

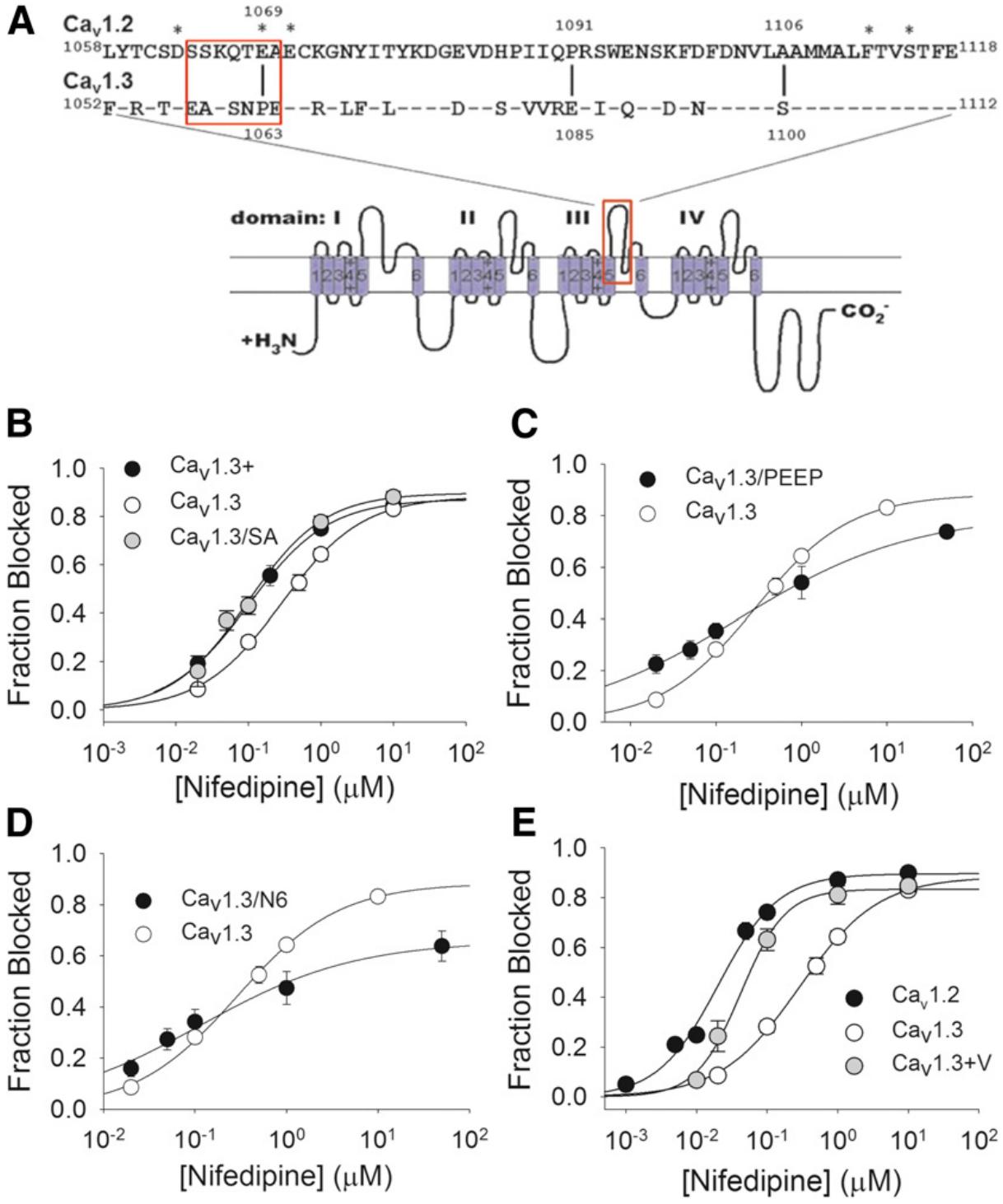

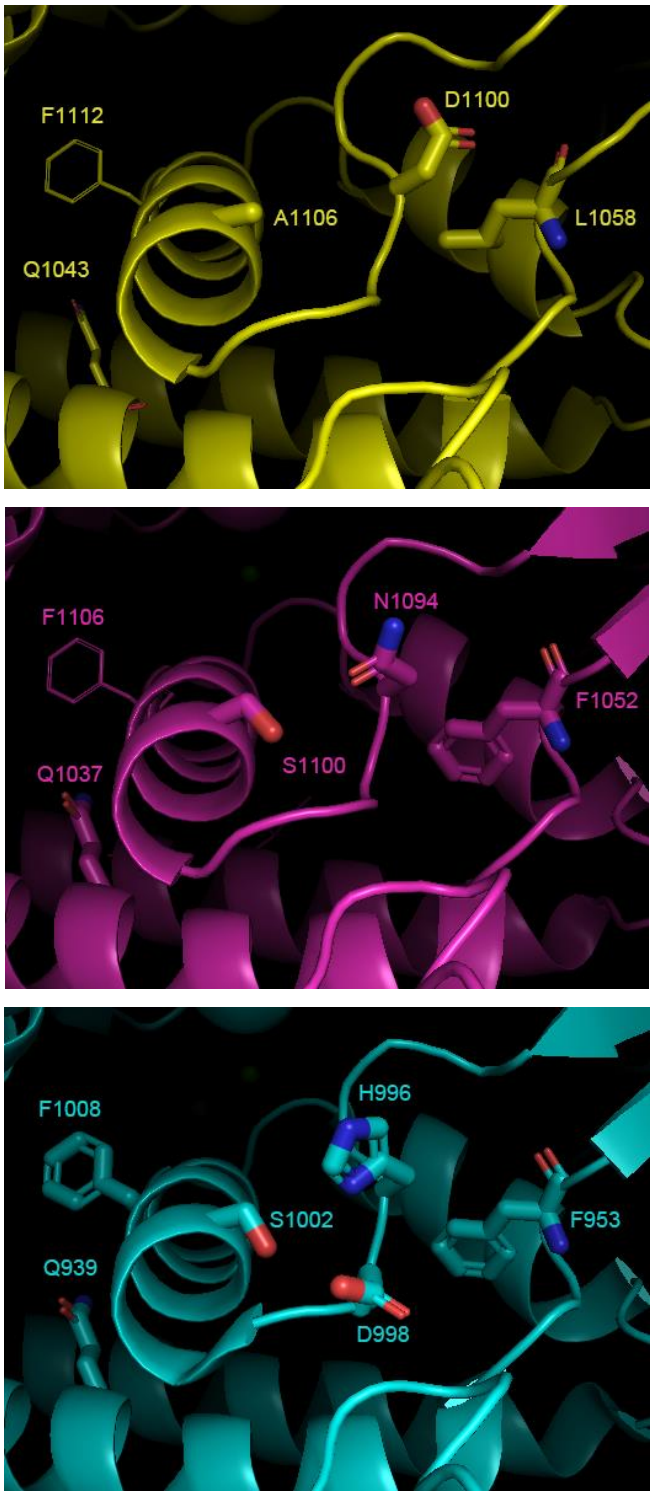

Figure 3.7. Homology models of $Ca_v1.2$ (yellow), $Ca_v1.3$ (purple), and CryoEM of $Ca_v1.1$ (cyan) at the backside of the 3P helix. $Ca_v1.3$ in the middle shows a potential H-bond between the $Ca_v1.3$-specific residues S1100 and N1094, while $Ca_v1.2$ with A1106 and 1100 does not. $Ca_v1.1$ also exhibits a potential H-bond between S1102 and H996 facilitated by D998.

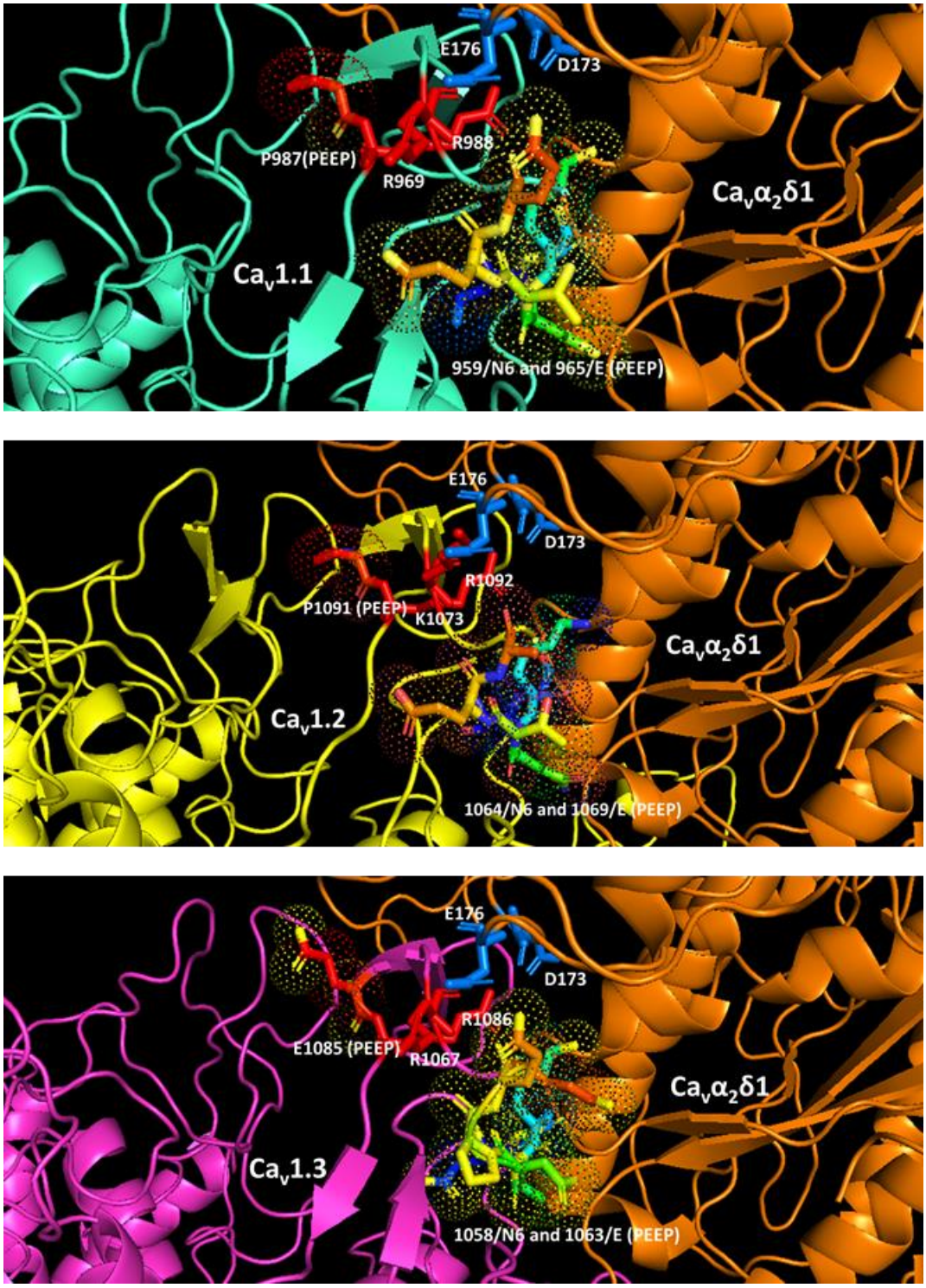

Figure 3.8. Cryo-EM structure of $Ca_v1.1$ (cyan) and 3D-models of $Ca_v1.2$ (yellow), $Ca_v1.3$ (purple) interacting with auxiliary subunit $Ca_v\alpha_2\delta$-1. The mutation sites in $Ca_v1.3$/N6 and $Ca_v1.3$/PEEP are near the interaction of Ca_v1 and $Ca_v\alpha_2\delta$-1. D173 and E176 in $Ca_v\alpha_2\delta$-1 interact with IIIS5-3P loop at R969 and R989 in $Ca_v1.1$, K1073, and K1092 in $Ca_v1.2$, and R1067 and R1086 in $Ca_v1.3$.

3.7 Combinational mutations of both transmembrane and loop in response to Nifedipine

Considering the promising but relatively modest nifedipine sensitivity shift of $Ca_v1.3$/MV in IIIS5 transmembrane and $Ca_v1.3$+ in extracellular IIIS5-3P loop, we asked whether the combination of these two mutations would generate an increased potency of nifedipine block. The mutant $Ca_v1.3$+V was created, and we reported its voltage-dependent activation and inactivation like all the channels we have characterized. $V_{1/2}$ inactivation of $Ca_v1.3$+V was reported to be -42 ± 0.3 (N = 4), shifted by -6mV compared with $Ca_v1.3$. $V_{1/2}$ activation of $Ca_v1.3$+V was reported to be -27 ± 0.8 (N = 8), not different from the wild-type (Table 3.1). As expected, the IC_{50} for the nifedipine block of $Ca_v1.3$+V was reduced compared to $Ca_v1.3$/MV and $Ca_v1.3$+. This mutant generated a value of 42 ± 5 nM (Figure 3.6.E), compared with 289 ± 30nM for $Ca_v1.3$ ($P < 0.001$), closer but still greater than IC_{50} of nifedipine block for $Ca_v1.2$ at 22nM ($P < 0.05$).

Considering the 20nM difference between the combinational mutant $Ca_v1.3$+V and $Ca_v1.2$, we tried to look for other amino acids in other DHP binding pockets to fill the remaining gap in nifedipine potency. Besides IIIS5 and IIIS5-3P loop in domain III, IIIS6 also contributes to the DHP binding pocket in $Ca_v1.2$, depicted in Figure 3.3.B (Hockerman et al., 1997c). Since this domain is highly conserved with only one divergent amino acid, $Ca_v1.2$/I1156, and $Ca_v1.3$/V1150, and mutation of $Ca_v1.2$/I1156 to alanine resulted in a significant decrease in DHP binding affinity (Peterson et al., 1997). We generated $Ca_v1.3$/V1150I but we found mutant yielded little to no current upon expression in tsA201 cells.

3.8 Molecular determinants in extracellular IIIS5-3P loop in response to FPL 64176

3.8.1 Significant amino acids in III5-3P loop to differentiate $Ca_v1.2$ and $Ca_v1.3$

We have made some progress in differentiating $Ca_v1.2$ and $Ca_v1.3$ in response to the universal L-VGCC antagonist, nifedipine in the drug class of dihydropyridine, and we shifted our attention to an agonist, a non-dihydropyridine compound FPL 64176 (methyl 2,5-dimethyl-4-[2-(phenylmethyl)benzoyl]-1H-pyrrole-3-carboxylate; FPL, Figure 3.10), which is calcium channel modulator specific for the L-VGCCs (Baxter et al., 1993; Ginap et al., 1993). Similar to the most common L-VGCC agonist Bay K 8644, FPL prolongs the opening of L-VGCCs during depolarization and slows the closing during repolarization (Rampe and Lacerda, 1991; Fan et al., 2000). Besides L-VGCCs, reconstruction of the DHP binding site was done in the P/Q-type

channel $Ca_v2.1$, and it conferred potentiation of current by FPL and potency by DHP antagonists (Sinnegger et al., 1997). The potentiation of $Ca_v1.2$ was well-characterized (Liu et al., 2003), but the modulation of $Ca_v1.3$ by FPL is not characterized. We compared the potency of FPL potentiation of current in $Ca_v1.2$ and $Ca_v1.3$ and modulation of deactivation.

Like the $Ca_v1.3$ mutants mentioned in chapter 3.6.3, we also characterized $Ca_v1.3$ mutants in NMDG-balanced solutions because application of FPL frequently induced outward current when the extracellular solution contained no NMDG (Figure 3.9.A). During the application of increasing concentrations of FPL, a higher-end concentration of FPL induces outward current and can be washed out by extracellular solution and returned to inward current. This observation suggests that FPL binding substantially alters the permeability of $Ca_v1.3$ to NMDG. We found that 10μM FPL stimulated the maximal increase in current in both $Ca_v1.2$ and $Ca_v1.3$, with higher concentrations leading to lower current potentiation. Therefore, to generate the EC_{50} values for FPL potentiation of current, we took the current amplitude at 10μM FPL to be 1 and normalized current amplitude at lower concentrations to that value for each cell. We determined the EC_{50} for potentiation of current amplitude in $Ca_v1.2$ by FPL at 103 ± 40 nM (Figure 3.10.A and D). The EC_{50} for potentiation of current amplitude in $Ca_v1.3$ was 854 ± 236nM ($P < 0.05$) (Figure 3.10.B and D). Thus, as with nifedipine, $Ca_v1.3$ is less sensitive to FPL than $Ca_v1.2$.

We next asked if the same amino acid that accounts for the differences in nifedipine potency in the block of $Ca_v1.2$ and $Ca_v1.3$ also account for the observed difference in FPL potency in potentiating current in these two channels. We found the EC_{50} for potentiation of current amplitude by FPL in $Ca_v1.3$+V to be 99 ± 5nM (Figure 3.10.C and D), indistinguishable from the EC_{50} for FPL potentiation of $Ca_v1.2$ at 103nM. We also found the EC_{50} for potentiation of current amplitude by FPL in $Ca_v1.3$/MV to be 737 ± 20nM, not different from the EC_{50} of $Ca_v1.3$ at 854nM (Figure 3.10.D). The results of these two mutants suggest that the molecular determinants of the difference in potency of FPL potentiation of current amplitudes lie within the IIIS5-3P loop. We were able to use standard solution sets for these experiments as FPL did not induce an outward current in $Ca_v1.2$, $Ca_v1.3$, $Ca_v1.3$+V, or $Ca_v1.3$/MV.

Considering the importance of this extracellular loop, we tried to measure FPL potency in $Ca_v1.3$+ in a standard solution set, but outward current was observed in the presence of FPL (Figure 3.9.A). However, the NMDG-solution set also did not generate useful data (Figure 3.9.B). We were unable to measure the potency of the FPL potentiation of this mutant because FPL induced

erratic changes in current amplitude and the accurate 10μM baseline for an authentic dose-response curve. Additional IIIS5-3P mutants such as $Ca_v1.3$/PEEP, $Ca_v1.3$/N6, and $Ca_v1.3$/SA were successfully measured to obtain the potency of FPL potentiation, but it was found that none of these mutants displayed increased sensitivity to potentiation of current induced by FPL compared with $Ca_v1.3$ (Table 3.1). In fact, $Ca_v1.3$/PEEP and $Ca_v1.3$/SA exhibited decreased sensitivity to potentiation of current by FPL. In the previous chapters, we have identified two regions of amino acid divergence between $Ca_v1.2$ and $Ca_v1.3$ within the IIIS5-3P loop, including $Ca_v1.2$/A1106 to $Ca_v1.3$/S1100 and $Ca_v1.2$ 1064~1070/ $Ca_v1.3$ 1058~64, to confer differences in sensitivity to nifedipine block but not in FPL potentiation of these two channel subtypes.

Next, we explored the IIIS5-3P loop and determined the significant amino acids to differentiate $Ca_v1.2$ and $Ca_v1.3$ potentiation by FPL (See Figure 3.6.A). We generated a switch from $Ca_v1.3$/F1052 to $Ca_v1.2$/L1058 and reported an EC_{50} for FPL potentiation of this $Ca_v1.3$/FL mutant at 275nM (Figure 3.11) in the NMDG-balanced solution as it unpredictably had outward currents in the standard solution set in the presence of a micromolar concentration of FPL. This result was significantly lower than that of $Ca_v1.3$ at 835nM ($P < 0.001$) but not as close as $Ca_v1.2$ or $Ca_v1.3$+V. We shifted our focus to a more highly conserved N-terminal region of the loop, which includes more amino acids in common between $Ca_v1.2$ and $Ca_v1.3$. A little further from the critical DHP interacting sites (Figure 3.11.A asterisk *), including the significant $Ca_v1.3$/S1100 mentioned in the previous section, we chose to mutate $Ca_v1.3$/Q1089, $Ca_v1.3$/D1092, and $Ca_v1.3$/N1094 into the corresponding $Ca_v1.2$/E1095, $Ca_v1.2$/K1098 and $Ca_v1.2$/D1010. With these three mutations plus and $Ca_v1.3$/SA, we generated the $Ca_v1.3$ mutant with four point-mutations as $Ca_v1.3$/QDNS. Unfortunately, like $Ca_v1.3$/VI we prepared in the previous chapter, this mutant failed to express detectable current. We incorporated the F1052L mutation into the QDNS mutant to create a new $Ca_v1.3$/FQDNS mutant. Fortunately, this mutant expressed well, and we were able to record its electric activity in the standard solution set without outward current induced by high concentration of FPL. The EC_{50} for FPL potentiation of the $Ca_v1.3$/FQDNS mutant was 133nM, close to that of $Ca_v1.2$ and $Ca_v1.3$+V at around 100nM (Figure 3.11). These three mutants have provided solid proof of the importance of $Ca_v1.3$/F1052 in differentiating FPL potentiation between $Ca_v1.2$ and $Ca_v1.3$. Moreover, the more conserved N-terminal portion of the IIIS5-3P loop, including Q1089, D1092, N1094, and S1100, also contribute to the differential potentiation of $Ca_v1.2$ and $Ca_v1.3$ by FPL (Figure 3.12).

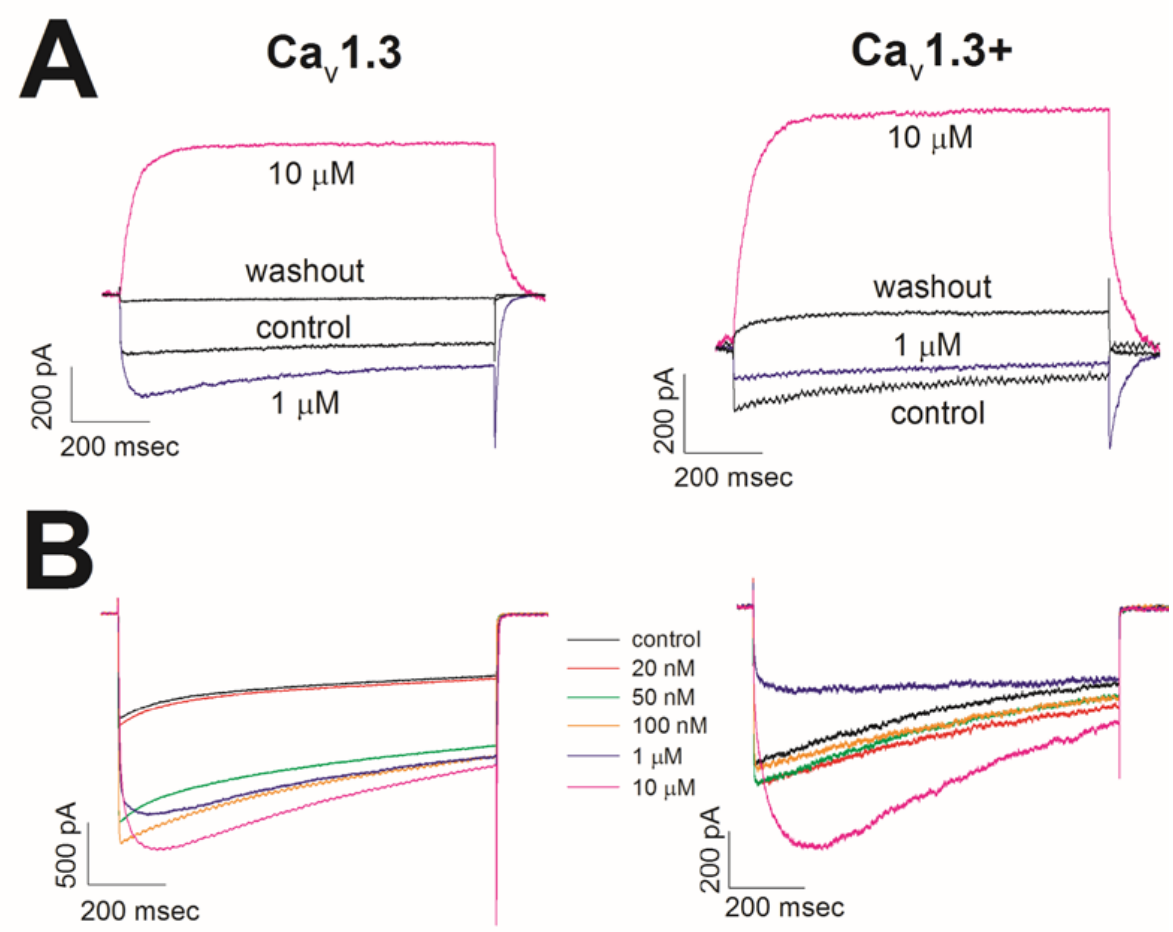

Figure 3.9. FPL 64176 effect on $Ca_v1.3$ and $Ca_v1.3+$ conducting currents. (**A**) Example traces of current through $Ca_v1.3$ (left) or $Ca_v1.3+$ (right) elicited with a step to 0 mV from a holding potential of -80mV using the standard solution set. FPL 64176 was applied at 1 and 10μM via extracellular perfusion as described in Chapter 2 materials and methods. (**B**) Example dose-response experiments with $Ca_v1.3$ and $Ca_v1.3+$ with FPL 64176 treatment using the NMDG-balanced solution set described in Chapter 2 material and methods. Note the current amplitude increase in $Ca_v1.3+$ at 50 and 100nM FPL and reduction in current amplitude at 1μM, even though channel activation is slower at lower concentrations.

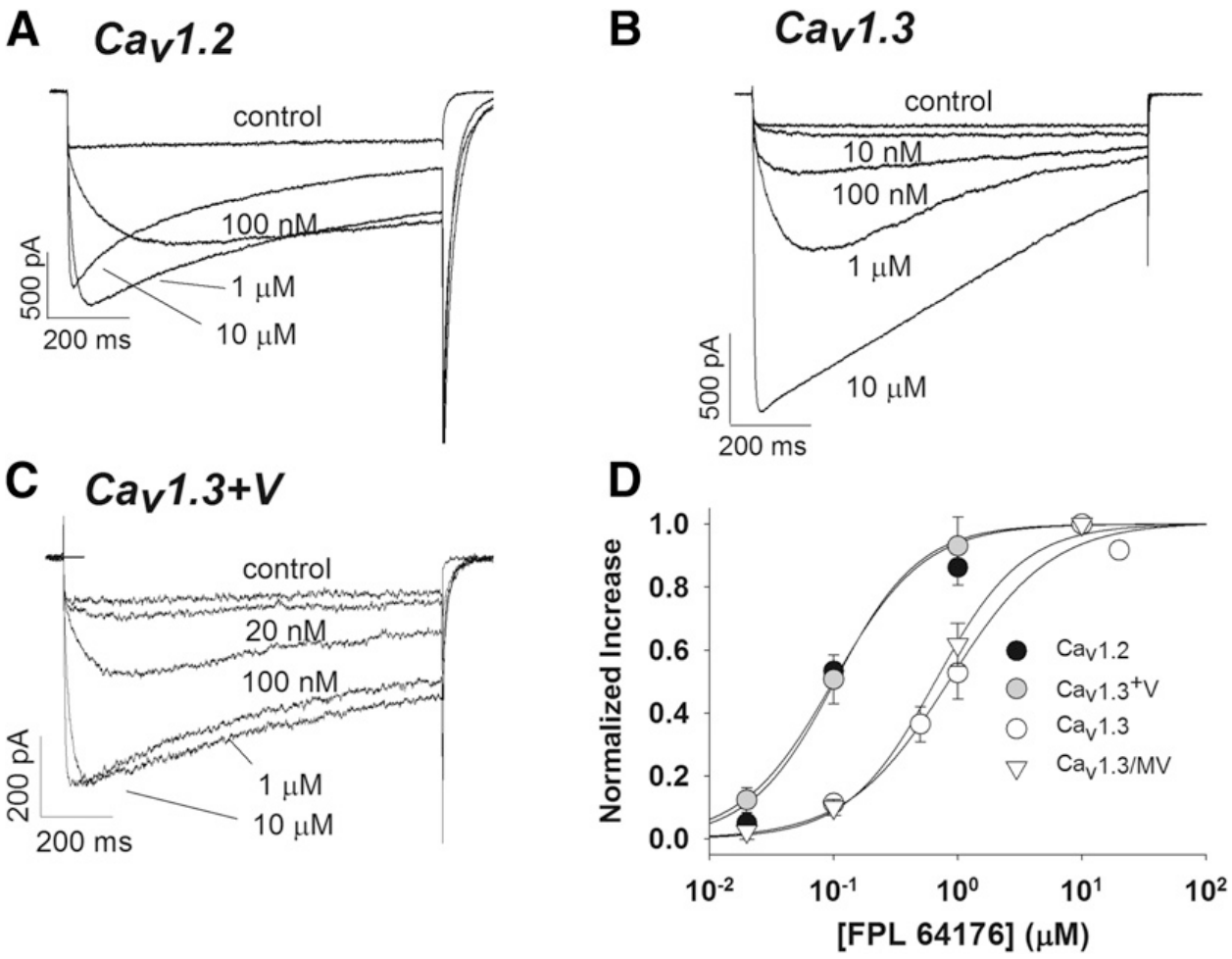

Figure 3.10. The potency of FPL 64176 potentiation of $Ca_v1.2$, $Ca_v1.3$, and mutant channels $Ca_v1.3$+V and $Ca_v1.3$/MV. (**A-C**) Example traces of $Ca_v1.2$, $Ca_v1.3$, and $Ca_v1.3$+V with indicated FPL concentrations in NMDG-balanced solution sets. Note the marked slowing of tail current in $Ca_v1.2$ that is absent in $Ca_v1.3$. $Ca_v1.3$+V has a moderately slow tail compared with the two wild-types. (**D**) Dose-response curves for FPL 64176 potentiation of $Ca_v1.2$, $Ca_v1.3$, and mutant channels $Ca_v1.3$+V and $Ca_v1.3$/MV. The EC_{50} values for FPL potentiation of current amplitude for $Ca_v1.2$ and $Ca_v1.3$ were 103 ± 40nM (N= 3~8) and 854 ± 236nM (N= 3~7), respectively ($P < 0.05$). The EC_{50} values for FPL potentiation of the mutant $Ca_v1.3$+V at 99 ± 5nM (N= 3~7) were not much different from that of $Ca_v1.2$ but were very different from that of $Ca_v1.3$ ($P < 0.005$). In contrast, the EC_{50} for FPL potentiation of the mutant $Ca_v1.3$/MV was 737 ± 20nM (N=5), not very different from that of $Ca_v1.3$. Data are shown as the mean fractional increase in current compared with 10μM FPL 64176 ± S.E.

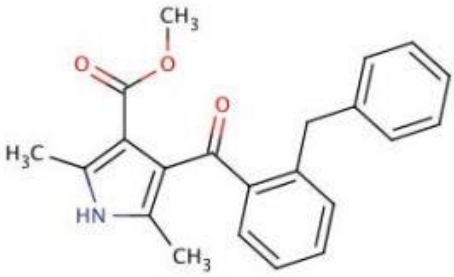

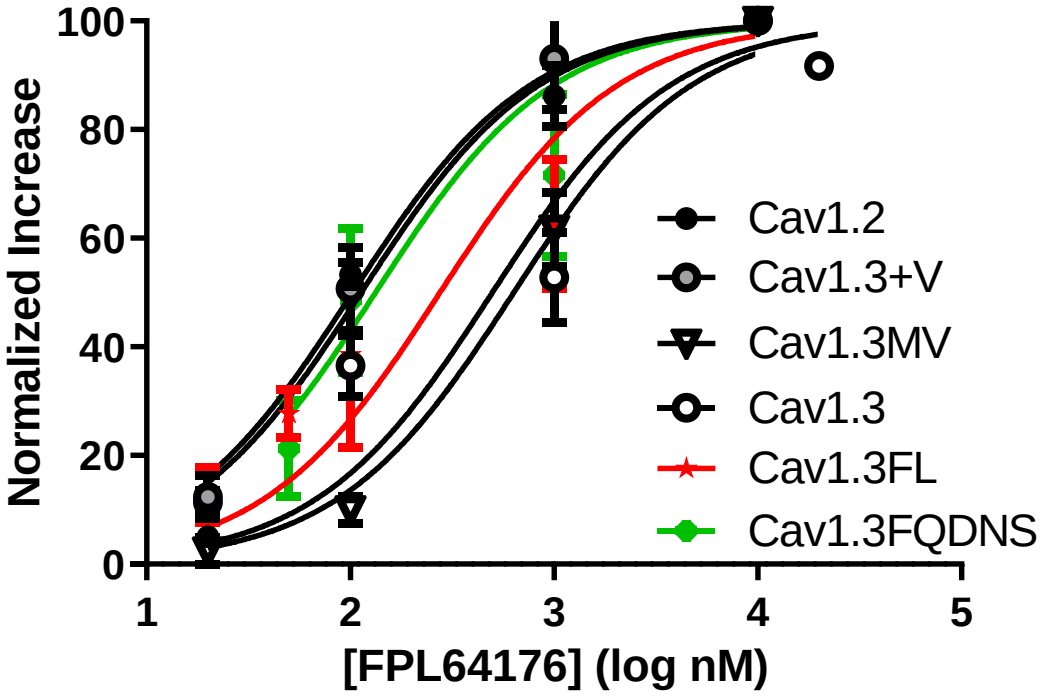

Figure 3.11. Structure of FPL64176 and its potentiation of $Ca_v1.2$, $Ca_v1.3$, and mutant channels. Dose-response curves for FPL 64176 potentiation of $Ca_v1.2$, $Ca_v1.3$, and mutant channels $Ca_v1.3$+V, $Ca_v1.3$/MV, $Ca_v1.3$ /FL, and $Ca_v1.3$/FQDNS (as extended from Figure 3.9.D). The EC_{50} values for FPL potentiation of current amplitude for $Ca_v1.3$/FL was 275 ± 12nM (log (2.44 ± 0.069), N= 3~17) and for $Ca_v1.3$/FQDNS was 133 ± 11nM (log(2.214 ± 0.047), N= 7~20). Both were significantly different from $Ca_v1.3$ ($P < 0.05$) but not $Ca_v1.2$. Data are shown as the mean fractional increase in current compared with 10μM FPL 64176 ± S.E.

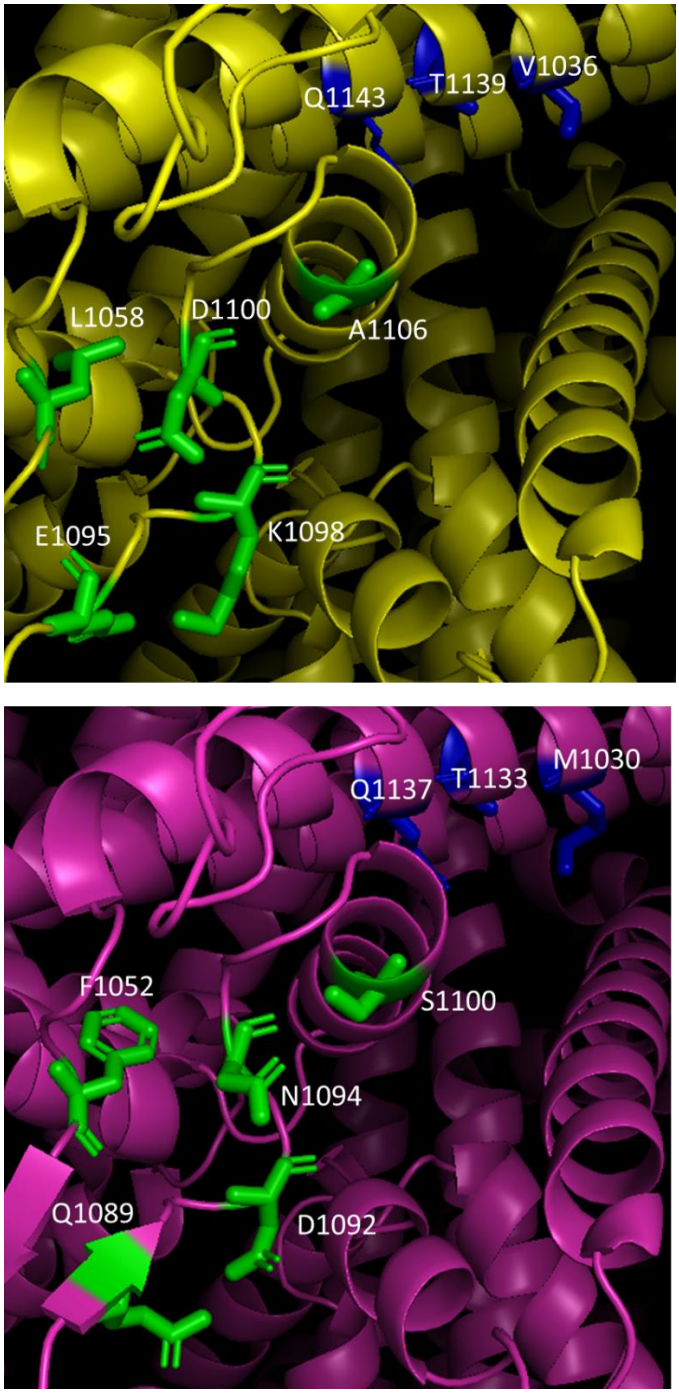

Figure 3.12. Homology models of $Ca_v1.2$ (yellow), $Ca_v1.3$ (purple) of the beginning of the 3P helix. The frame also includes significant amino acids in the transmembrane IIIS5 region. $Ca_v1.3$/F1052 to $Ca_v1.2$/L1058 mutation increased the potency of FPL potentiation. $Ca_v1.3$/N1094 to $Ca_v1.2$/D1100 without $Ca_v1.3$/FL mutation silenced the channel. $Ca_v1.3$ might exhibit a bigger hydrophobic guardian amino acid to inhibit the access of FPL.

3.8.2 Slowing kinetics of deactivation in $Ca_v1.3$ versus $Ca_v1.2$

During current measurements of Cav1.2 and Cav1.3 at a holding voltage of -80mV in response to FPL, we noticed strong effects on the kinetics of deactivation and the voltage-dependent activation of $Ca_v1.2$ and $Ca_v1.3$. The tail current changes in Figure 3.10.A and B are replotted with only baseline (control) and measurements in the presence of 10μM FPL in Figure 3.13.A and B with higher resolution on tail-current kinetics as a measure of the rate of deactivation. $Ca_v1.3$ displays a fast rate of closing with a single time constant (τ) at 0.41ms in the absence of FPL and a slower τ of 11ms in the presence of FPL (Figure 3.13.A; Table 3.2). In contrast, for $Ca_v1.2$, which has a much slower deactivation, two τs were observed (fast and slow) in the absence of FPL. However, a single slow τ is principally observed in the presence of FPL that is greater than both τs in the absence of FPL (Figure 3.13.B; Table 3.2).

Considering the difference in the kinetics of deactivation in $Ca_v1.3$ versus $Ca_v1.2$ in the absence of FPL, we compared the FPL-induced slowing of deactivation in both subtype channels by measuring the fraction of the tail current remaining 10 milliseconds after reaching a peak (R10). The R10 measured for both $Ca_v1.2$ and $Ca_v1.3$ in the absence of FPL was negligible as they both flatten out in the process of deactivation. In contrast, in the presence of 10 μM FPL, R10 in $Ca_v1.2$ was 0.67 ± 0.09, greater than that of $Ca_v1.3$ at 0.15 ± 0.02 (Figure 3.10.C; $P < 0.001$). This result indicated that $Ca_v1.2$ has a greater slowing of deactivation induced by FPL. Moreover, we also found that FPL shifted the $V_{1/2}$ activation of $Ca_v1.2$ by -26mV but only -10mV in $Ca_v1.3$ (Table 3.2). In addition to more potently potentiating current amplitude in $Ca_v1.2$ compared to $Ca_v1.3$, FPL also imposes stronger effects on deactivation kinetics and voltage-dependence of activation in $Ca_v1.2$ at a maximally effective concentration of 10μM.

Besides characterizing tail current kinetics in the deactivation of these two wild-type channels in response to FPL, we were curious whether the mutant channel $Ca_v1.3$/DHPi was also less sensitive to FPL than $Ca_v1.3$. Deactivation of $Ca_v1.3$/DHPi exhibited a single τ that was indistinguishable from that of wild-type $Ca_v1.3$ (Table 3.2), and this value was not altered after application of 10μM FPL (Figure 3.13.D and E), that both τs fell around 0.6 milliseconds. No significant increase in current amplitude was observed upon application of 10 μM FPL to $Ca_v1.3$/DHPi. The $V_{1/2}$ activation of $Ca_v1.3$DHPi in the presence of 10 μM FPL shifted by -9mV (Table 3.1). Since IIIS5 has shown clear evidence of a crucial role in FPL actions, we also examined the kinetics of deactivation of $Ca_v1.3$/MV (Figure 3.13.F) as it is the only mutant based

on the IIIS5 transmembrane region. $Ca_v1.3$/MV showed a deactivation in the absence of FPL, with a single τ (0.71 ± 0.04 milliseconds) that was slightly but statistically significantly greater than that of $Ca_v1.3$ at 0.41 ± 0.07 milliseconds (**P < 0.01) (Figure 3.13.G). In the presence of 10μM FPL, $Ca_v1.3$/MV displays a greater R10 at 0.52 ± 0.15 (*P < 0.05) compared to that of wild-type $Ca_v1.3$ (Figure 3.13.H). As for the reciprocal mutant $Ca_v1.2$/VM, the deactivation was not different from that of $Ca_v1.2$ either in the absence of the presence of FPL (Table 3.2). Thus, the M to V switch at position 1030 of $Ca_v1.3$ does not affect the FPL potency but does affect both deactivation and slowing of deactivation by FPL.

We were also interested in the kinetics of deactivation of new mutants we made to differentiate the FPL potentiation of $Ca_v1.2$ and $Ca_v1.3$. $Ca_v1.3$/FL and $Ca_v1.3$/FQDNS were measured in the same manner to see whether their tail current kinetics were slowed by FPL potentiation. Similar normalization was applied by framing a 25-millisecond duration starting from the tail current peak. A single exponential equation was fit to the normalized data. Plateau (Fractions in Table 3.2) was generated by using the formula f=a*(1-exp(-b*x)) with two parameters, along with τ values which are 1/b. We found that both $Ca_v1.3$/FL and $Ca_v1.3$/FQDNS have a very fast deactivation which was not significantly affected by FPL potentiation (Figure 3.14 and Table 3.2) like $Ca_v1.2$ or $Ca_v1.3$, but closer to $Ca_v1.3$/DHPi. We also found that the time constants for tail current decay in $Ca_v1.3$/FQDNS and $Ca_v1.3$/FL are decreased (i.e., decay is accelerated) upon application of FPL. The fast time constant, high plateau, and low R10 in the absence and presence of 10μM FPL suggest FPL potentiates current amplitude with no slowing of channel closing in these mutants. Altogether, we found $Ca_v1.3$/MV in transmembrane IIIS5 to regulate FPL-induced slowing of deactivation. On the other hand, $Ca_v1.3$/FL enhances the potency of FPL in potentiating current but diminished FPL regulation of channel closing.

Figure 3.13. Tail-current kinetics decay in the presence and absence of FPL 64176 in $Ca_v1.2$, $Ca_v1.3$, and mutant channels. (**A**) Example trace of 100-millisecond depolarization demonstrating tail-current decay in $Ca_v1.3$ in the presence or absence of 10μM FPL 64176. (**B**) Example trace of 100-millisecond depolarization demonstrating tail-current decay in $Ca_v1.2$ in the presence and absence of 10μM FPL 64716. (**C**) The R10 value (fraction of tail current remaining 10 milliseconds after peak) in the presence or absence of 10μM FPL was greater in $Ca_v1.2$ (0.67 ± 0.09, N =6) compared with that of $Ca_v1.3$ (0.15 ± 0.02, N=5) (***$P < 0.001$). (**D**) Example trace of 100-millisecond depolarization demonstrating tail-current decay in $Ca_v1.3$/DHPi in the presence and absence of 10μM FPL 64176. (**E**) The time constant for deactivation of $Ca_v1.3$/DHPi (τ =0.59 ± 0.11 milliseconds, N=5) was not affected by the presence of 10μM FPL (τ = 0.60 ± 0.04 milliseconds, N=5). (**F**) Example trace of 100-millisecond depolarizing demonstrating tail-current decay in $Ca_v1.3$/MV in the presence or absence of 10μM FPL 64176. (**G**) The time constant for deactivation of $Ca_v1.3$/MV in the absence of FPL followed a single time constant (τ = 0.70 ± 0.13 milliseconds, N=5) that was slower than that of $Ca_v1.3$ (**$P < 0.01$). (H) The R10 value for $Ca_v1.3$/MV tail current in the presence of 10 μM FPL (0.51 ± 0.15, N=5) was greater than that of $Ca_v1.3$ (*$P < 0.05$)

Figure 3.13 Continued

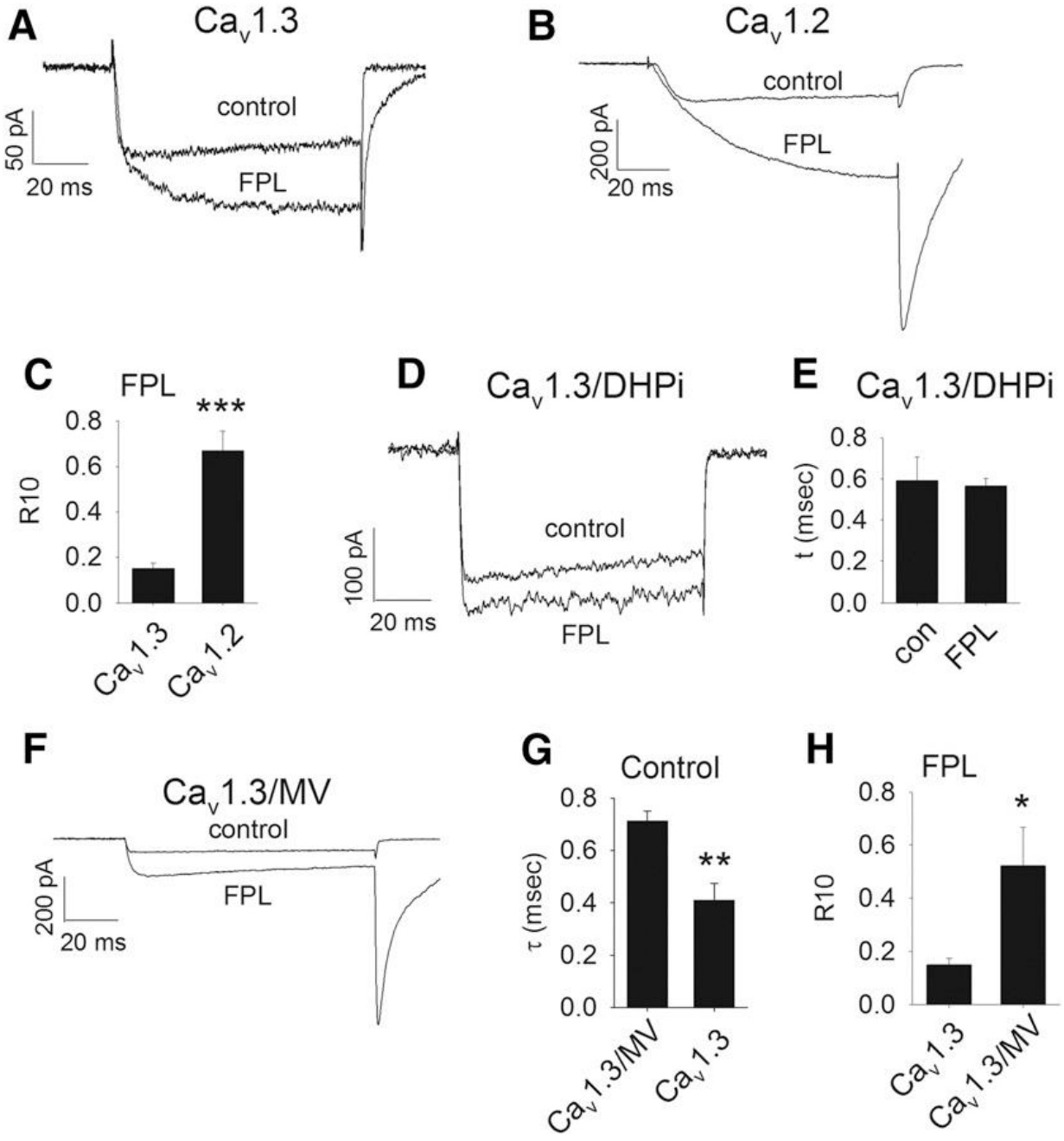

Figure 3.14. FPL potentiation and tail-current kinetics of $Ca_v1.3$/FL and $Ca_v1.3$/FQDNS. (**A**) Example trace of 100-millisecond depolarization demonstrating tail-current decay in $Ca_v1.3$ mutants in the presence or absence of 10μM FPL 64176 in $Ca_v1.3$/FQDNS (left) and $Ca_v1.3$/FL (right). (**B**) Bar graph of the fractional current closed (Plateau in the absence and presence of FPL) and R10 value (fraction of tail current remaining 10 milliseconds after the peak in the presence of FPL) measured of $Ca_v1.2$, $Ca_v1.3$, $Ca_v1.3$/FL, and $Ca_v1.3$/FQDNS. R10 of $Ca_v1.2$ was smaller than that of $Ca_v1.3$ and $Ca_v1.3$ mutants, and both wild-types decreased after FPL treatment, and the mutants remained stable. (**C**) Bar graph of time constant τ in the absence and presence of 10μM FPL, the measurement was relatively smaller in wild-type $Ca_v1.2$ and $Ca_v1.3$ but significantly greater after FPL treatment than that of $Ca_v1.3$/FL and $Ca_v1.3$/FQDNS (***P < 0.00001). $Ca_v1.3$/FL is also significantly different from $Ca_v1.3$/FQDNS in the presence of FPL (*P <0.05)

Figure 3.14 Continued

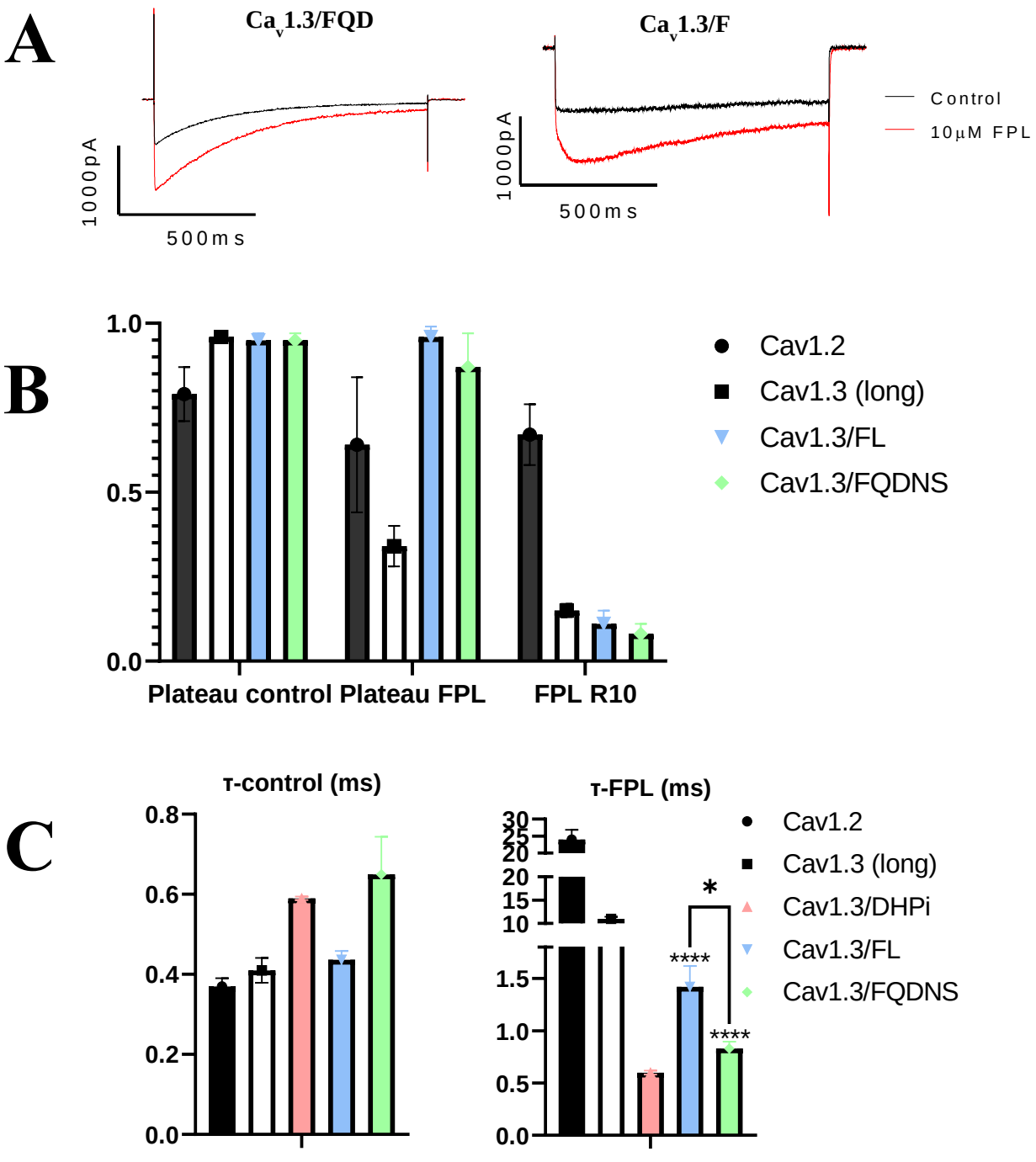

3.9 Discussion

3.9.1 Summary of characterization of $Ca_v1.2$, $Ca_v1.3$, and mutant channels

Table 3.1. Pharmacology and Voltage-Dependence of $Ca_v1.2$, $Ca_v1.3$, and Mutant Channels

Channel (+ β_3 & $\alpha_2\delta_1$)	Nifedipine IC_{50} (nM)	Nifedipine Hill Slope	Nifedipine Max %	FPL64176 EC_{50} (nM)
$Ca_v1.2$	22 ± 2 N = 3~12	1.0 ± 0.1	90 ± 3	103 ± 40 N = 3~8
$Ca_v1.3$ (long)	289 ± 30 N = 7	0.78 ± 0.05	88 ± 2	854 ± 236* N = 3~7
$Ca_v1.3$ 42a (short)	436 ± 24 N = 5~6	1.0 ± 0.05	91 ± 2	ND
$Ca_v1.3$/DHPi	~93000 N = 2~16	ND	ND	ND
$Ca_v1.3$/MV	89 ± 7 N = 5~7	1.3 ± 0.15	81 ± 2	737 ± 20 N = 3~7
$Ca_v1.2$/VM	39 ± 6 N = 4~6	0.83 ± 0.11	94 ± 4	ND
$Ca_v1.3$+	101 ± 4 N = 6~8	0.79 ± 0.02	87 ± 1	ND
$Ca_v1.3$+V	42 ± 5 N = 4~10	1.4 ± 0.16	83 ± 2	99 ± 5 N = 3~7
$Ca_v1.3$/PEEP	188 ± 28 N = 3~7	0.43 ± 0.02	80 ± 2	1166 ± 75 N = 4~5
$Ca_v1.3$/N6	116 ± 53* N = 5~9	0.52 ± 0.12	66 ± 5	813 ± 477* N = 8~12
$Ca_v1.3$/SA	99 ± 24 N = 4~5	0.82 ± 0.2	90 ± 5	2566 ± 952 N = 3~18
$Ca_v1.3$/FL	NA	NA	NA	275 ± 12* N = 3~17
$Ca_v1.3$/FQNDS	NA	NA	NA	133 ± 11 N = 7~20

*Balanced NMDG solutions

Table 3.1 (continued).

Channel (+ β_3 & $\alpha_2\delta_1$)	$V_{1/2}$ inact. (mV)	$V_{1/2}$ act. (mV)	$\triangle V_{1/2}$ act. FPL (mV)
$Ca_v1.2$	-41 ± 0.6 N = 6	-20 ± 0.5 N = 6	-26 ± 0.7 N = 7
$Ca_v1.3$ (long)	-36 ± 1.3 N = 5	-30 ± 1.5 N = 9	-10.2 ± 1.8 N = 9
$Ca_v1.3$ 42a (short)	-40 ± 1.2 N = 5	-28 ± 0.7 N = 5	ND
$Ca_v1.3$/DHPi	-27 ± 1.2 N = 5	-22 ± 1.1 N = 9	-9.5 ± 1.4 N = 6
$Ca_v1.3$/MV	-35 ± 0.5 N = 6	-26 ± 1.1 N = 23	ND
$Ca_v1.2$/VM	-38 ± 0.5 N = 6	-28 ± 1.2 N = 8	ND
$Ca_v1.3$+	-38 ± 1.6 N = 7	-27 ± 0.8 N = 12	ND
$Ca_v1.3$+V	-42 ± 0.3 N = 4	-28 ± 1.2 N = 8	-8.2 ± 1.8 N = 7
$Ca_v1.3$/PEEP	-36 ± 0.2 N = 3	-24 ± 1.0 N = 6	ND
$Ca_v1.3$/N6	-34 ± 0.6 N = 5	-22 ± 1.1 N = 9	ND
$Ca_v1.3$/SA	-49 ± 0.8 N = 12	-17 ± 0.8 N = 12	ND
Cav1.3/FL	-50 ± 0.6 N =11	-29 ± 0.3 N = 6	-2.78 ± 1.19 N = 10
Cav1.3/FQNDS	-42 ± 3.1 N =17	-3.14 ± 1.7 N = 22	-6.61 ± 1.32 N=13

*Balanced NMDG solutions

Table 3.2. Kinetics of tail current decay in the presence and absence of FPL 64176

Channel (+ β_3 & $\alpha_2\delta_1$)	Frac. Fast	τ-Fast (ms)	Frac Slow	τ-Slow (ms)
$Ca_v1.2$	0.79 ± 0.08	0.37 ± 0.05	0.18 ±0.08	6.5 ± 0.6
$Ca_v1.3$ (long)	0.96 ± 0.01	0.41± 0.07	NA	NA
$Ca_v1.3$/DHPi	0.94 ± 0.02	0.59 ± 0.01	NA	NA
$Ca_v1.3$+V	0.96 ± 0.01	0.70 ± 0.13	NA	NA
$Ca_v1.3$/MV	0.97 ± 0.01	0.71 ± 0.04*	NA	NA
$Ca_v1.2$/VM	0.96 ± 0.04	0.68 ± 0.15	NA	NA
$Ca_v1.3$/PEEP	0.96 ± 0.02	0.77 ± 0.08**	NA	NA
Cav1.3/FL	0.95 ± 0.05	0.43 ± 0.09	NA	NA
Cav1.3/FQNDS	0.95 ±0.05	0.65 ± 0.28	NA	NA

Channel (+ β_3 & $\alpha_2\delta_1$)	Frac. Slow FPL	τ-FPL (ms)	FPL R10	N
$Ca_v1.2$	0.64 ± 0.20	24 ± 7$^{\#}$	0.67 ± 0.09***	6
$Ca_v1.3$ (long)	0.34 ± 0.06	11 ± 1$^{\#\#\#}$	0.15± 0.02	5
$Ca_v1.3$/DHPi	NA	0.60 ± 0.04	ND	5
$Ca_v1.3$+V	0.84 ± 0.05	6.0 ± 1$^{\#\#}$	0.39 ± 0.07*	6
$Ca_v1.3$/MV	0.53 ± 0.13	39 ± 9$^{\#}$	0.52 ± 0.15*	5
$Ca_v1.2$/VM	0.73 ± 0.10	29 ± 7$^{\#\#}$	0.71 ± 0.08***	6
$Ca_v1.3$/PEEP	0.71 ± 0.18	12 ± 3$^{\#\#}$	0.34 ± 0.11	5
Cav1.3/FL	0.96 ± 0.03	1.42 ± 0.80***	0.11 ± 0.04	16
Cav1.3/FQNDS	0.87 ± 0.10	0.83 ± 0.20***	0.08 ± 0.03	9

*P < 0.05; **P < 0.01; ***P < 0.001 compared with Cav1.3.
#P < 0.05; ##P < 0.01; ###P < 0.001 compared with absence of FPL.

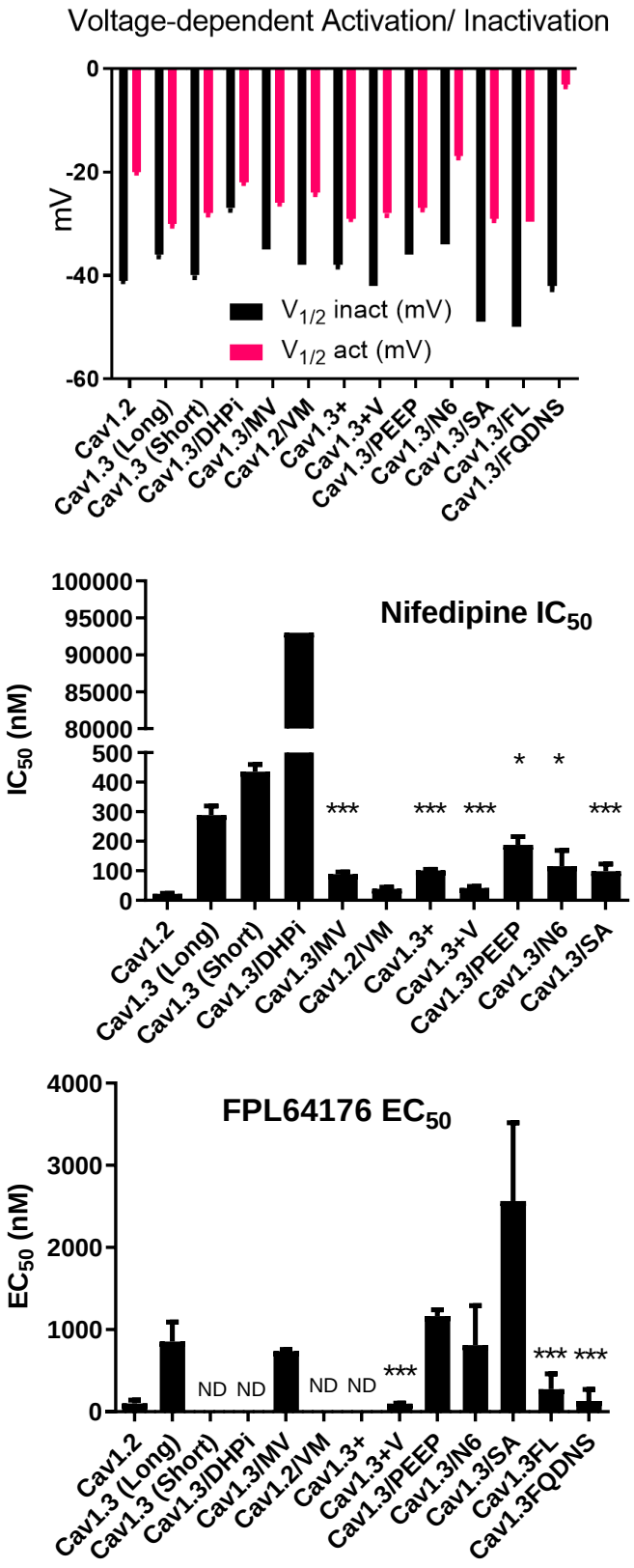

Figure 3.15. Summary of pharmacological and physiological measurements

3.9.2 Comparison between our results and past literature

Very little has been published regarding the molecular pharmacology of $Ca_v1.3$. However, the potency of $Ca_v1.3_{42}$ block by nimodipine and the voltage-dependence of activation and inactivation of that channel has been reported (Xu and Lipscombe, 2001). The $V_{1/2}$ activation we reported here is in good agreement with Xu and Lipscombe. Our choice of nifedipine among all the DHP antagonists available was due to its compact structure with no extended side chains, which might interact with amino acids outside the canonical DHP binding site. Our results showed an ~13-fold higher IC_{50} for the nifedipine block of $Ca_v1.3$ compared with $Ca_v1.2$, which is in line with the ~20-fold higher IC_{50} for nimodipine of $Ca_v1.3$ compared with $Ca_v1.2$ in Xu and Lipscombe's results. Even though no EC_{50} of agonist potentiation in $Ca_v1.3$ was previously reported, Xu and Lipscombe did report a modest shift in $V_{1/2}$ activation of $Ca_v1.3$ by 1μM concentration of DHP agonists Bay K 8644 (~-7 mV), which was in line with a modest leftward shift in $V_{1/2}$ activation we observed in Cav1.3 in the presence of 10μM FPL.

The binding affinity and block potency of the DHP antagonist PN200-110 (isradipine) for a $Ca_v1.3$ clone from the human pancreas ($Ca_v1.3_{8A}$) (Koschak et al., 2001) found that the K_D for [^{3}H]PN200-110 binding was not significantly different between $Ca_v1.3_{8A}$ and $Ca_v1.2$ cloned from rabbit cardiac muscle (Tanabe et al., 1987). However, the IC_{50} for the block of current by PN200-110 was shown to be 8.5-fold higher for $Ca_v1.3_{8A}$ than $Ca_v1.2$, which was very similar to the difference in nifedipine potency difference in blocking $Ca_v1.3$ and Cav1.2 in our study. The past studies have shown an invariably lower K_D value for binding of DHPs to L-type channels in isolated membranes compared to the IC_{50} values for the current block in electrophysiological measurements. One example we could find was PN200-110 measurements. K_D for [^{3}H]PN200-110 to the $Ca_v1.2$ clone used in Tanabe's study was 55 pM, whereas the IC_{50} for this compound block of current is 7nM (Peterson et al., 1997). Both studies indicated a single [^{3}H]PN200-110 binding site, which probably reflects the open, inactivated state of the channel at 0 mV. Thus, it is probable that the Hill slopes different from 1 that we observed for the nifedipine block of $Ca_v1.3$, and some of the mutant channels used in this study reflect the presence of distinct voltage-dependent channel conformations that regulate DHP affinity.

3.9.3 Conclusion

Our results suggest that relatively minor differences in transmembrane segment IIIS5 and the IIIS5-3P loop can largely account for the difference in potency of the nifedipine block of $Ca_v1.2$ and $Ca_v1.3$.

The IIIS5 helix is proved to be a critical component of the $Ca_v1.3$ DHP binding pocket since the mutation of T1033 and Q1037 in $Ca_v1.3$/DHPi results in a substantial loss of nifedipine potency (Figure 3.16). The single mutation in the side chains of $Ca_v1.3$/M1030 to $Ca_v1.2$/V1036 is projected to align to the same face of the IIIS5 helix as the T and Q residues required for high-potency DHP block (Mitterdorfer et al., 1996), supporting our finding that swapping the $Ca_v1.3$-specific residue at this position into $Ca_v1.2$ (V1036M) shifts nifedipine potency toward that of $Ca_v1.3$ and vice versa. These two exact mutations were later reproduced in another lab and showed the same results (Cooper et al., 2020). Interestingly, this swap of channel subtype-specific residues in this position also results in small reciprocal shifts in $V_{1/2}$ activation (Table 3.1). However, when they responded to the agonists, only the $Ca_v1.3$/MV mutant exhibited slower deactivation, both in the presence and absence of FPL (Table 3.2). This observation that decreasing the bulk of the amino acid side-chain at position M1030 in $Ca_v1.3$ affects voltage-dependence of activation, and the rate of tail-current decay suggests that position M1030 in IIIS5 (outer pore helix) may interact with IIIS6 (inner pore helix) in a manner that regulates channel gating. Models of DHP binding in $Ca_v1.2$ in previously published models suggest that amino acid residues directly interacting with DHP drugs are conserved between $Ca_v1.2$ and $Ca_v1.3$ (Cosconati et al., 2007; Tikhonov and Zhorov, 2009). To understand how subtle differences in amino acid sequence might account for a significant difference in nifedipine potency, we constructed homology models of $Ca_v1.2$ and $Ca_v1.3$ (Figure 3.3.A) based on the recently published high-resolution cryo-EM structure of $Ca_v1.1$ (Wu et al., 2016). With the help of homology models, we propose that the increase in side-chain bulk between $Ca_v1.2$ and $Ca_v1.3$ at position M1030/V1036 could potentially decrease the accessibility of nifedipine to the critical Q1037 and F1106 residues (Figure 3.4).

Besides IIIS5 transmembrane, the most divergent IIIS5-3P loop downstream of IIIS5 plays a critical role in the differentiation of $Ca_v1.2$ and $Ca_v1.3$ nifedipine inhibition sensitivity. Among all the mutants made based on the extracellular loop, $Ca_v1.3$/SA had the strongest effect on nifedipine potency. Additionally, the model predicts that S1100 in $Ca_v1.3$ can form a hydrogen bond with N1094, an interaction that could potentially constrain the movement of the 3P helix

during nifedipine binding (Figure 3.7, purple). On the other hand, the corresponding positions in $Ca_v1.2$ are occupied by an alanine residue (1106) and glutamate (1100), precluding the interaction of H-bonding formation (Figure 3.7, yellow). As for the actual cryo-EM structure of $Ca_v1.1$ colored in cyan in Figure 3.7, our finding indicates that S1100 of $Ca_v1.3$ is conserved in the corresponding position of $Ca_v1.1$ at S1002 and the position corresponding to N1094 of $Ca_v1.3$ is a histidine conserved in $Ca_v1.1$ at 996. These two residues, along with D998, may form a hydrogen bond in $Ca_v1.1$, which may contribute to the lower binding affinity of $Ca_v1.1$ for [^{3}H]PN200-110 at 270pM (Peterson et al., 1996) compared with $Ca_v1.2$ at 55pM (Peterson et al., 1997). Thus, our model suggests that the effect of the $Ca_v1.3$/SA mutation on nifedipine potency might be indirect and that the displacement of the 3P helix may be required for the high potency block of $Ca_v1.2$ by DHP antagonists.

Our studies of FPL, the non-dihydropyridine agonist, effects of potentiating $Ca_v1.2$, $Ca_v1.3$, and various mutant channels also yielded some novel results. Similar to DHP agonist Bay K, FPL shows a much higher potency in potentiating current amplitudes in $Ca_v1.2$ compared with $Ca_v1.3$ (Figure 3.9). This FPL potentiation difference can be attributed entirely to amino acid differences in the IIIS5-3P loop between these two subtypes. However, the conserved T1033 and Q1037 residues in IIIS5 are necessary for FPL action on $Ca_v1.3$, even though the nearby M1030V mutation did not increase the potency of FPL action in isolation. However, the inclusion of V1030 in $Ca_v1.3$+V was critical for stabilizing FPL potentiation of current and revealing the increased sensitivity of this mutant to FPL. Despite a complete loss of slowing deactivation by FPL, the FPL-induced shift in $V_{1/2}$ activation of $Ca_v1.3$/DHPi was not different from that of $Ca_v1.3$. This observation suggests the existence of distinct sites of action on $Ca_v1.3$ for these two characteristic effects of FPL on L-VGCC gating.

Other amino acid residues that confer the difference in sensitivity to FPL between $Ca_v1.2$ and $Ca_v1.3$ are located in the IIIS5-3P loop at $Ca_v1.3$/F1052 and $Ca_v1.2$/L1058. None of the mutations within the domain increased that increased nifedipine potency improved FPL potency at $Ca_v1.3$. Single mutation of $Ca_v1.3$/FL generated a ~5-fold shift of FPL potency from $Ca_v1.3$ to $Ca_v1.2$, while another mutant, $Ca_v1.3$/FQDNS, with four more amino acid changes in the C-terminal of the IIIS5-3P loop, was not significantly different from $Ca_v1.3$+V and $Ca_v1.2$ (Figure 3.10). Interestingly, in contrast to $Ca_v1.3$/MV, which drastically changed the tail current kinetics during deactivation in the presence of FPL, the mutants $Ca_v1.3$/FL and $Ca_v1.3$FQDNS exhibited a

minimal effect on deactivation kinetics. Similar to $Ca_v1.3$/DHPi in tail current decay but different in plateau measurements, they retained the fast, single exponential time constants while deactivating with small current availability (Figure 3.13). Also, $Ca_v1.3$/FL and $Ca_v1.3$/FQDNS showed opposite time constant change in the presence of FPL, but with a just minor difference. Therefore, we suspected that the divergent mutations in the C-terminal of the IIIS5-3P loop and T/Q in the IIIS5 transmembrane are involved in regulating the gating properties by slowing the voltage sensors. Unexpectedly, our results indicate that FPL potentiation of current amplitude and FPL slowing of deactivation are not coupled. A previous model was used to show slowed kinetics of activation and deactivation in physiological voltage range resulted from slower movement of the channel voltage sensors, which were required, through their cooperative movement, for channel opening (Fan et al., 2001). However, another study showed that FPL does not affect gating currents (i.e., voltage-sensor movement), and the speed at which the channel voltage sensors return to rest is not detectably affected by the drug, although the signature effect of FPL is a dramatic slowing of the ionic tail currents (McDonough et al., 2005). Altogether these results suggest that FPL enhances current amplitude and slows channel deactivation through different mechanisms.

In our studies of $Ca_v1.3$/N6 mutant, we made the unexpected observation that outward current often developed during an experiment. The standard solution set used in this study sets up a large NMDG gradient across the membrane. Mutations in the pore region of $Ca_v1.2$ were previously reported to lead to enhanced permeability of NMDG, as evidenced by a marked shift in reversal potential that was abolished by equalizing the NMDG concentration in the extracellular (Chapter 2) and intracellular solutions (Hockerman et al., 1995). Indeed, we found that, by equalizing the NMDG concentration in the intra- and extracellular solutions, the outward current observed in the $Ca_v1.3$/N6 mutant was diminished. In that case, we were able to complete the biophysical and pharmacological measurements reported in Table 3.1. Likewise, we found that $Ca_v1.3$ and $Ca_v1.3$+ mutant tended to undergo current reversal upon FPL application (Figure 3.8.A) that was abolished in $Ca_v1.3$ by equalizing the NMDG concentrations. However, even this maneuver left an unstable current when FPL was applied to $Ca_v1.3$+, and we were unable to determine an EC_{50} for FPL stimulation of this mutant (Figure 3.8.B). FPL was previously reported to alter the permeability of $Ca_v1.2$ (Fan et al., 2001), such that Cd^{2+} became a permeant ion, rather than a pore blocker, in the absence of Ca^{2+}. This fact implies that the changes in pore structure may be substantial. Studies on Bay K 8644 showed that the modification of cardiac L-type

channels also provided evidence in permeation properties affected by this drug, whose actions may share at least some similarities FPL (Leuranguer et al., 2003). Considering that the Bay K 8644-modified channels have altered rectification properties, passing inward current but little or no outward current, and FPL has no effect on gating steps, we rationalize that FPL affects only ion permeation of the channel. Thus, our observation that FPL can induce NMDG permeability in $Ca_v1.3$ is consistent with the notion that FPL binding may induce conformational changes in the IIIS5-3P loop that affect the ion selectivity of $Ca_v1.3$. Interestingly, neither $Ca_v1.3$+V nor $Ca_v1.3$/MV mutant conducted outward current in the presence of FPL, and $Ca_v1.3$/FL and $Ca_v1.3$/FQDNS mutants only infrequently conducted outward current in the standard solution set. This observation suggests that the M1030 and F1052 residues may play a role in the observed permeability changes in $Ca_v1.3$.

In summary, this study demonstrates that the reduced sensitivity of $Ca_v1.3$ to both nifedipine and FPL compared with $Ca_v1.2$ can be mainly attributed to amino acid differences within the previously defined DHP binding pocket. In the case of nifedipine, this difference can be attributed to the M/V divergence in the transmembrane domain IIIS5 and a S/A divergence in the IIIS5-3P loop. Our homology models suggest that divergence in the IIIS5 results in distinct stearic effects on drug binding, whereas the divergence in the IIIS5-3P loop may regulate displacement of the 3P helix upon ligand binding. In the case of a non-dihydropyridine agonist, FPL 64176, the sensitivity difference can be attributed to the F/L divergence in the IIIS-3P loop. M/V and F/L divergences may also attribute to the ion permeability in channel pores.

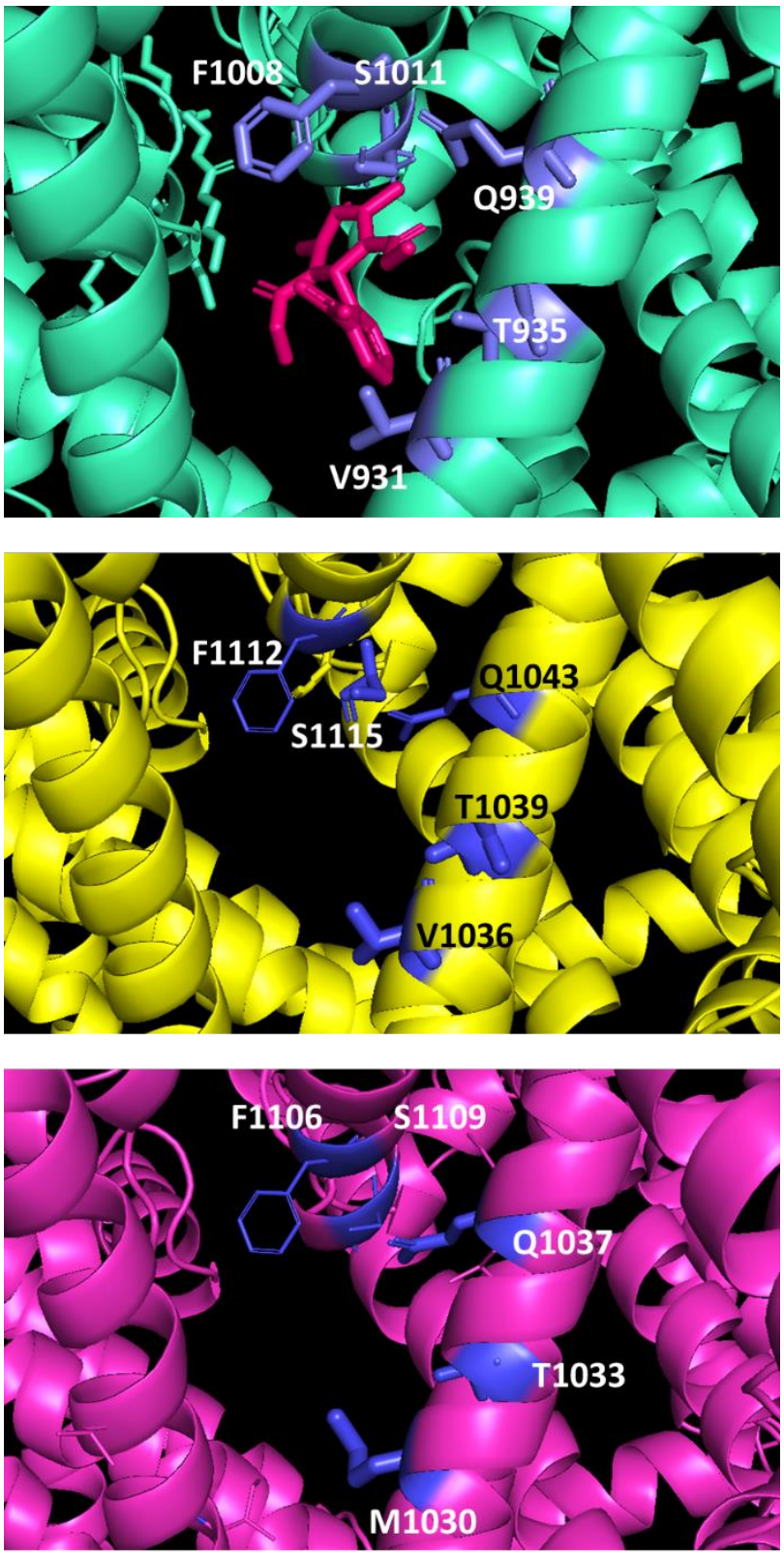

Figure 3.16. Nifedipine binding pockets, including previously identified amino acids in $Ca_v1.1$ (cyan), $Ca_v1.2$ (yellow), and $Ca_v1.3$ (purple).

CHAPTER 4. DIFFERENTIATION OF $CA_V1.2$ AND $CA_V1.3$ IN RESPONSE TO BETA SUBUNIT REGULATION

4.1 Introduction

As described in the previous chapter, the binding sites for current L-type channel inhibitors are in regions of near amino acid identity between Cav1 subtypes, making it difficult to find a rational basis for modifying known drug structures to achieve subtype selectivity (Wang et al., 2018). The 2020 phase III clinical trial for isradipine treating early-stage Parkinson's disease came out negative (Parkinson Study Group STEADY-PD Investigators, 2020). However, this study may have been hampered by dosing limitations on isradipine due to its strong cardiovascular effects. Besides Parkinson's disease, more studies implied that Cav1.3 is a potential therapeutical target for substance abuse disorders. Instead of developing strategies based on the known drug, we explored the intracellular interactions modulating Cav1.3 inactivated states.

4.1.1 $Ca_v1.3$ as an alternative strategy for treating substance abuse disorders

The report from the 2020 national survey on drug use and health has shown that 60.1 percent of the population over 12 years old, approximately 165.4 million people, used a substance in the past year (Substance Abuse and Mental Health Services Administration (SAMHSA) 2020). Extensive studies have been done to understand drug addiction on the reward pathway of the ventral tegmental area-nucleus accumbens (VTA-NAc) brain region, where dopamine is identified as the significant neurotransmitter (Nestler et al., 2005). However, not all addictive substances firmly release dopamine into the NAc (Nutt et al., 2015). Currently, FDA-approved drugs are not effective for stimulant use disorder, and there is an urgent need to explore novel strategies in an alternative pathway.

A variety of studies reveal the involvement of L-VGCC $Ca_v1.3$ in addiction to stimulants such as cocaine and amphetamines, suggesting its potential as a promising target. $Ca_v1.3$ is required for upregulation of dopamine D2L receptors and sensitization to amphetamine (Giordano et al., 2006) and recruitment of D2L receptors in the striatum upon cocaine withdrawal (Schierberl et al., 2012). Non-selective L-VGCC blocker nifedipine and isradipine reduced the rewarding effects and cocaine-seeking behavior in rodents (Shibasaki et al., 2010; Addy et al., 2018). The

prominent role of $Ca_v1.2$ in the prefrontal cortex and the hippocampus suggest that agents that suppress $Ca_v1.3$ activity, but spare $Ca_v1.2$ activity, may have fewer adverse neurological side effects. Accumulating evidence indicated that Ca^{2+} influx via $Ca_v1.3$ activity in dopaminergic neurons of VTA is a crucial step in the development of dependence on stimulant drugs, and developing $Ca_v1.3$-selective inhibitor is a viable strategy to treat stimulant use disorder.

4.1.2 Divergent intracellular domains in $Ca_v1.2$ and $Ca_v1.3$

Unlike the transmembrane domains, which were extensively studied in the previous chapter, the intracellular domains of the pore-forming α1 subunit of Ca_v1 channels are highly divergent, reflecting the coupling of different Ca_v1 channels to distinct signaling pathways. $Ca_v1.2$ and $Ca_v1.3$ interact with distinct proteins via these domains, and disruption of these interactions has been proposed as a handle for selective modulation of Ca_v1 subtype-selective signaling (Zuccotti et al., 2011). The Ca_v channels possess five distinct intracellular domains: N-terminal and C-terminal domains, as well as the I-II, II-III, and III-IV loops that connect the four homologous transmembrane domains shown earlier. One constant among all Ca_v channels is the interaction of the I-II loop with the auxiliary Ca_vβ-subunits (Chen et al., 2004; Pragnell et al., 1994; Van Petegem et al., 2004) accounts for the high amino acid identity of this domain between $Ca_v1.2$ and $Ca_v1.3$. These interactions play a critical role in the surface expression and voltage-dependence of all high voltage-activated (HVA) Ca^{2+} channels (i.e., Ca_v1 and Ca_v2 channels) (Dolphin et al., 2012). The C-terminal tails of $Ca_v1.2$ and $Ca_v1.3$ are divergent, especially in the distal portions, where they interact with separate arrays of regulatory and scaffolding proteins. We summarized the identified interacting proteins with these intracellular domains of $Ca_v1.2$ and $Ca_v1.3$ in Figure 4.1.B.

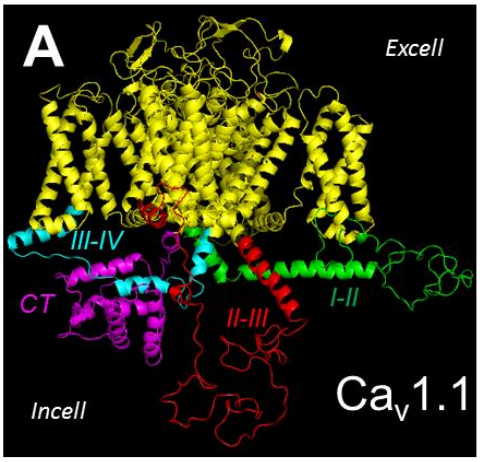

Figure 4.1. Intracellular domains of $Ca_v1.2$ and $Ca_v1.3$ are structurally and functionally divergent.

(**A**) Model (Wang et al., 2018) of $Ca_v1.2$ intracellular domains based on the CryEO structure of $Ca_v1.1$ with auxiliary subunits removed (Wu et al., 2016). (**B**) Amino acid identity of $Ca_v1.2$ and $Ca_v1.3$ intracellular domains and interacting proteins (Zuccotti et al., 2011).

B

Intracellular Domain	% Identity $Ca_v1.2/1.3$	Interacting Proteins
N Terminal	45	-
I-II loop	78	β-subunits
II-III loop	48	RyR2, PCLO, RIMS2
III-IV loop	93	-
C Terminal	51	CaM, CaMKII, STIM1, CIP, NIL-16, Actinin2, SK2, SHANK, densin
$Ca_v1.2$&1.3 both *$Ca_v1.2$ only, $Ca_v1.3$ only*		

4.2 The L-VGCC II-III loops modulate Ca^{2+}-secretion coupling

The intracellular loop connecting domain II and domain III of the L-VGCC α1 subunit is the largest cytoplasmic loop with 150 amino acids and also one of the most divergent regions between $Ca_v1.2$ and $Ca_v1.3$ (Zuccotti et al., 2011). Cav1.2 II-III loop was shown to effectively pull down syntaxin 1A, SNAP-25, and synaptotagmin (P65), and the loop peptide interrupts the association and completely blocks depolarization-evoked exocytosis and granule-localized Ca^{2+} influx (Wiser et al., 1999; Barg et al., 2002; Jacobo et al., 2009; Yasuda et al., 2010; Gandasi et al., 2017). Sharing only 48% amino acid identity, the intracellular loops of $Ca_v1.3$ and $Ca_v1.2$ are relatively divergent. Interestingly, the II-III loops of nearly all Ca_v channels, including $Ca_v1.1$ (Polster et al., 2018), $Ca_v1.2$ (Jacobo et al., 2009), $Ca_v2.1$ (Kim et al., 1997), $Ca_v2.2$ (Sheng et al., 1998), and $Ca_v2.3$ (Radhakrishnan et al., 2011), interact with multiple proteins to either anchor the channels in signaling complexes or regulate cell surface expression. Considering the divergent

homology shared in the cytoplasmic II-III loop between these two L-VGCC subtypes, we have not fully understood the role of the $Ca_v1.3$ II-III loop.

We examined the role of the II-III loop of $Ca_v1.2$ and $Ca_v1.3$ in the pancreatic β-cell line INS-1, which expresses both L-VGCC subtypes endogenously (Jacobo et al., 2009). We expressed the $Ca_v1.2$/II-III loop fused to eGFP and found it uncoupled $Ca_v1.2$ from ER Ca^{2+} release and enhanced glucose-stimulated action potential (GSAP) frequency by disrupting the SK channel (K_{Ca} 2.1-3) activation (Figure 4.2.C & E) (Wang et al., 2014). Interestingly, expression of $Ca_v1.3$/II-III loop fused to eGFP had the opposite effect on glucose-stimulated electrical activity, decreasing action potential frequency by ~80% (Figure 4.2.D & E). Compared to control INS-1 cells (Figure 4.2.A), $Ca_v1.2$/II-III and $Ca_v1.3$/II-III in β-cells display significantly different GSAP frequencies (Figure 4.2.E), suggesting distinct roles in β-cell electrical activity and providing evidence that specific regulation of these channels may be feasible.

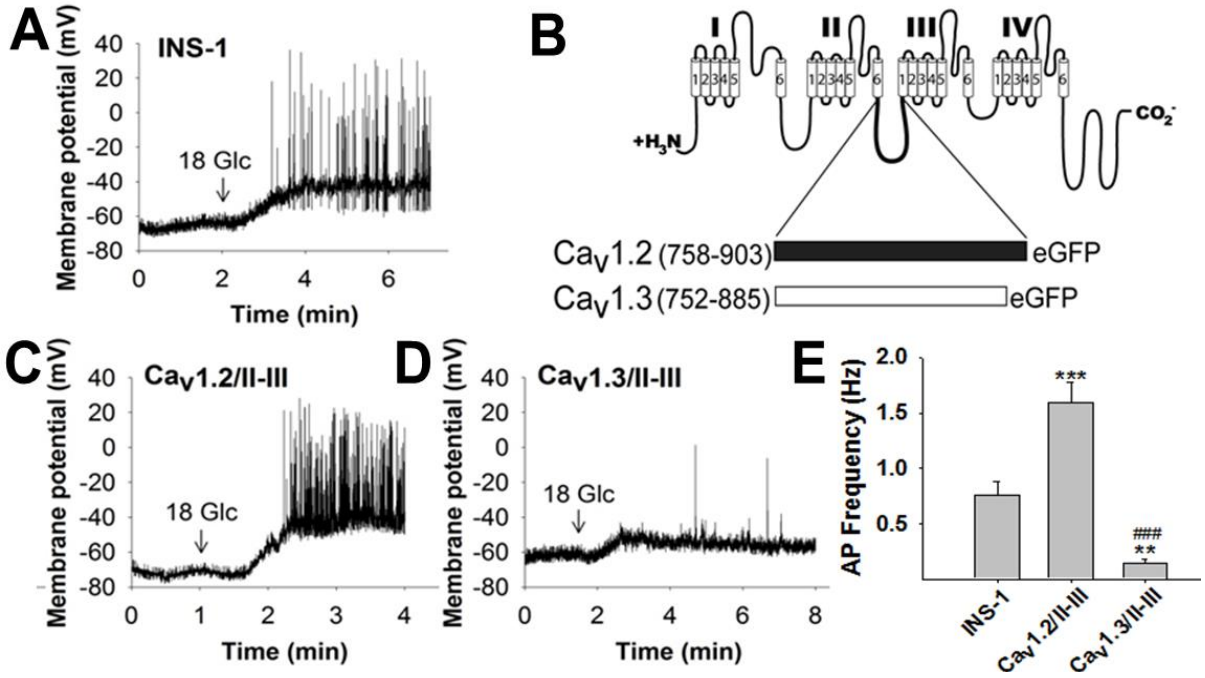

Figure 4.2. Differential effects of the $Ca_v1.2$ and $Ca_v1.3$ II-III loops in the pancreatic β-cell line INS-1. (**A**) Glucose-stimulated action potentials (GSAP) in control INS-1 cells. (**B**) Diagram of the $Ca_v1.2$ and $Ca_v1.3$ II-III loop-eGFP fusion proteins. (**C**) GSAP is enhanced in $Ca_v1.2$/II-III loop fused with eGFP cells. (**D**) GSAP is suppressed in the $Ca_v1.3$/II-III loop fused with eGFP. (**E**) Average GSAP frequency in control INS-1cells and INS-1 cells expressing the $Ca_v1.2$/II-III or $Ca_v1.3$/II-III loops. ***, $P < 0.001$ and **, $P < 0.01$ compared to control INS-1 cells; ###, $P < 0.001$ compared to $Ca_v1.2$/II-III loop expressing cells (student unpaired t-test) (Jarrad et al., unpubslihed).

4.3 The L-VGCC II-III loops modulate voltage-dependent inactivation

The inactivation state is the gating state when current conductance decreases. We are unable to observe the voltage-dependent opening of the inactivation gate because the channel's activation gate is mostly closed at potentials where inactivation is removed. A work-around exists to obtain information during the inactivated state by applying sufficiently long pre-pulse to observe the time-independent inactivation states (Molleman, 2002). Steady-state inactivation protocol depends on how many channels are locked in the inactivation state during the pre-pulse when a constant depolarizing pulse (opening the activation gates) is preceded by a variable pre-pulse then the evoked current will differ in amplitude.

The dramatic suppression of electrical activity by the $Ca_v1.3$/II-III in INS-1 cell suggests that $Ca_v1.3$ initiates action potentials in tissues where it is expressed. Therefore, we sought to understand the mechanism of the $Ca_v1.3$ II-III loop inhibited action potentials. $Ca_v1.3$ activates at more negative potential than $Ca_v1.2$ (Xu and Lipscombe 2001), and we found that $Ca_v1.3$/II-III did not alter the surface expression of $Ca_v1.3$ (data not shown) or L-VGCC current density (Jacobo et al., 2009) in INS-1 cells. This result further suggests that we should take a look at the activation and inactivation properties.

To test this property directly, we transfected the tSA-201 cells with either $Ca_v1.2$ or $Ca_v1.3$ along with the auxiliary subunits $\alpha_2\delta_1$ (Ellis et al., 1988) and β_3 (Castellano et al., 1993) with or without expression of $Ca_v1.3$/II-III loop fused with eGFP. We used $Ca_v\beta_3$ subunit in this set of experiments because both $Ca_v\beta_{2a}$ and $Ca_v\beta_3$ are expressed in pancreatic β-cells (Yang and Berggren 2006), but $Ca_v\beta_{2a}$ is tightly associated with $Ca_v1.2$ in the cardiovascular system (Shaw et al., 2013) while $Ca_v\beta_3$ is highly expressed in rat brain but not the heart which is more tightly associated with $Ca_v1.3$ (Castellano et al., 1993). We used whole-cell voltage clamp and conditioning pulses as described in Chapter 2 to determine the voltage-dependence activation and inactivation in the presence and absence of the $Ca_v1.3$/II-III loop.

The voltage-dependent inactivation of $Ca_v1.3$ was found to shift ~15 mV in the hyperpolarizing direction in the presence compared to the absence of the $Ca_v1.3$/II-III loop, but the voltage-dependent activation stayed unaltered (Figure 4.3.A & B). Interestingly, the expression of the $Ca_v1.3$/II-III loop did not change either voltage-dependence of activation or inactivation of $Ca_v1.2$ (Figure 4.3.B). $Ca_v1.3$ channel availability displaying the shift effect at threshold voltage for activation at ~ -40mV is indicated in Figure 4.3.A red box. Around 70% of $Ca_v1.3$ channels are

available to open at -40mV, while only 10% of $Ca_v1.3$ channels are available when co-expressed with $Ca_v1.3$/II-III. This marked reduction in $Ca_v1.3$ channel availability suggests that the -15mV shift in the voltage-dependence of inactivation induced by $Ca_v1.3$/II-III loop is sufficient to suppress the activation of $Ca_v1.3$ at physiologically relevant potentials. This observation is in line with the dramatic suppression of GSAPs in INS-1 cells in Figure 4.2. We also observed the same shift in a different solution set with calcium as charge carrier instead of barium, and expression of $Ca_v1.3$/II-III shifted the voltage-dependence inactivation of $Ca_v1.3$ from -31.10 ± 0.94 mV (N = 15) to -45.46 ± 3.97 mV (N = 7), which were not statistically different from the barium solution set (Figure 4.4). Besides $Ca_v1.2$ and $Ca_v1.3$, we also tested an alternative splicing variant of $Ca_v1.3$ exon 42a (Xu and Lipscombe 2001), with C-terminus tail truncated. The result interestingly showed no significant difference in the voltage-dependence of activation or inactivation upon co-expression with the $Ca_v1.3$/II-III loop (Figure 4.3.B). Moreover, P/Q-type channel $Ca_v2.1$ was not affected by $Ca_v1.3$/II-III in its voltage-dependent inactivation, but the activation shifted to more negative potentials. Additionally, P/Q-type $Ca_v2.1$ shares a much lower sequence identity with L-type $Ca_v1.3$ (Catterall 2000). These activation shifts suggest further that the common auxiliary subunits used in these experiments, $Ca_v\beta_3$ and $\alpha_2\delta_1$, may play a potential role in modulating VGCC activity by the $Ca_v1.3$/II-III loop.

A

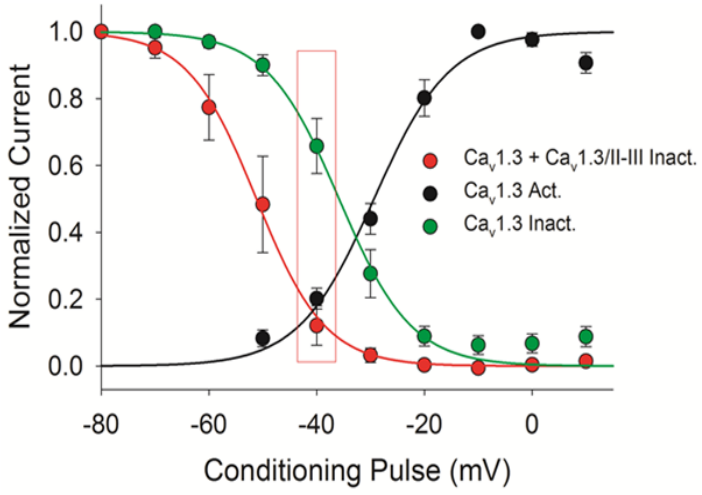

B

Channel	$V_{1/2}$ Inct. Control	$V_{1/2}$ Inact. $Ca_v1.3$/II-III	$V_{1/2}$ Act. Control	$V_{1/2}$ Act. $Ca_v1.3$/II-III
$Ca_v1.3$	-36.0 ± 1.3	-51.2 ± 0.6	-29.8 ± 1.5	-32.7 ± 0.5
$Ca_v1.3$ 42a	-40.3 ± 1.2	-42.6 ± 0.8	-28.0 ± 0.7	-30.1 ± 1.8
$Ca_v1.2$	-41.1 ± 0.6	-38.2 ± 0.8	-19.5 ± 0.5	-22.0 ± 1.3
$Ca_v2.1$	-25.5 ± 2.6	-22.5 ± 2.9	8.1 ± 3.2	-6.0 ± 3.4

Figure 4.3. Voltage-dependence of activation and inactivation in the presence and absence of $Ca_v1.3$/II-III loop. (**A**) Voltage-dependence of activation curve for $Ca_v1.3$ (black), steady-state inactivation curve for $Ca_v1.3$ in the absence (green) or presence (red) of the $Ca_v1.3$/II-III loop. The red box indicates the $Ca_v1.3$ channel availability at threshold voltage -40 mV. (**B**) Half-activation and -inactivation values for $Ca_v1.3$, $Ca_v1.3_{42a}$ (truncated form), $Ca_v1.2$, $Ca_v2.1$ in the presence or absence of the $Ca_v1.3$/II-III loop (Hockerman et al., unpublished).

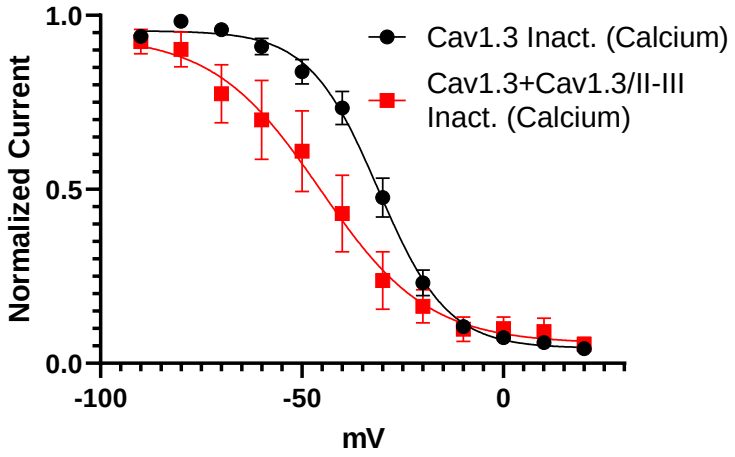

Figure 4.4. Voltage-dependence of inactivation of $Ca_v1.3$ in the presence and absence of $Ca_v1.3$/II-III loop in calcium solution sets. $Ca_v1.3$/II-III loop shifted the $V_{1/2}$ inactivation of $Ca_v1.3$ from -31.10 ± 0.94 mV (N = 15) -45.46 ± 3.97 mV (N = 7).

4.4 Identification of specific amino acid motifs in Cav1.3/II-III loop

4.4.1 Both N-terminus and C-terminus shift $Ca_v1.3$ inactivation

Next, we sought to identify the specific amino acids with the $Ca_v1.3$ II-III loop responsible for the modulation of $Ca_v1.3$ inactivation. We aligned the amino acid sequence of the II-III loop of both subtypes, which contains 151 amino acids in $Ca_v1.2$ and 135 amino acids in $Ca_v1.3$ (Figure 4.5.A). We created GFP fusions with N-terminus (NT) or C-terminus (CT) half of the $Ca_v1.3$/II-III loop as described in Chapter 2 and found that both were capable of shifting the inactivation of $Ca_v1.3$ when co-expressed in tSA-201 cells with $\alpha_2\delta_1$ and β_3 subunits to hyperpolarizing potentials (Figure 4.5.B). Interestingly, the NT half and CT half of $Ca_v1.3$/II-III have different effects: the NT half shifted the $V_{1/2}$ inactivation by -6 mV to -40.04 ± 1.11 mV, while the CT half shifted by -10.5 mV to -44.2 ± 0.90 mV. Thus, both the N-terminal and C-terminal halves of the $Ca_v1.3$ II-III loop are capable of modulating $Ca_v1.3/Ca_v\beta_3$ inactivation, with the greater effect exerted by the C-terminal half.

4.4.2 Peptides containing putative SH3 and GK domain ligands shift $Ca_v1.3$ inactivation

To further refine the specific determinants of the shift, we searched for protein-protein interaction motifs within the $Ca_v1.3$ II-III loop. The $Ca_v1.3$ II-III loop contains proline-rich regions,

especially the canonical PxxP amino acid motifs recognized as SH3-binding domains (Teyra et al., 2017). SH3 domains are protein molecules that mediate protein-protein interactions in many eukaryotic signal transduction pathways. We next designed synthetic peptides based on PXXP motifs, trying to mimic the interactions between $Ca_v1.3$/II-III loop and SH3-containing regions.

We generated the synthetic peptides corresponding to the potential interaction sites and introduced 10μM peptides to the cell in whole-cell patch-clamp by back-filling patch pipette, waiting for at least 3 minutes after going whole-cell (break-in) before running steady-state inactivation protocol, described in Chapter 2, allowing the diffusion and delivery of peptides into the cell.

The peptide P1-1 (Ac-DEDKDPYPPCDVPGEE-NH_2, 987-1002) in the N-terminal half of the Cav1.3 II-III loop includes a putative SH3 domain ligand (PYPPCDVP; atypical) unique to $Ca_v1.3$. This P1-1 peptide shifted the $V_{1/2}$ of steady-state inactivation by -6.5 mV to -41.4 ± 1.32 mV, which reproduced the effect of the entire NT half of the $Ca_v1.3$/II-III loop. In contrast, we generated a control peptide P1-2 (Ac-DEDKDGYPGCDVPGEE-NH_2) by replacing proline residues of the first PXXP motif with glycine. The peptide P1-2 showed no effect on steady-state inactivation and generated a $V_{1/2}$ inactivation at -33.57 ± 0.89 mV (Figure 4.5.C).

As for the CT half of the $Ca_v1.3$/II-III loop, we were initially interested in the peptides containing another SH3 domain ligand with a PXXP motif. We generated two peptides, P2-1 (Ac-EEEDEPEVPAGPRPRR-NH_2, 1006-1021; class VIII) and control P2-2 (Ac-EEEDEGEVGAGPRPRR-NH_2) with the proline to glycine switch. However, both peptides showed no effect on $Ca_v1.3$ inactivation, displaying the $V_{1/2}$ inactivation at -30.99 ± 1.32 mV (N = 13) for P2-1 and at -31.72 ± 0.94 mV (N = 13) for P2-2. Interestingly, the third peptide, P3-1 (Ac-RRISELNMKEKIAPIPE-NH_2, 1021-1036) we generated did not have a typical SH3 domain ligand but displayed two prolines. This peptide shifted the $V_{1/2}$ inactivation by -16 mV to -44.26 ± 2.46 mV (N = 7), similar to the entire CT half of the $Ca_v1.3$/II-III loop. The same peptide in which the proline residues were replaced with glycine residues, P3-2(Ac-RRISELNMKEKIAGIGE-NH_2), induced an identical shift (Figure 4.5.C) to -44.79 ± 4.18 mV (N = 10). Even though both P3-1 and P3-2 contain no SH3 domain ligand, these two peptides contain a protein kinase (PKG) phosphorylation site RRISE. This site is required for PKG inhibition of $Ca_v1.3$ at S860 (Sandoval et al., 2017) but not conserved in $Ca_v1.2$.

As P3-1 and P3-2 share very similar activity on $Ca_v1.3/\beta_3$ inactivation and marked similarity in amino acid motifs to other proteins shown to be ligands for Guanylate Kinase (GK) domains (Zhu et al., 2011), represented by the mitotic spindle protein LGN (Figure 4.6.A). The scaffolding RxxS is very common among GK-binding domains. Interestingly, several studies have shown that the SH3 domain and GK domain in an SH3-GK tandem interact with each other forming an integral structural unit, so it is not surprising that a GK ligand might exist close to the SH3 ligand in peptide P3-1. We initially assessed the activity of P3-1 and P3-2 at a concentration of 10μM. However, we asked whether this inactivation modulation is concentration dependent. We applied 10, 100, 1000 nM of either P3-1 or P3-2 in addition to 10μM and generated the $V_{1/2}$ inactivation curves. We normalize the measurements to the highest shift at 10μM to obtain EC_{50} values based on fitting data to a single binding site model. The activities of peptides P3-1 and P3-2 in shifting the inactivation of $Ca_v1.3/\beta_3$ are dose-dependent, with EC_{50} values of 535.2 and 563 nM, respectively, when measured 3 minutes after break-in, and 231 and 301nM when measuring 10 minutes after break-in (Figure 4.6.B & C). Thus, a modest effect on the voltage-dependence of $Ca_v1.3$ inactivation is explicitly induced by a putative SH3 domain ligand in the NT half of the $Ca_v1.3$/II-III loop. However, the larger shift induced by the CT tail of the $Ca_v1.3$/II-III loop is mimicked by a potential GK domain ligand that contains a PKG phosphorylation site linked to inhibition of $Ca_v1.3$ activity.

4.4.3 Determine the minimum peptide to reproduce the shift

As P3-1/P3-2 contain 17 amino acids, we tried to determine the minimum peptide that reproduces the shift in $Ca_v1.3$ $V_{1/2}$ inactivation. Minimization of the required amino acid sequence is desirable not only to guide medicinal chemistry efforts to make more drug-like molecules but also to guide the construction of DNA-encoded libraries for the discovery of $Ca_v\beta$ subunit SH3 and GK domain ligands. In addition, the presence of an inhibitory PKG phosphorylation site within the P3-1 peptide strongly suggests that phosphorylation may regulate the activity of P3-1. We further generated the synthetic peptide P4-1 (Ac-<u>RRISE</u>LNMKEK-NH_2) without the PXXP motif, but the conserved PKG phosphorylation site (Ser 860) of $Ca_v1.3$ and P4-2 (Ac-<u>RRIDE</u>LNMKEK-NH_2) with serine replaced by aspartic acid to potentially interrupt the PKG phosphorylation. However, neither peptide could reproduce the shift or any statistically different modulation. $V_{1/2}$

inactivation of P4-1was shown to be -34.07 ± 2.94 mV (N =12), and the $V_{1/2}$ inactivation of P4-2 was -33.06 ± 3.22 (N = 5), both not different from -36 mV control value.

The four amino acids, PIPE or GIGE, are obviously required to shift the inactivation. The length of peptides is likely a critical factor to assist either protein folding or interactions with potential GK or SH3 domain in additional intracellular molecules. We proceeded with the next step to explore the inactivation of $Ca_v1.3$ by the minimum effective peptide P3-1 and identify the interactions with modulators containing GK or SH3 domains.

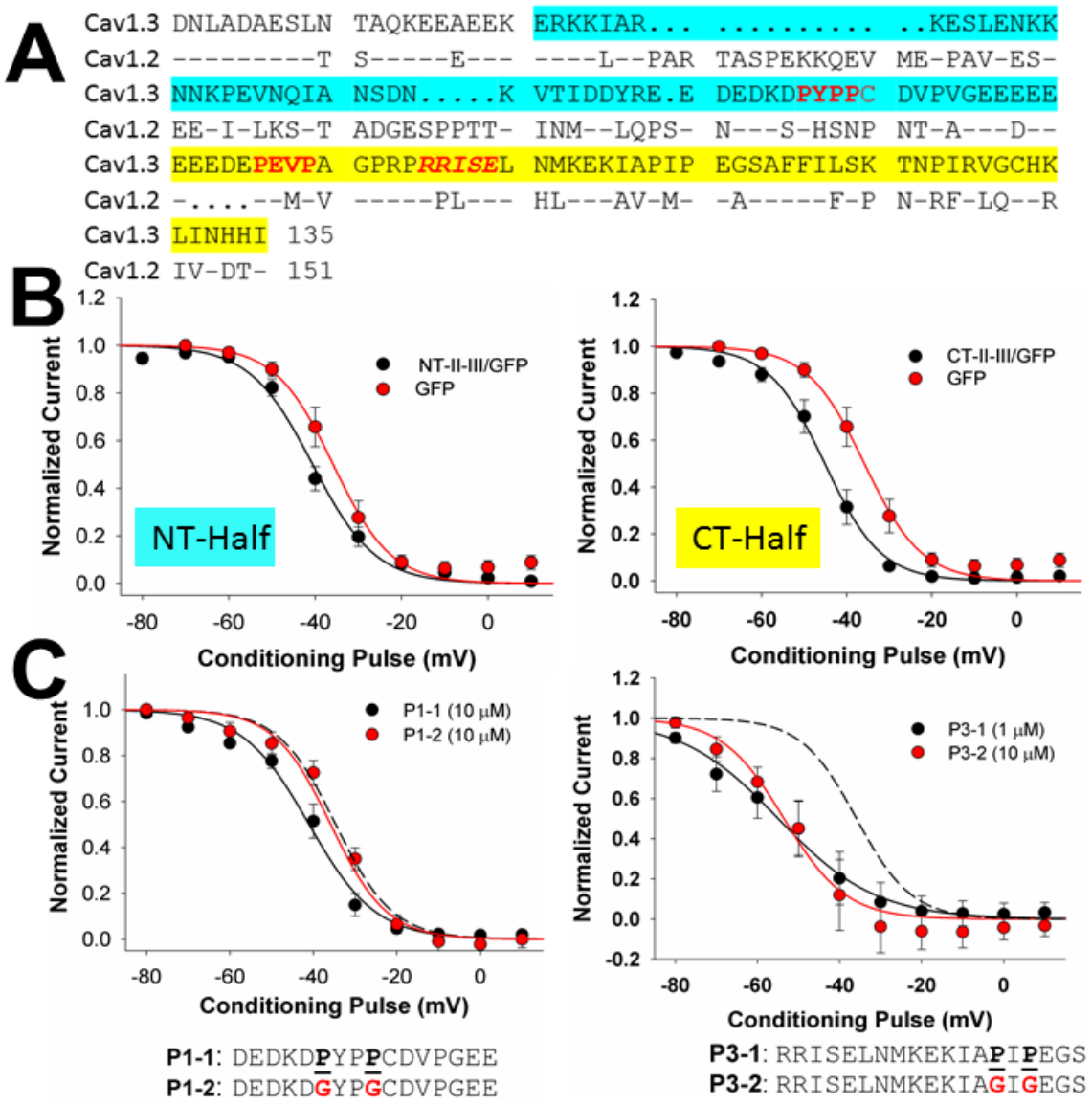

Figure 4.5. Identification of specific amino acid motifs within the $Ca_v1.3$ II-III loop that modulated inactivation of $Ca_v1.3/\beta_3$. (**A**) Amino acid alignment of the $Ca_v1.2$ and $Ca_v1.3$ II-III loop. N-terminus is in blue, and the C-terminus is in yellow. Putative SH3 domain ligands are indicated in red, and PKG site in red italics. Dots in $Ca_v1.3$ indicate gaps with alignment with $Ca_v1.2$, and dashes display identical amino acids. (**B**) Modulation of steady-state inactivation by NT or CT terminal halves of $Ca_v1.3$ II-III loops fused to eGFP. $V_{1/2}$ inactivation with NT half was -40.04 ± 1.11 mV (N = 8), while the $V_{1/2}$ inactivation with CT half was -44.2 ± 0.90 mV (N = 4). (**C**) Left: NT peptide P1-1 containing a putative SH3 ligand reproduces the effect of the entire NT half of the $Ca_v1.3$/II-III loop. $V_{1/2}$ inactivation of peptide P1-1: 41.4 ± 1.32 Mv (N =19); $V_{1/2}$ inactivation of peptide P1-2: -33.57 ± 0.89 mV (N=12). Right: Two CT peptides (P3-1 and 2), without SH3 domain ligands, recapitulate the effect of the entire CT half of the $Ca_v1.3$/II-III loop. $V_{1/2}$ inactivation of peptide P3-1: -44.26 ± 2.46 mV (N = 7), $V_{1/2}$ inactivation of peptide P3-2: -44.79 ± 4.18 mV (N = 10).

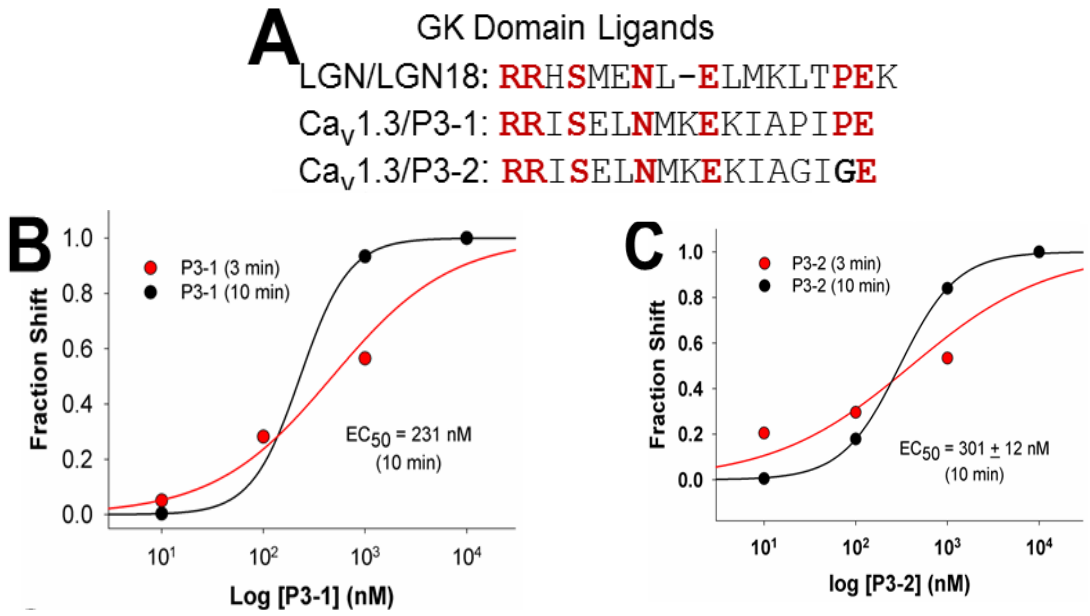

Figure 4.6. P3-1/P3-2 contain putative GK domain ligands to regulate $Ca_v1.3$. (**A**) Alignment of LGN GK ligand domain, P3-1 & P3-2. (**B-C**) Dose-response curves for P3-1 and P3-2 induced shifts in $Ca_v1.3$ $V_{1/2}$ inactivation. 3 minutes and 10 minutes: time from break-in to start of the experiment. EC_{50} values of P3-1: 535.2 nM at 3 minutes and 231 nM at 10minutes. EC_{50} values of P3-2: 231 nM at 3 minutes and 301 nM at 10 minutes.

4.5 $Ca_v1.3$ II-III peptide P1-1modulation in other L-VGCCs

Given the strong effect of the P3-1 and P3-2 peptides on the inactivation of the full-length $Ca_v1.3/\beta_3$ channel, we assessed the activity of these peptides on other Ca^{2+} channels. Unlike the $Ca_v1.3$/II-III loop mentioned in Figure 4.3, the peptide P3-1 shifts inactivation of the truncated $Ca_v1.3_{42a}$ splice variant, which is detected along with the full-length variant in the brain (Hell et al., 1993). P3-1 shifts the $V_{1/2}$ inactivation from -40mV to -53 mV (Figure 4.7.A). We next examined the effect of the P3-1 peptide on $Ca_v1.2/\beta_3$. We found that P3-1 shifts the voltage dependence of inactivation of $Ca_v1.2$ to more positive potentials by 15mV (Figure 4.7.B). Thus, the P3-1 peptide can modulate both $Ca_v1.3/\beta_3$ and $Ca_v1.2/\beta_3$, but in a manner to decrease the availability of $Ca_v1.3$ but not $Ca_v1.2$. We also found that P3-2 had the same effect on $Ca_v1.2$, similar to P3-1, with statistically different inactivation shifts 10 minutes after break-in (data not shown).

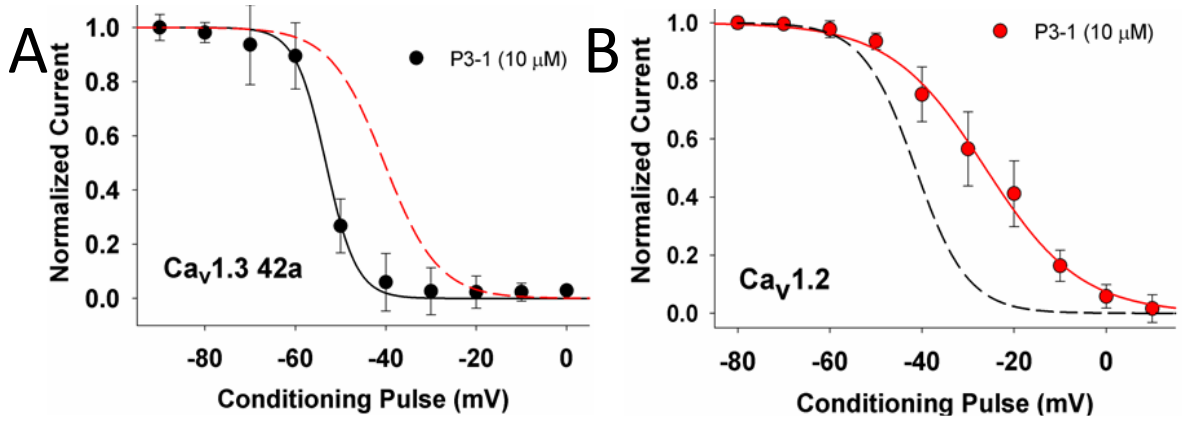

Figure 4.7. P3-1 peptide has opposite effects on $Ca_v1.3_{42a}/\beta_3$ and $Ca_v1.2/\beta_3$ inactivation. **(A)** $V_{1/2}$ inactivation for $Ca_v1.3_{42a}$: -53 ± 0.6 mV (N = 7). **(B)** $V_{1/2}$ inactivation for $Ca_v1.2$: -27.19 ± 2.30 mV (N = 9). Dashed lines indicated inactivation curves for the indicated channel in the absence of peptide.

4.6 Auxiliary $Ca_v\beta$ subunit modulates $Ca_v1.3$ inactivation

4.6.1 Auxiliary $Ca_v\beta$ subunit is required to shift $Ca_v1.3$ inactivation

Considering the SH3 domain ligand and GK domain ligand in the effective peptides P1-1 and P3-1, we hypothesized that the $Ca_v1.3$ II-III loop and derivative peptides target auxiliary β subunit since they all contain both an SH3 domain and a GK domain. Therefore, we asked whether $Ca_v\beta$ can be putative interacting partners with the II-III loop of $Ca_v1.3$, then we asked if the robust shift in inactivation induced by co-expression of $Ca_v1.3$ with the $Ca_v1.3$/II-III loop/GFP fusion (Figure 4.3.B) requires the presence of a $Ca_v\beta$ subunit.

As expected, in the absence of $Ca_v\beta_3$, the $V_{1/2}$ inactivation of $Ca_v1.3$ is shifted to the depolarizing direction, and the voltage dependence is much shallower than $Ca_v1.3$ channels expressing $Ca_v\beta_3$ (Figure 4.8). Remarkably, the voltage dependence of inactivation in $Ca_v1.3$ channels without the $Ca_v\beta_3$ subunit was utterly insensitive to the $Ca_v1.3$/II-III/GFP fusion presence. Thus, $Ca_v\beta$ subunits appear to play a vital role in the modulation of $Ca_v1.3$ inactivation by amino acid motifs within the II-III loop. This observation has prompted us to ask whether divergent $Ca_v\beta$ subunit subtypes would modulate voltage-dependent inactivation of $Ca_v1.3$ expressed with $Ca_v1.3$/II-III loop in a different manner. We hypothesize that the II-III loop of $Ca_v1.3$ may interact with specific auxiliary β subunits, unlike the canonical interaction of the I-II loop of all HVA Ca^{2+} channels with all subtypes of β subunits.

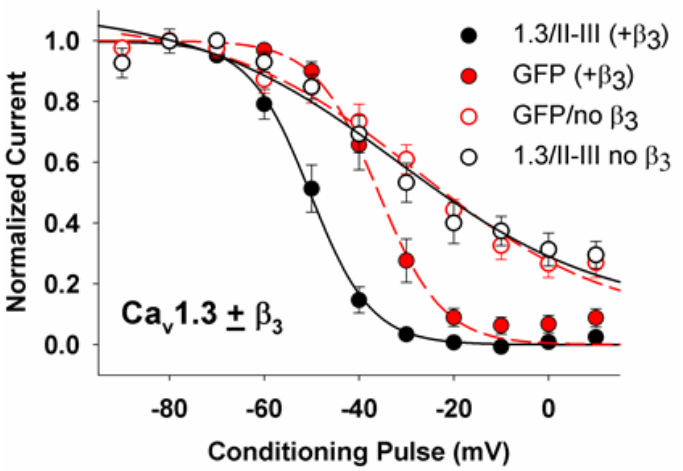

Figure 4.8. The modulation of $Ca_v1.3$ inactivation by the $Ca_v1.3$/II-III loop requires a $Ca_v\beta$ subunit. $Ca_v1.3$ was expressed in tSA-201 cells with α2δ1 subunit and GFP with or without the $Ca_v\beta_3$ subunit (red closed or open symbols, respectively). Channels with or without $Ca_v\beta_3$ were co-expressed with the $Ca_v1.3$/II-III/GFP fusion (black closed or open symbols, respectively). Voltage-dependence of inactivation was determined as described before. $V_{1/2}$ inactivation for $Ca_v1.3$ without $Ca_v\beta_3$ is -27.57 ± 2.90 mV (N = 7), and for $Ca_v1.3$ co-expressed with $Ca_v1.3$/II-III but no $Ca_v\beta_3$ is -29.81 ± 1.07 mV (N = 13).

4.6.2 $Ca_v\beta$ subunits contain SH3 domains and GK domains

An α-helical segment of the intracellular I-II loop of Ca_v channels binds to the auxiliary β-subunits of Ca_v channels, and several structures of β-subunits bound to a peptide corresponding to the so-called α1 interacting domain (AID) have been reported (Chen et al., 2004; Van Petegem et al., 2004; Opatowsky et al., 2004). $Ca_v\beta$ core consists of an SH3 domain interrupted by a HOOK domain and a GK domain. The AID binds to a groove on the periphery of the GK domain and occupies a tiny area of the SH3/HOOK-GK motif, suggesting further interactions with the $Ca_v\alpha$ subunit (Chen et al., 2004) (Figure 4.9.A). Putative locations of peptide P1-1 and P3-1 sequences in the II-III loop of $Ca_v1.3$ are shown in Figure 4.9.B. The IIS6 helix is highlighted because several mutations in this helix have substantial effects on the voltage-dependence of inactivation of $Ca_v1.2$ (Liveneh et al., 2006; Hohaus et al., 2005). Thus, engagement of the SH3 ligand domain and putative GK ligand domain in the II-III loop of $Ca_v1.3$ by the $Ca_v\beta$ subunits is poised to influence the disposition of the IIS6 helix.

Given that peptides P1-1 and P3-1 contain putative ligands for SH3 domains and GK domains, respectively, we propose that these peptides regulate $Ca_v1.3$ inactivation via binding to $Ca_v\beta$ subunits and disrupting interactions with the $Ca_v1.3$/II-III loop. This regulation may mimic

the physiological inhibition of $Ca_v1.3$ by PKG phosphorylation since the $Ca_v\beta$ subunit GK domain is proposed to bind a non-phosphorylated ligand (Zhu et al., 2011). Thus, phosphorylation of PKG site serine residue in the II-III loop of $Ca_v1.3$ may inhibit channel activity by disrupting the binding of this motif to the GK domain of $Ca_v\beta$ subunits. The binding of $Ca_v\beta$ subunits to all HVA Ca^{2+} channel α1 subunits via the AID domain in the I-II loop is critical for proper channel function, and interruption of this interaction with small molecules (Young et al., 1998; Chen et al., 2018), or nanobodies (Morgenstern et al., 2019) profoundly inhibits channel activity.

However, this approach does not achieve channel subtype specificity. We hypothesize that the $Ca_v1.3$ sequence represented by peptide P3-1, which is unique among all HVA Ca^{2+} channels, mediates a $Ca_v1.3$-specific inhibitory interaction with $Ca_v\beta_3$ and likely other $Ca_v\beta$ subunits (Figure 4.9.C).

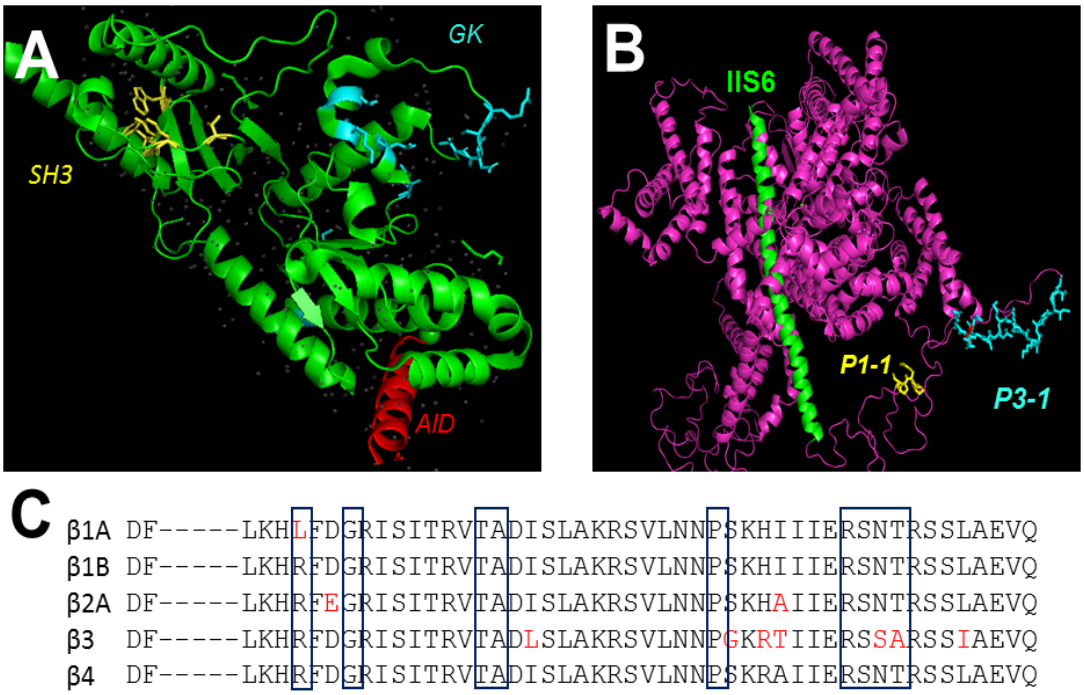

Figure 4.9. $Ca_v\beta$ subunits contain SH3 domains and GK domains. (**A**) Structure of the β1A subunit bound to the AID peptide (red) (Chen et al., 2004). Yellow-SH3 domain amino acid residues involved in ligand binding. Cyan-putative amino acid residues involved in GK domain ligand binding. (**B**) Position of the PXXP motif of P1-1 and P3-1 sequence within the II-III loop of a model of $Ca_v1.3$. (**C**) Alignment of putative GK domain residues from the five major $Ca_v\beta$ subunit subtypes involved in ligand binding (Zuccotti et al., 2011). Boxes indicate key positions for interacting with GK domain ligands.

4.6.3 $Ca_v\beta$ selectivity in regulating $Ca_v1.2$ and $Ca_v1.3$ inactivation

It is clear that $Ca_v\beta_{1b}$, $Ca_v\beta_2$, $Ca_v\beta_3$, and $Ca_v\beta_4$ are all present in the brain (Schlick et al., 2010). However, $Ca_v\beta_3$ and $Ca_v\beta_4$ were shown to complex with ~40% each of the total L-type channels in the cerebral cortex and hippocampus (Pichler et al., 1997). The alignment of the putative GK domain ligand binding site shown in Figure 4.8.C indicates a high degree of identity across β subunit subtypes. However, it is possible that the β subunit subtypes may influence the activity of P3-1 and related peptides in regulating $Ca_v1.3$ inactivation. Therefore, we performed the experiments shown in Figure 4.5.C with 10 μM P3-1 peptide using cells co-expressing $Ca_v1.3$, $\alpha_2\delta_1$, and β_{1b}, β_{2a}, or β_4. We expected that the P3-1 peptide would shift $V_{1/2}$ inactivation significantly regardless of the β-subunit subtype, but that potency or magnitude of the shift may differ. Since the predominant L-type Ca^{2+} channel in the cardiovascular system is $Ca_v1.2/\beta_2/\alpha_2\delta_1$, we will determine if the P3-1 peptide regulates the inactivation of this subunit combination. We expect that, as we observed with $Ca_v1.2/\beta_3/\alpha_2\delta_1$, P3-1 will not enhance the inactivation of the $Ca_v1.2/\beta_2/\alpha_2\delta_1$ channel. Such a result would suggest that the mechanism of action of P3-1 might permit inhibition of $Ca_v1.3$ with minimal effects on vascular tone or cardiac contractility.

4.6.3.1 β subunit-dependence of P3-1 modulation of inactivation

To determine if the modulation of $Ca_v1.3$ steady-state inactivation was dependent upon the β subunit subtype, we expressed full-length $Ca_v1.3$ with $\alpha_2\delta_1$ and each of the other three β subunit subtypes in tsA-201 cells and measured $V_{1/2}$ inactivation in the presence and absence of 10 μM P3-1 in the pipette. $Ca_v\beta_4$ showed very similar $V_{1/2}$ inactivation either in the presence or absence of 10μM P3-1, and prolonged exposure to P3-1 did not change the observation (Figure 4.10.D; Table 4.1). As for $Ca_v\beta_{2a}$, $Ca_v1.3$ channels co-expressed with $\alpha_2\delta$-1 and $Ca_v\beta_{2a}$ exhibited a $V_{1/2}$ inactivation -5 mV more negative than control 3 minutes after the break-in and -7 mV more negative than control after 10 minutes with 10 μM (Figure 4.10.C; Table 4.1). $Ca_v1.3$ channels co-expressed with $\alpha_2\delta_1$ and $Ca_v\beta_{1b}$, exhibited a $V_{1/2}$ inactivation ~15 mV more negative than control 3 minutes after break-in with 10 μM P3-1 in the pipette. However, this modulation was transient, as it declined to an ~3 mV shift by 10 minutes post break-in (Figure 4.10.B; Table 4.1). This might suggest a transient interaction between $Ca_v\beta_{1b}$ and $Ca_v\alpha_1$, which is not found in other subunits. Moreover, we compared the relative shift among four subunits 3 minutes and 10 minutes after

break-in (Figure 4.10.E & F; Table 4.1). Except for $Ca_v\beta_4$, all other three subunits shifted after the prolonged expression of P3-1. $Ca_v\beta_{1b}$ showed a very dramatic temporary modulation of $V_{1/2}$ inactivation compared to other subunits. It is exciting that $Ca_v\beta_3$, which is the most tightly correlated with $Ca_v1.3$ in our physiological and clinical interest, shows the most significant modulation in either short or prolonged exposure of peptide P3-1.

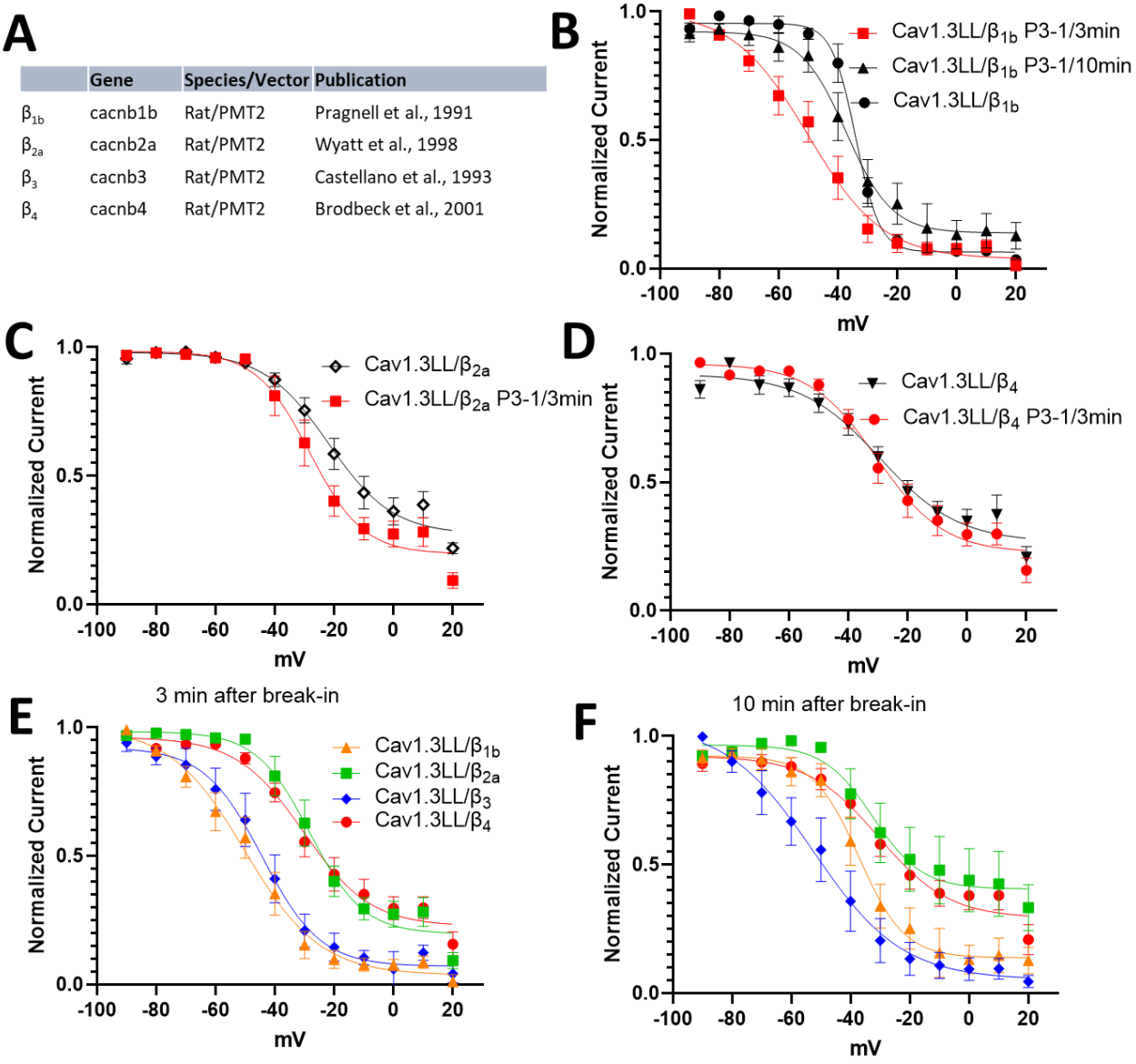

Figure 4.10. Voltage-dependence inactivation of $Ca_v1.3$ when co-expressed with different auxiliary $Ca_v\beta$ subunits and $\alpha_2\delta_1$ in the absence and presence of 10μM P3-1 peptide. (**A)** $Ca_v\beta$ subunits used in experiments. (**B-D**) The voltage-dependence inactivation curve of $Ca_v1.3$ with $Ca_v\beta_{1b}$, $Ca_v\beta_{2a}$, $Ca_v\beta_4$ in the absence and presence of 10μM P3-1. (**E-F**) Comparisons of 4 auxiliary subunits modulating $Ca_v1.3$ inactivation in the presence of 10μM P3-1 3 minutes and 10 minutes after the break-in. Refer to Table 4.1 for detailed measurements.

4.6.3.2 P3-1 regulation in $Ca_v1.2/\beta_{2a}/\alpha_2\delta_1$

Since all the previous measurements were done with the expression of $Ca_v\beta_3$, which is not the predominant form to associate with $Ca_v1.2$, we tested peptide P3-1 on $Ca_v1.2$ with co-expression of $Ca_v\beta_{2a}$ and $\alpha_2\delta_1$. Moreover, $Ca_v1.2$ requires a β_{2a} subunit for PKG phosphorylation (Yang et al., 2007). The inactivation for $Ca_v\beta_{2a}$ is significantly more positive than that for $Ca_v\beta_3$, and P3-1 also shifted the $V_{1/2}$ inactivation to a more positive voltage (Figure 4.11 and Table 4.1).

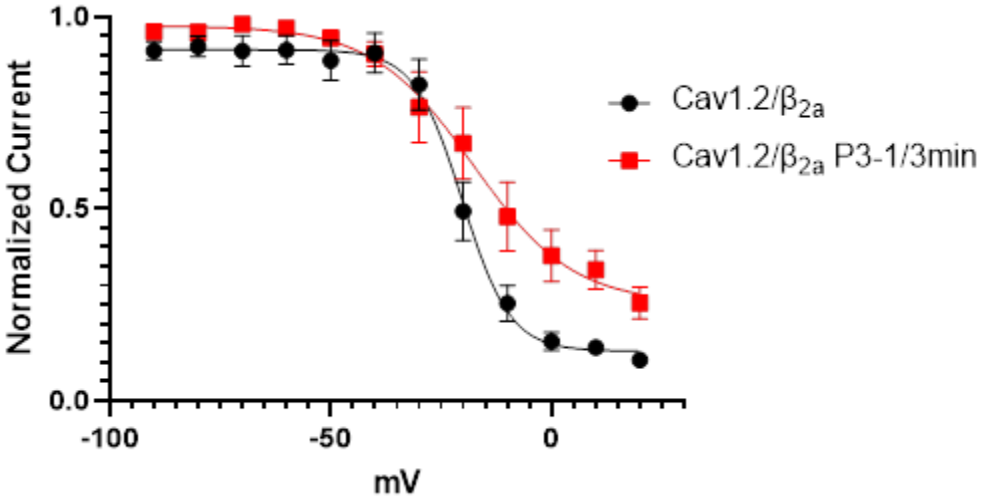

Figure 4.11. Voltage-dependence inactivation of $Ca_v1.2$ when co-expressed the auxiliary $Ca_v\beta_{2a}$ in the presence and absence of 10μM P3-1 peptide. See Table 4.1 for detailed measurements.

Table 4.1. $V_{1/2}$ inactivation of $Ca_v1.2$ and $Ca_v1.3$ co-expressed with auxiliary subunits $\alpha_2\delta_1$ and different β subunits in the absence and presence of 10μM peptide P3-1, 3 minutes, and 10 minutes after the break-in. Measurements highlighted in blue showed **** P<0.0001 when unpaired t-test was done between control and 10μM P3-1 in the pipette.

Cav	β	Control (mV)	10μM P3-1 3min (mV)	10μM P3-1 10min (mV)
Cav1.3	β_{1b}	-34.00 ± 0.63 (N=7)	-50.10 ± 2.51 (N=9)	-37.22 ± 2.20 (N=7)
	β_{2a}	-23.00 ± 2.19 (N=5)	-28.22 ± 1.92 (N=7)	-31.61 ± 1.77 (N=5)
	β_3	-29.50 ± 1.58 (N=7)	-44.26 ± 2.45 (N=7)	-48.89 ± 0.55 (N=4)
	β_4	-29.33 ± 3.13 (N=10)	-30.36 ± 2.18 (N=18)	-30.56 ± 3.02 (N=14)
Cav1.2	β_{2a}	-20.19 ± 1.14 (N=7)	-17.80 ± 3.26 (N=5)	-13.90 ± 2.41 (N=3)
	β_3	-41.10 ± 0.60 (N=7)	-27.19 ± 2.30 (N=9)	-17.99 ± 4.24 (N=8)

4.7 Frequency-dependence of verapamil block enhanced by P3-1

Verapamil was introduced in Chapter 1.5.3 as a calcium channel blocker to treat hypertension, angina, and supraventricular tachycardia. Verapamil exhibits frequency-dependent block to antagonize $Ca_v1.2$ undergoing high-frequency depolarizations, the result of a higher drug affinity for the inactivated state of the channel (Lee and Tsien, 1983; Johnson et al., 1996; Nawrath and Wegner, 1997). (±)-Verapamil (Sigma/RBI, Natick, MA) was dissolved in bath saline and applied to cells using the previously described perfusion system with constant exchange of the bath solution. I_{Ba} current was measured in the standard Silverman solution set mentioned in Chapter 2. The stock solution was prepared in 100mM and 70% ethanol.

The frequency-dependent block of $Ca_v1.3$ was measured in the absence (black symbols) or presence (red symbols) of 30 μM Verapamil (Figure 4.12). A frequency-dependent protocol was applied in which cells were depolarized from a holding potential of -60mV to +10mV for 100 ms every second. Block was brought to equilibrium with the indicated concentration at 0.05 Hz, followed by a 20-pulse train of depolarization given at 1Hz. Verapamil showed significant frequency-dependent drug block accumulation at the end of a 20-pulse stimulation. The asterisks indicate significant differences between the current remaining at the end of the train in the absence and presence of verapamil.

There is no statistical difference between either group in the presence and absence of P3-1 without verapamil, but there is a considerable difference when verapamil is in the perfusion. Only 20 percent of the current is blocked when only verapamil is applied, but with 10 μM P3-1 in the pipette, 30 μM verapamil blocked over 40% of current by the end of 20 pulses train of depolarization. We used one-phase decay to estimate the plateau of the frequency-dependent block, and P3-1 increased the block by 20 percent. These results are consistent with our previous experiments showing that P3-1 enhances the inactivation of $Ca_v1.3/\beta_3$.

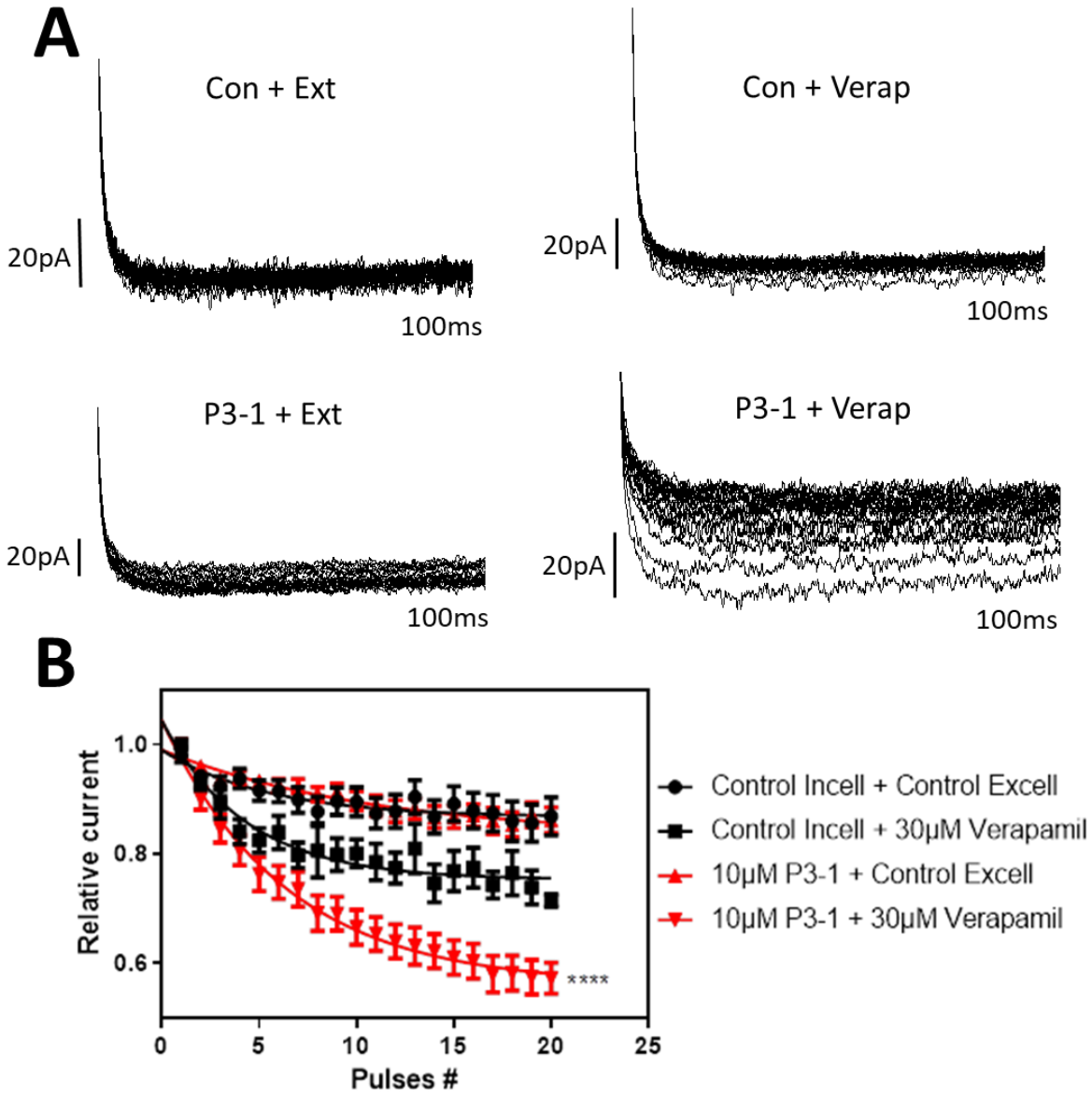

Figure 4.12. Frequency-dependence of block in $Ca_v1.3$ with or without 10μM P3-1 in the intracellular solution and in the absence or presence of 30μM verapamil. (**A**) Example trains of 20 depolarizations at 1 Hz in the presence of indicated agents. (**B**) The asterisks showed the unpaired t-test in the absence and presence of P3-1 with 30μM verapamil block (****, $P < 0.0001$). Plateau of the frequency-dependent block: (1) Control Incell + Control Excell: 0.87; (2) Control Incell +30 μM Verapamil: 0.75; (3) 10μM P3-1 + Control Exell: 0.83; (4) 10μM P3-1 + 30 μM Verapamil: 0.56.

4.8 Discussion

4.8.1 Conclusion

In contrast to the well-studied and highly conserved small molecule drug-binding pockets, we explored the intracellular interactions between subunit $Ca_v\beta$ and Ca_v α_1. However, our understanding of the precise binding nature of the interactions of the intracellular domains of Ca_v1 and $Ca_v\beta$ is limited since Cryo-EM structures do not resolve many of these interactions. Our lab has established the findings of Ca_v1 II-III loop activity in Ca^{2+} -induced Ca^{2+} release in pancreatic β-cells (Jacobo et al., 2009; Wang et al., 2014; Pratt et al., 2015), and we found that expression of $Ca_v1.3$/II-III loop silence the glucose-stimulated action potentials in INS-1 cells. Oppositely, the $Ca_v1.2$/II-III loop increases action potential firing.

We sought to understand how the expression of the $Ca_v1.3$/II-III loop could suppress glucose-stimulated action potential frequency in INS-1 cells, reasoning that the mechanism could present a novel therapeutic strategy to inhibit Cav1.3 selectively. We characterized the voltage-dependence of activation and inactivation of different $Ca_v\alpha_1$ subunits, co-expressed with $Ca_v\beta_3$, $Ca_v\alpha_2\delta_1$, and $Ca_v1.3$/II-III loop fused with eGFP in transfected tsA-201 cells. The long-form $Ca_v1.3$ turned out to be the only subunit modulated by the $Ca_v1.3$/II-III loop, which shifted the inactivation by -15 mV to a more hyperpolarizing voltage. The shifted voltage range suggests an innovative approach to antagonize $Ca_v1.3$ by modulating the channel availability.

Next, we tried to locate the molecular determinants in the $Ca_v1.3$/II-III loop, which could reproduce the inactivation shift. We generated the desired peptides and introduced them into patch pipettes, waiting for at least three minutes before experiments. Then, we divided the $Ca_v1.3$/II-III loop into C-terminal and N-terminal halves, and they could reproduce the inactivation shift together. Therefore, we dissected both termini into shorter truncated peptides, including putative SH3 and GK domain ligands (P1-1, P2-1, and P3-1), and control peptides (P1-2, P2-2, and P3-2) designed to test the involvement of SH3 domain ligands, which required the prolines. P1-1 could reproduce the inactivation shift induced by N-terminal, and P2-1 could not as expected. Neither P2-1 nor P2-2 altered the voltage dependence of inactivation of $Ca_v1.3$. Interestingly, both P3-1 in C-terminal and the control peptide P3-2 could reproduce the -15 mV shift, and P3-1 is the shortest effective peptide that could introduce this significant shift. We also tested P3-1 on $Ca_v1.2$ and $Ca_v1.3_{42A}$. We found that P3-1 shifted the inactivation of $Ca_v1.2$ to a more positive voltage, which

further supports the possibility of differential regulation of $Ca_v1.2$ and $Ca_v1.3$ by $Ca_v1.3$/II-III loop. Surprisingly, unlike the results in the presence of the $Ca_v1.3$/II-III loop, P3-1 successfully shifted $Ca_v1.3_{42A}$ to a hyperpolarizing voltage by -13 mV, suggesting the modulation of $Ca_v1.3/\beta_3$ by the P3-1 peptides is independent of C-terminal regulation.

Since the peptides we generated exhibit putative SH3 and GK domain ligands, we were curious whether the $Ca_v\beta$ subunit, which contains both SH3 and GK domains, might modulate the voltage-dependent inactivation shift together with the $Ca_v1.3$/II-III loop. Furthermore, we were curious whether the β subunit was required for peptide modulation of Cav1.3, and if so, whether there is any selectivity for specific β subunits. We found that $Ca_v\beta$ was required to shift the inactivation in the presence of the $Ca_v1.3$/II-III loop. Since $Ca_v1.3$ is highly associated with $Ca_v\beta_3$ and $Ca_v\beta_4$, we asked whether there exists $Ca_v\beta$ specificity interacting with $Ca_v1.3$. Among four $Ca_v\beta$ subunits we tested in $Ca_v1.3$, $Ca_v\beta_4$ did not alter channel gating in the presence of peptide P3-1. On the other hand, when co-expressed with $Ca_v\beta_{2a}$, P3-1 shifted steady-state inactivation of $Ca_v1.3$ by -5mV. P3-1 shifted the inactivation of $Ca_v1.3$ co-expressed with $Ca_v\beta_{1b}$ by -15 mV measured 3 minutes after break-in, but this significant shift was transient and was not detected when $V_{1/2}$ inactivation was measured 10 min after the break-in.

Moreover, we tested the effect of P3-1 on steady-state inactivation of the most prevalent VGCC in the cardiovascular system, $Ca_v1.2/\beta_{2a}$, and found that it shifted $V_{1/2}$ inactivation by +2 mV 3 minutes after the break-in and by +6 mV 10 min after the break-in. Thus, our results show that the P3-1 peptide preferentially shifts $V_{1/2}$ inactivation of $Ca_v1.3$ channels coupled to the β3 subunits to more negative potentials. As shown in Figure 4.3, this reduces the availability of $Ca_v1.3$ channels for opening. In contrast, the positive shift in $V_{1/2}$ inactivation of $Ca_v1.2/\beta_{2a}$ induced by P3-1 will not interfere with $Ca_v1.2$ channel gating at physiologically relevant voltages.

Our experiments showing that P3-1 potentiates verapamil block of $Ca_v1.3$ are exciting for two reasons. First, it supports our conclusion that P3-1 stabilizes the inactivated state of $Ca_v1.3$ since verapamil preferentially binds to the inactivated state of the channel (Dilmac 2004). Second, it suggests that the β subunit-selective modulation of $Ca_v1.3$ by P3-1 offers a strategy to make an existing drug more potent in blocking $Ca_v1.3$. To further examine the regulation of $Ca_v\beta$ regulating the channel gating in the presence of $Ca_v1.3$/II-III loop, we were interested in whether phenylalkylamine binds to P3-1 treated $Ca_v1.3$ with a higher affinity. Excitingly, 10 μM P3-1

increased the blocking by 30% in the presence of 30 μM Verapamil. This observation provides solid support on P3-1 modulating channel opening probability.

4.8.2 $Ca_v\beta$ regulation of L-VGCC gating

In summary, our results suggest that the $Ca_v1.3$/II-III loop contains motifs that interact preferentially with the $Ca_v\beta_3$ subunit to regulate channel inactivation, and short peptide mimics of these regions can regulate inactivation in a β subunit-dependent manner. The final challenge and future direction include understanding the molecular mechanism of the $Ca_v1.3$/II-III loop interacting with $Ca_v\beta$ to alter the channel opening and developing a therapeutic strategy based on the selectivity of P3-1 modulation of $Ca_v1.3$ co-expressed with $Ca_v\beta_3$. A prevalent model of $Ca_v\beta$ regulating L-type channels includes the intracellular I-II loop, C-, and N-termini forming a "hinged lid" to occlude the pore by biding to the pore-lining regions of S6 segments (Stotz et al., 2000) or the disruption of IVS6-AID linker by $Ca_v\beta$ (Findeisen et al., 2009). In addition, besides the intracellular I-II loop, $Ca_v\beta$ interacts with the IQ motif in the C-terminal of $Ca_v1.2$ (Lao et al., 2008; Zhang et al., 2005; Soldatov 2012), III-IV loop, and N-/C- termini in other VGCCs (Qin et al., 1997; Tareilus et al., 1997; Walker et al., 1998 and 1999). However, these low-affinity interactions only impose significant effects when $Ca_v\beta$ SH3-HOOK is near $Ca_v\alpha_1$ (Chen et al., 2009). Additionally, the previous studies have not found solid gating alterations of $Ca_v\beta$ on $Ca_v\alpha_1$ in the AID-independent manner (See Braei and Yang 2010 for review).

We were able to observe the intramolecular interactions of the intracellular II-III loop and β subunits in both endogenous INS-1 cell lines and heterologous expression systems in tsA-201 cells, but not in two-way immunoblotting (data not shown). Thus, the presence of intracellular I-II loop and other parts of Ca_v1 might intensify the changes of VDI in $Ca_v1.3$. In addition, oligomerization of $Ca_v\beta$ (Lao et al., 2010) provides more insights into interlaced $Ca_v\beta$ binding with various parts of $Ca_v\alpha_1$. However, whether the P3-1 can produce a compelling therapeutic effect on gating modulation without nonspecific targeting is called into question, as they are not naturally existing peptides. Thus, to fully understand the intracellular II-III loop and $Ca_v\beta$ regulation of VGCC gating, we need to examine different pairs in different tissues, cell types, subcellular locations, and at different developmental stages.

CHAPTER 5. RYR2 AND IRBIT REGULATION IN B-CELL ELECTRICAL ACTIVITY

5.1 Introduction

Ca^{2+} signaling in β-cell function during the process of glucose-induced insulin secretion (GSIS) includes L-type voltage-gated calcium channel (L-VGCCs)-induced Ca^{2+} influx and Ca^{2+}-induced Ca^{2+} release (CICR) from intracellular stores modulated by ryanodine receptors (RyRs) and inositol 1,4,5-triphosphate receptors (IP_3Rs). ER Ca^{2+} dysregulation is associated with insulin reduction and pancreatic β-cell death, the pathological cause of type 1 and type 2 diabetes (Stein et al., 1997; Gilon et al., 2014; Tersey et al., 2012; Tong et al., 2015). The roles of VGCCs in β-cell function are now better understood, but pancreatic β-cell ER Ca^{2+} loss is not well studied (Yamamoto et al., 2019).

The primary Ca^{2+} channels, transporters, and receptors in β-cells were summarized in Chapter 1.6. Among three subtypes of RyRs, RyR2 is the predominant RyR found in β-cells and activated by Ca^{2+} influx through either $Ca_v1.2$ or $Ca_v1.3$ following depolarization elicited by inhibition of the K_{ATP} channel (Bruton et al., 2002; Johnson et al., 2004). RyR2 was found to induce insulin secretion at low glucose concentration (3mM) but not in higher glucose concentration (Johnson et al., 2004). This biphasic response was explained by RyR's open probability (Bezprozavanny et al., 1991) and the solved structure (de Georges et al., 2016), showing two Ca^{2+} binding sites with different affinities that stimulate or inhibit channel opening. RyR dysfunction induces ER Ca^{2+} leak under ER stress conditions (Yamatoto et al., 2019). Deletion of RyR2 was shown to perturb multiple signaling pathways, including Ca^{2+} dynamics, insulin secretion, cortical f-actin density, and glucose-stimulated electrical activity in INS-1 cells (Stantulli et al., 2017b; Luciani et al., 2008; Dixit et al., 2013).

Interestingly, our preliminary data (Rantz et al., unpublished) observed increased ER Ca^{2+} release from IP_3R in $RyR2^{KO}$ INS-1cells response to glucose or tolbutamide stimulation. Thus, we asked whether the IP_3R binding protein released with inositol 1,4,5-triphosphate (IRBIT, also called AHCYL1 or DCAL) is modulated in this process. IRBIT is a regulatory protein that modulates IP_3 receptors, $Na^+/HCO3^-$ co-transporters, Cl^- channel CFTR, Cl^-/HCO_3^- exchanger, and Ca^{2+} flux between ER and mitochondria, and production of PIP_2 in the plasma membrane (Ando et al., 2014; Santulli and Marks 2015; Itoh et al., 2021). Thus, IRBIT's most vital role in ER Ca^{2+}

homeostasis is competing with IP_3 for the common binding site on IP_3R and suppressing IP_3R activation (Ando et al., 2003, 2006).

We hypothesize that RyR2 is a hub for regulating Ca^{2+} signaling in pancreatic β-cells, and IRBIT activity is a critical component of the RyR2 signaling complex. We also propose that IRBIT activity is regulated by Ca^{2+} release from ER via activation of Ca^{2+} -dependent kinases. Additionally, we expect that altered RyR2/IRBIT signaling may contribute to the deficits in β-cell function observed in type 2 diabetes.

5.2 Current density of INS-1 knock-outs

To determine the role of RyR2 in pancreatic β-cells, we knock-out RyR2 and/or IRBIT in INS-1 cell lines and generated RyR2-knockout and IRBIT-knockout INS-1 cell lines. To assess the current density of functional VGCCs in the membranes of these INS-1 cells, we recorded the capacitance of a single INS-1cell before applying the current-voltage relation in the standard solution set, which contains barium as a charge carrier for measuring calcium current activity.

5.2.1 Capacitance measurements

Cell membrane capacitance is measured because the electrical property of capacitance, which is the capacity to separate and store electric charge, is proportional to the area of the capacitor, which is the biological membrane. The capacitance of a cell is directly proportional to the surface area of its cell membrane (Hille, 1978). A β-cell with a diameter of 15μm can have a capacitance of ~7pF, supported by the experimental measurement (Göpel et al., 1999). We obtained the capacitance measurements using built-in capacitance dithering capacity in Axopatch 200B (Molecular Devices).

5.2.2 Current amplitude measurements

The amplitude of VGCC-mediated current relates to the total number of functional VGCCs on the cell surface. The current-voltage relationship was used to generate the whole-cell currents evoked by voltage steps from -70mV to +50mV in 10mV increments, from a holding potential of

-80mV. We measured the peak currents at each voltage step with on-line leak subtraction (p/-4) in a standard solution set containing barium.

5.2.3 Current density of INS-1 and knock-outs

We generated the current density by using the peak current (pA) elicited during a 12-voltage step I-V ensemble recording (see Chapter 2) and dividing by membrane capacitance (pF). The peak current did not always occur at the same voltage between cells but was usually elicited at either -10 mV, 0 mV, or +10 mV. In Figure 5.1.A, example traces of three INS-1 cell lines are shown with current-voltage relation, and the peak currents were recorded to generate the statistics in Figure 5.1.B and 5.1.C. The VGCC current densities measured at 0mV in control INS-1, $RyR2^{KO}$ and $IRBIT^{KO}$ are: 16.71 ± 2.26 pA/pF (N = 11), 27.53 ± 3.90 pA/pF (N = 23), 23.47 ± 1.77 (N = 19) pA/pF respectively (Figure 5.1.B). Unpaired t-tests were done to compare the two cell lines out of three cell lines: INS-1 is significantly different from either $RyR2^{KO}$ (****, $P <$ 0.0001) or $IRBIT^{KO}$ (****, $P <$0.0001), and $RyR2^{KO}$ and $IRBIT^{KO}$ are also distinct from each other (***, $P <$0.001). We generated the results for Figure 5.1.B by measuring VGCC current densities measured from -70mV to +50mV at a 10mV increment (Figure 5.1.C), which is in line with the observation we had at peak current density. Multiple unpaired t-tests were done among three cell lines at thirteen voltages, and the results are shown in Table 5.1. We measured their voltage-dependence of activation and reported no difference (Figure 5.2.A). We also applied Tris-barium and calcium-based extracellular solution measurements and saw the same trend (Figure 5.2.B).

The total whole-cell Ba^{2+} current in the INS-1 cell is comprised of at least three different VGCC, $Ca_v1.2$, $Ca_v1.3$, $Ca_v2.1$, and $Ca_v2.3$ (Yang and Berggren 2006). VGCC current density in $RYR2^{KO}$ nearly doubled compared to the control, while $IRBIT^{KO}$ also significantly increases the current density. To determine if the upregulation of current density observed in RyR and IRBIT knock-out cells is subtype-specific, we measured the fraction of L-type current (i.e., $Ca_v1.2$ and $Ca_v1.3$) in control and knock-out cells.

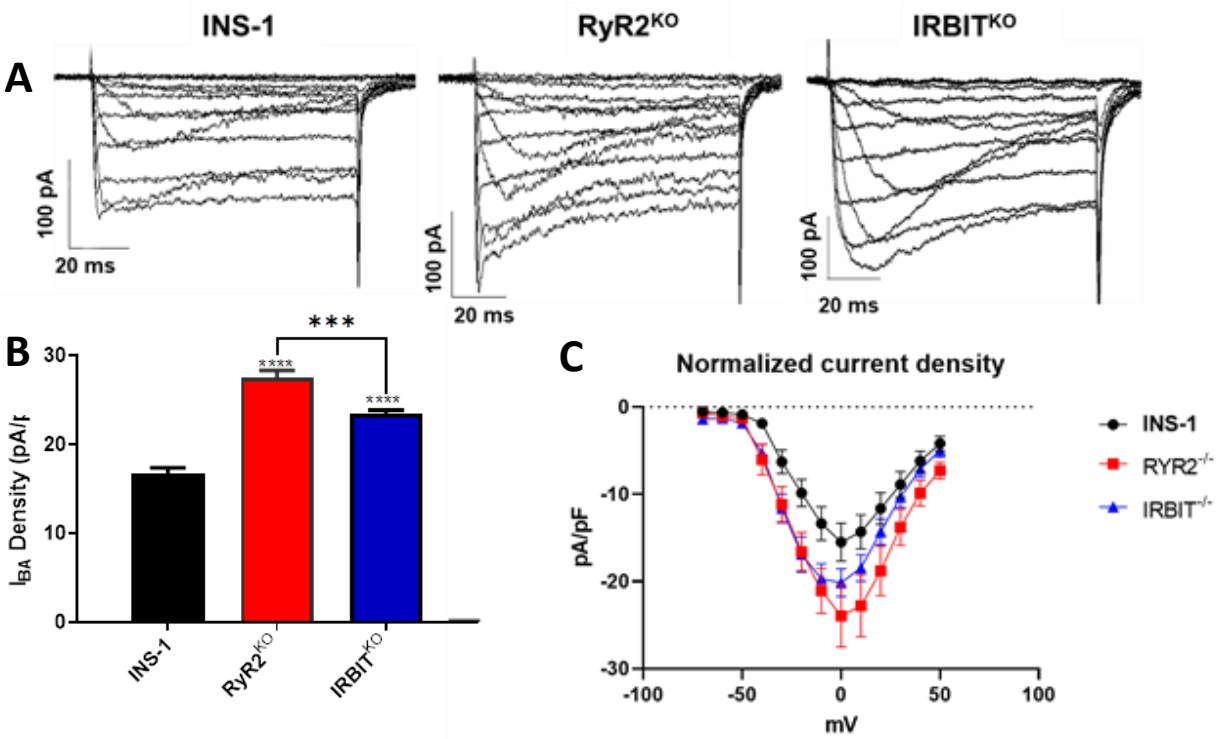

Figure 5.1. Current density of INS-1 cells and knockouts. (**A**) Example traces of current-voltage (I-V) relationship of INS-1, RyR2^{KO} and IRBIT^{KO} cells. (**B**) Voltage-gated Ca^{2+} Channel (VGCC) peak current density measured in INS-1 (black), RyR2^{KO} (red) and IRBIT^{KO} (blue) with perfusion of Ba^{2+} -based extracellular solution, and current density is greater in RyR2^{KO} than IRBIT^{KO} (****, P <0.0001) and control INS-1 cells (***, P < 0.001). (**C**) Voltage-gated Ca^{2+} channel (VGCC) current density measured from -70 mV to +50 mV. Multi-unpaired t-tests were done between two of each cell lines and it supports the single-value observation in (B). The P-values are recorded in the Table 5.1.

Table 5.1 Current densities and unpaired t-tests P-values of VGCC currents among control, $RyR2^{KO}$, and $IRBIT^{KO}$ INS-1 cell lines at stepping voltages from -70 mV to +50 mV.

mV	INS-1 (pA/pF)	$RyR2^{KO}$ (pA/pF)	$IRBIT^{KO}$ (pA/pF)	INS-1 vs $RyR2^{KO}$ (P-value)	INS-1 vs $IRBIT^{KO}$ (P-value)	$RyR2^{KO}$ vs $IRBIT^{KO}$ (P-value)
-70	-0.5485	-0.6998	-1.386	0.20602	**0.020078**	0.051665
-60	-0.6276	-1.052	-1.315	**0.027653**	**0.01916**	0.380116
-50	-0.8689	-1.294	-1.841	0.104478	**0.004648**	0.119369
-40	-1.886	-6.032	-5.281	**0.029084**	**0.004437**	0.710831
-30	-6.291	-11.16	-11.61	0.053856	**0.019226**	0.862405
-20	-9.874	-16.59	-16.90	**0.017896**	**0.010611**	0.917676
-10	-12.06	-21.07	-19.69	**0.004752**	**0.002367**	0.412791
0	-13.72	-26.73	-20.14	**0.002309**	**0.0045**	**0.017986**
10	-12.97	-24.35	-18.43	**0.0059**	**0.018696**	0.088543
20	-11.65	-19.57	-14.33	**0.023781**	0.264269	0.106316
30	-8.880	-14.36	-10.31	**0.037433**	0.459539	0.097638
40	-6.185	-10.31	-7.147	**0.02959**	0.514106	0.070089
50	-4.194	-7.275	-4.970	**0.021708**	0.508468	0.073153

*All current densities were averaged (standard deviation not shown, N= 11~ 24). Multiple unpaired Welch's t-tests were used to estimate the significance, and all values smaller than 0.05 are in bold.

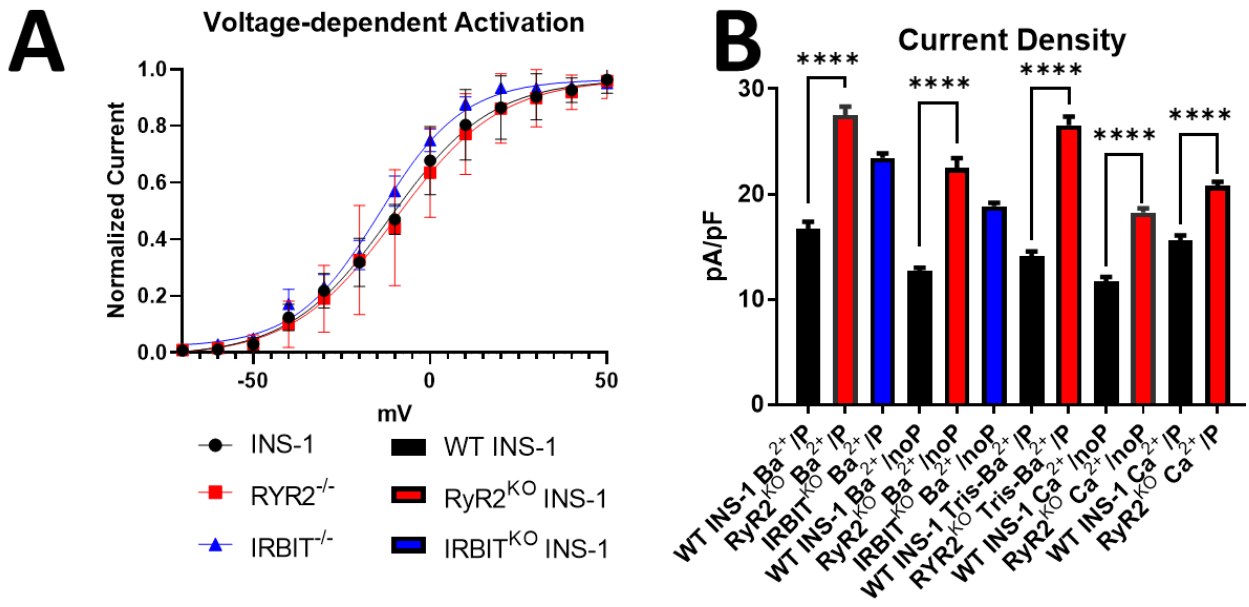

Figure 5.2. Biophysical characterization of control, RyR2^{KO} and IRBIT^{KO} INS-1 cells. (**A**) Voltage-dependent activation of three cell lines and no significant difference was reported. (**B**) Current density of INS-1 cells and RyR2^{KO} in three solution sets with or without prolonged perfusion. Current densities (pA/pF) in (1) Ba^{2+} solution sets with perfusion were reported in Figure 5.2; (2) Ba^{2+} solution sets with no perfusion: WT: 12.73 ± 1.00 (N = 14), RyR2^{KO}: 22.42 ± 4.26 (N = 22); (3) Tris-Ba^{2+} solution sets with perfusion: WT: 14.13 ± 1.64 (N = 14), RyR2^{KO}: 26.56 ± 3.06 (N = 14); (4) Ca^{2+} solution sets with perfusion: WT: 15.60 ± 1.73 (N = 12), RyR2^{KO}: 26.56 ± 3.06 (N = 14); (5) Ca^{2+} solution sets without perfusion: WT: 11.74 ± 1.45 (N = 13), RyR2^{KO}: 18.26 ± 1.63 (N = 16).

5.3 Identification of VGCC subtypes

Given the significant increase in VGCC current density, we asked which VGCC subtype is upregulated. L-VGCC is the predominant VGCC in mouse β-cells over other types such as P/Q-type and R-type VGCCs. To determine if the fraction of L-type current relative to total current is changed upon RyR2 or IRBIT deletion, we applied 5μM nifedipine to control, RyR2^{KO}, and IRBIT^{KO} cells under voltage clamp and measured the fraction block in each cell line. Cells were held at -80 mV and stepped to 10 mV for 100 ms at a frequency of 0.05 Hz. In control INS-1 cells, 5μM nifedipine blocked ~20 percent of whole-cell current, and this fraction was not different in RyR2^{KO} or IRBIT^{KO} cells (Figure 5.3). Thus, the mechanism that leads to the increase in the whole-cell VGCC current in the KO cell lines does not change the proportion of L-type to non-L-type current and is likely, not subtype-specific. Thus, the upregulation of VGCC current density might

be due to P/Q-type or R-type VGCC increase in the β-cells, or more likely, all existing VGCCs are upregulated in the knock-out cell lines that no selective VGCC antagonist can differentiate the subtypes.

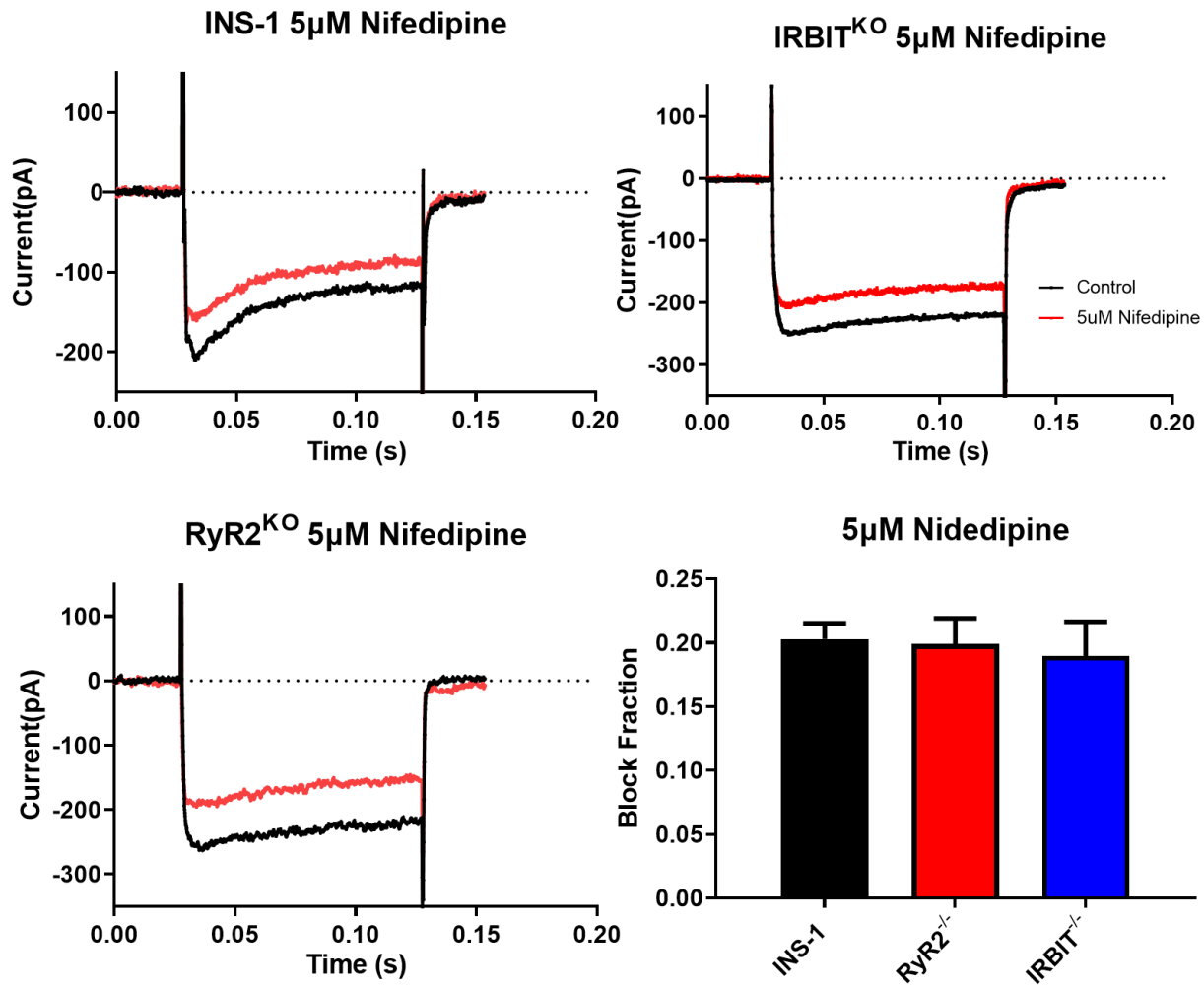

Figure 5.3. Example traces of 5μM nifedipine block on control, RyR2^{KO} and IRBIT^{KO} INS-1 cells, in the absence or (red) in the presence (black) of 5 μM nifedipine. Fractional block was calculated for three lines. Control INS-1 (black): 0.20 ± 0.05 (N = 20); RyR2^{KO} (red): 0.20 ± 0.11 (N = 29); IRBIT^{KO} (blue): 0.19 ± 0.08 (N =8). Unpaired t-tests among three cell lines showed no statistical difference.

5.5 Glucose-stimulated action potential in INS-1 cells

Since glucose stimulates electrical activity in the form of trains of action potentials in pancreatic β-cells, we next asked if deletion of RyR2 or IRBIT from INS-1 cells regulates this activity. Perforated whole-cell patch-clamp is a variant of the patch-clamp technique used to measure the sum activity of ion channels in the plasma membrane of a single cell. It was developed to maintain the cytoplasm so that the intracellular solution does not wash out crucial elements of signaling cascades or metabolism during the experiment (Molleman 2002). Whole-cell perforated patch configuration was used with INS-1, $RyR2^{KO}$, and $IRBIT^{KO}$ cells to measure action potentials in I=0 current-clamp mode. The patch resistance was monitored until it reached 200 MΩ, then we applied 40μM diazoxide, the K_{ATP} channel activator, which effectively hyperpolarized the cell membrane potential. Diazoxide binds to sites on SUR1, increasing K_{ATP} channel open probability (Drews et al., 2010). Once the cell stabilized at the correct resting membrane potential (~ -65 mV), 18mM glucose in the standard solution set was applied via extracellular perfusion.

5.5.1 $RyR2^{KO}$ GSAP and SK channel regulation

Upon inhibition of action potentials started firing, trains of action potentials were recorded for a minimum of three minutes. The average action potential frequencies were determined using uniform bursts of action potentials and excluding gaps between bursts. We found that the GSAP frequency is doubled by RyR2 deletion. Control INS-1 cells displayed an action potential frequency of 0.94 ± 0.27 Hz (N = 9) while that in $RyR2^{KO}$ cell was 2.16 ± 0.36 Hz (N = 15). Moreover, we applied the compound apamin, a blocker of the SK ($K_{Ca}3$) channel, antagonizing the Ca^{2+} -activated K^+ outward current, stimulating action potential firing and reducing action potential amplitudes in control INS-1 cells (Figure 5.4.A and Jacobson et al., 2010). In contrast, $RyR2^{KO}$ cells did not respond to 1μM apamin application (Figure 5.4.A and 5.4.B).

We further analyzed the INS-1 cell action potential bursts. Glucose-stimulated action potentials can be dissected into the following phases: (1) β-cell action potential upstrokes are mainly associated with regenerative action of L-VGCCs; (2) β-cell action potential repolarization associated with Ca^{2+} -dependent inactivation and voltage-dependent inactivation of Na^+ channels along with activation of delayed rectifying $K_v2.1$ and BK channels; (3) β-cell action potential plateau is influenced by SK channel and two-pore K^+ channel (Rorsman and Ashcroft 2018).

Afterhyperpolarization (APH) is a principal feedback mechanism controlling the frequency and patterning of action potentials. APHs are driven by SK channel currents, maintained after repolarization, driving the membrane potential to more negative values and prolonging the time interval between action potentials (i.e., decreasing frequency). To explain our results in action potential frequency, we also measured the AHP in both control and $RyR2^{KO}$ INS-1 cells by subtracting the lowest potential by the previous plateau. The AHPs measured for INS-1 and $RyR2^{KO}$ generated using weighted average were: -11.52 mV (N=8, n=9310) and -5.976 mV (N=14, n=21241) respectively in the absence of 1μM apamin, -5.380 mV (N=6, n=5371) and -6.957 mV (N=6, n=7018) respectively in the presence of 1μM apamin. The action potential amplitudes are not statistically different in INS-1 and $RyR2^{KO}$ cells in the absence and presence of apamin (data not shown). Thus, the increased glucose-stimulated action potential frequency, the unresponsiveness of action potential frequency to apamin, and the reduced AHP amplitude in $RyR2^{KO}$ cell all argue that SK channels are not activated during glucose stimulation in $RyR2^{KO}$ cells.

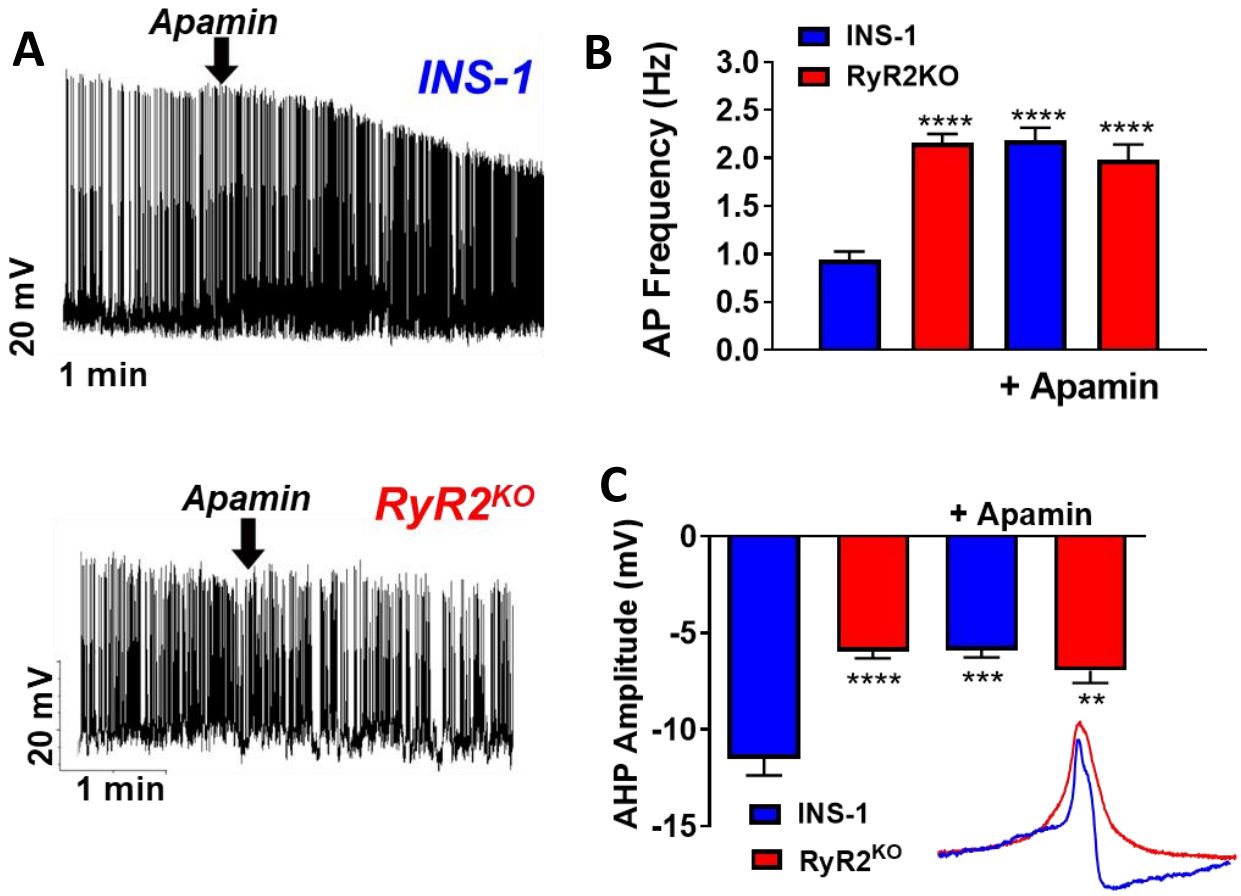

Figure 5.4. Glucose-activated action potentials of control and RyR2^{KO} INS-1 cells. (**A**) Example action potentials (APs) elicited by 18mM glucose are more frequent in RyR2^{KO} than control, and upon the addition of 1μM apamin action potentials of control INS-1 increase while RyR2^{KO} stayed unchanged. (**B**) Average AP frequency measured in control and RyR2^{KO} INS-1 cells in the absence and presence of 1μM apamin. (**C**) Afterhyperpolarization (AHP) measure in control and RyR2^{KO} INS-1 cells in the absence and presence of apamin and representative traces of INS-1 and RyR2^{KO} in the absence of apamin. AHPs in INS-1 and RyR2^{KO} cells were -11.52 mV (N=8, n=9310) and -5.976 mV (N=14, n=21241) respectively in the absence of 1μM apamin, -5.380 mV (N=6, n=5371) and -6.957 mV (N=6, n=7018) respectively in the presence of 1μM apamin. N means the number of single cells, and n means the number of action potentials measured.

5.5.2 IRBIT^{KO} GSAP

In the light of the marked increase in current density in IRBIT^{KO} cells, we also examined its role in regulating GSAP in INS-1 cells. However, IRBIT^{KO} cells have volatile electrical activity. Among 25 cells that responded to glucose stimulation, only three cells showed stable firing for more than 500 action potentials. Most of the cells had either short, grouped bursts in between long silent intervals or had a progressive decrease in both action potential amplitude and frequency during 18mM glucose stimulation. Action potential frequency ranged from 0.57 to 2.93 Hz among the 25 cells, with an average of the most stable cells at 1.91 ± Hz (N =2, n =1432) and an average of all cells including intermittent bursts or in response to current injection (if glucose did not stimulate electrical activity) of 1.62 ± 0.77 Hz (N =25, n =9678) (Figure 5.5). Based on limited data, we observed the action potential frequency in IRBIT^{KO} with 1μM apamin slightly decreased compared to experiments in control INS-1 cells or RyR2^{KO} cells. Moreover, we observed very slow action upstrokes and repolarization in the limited stable IRBIT^{KO} cells (Figure 5.6).

The difficulty of obtaining GSAP of IRBIT^{KO} cells does raise some interesting questions. Deletion of IRBIT was confirmed to upregulate IP_3R activity and potentially influence store-operated Ca^{2+} entry (SOCE) and conductance of other ion channels. In addition, long silent intervals between grouped bursts, slowed upstroke and APH, and reduced amplitude suggests a role for IRBIT in cross-talk with additional ion channels, potentially calcium and potassium channels.

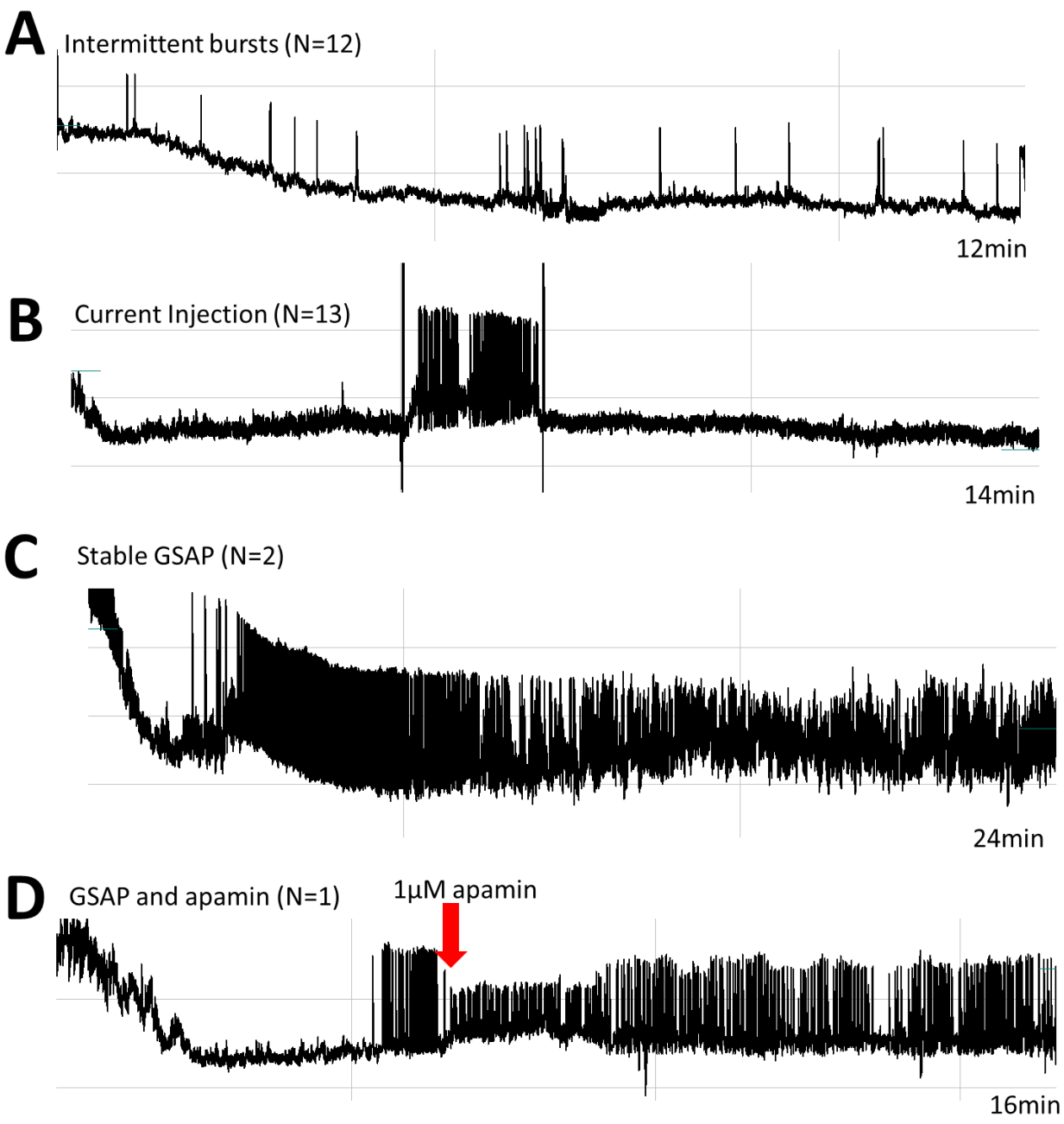

Figure 5.5. Example traces of current-clamp measurements of IRBIT^{KO} INS-1 cells in response to 18mM glucose. (**A**) 12 cells showed intermittent grouped action potentials in the presence of 18mM glucose. (**B**) 13 cells did not respond to 18mM glucose stimulation but did respond to current injections. (**C**) 2 cells responded to 18mM glucose like control and RyR^{KO} cells. (**D**) One cell responded to 18mM glucose, and 1μM apamin reduced action potential magnitude and the frequency slightly from 1.11 Hz (n=60) to 0.66 Hz (n=291).

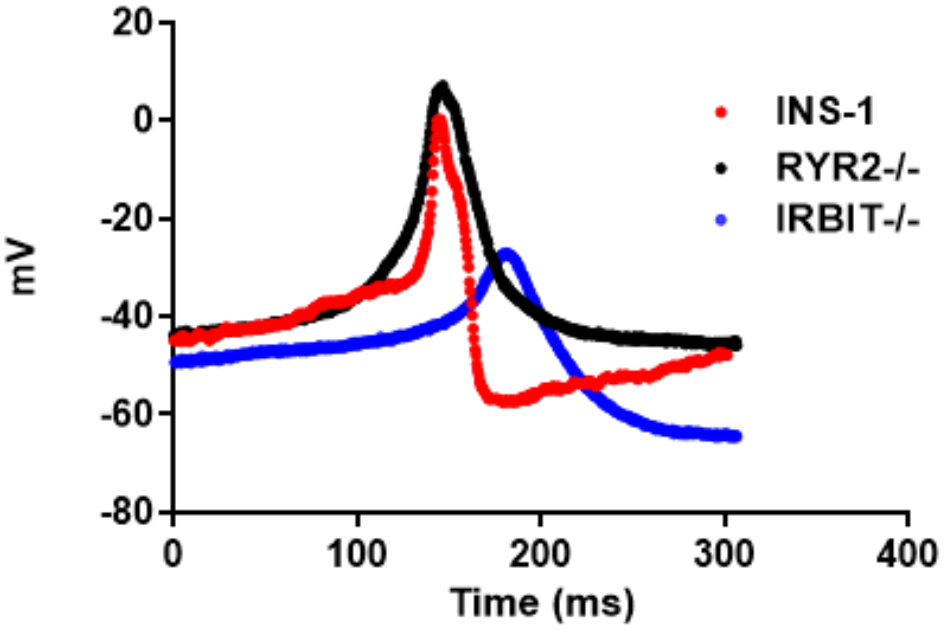

Figure 5.6. Afterhyperpolarization (AHP) measured in control, RyR2^{KO} (Figure 5.4.C), and IRBIT^{KO} INS-1 cells in the presence of 18 mM glucose. Since IRBIT^{KO} INS-1 cells have a very slow upstroke and afterhyperpolarization with minimal sample size (N=2), we do not report the statistical analysis.

5.6 PIP$_2$ potentially regulates current density and GSAP in the knock-outs

5.6.1 PIP$_2$ and ion channel modulation

PIP$_2$ is a plasma membrane lipid, contributing to numerous intracellular signaling events, including regulation of many ion channels via binding at the plasma membrane (Hille et al., 2015; Hilgemann et al., 2018). G_qPCR induced PIP$_2$ hydrolysis by phospholipase C (PKC) is the primary driver of dynamic PIP$_2$ level change (Suh and Hillie 2002; Harraz et al., 2020). PIP$_2$ contributes to the negatively charged inner leaflet of the plasma membrane, attracting cations, including Ca^{2+} (McLaughlin et al., 2002; Won et al., 2006). How PIP$_2$ modulates K^+ channels has been extensively studied (Hille et al., 2015), and PIP$_2$ enhances rat SK channel activity via CaM-SK channel complex (Lu et al., 2002; Zhang et al., 2014).

We briefly discussed the PIP$_2$ regulation of K_{ATP} channels, TRP channels, and GPCR in Chapter 1. However, how exactly PIP$_2$ potentially contributes to Ca^{2+} dysregulation and pancreatic β-cell apoptosis is not well understood. Our preliminary data observed reduced PLC activity

(Rantz et al., unpublished) and elevated PIP_2 (Harvey et al., unpublished) in $RyR2^{KO}$ INS-1 cells. Notably, the deletion of PIP_2 induces voltage-independent inhibition of VGCCs (Wu et al., 2002; Gamper et al., 2004; Roberts-Crowley et al., 2009). Additionally, production of PIP_2 and PIP_3 upon PI3K activation recruits PKB to the membrane, phosphorylating $Ca_v\beta_{2a}$ at S574 and increasing the channel expression and conductance (Viard et al., 2004). Thus, we asked whether PIP_2 plays a regulatory role in upregulating HVA Ca^{2+} channel activity to compensate for the loss of RyR2 and IRBIT.

5.6.2 PIP_2 and Ca^{2+} current inhibition

To closely monitor the quantitative change in Ca^{2+} current activity regulated by PIP_2, we introduced a rapamycin-induced dimerization of translocating phosphatases to hydrolyze PIP_2 at the plasma membrane (Hammond et al., 2012). This enzymatic chimera is fused with the FKBP (FK506 binding protein 12)-rapamycin-FRB (fragment of mTOR that binds rapamycin) ternary complex, used to recruit enzymes to the plasma membrane (Banaszynski et al., 2005; Varnai et al., 2006; Inobe and Nukina 2016). This chimera is a fusion protein named Pseudojanin (PJ), consisting of two phosphatases and converting PIP_2 to PI4P and further dephosphorylating PI4P (phosphatidylinositol 4-phosphate) into PI (phosphatidylinositol) (Varnai et al., 2006; Hammond et al., 2012). Thus, PJ is recruited to the plasma membrane upon rapamycin induction, decreasing PIP_2 and PI4P levels (Figure 5.7.A). Interestingly, rapamycin and FK506 target the RyR Calstabins, and prolonged exposure induces ER calcium dysregulation and mitochondrial dysfunction (Lombardi et al., 2017 a & b).

We transfected the control and $RyR2^{KO}$ INS-1 cells with Lyn11-FRB-CFP and PJ or Lyn11-FRB-CFP and PJ-dead and applied the whole-cell voltage clamp. We measured the current change of two transfections in two cell lines in the absence and presence of 1 μM Rapamycin. First, we measured the Ca^{2+} current change using standard Ba^{2+} solution set in the +10mV pulse protocol held at -80mV. We found that $RyR2^{KO}$ cells had a higher fractional block than wild-type INS-1 cells in response to rapamycin when PJ is expressed, and PJ dead did not show significant alterations (Figure 5.7.B). In addition, we measured the current density of two cell lines. Although the current density in $RyR2^{KO}$ is very variable, the decrease from group PJ to PJ-D is consistent (Figure 5.7.D). We calculated the fractional decrease of average current density before and after rapamycin treatment, and the normalized results supported that $RyR2^{KO}$ cells show a greater Ca^{2+}

current decrease than WT INS-1 cells in response to rapamycin, expressed with or without PJ (Figure 5.7.C). The decrease of current density and current in pulse protocols is very consistent. Thus, our result still supports our hypothesis that hydrolysis of PIP_2 might downregulate HVA Ca^{2+} channel activity.

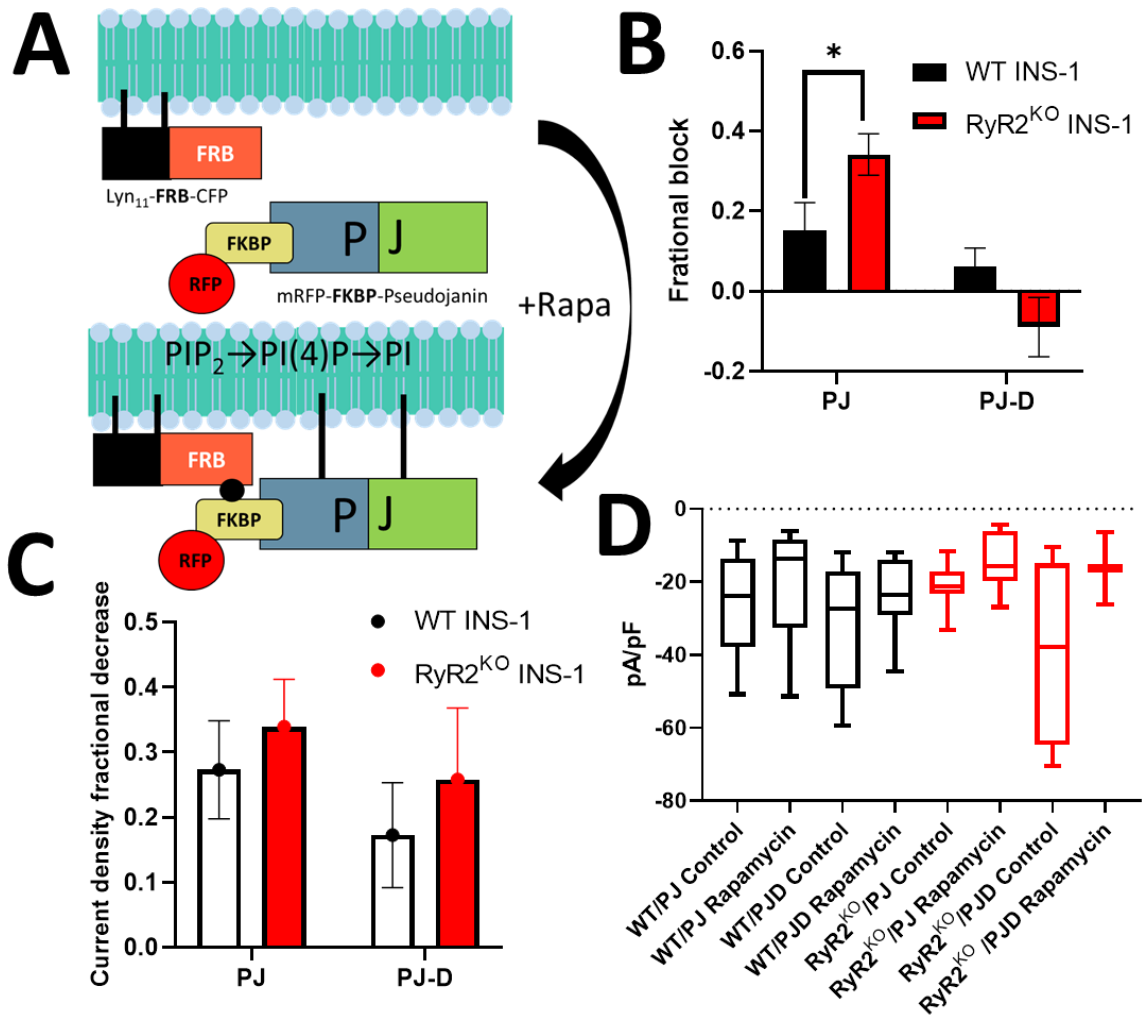

Figure 5.7. PIP_2 hydrolysis and Ca^{2+} current inhibition in control and $RyR2^{KO}$ INS-1 cells. (**A**) Rapamycin induces the translocation of FKBP fused with pseudojanin (PJ) and RFP (red fluorescence protein) to the plasma membrane (PM) and forms the complex with PM-anchored FRB. PJ converts PIP_2 into PI(4)P and further into PI. (**B**) Fractional block of wild-type and $RyR2^{KO}$ INS-1 cells expressed with PJ or PJ-D in the presence of 1μM rapamycin. WT: 0.15 ± 0.25 (N = 13) with PJ, 0.06 ± 0.13 (N = 8) with PJ-D; $RyR2^{KO}$: 0.34 ± 0.19 (N = 14) with PJ (*P < 0.05), -0.09 ± 0.15 (N =4). (**C-D**) Current density of WT and RyR2KO INS-1 cells expressed with PJ or PJ-D in the absence and presence of 1μM rapamycin. (C) Fractional change of current density in response to 1μM rapamycin. (D) Boxplot of eight data sets.

5.7 Discussion

5.7.1 Conclusion

We generated the $RyR2^{KO}$ INS-1 cell line to understand the role of RyR2 in pancreatic β-cell functions. These studies were prompt by our lab's previous work showing that expression of the $Ca_v1.2$II/III loop disrupts Ca^{2+} -induced Ca^{2+} release, likely by uncoupling $Ca_v1.2$ activity from activation of RyR2 (Jacobo et al., 2009; Wang et al., 2014; Pratt et al., 2015). Meanwhile, we observed the downregulation of IRBIT, an IP_3R inhibitory binding protein, in $RyR2^{KO}$ cells (Harvey and Rantz., unpublished). Thus, we generated the $IRBIT^{KO}$ INS-1 cell line to explore the ER Ca^{2+} channel dysregulation and impaired beta-cell function. We characterized the current density of the control, $RyR2^{KO}$, and $IRBIT^{KO}$ INS-1 cells using whole-cell voltage-clamp in three different solution sets with either Ba^{2+} or Ca^{2+} as the charge carrier. We found that the current density is doubled in $RyR2^{KO}$ cells compared to the control, and the current density of $IRBIT^{KO}$ increased by half of the wild-type. Given the dramatic increase in current density, we asked which VGCC was upregulated in the knock-out cell lines. Therefore, we applied the L-type selective inhibitor nifedipine, and 5μM nifedipine blocked 20 percent of the Ca^{2+} current among all three cell lines. The pharmacological result suggests a consistent upregulation of all VGCCs in the knock-out cell lines.

Next, we examined how these cells respond to glucose stimulus in a whole-cell perforated patch-clamp. We found that the action potential frequency also doubled in $RyR2^{KO}$ compared to the wild-type INS-1 cells. $IRBIT^{KO}$ cells showed extremely variable electrical activities in response to glucose stimulation, including $RyR2^{KO}$ -like GSAP, no response to glucose stimulus but current injection and intermittent grouped bursts. Additionally, we applied apamin, the SK channel blocker, to investigate whether we are able to see apamin-induced action potential increase in knock-out cells. Interestingly, apamin could double the action potential frequency in INS-1 cells but not in $RyR2^{KO}$ and $IRBIT^{KO}$ cells, suggesting the loss of SK channel activation when RyR2 or IRBIT is deleted. SK channel activity is a major contributor to the AHP in INS-1 cells, and AHP magnitude in $RyR2^{KO}$ is diminished and similar to that in apamin-treated control INS-1 cells. Thus, the alterations in GSAP frequency and the decrease in AHP amplitude in $RyR2^{KO}$ cells that parallel those measured in control INS-1 cells in the presence of apamin strongly argue that RyR2 activity is required for SK channel activation and modulation of glucose-stimulated electrical activity.

On the other hand, the mystery of upregulated current density has not been solved. Our preliminary data revealed reduced PLC activity and increased PIP_2 in $RyR2^{KO}$ INS-1 cells, and PIP_2 modulates various proteins at the plasma membrane, including upregulation of the HVA Ca^{2+} channel activity. Therefore, we proposed that upregulated PIP_2 might explain the upregulation of the HVA Ca^{2+} channels. Thus, we introduced the membrane anchor (Lyn11-FRB) and the translocatable fluorescence-tagged phosphatase, pseudojanin (PJ), to control the PIP_2 activity in the plasma membrane in the whole-cell patch-clamp experiments. We transfected control and $RyR2^{KO}$ INS-1 cells with Lyn11-FRB and PJ or PJ-dead (PJ-D) and induced the co-localization of Lyn11-FRB/PJ at the plasma membrane and PIP_2 hydrolysis using 1μM rapamycin. We observed a greater current inhibition in $RyR2^{KO}$ than wild-type with active PJ held at +10 mV. Additionally, the cells with PJ-D did not show a significant current decrease in response to rapamycin. We also examined the current density in four transfection conditions in the absence and presence of rapamycin and detected a uniform decrease in current density in the presence of rapamycin through all groups. Overall, increased PIP_2 hydrolysis on the plasma membrane in $RyR2^{KO}$ might explain the upregulation of Ca^{2+} channel activity in channel expression and GSAP.

5.7.2 Proposed models

We propose several models below to explain our observations in WT, $RyR2^{KO,}$ and $IRBIT^{KO}$ INS-1 cell lines. IRBIT binds to PIP kinases to form signaling complexes (Ando et al., 2015). We also observed sharply decreased basal PLC activity, IP_3 levels (Rantz et al., unpublished), IRBIT protein level, and insulin secretion (Harvey et al., unpublished) in $RyR2^{KO}$ cells. We proposed a model below to explain an increase in basal levels of PIP_2.

Glucose-stimulated L-VGCC activation (mainly $Ca_v1.2$) (see Section 1.6) activates calcium-induced calcium release (CICR) from IP_3R and RyR2 in INS-1 cells. Two Ca^{2+} binding sites with different affinities on RyR2 allow divergent responses to glucose concentrations. At low glucose conditions in control INS-1 cells, we propose an unaltered IRBIT level, which keeps the inactive form of IP_3R and limits the Ca^{2+} release from ER stores. Thus, a low glucose condition allows Ca^{2+} leak from RyR2 and a regular insulin exocytosis activity. On the other hand, high glucose concentration activates the SK channel, slows the afterhyperpolarization, and slows the action potential frequency. In the $RyR2^{KO}$ INS-1 cells, a reduced cytosolic IRBIT level enhances IP_3R releasing Ca^{2+} from ER stores. As a result, no Ca^{2+} leak goes through RyR2 and reduces basal

insulin secretion. The high glucose condition does not activate the SK channel, and little afterhyperpolarization is observed with high action potential frequency (Figure 5.9).

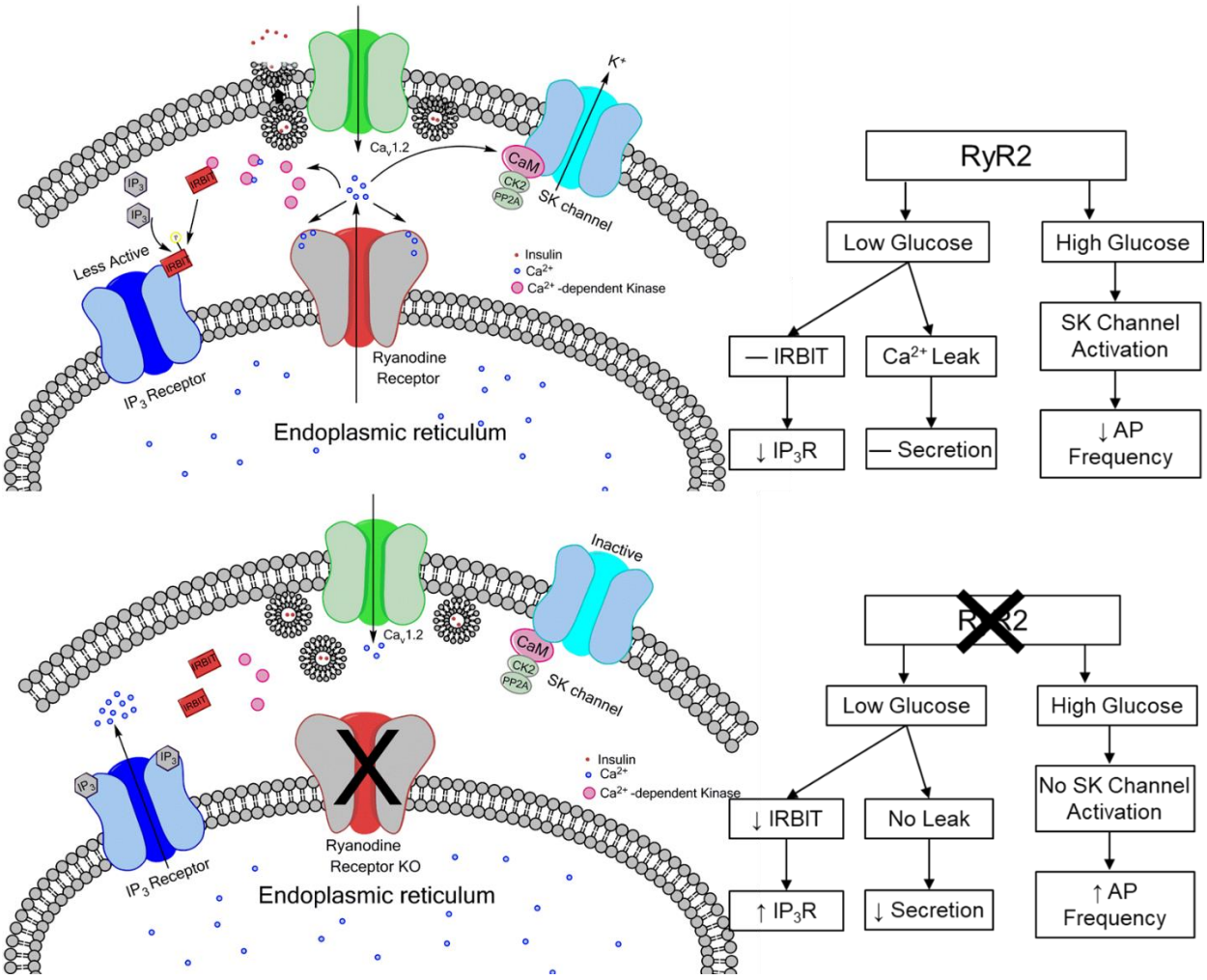

Figure 5.8. Models of ER Ca^{2+} regulation in control and $RyR2^{KO}$ INS-1 cells in response to low and high glucose stimulation.

CHAPTER 6. FUTURE DIRECTIONS

6.1 Development of selective L-VGCC subtype inhibitor

We have identified several molecular determinants to differentiate $Ca_v1.2$ and $Ca_v1.3$ in Chapter 3, and we ask whether we can develop a selective L-VGCC subtype antagonist based on our existing findings in our future directions. Three classes of L-VGCC antagonists, DHP, PAA, and BZT, show higher resistance in $Ca_v1.3$ than $Ca_v1.2$ but no selectivity. Therefore, developing either $Ca_v1.2$ or $Ca_v1.3$ inhibitors becomes challenging if we try to modify the existing small molecules. However, peptide toxins, a popular area in the 80s and 90s, are not considered and studied using modern techniques in current research. Previous studies showed that calcicludine (CaC), an L-VGCC selective peptide toxin, couples to DHP blockers allosterically and increases DHP binding affinity (Wang et al., 2007; Also see Section 1.5.5). Our preliminary data (Wang 2015) showed that CaC binding site adjacent to the selectivity filter in the extracellular IIIS5-3P loop is not conserved in $Ca_v1.3$. Our chimeric channel $Ca_v1.3+$, the $Ca_v1.2$-like $Ca_v1.3$ expressed $Ca_v1.2$ IIIS-3P loop, rescued the CaC sensitivity (Figure 6.1.B) without changing the voltage-dependent activation and inactivation (data not shown; Wang et al., unpublished).

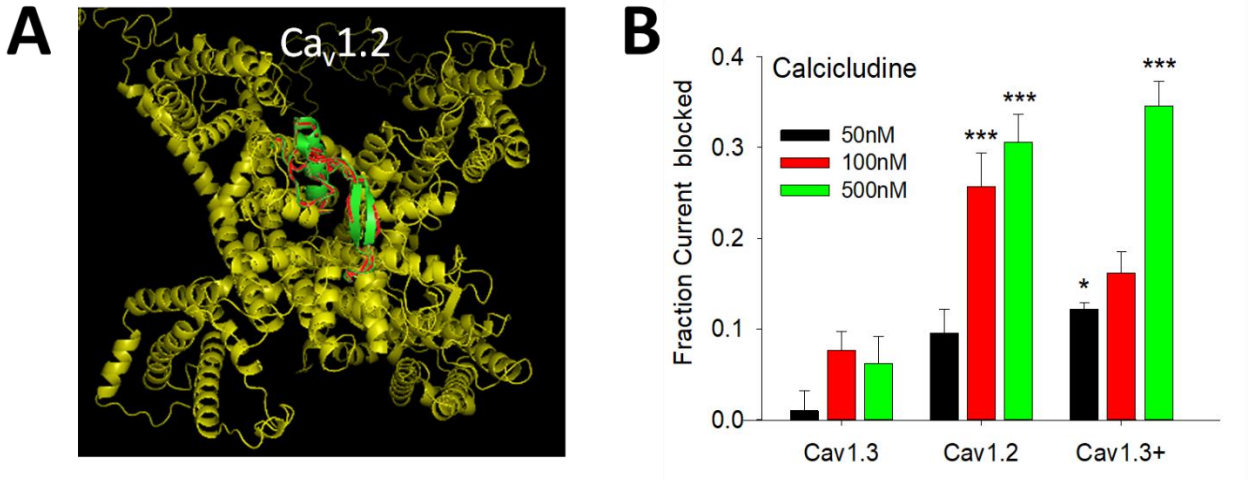

Figure 6.1. Calcicludine selectively binds to $Ca_v1.2$ by interacting with the IIIS5-3P loop. (**A**) Topical view of calcicludine binding to IIIS5-3P loop of $Ca_v1.2$ in 3D model. (**B**) Calcicludine inhibits the Ca^{2+} current conducted by $Ca_v1.2$, $Ca_v1.3$, and chimeric $Ca_v1.3+$ expressed with $Ca_v1.2$/IIIS-3P loop. Replacing the IIIS-3P loop of $Ca_v1.3$ rescued the calcicludine sensitivity.

Next, we ask whether we can find the molecular determinants in CaC that reproduce the block of $Ca_v1.2$. Several studies suggest the significant amino acids lying in the middle region of CaC, containing three positively-charged lysines (Nishio et al., 1999; Gilquin et al., 1999) (Figure 6.2.A). We first synthesized a cyclized version of peptide A containing an extra N-terminal cysteine residue to enable a disulfide crosslink with the native cys 32 (Figure 6.2.A) and confirmed peptide A binding $Ca_v1.2$/IIIS5-3P in BLI assay (Wang et al., unpublished).

Furthermore, we generated additional peptides based on peptide A to use in electrophysiological experiments. We inserted a cysteine at position 23 or position 24 to form a disulfide bond with native cysteine at position 33 (originally 32) (Figure 6.2.B). We first measured the dose responses of peptide 23-33, and they reduced the efficacy compared to the full-length CaC. Even at the saturated 10μM, only 20 percent is blocked in $Ca_v1.2$. Interestingly, when we tested this peptide in $Ca_v1.3$ without conserved CaC binding pocket in IIIS5-3P loop, we observed a higher sensitivity to peptide 23 (Figure 6.3.A) and 10μM might not saturate the binding given the increasing fractional block compared to $Ca_v1.2$. However, because of the limited range of antagonizing on both $Ca_v1.2$ and $Ca_v1.3$, we were unable to fit into the dose-response curve and report a valid IC_{50}. In addition, we tested 10μM peptide 24 and a fusion peptide with amlodipine, which might increase the efficacy of CaC peptide and increases the selectivity of DHP. Peptide 24 showed a slightly lower but not significantly different binding affinity in $Ca_v1.2$ compared to peptide 23. Amlodipine-Za showed a stable blocking at 40 percent in a limited sample size (Figure 6.3.B).

We will further examine the binding of peptide 24 and amlodipine-Za with $Ca_v1.2$ and $Ca_v1.3$ in multiple concentrations and examine the potential of DHP-CaC peptide in developing selective L-type VGCC antagonists.

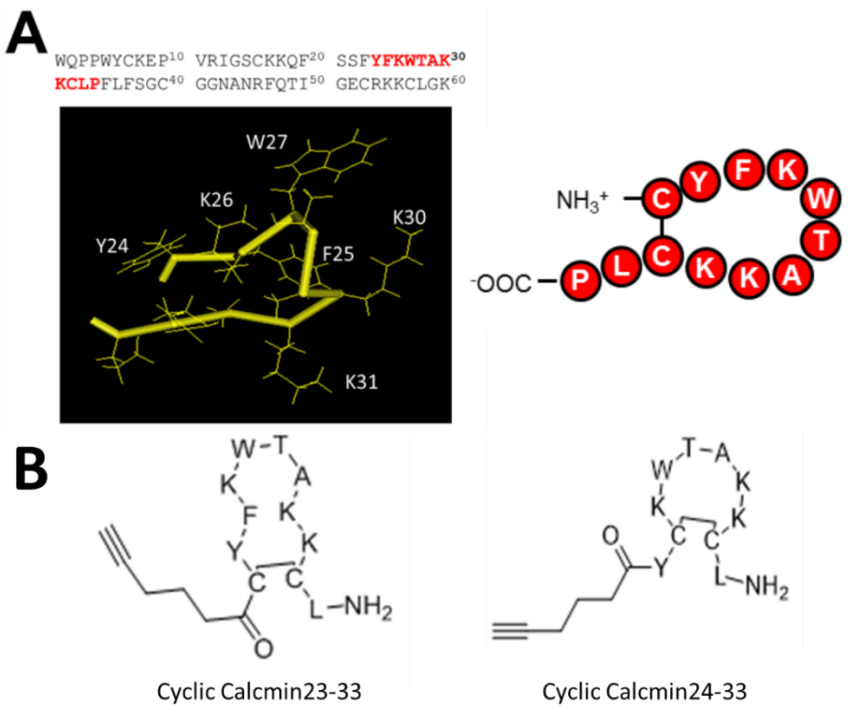

Figure 6.2. A 12 a.a peptide derived from CaC blocks $Ca_v1.2$. (**A**) The amino acid sequence of calcicludine and 3-D structure of an external loop containing three positively charged lysines. This loop was mimicked using the 12 a.a disulfide cross-linked peptide A (Red). (**B**) Alkined peptide A forms a disulfide bond at position 23 (Cyclic Calcmin 23-33) and position 24 (Cyclic Calcmin 24-33).

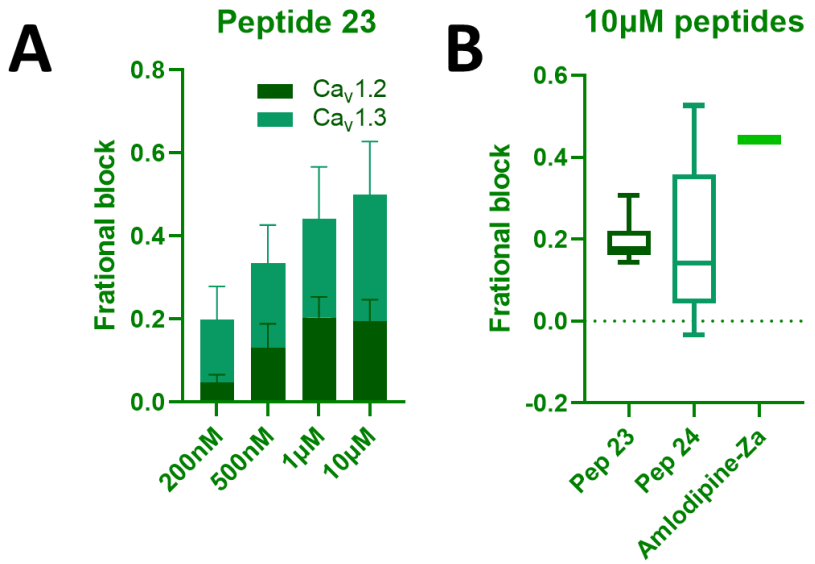

Figure 6.3. Dose responses of $Ca_v1.2$ and $Ca_v1.3$ in response to peptide 23 (A), peptide 24, and the DHP-fused peptide (B). (**A**) Fractional block of $Ca_v1.2$ and $Ca_v1.3$ in the presence of 200nM, 500nM, 1μM, and 10μM peptide 23. (N = 4~16 for each concentration). (**B**) Fractional block of $Ca_v1.2$ in response to 10μM peptide 23, peptide 24 and amlodipine-Za (N = 3~11).

6.2 Explore $Ca_v\beta$ regulation $Ca_v1.3$/II-III loop

6.2.1 Immunoprecipitation of $Ca_v1.3$/II-III and β_3

6.2.1.1 No direct interaction between $Ca_v1.3$/II-III and β_3

In the previous sections, we were impressed by the $Ca_v\beta_3$ subunit regulation of $Ca_v1.3$ voltage-dependent inactivation in the presence of the $Ca_v1.3$/II-III loop. Therefore, we asked whether we can detect direct interaction between the $Ca_v1.3$/II-III loop and $Ca_v\beta_3$. We generated the $Ca_v1.3$/II-III loop fused with FLAG tag (Flag-D23) and expected the co-immunoprecipitation with rat $Ca_v\beta_3$ (Castellano et al., 1993). We prepared the protein lysates from transfected tsA-201 cells (See Section 2.5). Both constructs were examined by electrophoresis (data not shown) and immunoblotting (Figure 6.4.A), and both anti-FLAG and anti-β_3 antibodies recognize "ladder"-like bands in both Flag-D23 and $Ca_v\beta_3$. We pulled down the mixed Flag-D23/β_3 protein lysates using anti-Flag agarose beads, blotted with anti-β_3. However, we were unable to detect the β_3 bands in the elution (Figure 6.4.B). Thus, there might not be strong or direct interactions between the $Ca_v1.3$/II-III loop and $Ca_v\beta_3$ in denatured form, but we might observe multi-way non-covalent interactions or covalent interactions, which only potentially happen on the plasma membrane.

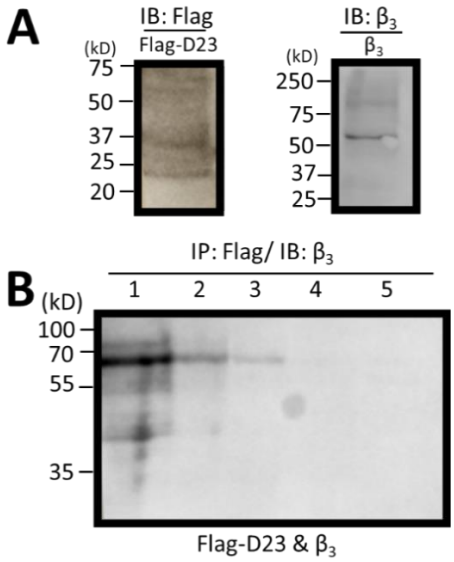

Figure 6.4. Immunoblotting of $Ca_v1.3$/II-III loop and $Ca_v\beta_3$. (**A**) Flag-D23 can be detected by anti-FLAG antibody, and $Ca_v\beta_3$ can be detected by the anti-$Ca_v\beta_3$ antibody. (**B**) Co-immunoprecipitation of $Ca_v1.3$/II-III loop and $Ca_v\beta_3$, pulled-down by anti-FLAG agarose beads and blotted by anti-β_3. Lane 1-5: Supernatant after IP, Wash collection 1, Wash collection 2, Elution 1, and Elution 2.

6.2.1.2 C-terminus of L-VGCCs in $Ca_v1.3$ inactivation

The carboxy-terminal tails of $Ca_v1.2$ and $Ca_v1.3$ modulate calcium-dependent inactivation (CDI) and voltage-dependent inactivation (VDI), as mentioned in sections 1.4.5 and 1.4.7. In section 4.2, we observed no change in $Ca_v1.3_{42a}$ inactivation in the presence of the $Ca_v1.3$/II-III loop. Thus, we were inspired to include the role of the C-terminus in $Ca_v\beta$ regulated $Ca_v1.3$ inactivation.

We proposed a three-way co-immunoprecipitation including $Ca_v1.3$/C-terminus, $Ca_v1.3$/II-III, and $Ca_v\beta_3$. Interestingly, Gomez-Ospina's research also showed that the C-terminus of $Ca_v1.2$ was found in the nucleus of neurons but not in the membrane and cytosol, and oppositely, the intracellular II-III loop was only found in the membrane and cytosol but not in the nucleus (Gomez-Ospina et al., 2006). Therefore, to prevent the truncated channels from degradation or misfolding during lysis, we will choose to transfect Flag-D23 into INS-1 cell lines with stably expressed C-terminus (DCTS) with endogenous $Ca_v\beta_3$.

6.2.2 Examine the effect of other intracellular regions of $Ca_v\beta$ on II-III loop interaction with $Ca_v\beta$

Since we are having difficulties detecting the two-way intramolecular interactions of the II-III loop and $Ca_v\beta$, we will consider other intracellular regions of $Ca_v\alpha1$. Multiple studies have shown that $Ca_v\beta$ interacts with N-, C-termini, and III-IV loop (Qin et al., 1997; Tareilus et al., 1997; Walker et al., 1998 & 1999). In addition to the C-terminal effect on CDI (See section 1.4.5), III-IV interacts with the I-II loop in a $Ca_v\beta$-dependent manner modulating $Ca_v2.1$ VDI (Geib et al., 2002). Thus, it is very likely that the II-III loop interacts with the I-II loop to modulate $Ca_v1.3$ inactivation instead of a single effect. Nonetheless, the intracellular regions of $Ca_v\alpha1$ have not been solved, and the exact interactions were not well understood. We can generate I-II loop mutations to disrupt the potential interaction with the II-III loop and recover the $Ca_v1.3$/II-III-induced inactivation shift.

In addition, the regulation of $Ca_v1.3$/$Ca_v\beta$ inactivation by the $Ca_v1.3$/II-III loop and corresponding peptides might result from disruption of $Ca_v\beta_3$ oligomerization. We found that most of the Cryo-EM structures of $Ca_v\beta$ showed dimerization (Figure 6.5). Thus, $Ca_v\beta$ oligomerization can be either homo- or hetero by interaction with other $Ca_v\beta$ subtypes, and it does not affect the

channel expression on the plasma membrane (Lao et al., 2010). However, we do not know whether these oligomers can interact with multiple intracellular regions of $Ca_v\alpha1$.

One way to test if the P3-1/P3-2 peptides are disrupting $Ca_v\beta_3$ oligomerization would be to run a non-denaturing PAGE followed by immunoblotting for $Ca_v\beta_3$ as in Lao et al., 2010 but in the presence or absence of the peptides. Moreover, we can examine the homo- and hetero-oligomerization of $Ca_v\beta$ affecting the $Ca_v1.3$/II-III-induced inactivation shift as we already showed that $Ca_v\beta$ expression is subtype-specific in regulating the inactivation.

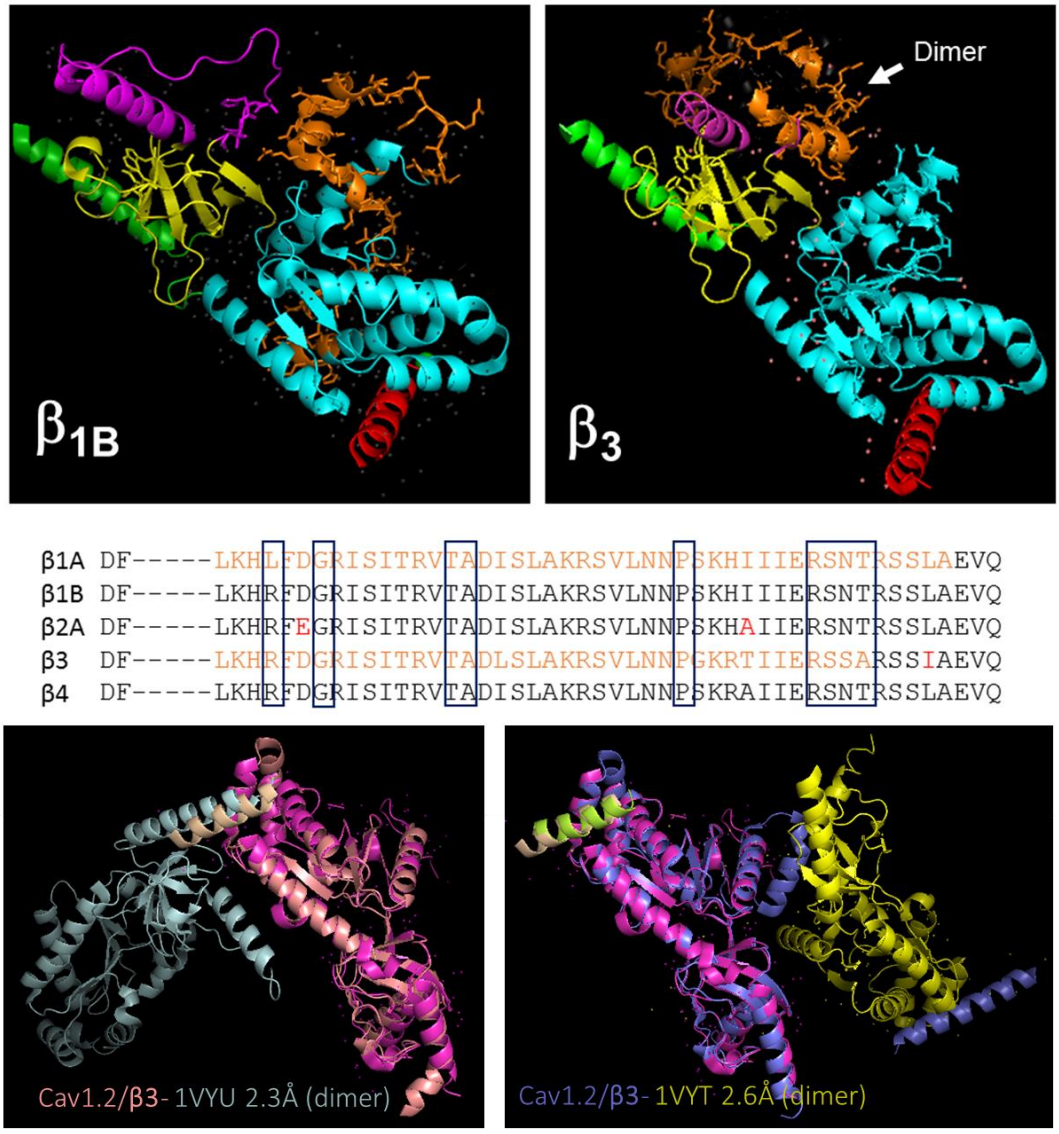

Figure 6.5. Cryo-EM structures of $Ca_v\beta$ and sequence alignment of GK domains involved in ligand binding (Zuccotti et al., 2011). Boxes indicate key positions for interacting for GK domain ligands.

6.2.3 Examine P3-1 regulation of isradipine block

Small molecule inhibitors of L-VGCC prefer to bind to the inactivated state (30, 63, 64), and the potency is greater for $Ca_v1.2$ than $Ca_v1.3$. We have shown that the P3-1 peptide derived from the $Ca_v1.3$/II-III loop enhances the inactivation of $Ca_v1.3$ at hyperpolarized potentials (See Chapter 4). Thus, we propose that P3-1 could enhance the potency of currently FDA-approved drugs for the block of $Ca_v1.3$. To examine this possibility, we will express $Ca_v1.3/\beta_3/\alpha_2\delta_1$ in HEK 293 cells and measure the potency of drug block in the presence or absence of 10 μM P3-1 peptide in the patch pipette.

We will use the DHP isradipine, which penetrates the blood-brain barrier (Rostein et al., 2015) and is associated with a decrease in risk for Parkinson's disease (Ritz et al., 2009). Isradipine also reduces cocaine-seeking in rats (Addy et al., 2018). However, Isradipine was ineffective in suppressing the subjective effects of cocaine in human subjects (Johnson et al., 2004) and failed to show significant slowing of early-stage PD progression (Parkinson Study Group STEADY-PD Investigators, 2020). On the other hand, both studies concluded that dosing limitations imposed by cardiovascular side effects confounded the study.

The IC_{50} of the isradipine block of $Ca_v1.3$ will be assessed as described in Chapter 2 using a holding potential of -60 mV or -80mV. At -60 mV, an appreciable fraction of channels are inactivated in the presence, but not the absence of P3-1 peptide. At -80 mV, the fraction of inactivated channels is negligible in both cases (Figure 5.4.C). Therefore, we expect that any difference in potency of isradipine in the presence or absence of P3-1 will be minimal while using -80 mV as the holding potential, but that a significant decrease in IC_{50} will be stimulated by P3-1 when the holding potential is -60 mV. This result would be physiologically significant since the resting membrane potential of dopaminergic VTA neurons is -55 mV (Khaliq et al., 2010). To assess the selectivity of any potentiation of the block by P3-1, we will also measure the IC_{50} for the isradipine block of $Ca_v1.2/\beta_3/\alpha_2\delta_1$ as described. Since P3-1 does not change the fraction of inactivated $Ca_v1.2$ channels at these voltages, we expect that the inclusion of P3-1 will not affect the IC_{50} of isradipine at either holding potential.

6.3 Characterize ER Ca^{2+} homeostasis regulatory proteins

6.3.1 Examine PIP_2 hydrolysis and Ca^{2+} activity in $IRBIT^{KO}$

We have characterized the wild-type and $RyR2^{KO}$ INS-1 cells in Section 5.5 and observed a greater decrease in VGCC activity in response to rapamycin-induced PIP_2 in hydrolysis in $RyR2^{KO}$ cells compared to control INS-1 cells. Therefore, we will examine the $IRBIT^{KO}$ cell line with the same experimental setup. We expect to see a result close to $RyR2^{KO}$ since $IRBIT^{KO}$ cells also exhibit a current density higher than control.

6.3.2 Examine PIP_2 hydrolysis regulation of $Ca_v\beta$

The research projects of PIP_2 regulating ion channels have been focusing on K^+ channels, and only a few studies showed PIP_2 modulation of voltage-gated Ca^{2+} channels. However, $Ca_v\beta_{2a}$ phosphorylation is facilitated by PIP_2 and increases VGCC expression on the plasma membrane, indicating the positive association between PIP_2 and VGCC current activity (Viard et al., 2004). Furthermore, our results in Section 5.3 suggest a consistent upregulation of all VGCCs in $RyR2^{KO}$ and $IRBIT^{KO}$ cells. Therefore, we can explore whether this PIP_2 is $Ca_v\beta$ subtype-specific and tissue-specific.

We can generate $Ca_v\beta$ mutants to disrupt the PIP_2 regulation of $Ca_v\beta$ and examine the HVA Ca^{2+} channel activity in WT and knock-out INS-1 cells. We can also use pharmacological methods to inhibit $Ca_v\beta$. A variety of $Ca_v\beta$ antagonists have been developed to disrupt $Ca_v\alpha1$-$Ca_v\beta$ (especially $Ca_v2.2$) and reduces trafficking, including small molecules (Chen et al., 2018; Rajesh et al., 2019) and engineered nanobody (Morgenstern et al., 2019) with no $Ca_v\beta$ specificity. Therefore, we can introduce $Ca_v\beta$ antagonists to compare the pharmacological disruption of $Ca_v\alpha1$-$Ca_v\beta$ and PIP_2 induced $Ca_v\alpha1$-$Ca_v\beta$ alterations.

6.3.3 Characterize other Ca^{2+} channel or related knock-outs

In addition to RyR2 and IRBIT in β-cells, many other Ca^{2+} channels and Ca^{2+} -related proteins appeal to us. We have knocked out the L-VGCC $Ca_v1.2$ and $Ca_v1.3$ and the cytomatrix active zone protein piccolo (Harvey et al., unpublished). We characterized the current density, GSAP, and nifedipine block of these channels and will explain our observations below.

We generated the current density of $Ca_v1.2^{KO}$, $Ca_v1.3^{KO}$, and $PCLO^{KO}$ in the standard Ba^{2+} solution set. We found that $Ca_v1.2^{KO}$ and $PCLO^{KO}$ showed a slightly lower current density than that of control, but $Ca_v1.3^{KO}$ almost doubled the value like $RyR2^{KO}$ cells (Figure 6.6.A). Next, we asked how would $Ca_v1.2^{KO}$ and $Ca_v1.3^{KO}$ INS-1 cells react to 5 μM nifedipine. Interestingly, we could not record $Ca_v1.2^{KO}$ in the standard Ba^{2+} solution sets, as they all ran down very fast or jumped around (data not shown). This observation was also expected because $Ca_v1.2$ is the predominant L-VGCCs in INS-1 cells. On the other hand, we examined the fractional block by 5μM nifedipine in $Ca_v1.3^{KO}$ cells and found that nifedipine had a slightly higher block than control INS-1 cells (Figure 6.6.B). A compensatory $Ca_v1.2$ upregulation can explain this higher fractional block. Indeed, $Ca_v1.2$ is reported to be upregulated in the β-cells of $Ca_v1.3$ β-cell-specific knock-out mice (Namkung et al., 2001).

Furthermore, we asked whether $Ca_v1.2^{KO}$, $Ca_v1.3^{KO}$, and $PCLO^{KO}$ can regulate glucose-stimulated action potentials differently from control INS-1 cells. However, the observation of GSAP in response to 18 mM glucose became challenging, like the $IRBIT^{KO}$ recordings in Chapter 5. Both $Ca_v1.2^{KO}$ and $Ca_v1.3^{KO}$ were activated with continuous action potentials at the beginning of experiments without glucose or tolbutamide stimulation. A tiny portion of the cells could respond to 18 mM glucose or tolbutamide, while most of the cells either did not respond to glucose after diazoxide treatment or continued firing action potentials despite the application of diazoxide. We showed the action potential frequency of continuous bursts during diazoxide addition, 18 mM glucose (or glucose + current injection), 200μM tolbutamide (or tolbutamide + current injection) of $Ca_v1.2^{KO}$ and $Ca_v1.3^{KO}$ in Figure 6.7.C and Table 6.1. Since $Ca_v1.2$ and $Ca_v1.3$ are the predominant VGCCs controlling the upstrokes of action potentials, our observation of no prolonged action potentials in response to either glucose or tolbutamide is consistent with the role of $Ca_v1.2$ or $Ca_v1.3$ in controlling the upstroke of action potentials. $PCLO^{KO}$ cells behaved like WT INS-1 cells with a non-significant slight increase in AP frequency (Figure 6.6.D), while the $Ca_v1.2^{KO}$ and $Ca_v1.3^{KO}$ doubled the GSAP from the small portion of glucose-responsive cells.

We extracted some interesting information from $Ca_v1.2^{KO}$, $Ca_v1.3^{KO}$, and $PCLO^{KO}$ INS-1 cells, but they are not enough to answer the questions that remained in Chapter 5. The next target will be the generation of IP_3R knock-out, which will be directly related to the results of $RyR2^{KO}$ and $IRBIT^{KO}$. We will examine IP_3RKO regulation of β-cell electrical activity and associated insulin secretion and β-cell survival.

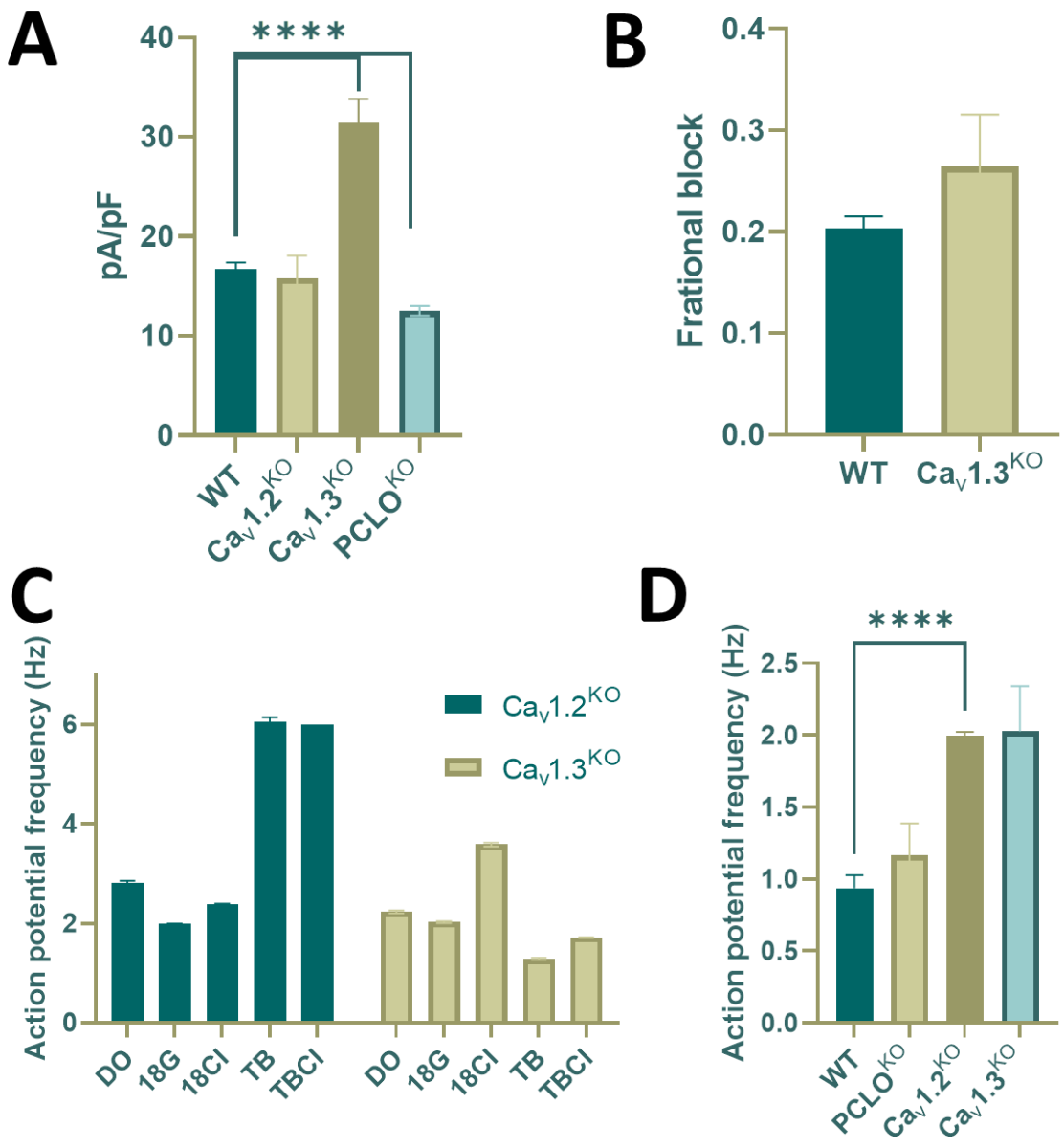

Figure 6.6. Characterization of current density, nifedipine block, and GSAP in $Ca_v1.2^{KO}$, $Ca_v1.3^{KO}$, and $PCLO^{KO}$ INS-1 cells. (**A**) The current density (pA/pF) of WT and knock-outs. WT: 16.71 ± 2.26 (N = 11); $Ca_v1.2^{KO}$: 15.82 ± 9.03 (N = 16); $Ca_v1.3^{KO}$: 31.44 ± 12.63 (N = 8) (****P < 0.0001), and $PCLO^{KO}$: 12.53 ± 2.10 (N = 18) (****P < 0.0001). (**B**) 5μM nifedipine block of WT and $Ca_v1.3^{KO}$ INS-1 cells: WT: 0.20 ± 0.055 (N = 20); $Ca_v1.3^{KO}$: 0.26 ± 0.16 (N = 10). (**C**) Action potential frequency of glucose/ tolbutamide stimulated action potentials in $Ca_v1.2^{KO}$ and $Ca_v1.3^{KO}$ INS-1 cells. Values are reported in Table 6.1. (**D**) Action potential frequency (Hz) of 18 mM glucose-stimulated action potentials in WT, $Ca_v1.2^{KO}$, $Ca_v1.3^{KO}$, and $PCLO^{KO}$ INS-1 cells. WT: 0.94 ± 0.27 (N = 9); $Ca_v1.2^{KO}$: 2.00 ± 0.06 (N = 5); $Ca_v1.3^{KO}$: 2.03 ± 0.32 (N = 2); $PCLO^{KO}$: 1.17 ± 0.69 (N = 10).

Table 6.1. Action potentials of $Ca_v1.2^{KO}$ and $Ca_v1.3^{KO}$ in response to 18 mM glucose and 200 μm tolbutamide in whole-cell perforated patch-clamp.

	$Ca_v1.2^{KO}$				$Ca_v1.3^{KO}$			
Treatment	AP (Hz)	Std. (Hz)	(N) Cell counts	(n) AP counts	AP (Hz)	Std. (Hz)	(N) Cell counts	(n) AP counts
Diazoxide	2.82	1.60	18	2132	2.23	0.94	13	930
18mM Glucose	2.00	0.06	5	314	2.03	0.32	2	206
18G Current Injection	2.38	1.08	9	3396	3.58	1.16	3	985
Tolbutamide	6.05	2.00	3	511	1.29	0.41	4	335
T Current Injection	6.00	0	1	285	1.72	0.22	2	478

REFERENCES

Abderemane-Ali, F., Findeisen, F., Rossen, N. D., & Minor, D. L. (2019). A Selectivity Filter Gate Controls Voltage-Gated Calcium Channel Calcium-Dependent Inactivation. *Neuron*, *101*(6), 1134–1149.e3. https://doi.org/10.1016/j.neuron.2019.01.011

Abou-Sleiman, P. M., Muqit, M. M. K., & Wood, N. W. (2006). Expanding insights of mitochondrial dysfunction in Parkinson's disease. *Nature Reviews Neuroscience*, *7*(3), 207–219. https://doi.org/10.1038/nrn1868

Acosta, C., & Santa Cruz, F. (2018). Hypertension: A Companion to Braunwald's Heart Disease 3rd Edition, 2018. Elsevier Inc. George L. Bakrisand Matthew Sorrentino. *Anales de La Facultad de Ciencias Médicas (Asunción)*, *51*(2), 87–88. https://doi.org/10.18004/anales/2018.051(02)87-088

Adams, P., Ben-Johny, M., Dick, I., Inoue, T., & Yue, D. (2014). Apocalmodulin Itself Promotes Ion Channel Opening and Ca2+ Regulation. *Cell*, *159*(3), 608–622. https://doi.org/10.1016/j.cell.2014.09.047

Addy, N. A., Nunes, E. J., Hughley, S. M., Small, K. M., Baracz, S. J., Haight, J. L., & Rajadhyaksha, A. M. (2018). The L-type calcium channel blocker, isradipine, attenuates cue-induced cocaine-seeking by enhancing dopaminergic activity in the ventral tegmental area to nucleus accumbens pathway. *Neuropsychopharmacology*, *43*(12), 2361–2372. https://doi.org/10.1038/s41386-018-0080-2

Adriaenssens, A. E., Svendsen, B., Lam, B. Y. H., Yeo, G. S. H., Holst, J. J., Reimann, F., & Gribble, F. M. (2016). Transcriptomic profiling of pancreatic alpha, beta and delta cell populations identifies delta cells as a principal target for ghrelin in mouse islets. *Diabetologia*, *59*(10), 2156–2165. https://doi.org/10.1007/s00125-016-4033-1

Affolter, H., & Coronado, R. (1985). Agonists Bay-K8644 and CGP-28392 open calcium channels reconstituted from skeletal muscle transverse tubules. *Biophysical Journal*, *48*(2), 341–347. https://doi.org/10.1016/s0006-3495(85)83789-9

Akiyama, T., Yamazaki, T., Mori, H., & Sunagawa, K. (2004). Effects of Ca2+ channel antagonists on acetylcholine and catecholamine releases in the in vivo rat adrenal medulla. *American Journal of Physiology-Regulatory, Integrative and Comparative Physiology*, *287*(1), R161–R166. https://doi.org/10.1152/ajpregu.00609.2003

Al Kury, L. T. (2020). Calcium Homeostasis in Ventricular Myocytes of Diabetic Cardiomyopathy. *Journal of Diabetes Research*, *2020*, 1–12. https://doi.org/10.1155/2020/1942086

Albillos, A., Gandía, L., Michelena, P., Gilabert, J. A., del Valle, M., Carbone, E., & García, A. G. (1996). The mechanism of calcium channel facilitation in bovine chromaffin cells. *The Journal of Physiology*, *494*(3), 687–695. https://doi.org/10.1113/jphysiol.1996.sp021524

Almers, W., & McCleskey, E. W. (1984). Non-selective conductance in calcium channels of frog muscle: calcium selectivity in a single-file pore. *The Journal of Physiology*, *353*(1), 585–608. https://doi.org/10.1113/jphysiol.1984.sp015352

Alseikhan, B. A., DeMaria, C. D., Colecraft, H. M., & Yue, D. T. (2002). Engineered calmodulins reveal the unexpected eminence of Ca2+ channel inactivation in controlling heart excitation. *Proceedings of the National Academy of Sciences*, *99*(26), 17185–17190. https://doi.org/10.1073/pnas.262372999

Altier, C. (2012). GPCR and Voltage-Gated Calcium Channels (VGCC) Signaling Complexes. *Subcellular Biochemistry*, 241–262. https://doi.org/10.1007/978-94-007-4765-4_13

Ämmälä, C., Ashcroft, F. M., & Rorsman, P. (1993). Calcium-independent potentiation of insulin release by cyclic AMP in single β-cells. *Nature*, *363*(6427), 356–358. https://doi.org/10.1038/363356a0

Ämmälä, C., Eliasson, L., Bokvist, K., Berggren, P. O., Honkanen, R. E., Sjoholm, A., & Rorsman, P. (1994). Activation of protein kinases and inhibition of protein phosphatases play a central role in the regulation of exocytosis in mouse pancreatic beta cells. *Proceedings of the National Academy of Sciences*, *91*(10), 4343–4347. https://doi.org/10.1073/pnas.91.10.4343

Anderson, P. A., & Greenberg, R. M. (2001). Phylogeny of ion channels: clues to structure and function. *Comparative Biochemistry and Physiology Part B: Biochemistry and Molecular Biology*, *129*(1), 17–28. https://doi.org/10.1016/s1096-4959(01)00376-1

Ando, H., Kawaai, K., & Mikoshiba, K. (2014). IRBIT: A regulator of ion channels and ion transporters. *Biochimica et Biophysica Acta (BBA) - Molecular Cell Research*, *1843*(10), 2195–2204. https://doi.org/10.1016/j.bbamcr.2014.01.031

Ando, H., Mizutani, A., Kiefer, H., Tsuzurugi, D., Michikawa, T., & Mikoshiba, K. (2006). IRBIT Suppresses IP3 Receptor Activity by Competing with IP3 for the Common Binding Site on the IP3 Receptor. *Molecular Cell*, *22*(6), 795–806. https://doi.org/10.1016/j.molcel.2006.05.017

Ando, H., Mizutani, A., Matsu-ura, T., & Mikoshiba, K. (2003). IRBIT, a Novel Inositol 1,4,5-Trisphosphate (IP3) Receptor-binding Protein, Is Released from the IP3 Receptor upon IP3 Binding to the Receptor. *Journal of Biological Chemistry*, *278*(12), 10602–10612. https://doi.org/10.1074/jbc.m210119200

Andranovits, S., Beyl, S., Hohaus, A., Zangerl-Plessl, E. M., Timin, E., & Hering, S. (2017). Key role of segment IS4 in Cav1.2 inactivation: link between activation and inactivation. *Pflügers Archiv - European Journal of Physiology*, *469*(11), 1485–1493. https://doi.org/10.1007/s00424-017-2038-3

Antzelevitch, C., Pollevick, G. D., Cordeiro, J. M., Casis, O., Sanguinetti, M. C., Aizawa, Y., Guerchicoff, A., Pfeiffer, R., Oliva, A., Wollnik, B., Gelber, P., Bonaros, E. P., Burashnikov, E., Wu, Y., Sargent, J. D., Schickel, S., Oberheiden, R., Bhatia, A., Hsu, L. F., . . . Wolpert, C. (2007). Loss-of-Function Mutations in the Cardiac Calcium Channel Underlie a New Clinical Entity Characterized by ST-Segment Elevation, Short QT Intervals, and Sudden Cardiac Death. *Circulation*, *115*(4), 442–449. https://doi.org/10.1161/circulationaha.106.668392

Arikkath, J., & Campbell, K. P. (2003). Auxiliary subunits: essential components of the voltage-gated calcium channel complex. *Current Opinion in Neurobiology*, *13*(3), 298–307. https://doi.org/10.1016/s0959-4388(03)00066-7

Asfari, M., Janjic, D., Meda, P., Li, G., Halban, P. A., & Wollheim, C. B. (1992). Establishment of 2-mercaptoethanol-dependent differentiated insulin-secreting cell lines. *Endocrinology*, *130*(1), 167–178. https://doi.org/10.1210/endo.130.1.1370150

Ashcroft, F. M., Harrison, D. E., & Ashcroft, S. J. H. (1984). Glucose induces closure of single potassium channels in isolated rat pancreatic β-cells. *Nature*, *312*(5993), 446–448. https://doi.org/10.1038/312446a0

Ashcroft, F. M., Proks, P., Smith, P. A., Ämmälä, C., Bokvist, K., & Rorsman, P. (1994). Stimulus-secretion coupling in pancreatic β cells. *Journal of Cellular Biochemistry*, *55*(S1994A), 54–65. https://doi.org/10.1002/jcb.240550007

Ashcroft, F. M., & Rorsman, P. (1989). Electrophysiology of the pancreatic β-cell. *Progress in Biophysics and Molecular Biology*, *54*(2), 87–143. https://doi.org/10.1016/0079-6107(89)90013-8

Ashcroft, S. J. H., Hedeskov, C. J., & Randle, P. J. (1970). Glucose metabolism in mouse pancreatic islets. *Biochemical Journal*, *118*(1), 143–154. https://doi.org/10.1042/bj1180143

Back, S. H., & Kaufman, R. J. (2012). Endoplasmic Reticulum Stress and Type 2 Diabetes. *Annual Review of Biochemistry*, *81*(1), 767–793. https://doi.org/10.1146/annurev-biochem-072909-095555

Bader, P. L., Faizi, M., Kim, L. H., Owen, S. F., Tadross, M. R., Alfa, R. W., Bett, G. C. L., Tsien, R. W., Rasmusson, R. L., & Shamloo, M. (2011). Mouse model of Timothy syndrome recapitulates triad of autistic traits. *Proceedings of the National Academy of Sciences*, *108*(37), 15432–15437. https://doi.org/10.1073/pnas.1112667108

Bai, X. C., Yan, Z., Wu, J., Li, Z., & Yan, N. (2016). The Central domain of RyR1 is the transducer for long-range allosteric gating of channel opening. *Cell Research*, *26*(9), 995–1006. https://doi.org/10.1038/cr.2016.89

Baig, S. M., Koschak, A., Lieb, A., Gebhart, M., Dafinger, C., Nürnberg, G., Ali, A., Ahmad, I., Sinnegger-Brauns, M. J., Brandt, N., Engel, J., Mangoni, M. E., Farooq, M., Khan, H. U., Nürnberg, P., Striessnig, J., & Bolz, H. J. (2010). Loss of Cav1.3 (CACNA1D) function in a human channelopathy with bradycardia and congenital deafness. *Nature Neuroscience*, *14*(1), 77–84. https://doi.org/10.1038/nn.2694

Baker, M. R., Fan, G., Seryshev, A. B., Agosto, M. A., Baker, M. L., & Serysheva, I. I. (2021). Cryo-EM structure of type 1 IP3R channel in a lipid bilayer. *Communications Biology*, *4*(1). https://doi.org/10.1038/s42003-021-02156-4

Baldelli, P., Hernández-Guijo, J. M., Carabelli, V., Novara, M., Cesetti, T., Andrés-Mateos, E., Montiel, C., & Carbone, E. (2004). Direct and Remote Modulation of L-Channels in Chromaffin Cells: Distinct Actions on α1C and α1D Subunits? *Molecular Neurobiology*, *29*(1), 73–96. https://doi.org/10.1385/mn:29:1:73

Banaszynski, L. A., Liu, C. W., & Wandless, T. J. (2005). Characterization of the FKBP·Rapamycin·FRB Ternary Complex. *Journal of the American Chemical Society*, *127*(13), 4715–4721. https://doi.org/10.1021/ja043277y

Bandyopadhyay, D., Salazar, T., & Gonzalez, A. (2017). Dihydropyridines as Calcium Channel Blockers: An Overview. *Journal of Analytical & Pharmaceutical Research*, *5*(4), 00148. https://doi.org/10.15406/japlr.2017.05.00148

Bannister, R. A., & Beam, K. G. (2013). CaV1.1: The atypical prototypical voltage-gated Ca2+ channel. *Biochimica et Biophysica Acta (BBA) - Biomembranes*, *1828*(7), 1587–1597. https://doi.org/10.1016/j.bbamem.2012.09.007

Bao, X. (2012, March). Impact of calcium channel antagonists for estrogen action on the endometrial carcinoma HEC-1A cells. *Zhonghua Fu Chan Ke Za Zhi*, *47*(3), 212–217.

Barg, S., Eliasson, L., Renstrom, E., & Rorsman, P. (2002). A Subset of 50 Secretory Granules in Close Contact With L-Type Ca2+ Channels Accounts for First-Phase Insulin Secretion in Mouse -Cells. *Diabetes*, *51*(Supplement 1), S74–S82. https://doi.org/10.2337/diabetes.51.2007.s74

Barg, S., Ma, X., Eliasson, L., Galvanovskis, J., Göpel, S. O., Obermüller, S., Platzer, J., Renström, E., Trus, M., Atlas, D., Striessnig, J., & Rorsman, P. (2001). Fast Exocytosis with Few Ca2+ Channels in Insulin-Secreting Mouse Pancreatic B Cells. *Biophysical Journal*, *81*(6), 3308–3323. https://doi.org/10.1016/s0006-3495(01)75964-4

Barker, C. J., & Berggren, P. O. (2013). New Horizons in Cellular Regulation by Inositol Polyphosphates: Insights from the Pancreaticβ-Cell. *Pharmacological Reviews*, *65*(2), 641–669. https://doi.org/10.1124/pr.112.006775

Barnett, D. W., Pressel, D. M., & Misler, S. (1995). Voltage-dependent Na+ and Ca2+ currents in human pancreatic islet ?-cells: evidence for roles in the generation of action potentials and insulin secretion. *Pflugers Archiv European Journal of Physiology*, *431*(2), 272–282. https://doi.org/10.1007/bf00410201

Baroudi, G., Qu, Y., Ramadan, O., Chahine, M., & Boutjdir, M. (2006). Protein kinase C activation inhibits Cav1.3 calcium channel at NH2-terminal serine 81 phosphorylation site. *American Journal of Physiology-Heart and Circulatory Physiology*, *291*(4), H1614–H1622. https://doi.org/10.1152/ajpheart.00095.2006

Barrett, C. F., & Tsien, R. W. (2008). The Timothy syndrome mutation differentially affects voltage- and calcium-dependent inactivation of CaV1.2 L-type calcium channels. *Proceedings of the National Academy of Sciences*, *105*(6), 2157–2162. https://doi.org/10.1073/pnas.0710501105

Barttfeld, P., Wicker, B., Cukier, S., Navarta, S., Lew, S., & Sigman, M. (2011). A big-world network in ASD: Dynamical connectivity analysis reflects a deficit in long-range connections and an excess of short-range connections. *Neuropsychologia*, *49*(2), 254–263. https://doi.org/10.1016/j.neuropsychologia.2010.11.024

Bason, C., Lorini, R., Lunardi, C., Dolcino, M., Giannattasio, A., d'Annunzio, G., Rigo, A., Pedemonte, N., Corrocher, R., & Puccetti, A. (2013). In Type 1 Diabetes a Subset of Anti-Coxsackievirus B4 Antibodies Recognize Autoantigens and Induce Apoptosis of Pancreatic Beta Cells. *PLoS ONE*, *8*(2), e57729. https://doi.org/10.1371/journal.pone.0057729

Baumann, L., Gerstner, A., Zong, X., Biel, M., & Wahl-Schott, C. (2004). Functional Characterization of the L-type Ca2+Channel Cav1.4α1 from Mouse Retina. *Investigative Opthalmology & Visual Science*, *45*(2), 708. https://doi.org/10.1167/iovs.03-0937

Baxter, A. J. G., Dixon, J., Ince, F., Manners, C. N., & Teague, S. J. (1993). Discovery and synthesis of methyl 2,5-dimethyl-4-[2-(phenylmethyl)benzoyl]-1H-pyrrole-3-carboxylate (FPL 64176) and analogs: the first examples of a new class of calcium channel activator. *Journal of Medicinal Chemistry*, *36*(19), 2739–2744. https://doi.org/10.1021/jm00071a004

Bazzazi, H., Ben Johny, M., Adams, P., Soong, T., & Yue, D. (2013). Continuously Tunable Ca2+ Regulation of RNA-Edited CaV1.3 Channels. *Cell Reports*, *5*(2), 367–377. https://doi.org/10.1016/j.celrep.2013.09.006

Beauvois, M. C., Merezak, C., Jonas, J. C., Ravier, M. A., Henquin, J. C., & Gilon, P. (2006). Glucose-induced mixed [Ca2+]c oscillations in mouse β-cells are controlled by the membrane potential and the SERCA3 Ca2+-ATPase of the endoplasmic reticulum. *American Journal of Physiology-Cell Physiology*, *290*(6), C1503–C1511. https://doi.org/10.1152/ajpcell.00400.2005

BECHEM, M., & SCHRAMM, M. (1987). Calcium-Agonists. *Journal of Molecular and Cellular Cardiology*, *19*, 63–75. https://doi.org/10.1016/s0022-2828(87)80005-6

Bech-Hansen, N. T., Naylor, M. J., Maybaum, T. A., Pearce, W. G., Koop, B., Fishman, G. A., Mets, M., Musarella, M. A., & Boycott, K. M. (1998). Loss-of-function mutations in a calcium-channel α1-subunit gene in Xp11.23 cause incomplete X-linked congenital stationary night blindness. *Nature Genetics*, *19*(3), 264–267. https://doi.org/10.1038/947

Becker, C., Jick, S. S., & Meier, C. R. (2008). Use of antihypertensives and the risk of Parkinson disease. *Neurology*, *70*(Issue 16, Part 2), 1438–1444. https://doi.org/10.1212/01.wnl.0000303818.38960.44

Benkert, P., Biasini, M., & Schwede, T. (2010). Toward the estimation of the absolute quality of individual protein structure models. *Bioinformatics*, *27*(3), 343–350. https://doi.org/10.1093/bioinformatics/btq662

Benner, C., van der Meulen, T., Cacéres, E., Tigyi, K., Donaldson, C. J., & Huising, M. O. (2014). The transcriptional landscape of mouse beta cells compared to human beta cells reveals notable species differences in long non-coding RNA and protein-coding gene expression. *BMC Genomics*, *15*(1), 620. https://doi.org/10.1186/1471-2164-15-620

Berger, S. M., & Bartsch, D. (2014). The role of L-type voltage-gated calcium channels Cav1.2 and Cav1.3 in normal and pathological brain function. *Cell and Tissue Research*, *357*(2), 463–476. https://doi.org/10.1007/s00441-014-1936-3

Berggren, P. O., Yang, S. N., Murakami, M., Efanov, A. M., Uhles, S., Köhler, M., Moede, T., Fernström, A., Appelskog, I. B., Aspinwall, C. A., Zaitsev, S. V., Larsson, O., de Vargas, L. M., Fecher-Trost, C., Weißgerber, P., Ludwig, A., Leibiger, B., Juntti-Berggren, L., Barker, C. J., . . . Flockerzi, V. (2004). Removal of Ca2+ Channel β3 Subunit Enhances Ca2+ Oscillation Frequency and Insulin Exocytosis. *Cell*, *119*(2), 273–284. https://doi.org/10.1016/j.cell.2004.09.033

Berjukov, S., Aczel, S., Beyer, B., Kimball, S. D., Dichtl, M., Hering, S., & Striessnig, J. (1996). Extra- and intracellular action of quaternary devapamil on muscle L-type Ca2+-channels. *British Journal of Pharmacology*, *119*(6), 1197–1202. https://doi.org/10.1111/j.1476-5381.1996.tb16022.x

Berridge, M. J. (1993). Inositol trisphosphate and calcium signalling. *Nature*, *361*(6410), 315–325. https://doi.org/10.1038/361315a0

Berridge, M. J., Bootman, M. D., & Roderick, H. L. (2003). Calcium signalling: dynamics, homeostasis and remodelling. *Nature Reviews Molecular Cell Biology*, *4*(7), 517–529. https://doi.org/10.1038/nrm1155

Berridge, M. J., Lipp, P., & Bootman, M. D. (2000). The versatility and universality of calcium signalling. *Nature Reviews Molecular Cell Biology*, *1*(1), 11–21. https://doi.org/10.1038/35036035

Berry, C., Lal, M., & Binukumar, B. K. (2018). Crosstalk Between the Unfolded Protein Response, MicroRNAs, and Insulin Signaling Pathways: In Search of Biomarkers for the Diagnosis and Treatment of Type 2 Diabetes. *Frontiers in Endocrinology*, *9*. https://doi.org/10.3389/fendo.2018.00210

Bers, D. (1999). Ca channels in cardiac myocytes: structure and function in Ca influx and intracellular Ca release. *Cardiovascular Research*, *42*(2), 339–360. https://doi.org/10.1016/s0008-6363(99)00038-3

Bers, D. M. (2002). Cardiac excitation–contraction coupling. *Nature*, *415*(6868), 198–205. https://doi.org/10.1038/415198a

Bertoni, M., Kiefer, F., Biasini, M., Bordoli, L., & Schwede, T. (2017). Modeling protein quaternary structure of homo- and hetero-oligomers beyond binary interactions by homology. *Scientific Reports*, *7*(1), 10480. https://doi.org/10.1038/s41598-017-09654-8

Beyl, S., Kügler, P., Kudrnac, M., Hohaus, A., Hering, S., & Timin, E. (2009). Different pathways for activation and deactivation in CaV1.2: a minimal gating model. *Journal of General Physiology*, *134*(3), 231–241. https://doi.org/10.1085/jgp.200910272

Bezanilla, F. (2000). The Voltage Sensor in Voltage-Dependent Ion Channels. *Physiological Reviews*, *80*(2), 555–592. https://doi.org/10.1152/physrev.2000.80.2.555

Bezprozvanny, I. (2009). Calcium signaling and neurodegenerative diseases. *Trends in Molecular Medicine*, *15*(3), 89–100. https://doi.org/10.1016/j.molmed.2009.01.001

Bezprozvanny, I., Scheller, R., & Tsien, R. (1995). Functional impact of syntaxin on gating of N-type and Q-type calcium channels. *Nature*, *378*(6557), 623–626. https://doi.org/10.1038/378623a0

Bezprozvanny, L., Watras, J., & Ehrlich, B. E. (1991). Bell-shaped calcium-response curves of lns(l,4,5)P3- and calcium-gated channels from endoplasmic reticulum of cerebellum. *Nature*, *351*(6329), 751–754. https://doi.org/10.1038/351751a0

Bhat, S., Dao, D. T., Terrillion, C. E., Arad, M., Smith, R. J., Soldatov, N. M., & Gould, T. D. (2012). CACNA1C (Cav1.2) in the pathophysiology of psychiatric disease. *Progress in Neurobiology*, *99*(1), 1–14. https://doi.org/10.1016/j.pneurobio.2012.06.001

Bienert, S., Waterhouse, A., de Beer, T., Tauriello, G., Studer, G., Bordoli, L., & Schwede, T. (2016). The SWISS-MODEL Repository—new features and functionality. *Nucleic Acids Research*, *45*(D1), D313–D319. https://doi.org/10.1093/nar/gkw1132

Bito, M., Tomita, T., Komori, M., Taogoshi, T., Kimura, Y., & Kihira, K. (2013). The Mechanisms of Insulin Secretion and Calcium Signaling in Pancreatic β-Cells Exposed to Fluoroquinolones. *Biological and Pharmaceutical Bulletin*, *36*(1), 31–35. https://doi.org/10.1248/bpb.b12-00425

Blodgett, D. M., Nowosielska, A., Afik, S., Pechhold, S., Cura, A. J., Kennedy, N. J., Kim, S., Kucukural, A., Davis, R. J., Kent, S. C., Greiner, D. L., Garber, M. G., Harlan, D. M., & diIorio, P. (2015). Novel Observations From Next-Generation RNA Sequencing of Highly Purified Human Adult and Fetal Islet Cell Subsets. *Diabetes*, *64*(9), 3172–3181. https://doi.org/10.2337/db15-0039

Bock, G., Gebhart, M., Scharinger, A., Jangsangthong, W., Busquet, P., Poggiani, C., Sartori, S., Mangoni, M. E., Sinnegger-Brauns, M. J., Herzig, S., Striessnig, J., & Koschak, A. (2011). Functional Properties of a Newly Identified C-terminal Splice Variant of Cav1.3 L-type Ca2+ Channels*. *Journal of Biological Chemistry*, *286*(49), 42736–42748. https://doi.org/10.1074/jbc.m111.269951

Bonner, C., Kerr-Conte, J., Gmyr, V., Queniat, G., Moerman, E., Thévenet, J., Beaucamps, C., Delalleau, N., Popescu, I., Malaisse, W. J., Sener, A., Deprez, B., Abderrahmani, A., Staels, B., & Pattou, F. (2015). Inhibition of the glucose transporter SGLT2 with dapagliflozin in pancreatic alpha cells triggers glucagon secretion. *Nature Medicine*, *21*(5), 512–517. https://doi.org/10.1038/nm.3828

Bourdin, B., Briot, J., Tétreault, M. P., Sauvé, R., & Parent, L. (2017). Negatively charged residues in the first extracellular loop of the L-type CaV1.2 channel anchor the interaction with the CaVα2δ1 auxiliary subunit. *Journal of Biological Chemistry*, *292*(42), 17236–17249. https://doi.org/10.1074/jbc.m117.806893

Boussif, O., Lezoualc'h, F., Zanta, M. A., Mergny, M. D., Scherman, D., Demeneix, B., & Behr, J. P. (1995). A versatile vector for gene and oligonucleotide transfer into cells in culture and in vivo: polyethylenimine. *Proceedings of the National Academy of Sciences*, *92*(16), 7297–7301. https://doi.org/10.1073/pnas.92.16.7297

Boycott, K. M., Pearce, W. G., & Bech-Hansen, N. T. (2000). Clinical variability among patients with incomplete X-linked congenital stationary night blindness and a founder mutation in CACNA1F. *Canadian Journal of Ophthalmology*, *35*(4), 204–213. https://doi.org/10.1016/s0008-4182(00)80031-9

Brady, P. A., Alekseev, A. E., Aleksandrova, L. A., Gomez, L. A., & Terzic, A. (1996). A disrupter of actin microfilaments impairs sulfonylurea-inhibitory gating of cardiac KATP channels. *American Journal of Physiology-Heart and Circulatory Physiology*, *271*(6), H2710–H2716. https://doi.org/10.1152/ajpheart.1996.271.6.h2710

Braun, M., Ramracheya, R., Bengtsson, M., Zhang, Q., Karanauskaite, J., Partridge, C., Johnson, P. R., & Rorsman, P. (2008). Voltage-Gated Ion Channels in Human Pancreatic -Cells: Electrophysiological Characterization and Role in Insulin Secretion. *Diabetes*, *57*(6), 1618–1628. https://doi.org/10.2337/db07-0991

Braun, M., Ramracheya, R., Johnson, P. R., & Rorsman, P. (2009). Exocytotic Properties of Human Pancreatic β-cells. *Annals of the New York Academy of Sciences*, *1152*(1), 187–193. https://doi.org/10.1111/j.1749-6632.2008.03992.x

Brauns, T., Prinz, H., Kimball, S. D., Haugland, R. P., Striessnig, J., & Glossmann, H. (1997). L-Type Calcium Channels: Binding Domains for Dihydropyridines and Benzothiazepines Are Located in Close Proximity to Each Other†. *Biochemistry*, *36*(12), 3625–3631. https://doi.org/10.1021/bi9613584

Brillantes, A. M., Allen, P., Takahashi, T., Izumo, S., & Marks, A. R. (1992). Differences in cardiac calcium release channel (ryanodine receptor) expression in myocardium from patients with end-stage heart failure caused by ischemic versus dilated cardiomyopathy. *Circulation Research*, *71*(1), 18–26. https://doi.org/10.1161/01.res.71.1.18

Briot, J., Mailhot, O., Bourdin, B., Tétreault, M. P., Najmanovich, R., & Parent, L. (2018). A three-way inter-molecular network accounts for the CaVα2δ1-induced functional modulation of the pore-forming CaV1.2 subunit. *Journal of Biological Chemistry*, *293*(19), 7176–7188. https://doi.org/10.1074/jbc.ra118.001902

Brodbeck, J., Davies, A., Courtney, J. M., Meir, A., Balaguero, N., Canti, C., Moss, F. J., Page, K. M., Pratt, W. S., Hunt, S. P., Barclay, J., Rees, M., & Dolphin, A. C. (2002). The Ducky Mutation in Cacna2d2 Results in Altered Purkinje Cell Morphology and Is Associated with the Expression of a Truncated α2δ-2 Protein with Abnormal Function. *Journal of Biological Chemistry*, *277*(10), 7684–7693. https://doi.org/10.1074/jbc.m109404200

Bruton, J. D., Lemmens, R., Shi, C., Persson-Sjögren, S., Westerblad, H., Ahmed, M., Pyne, N. J., Frame, M., Furman, B. L., & Islam, M. S. (2002). Ryanodine receptors of pancreatic β-cells mediate a distinct context-dependent signal for insulin secretion. *The FASEB Journal*, *17*(2), 301–303. https://doi.org/10.1096/fj.02-0481fje

Buraei, Z., & Yang, J. (2010). The β Subunit of Voltage-Gated Ca2+ Channels. *Physiological Reviews*, *90*(4), 1461–1506. https://doi.org/10.1152/physrev.00057.2009

Busquet, P., Hetzenauer, A., Sinnegger-Brauns, M. J., Striessnig, J., & Singewald, N. (2008). Role of L-type Ca2+ channel isoforms in the extinction of conditioned fear. *Learning & Memory*, *15*(5), 378–386. https://doi.org/10.1101/lm.886208

Cabrera, O., Berman, D. M., Kenyon, N. S., Ricordi, C., Berggren, P. O., & Caicedo, A. (2006). The unique cytoarchitecture of human pancreatic islets has implications for islet cell function. *Proceedings of the National Academy of Sciences*, *103*(7), 2334–2339. https://doi.org/10.1073/pnas.0510790103

Cai, D., Mulle, J. G., & Yue, D. T. (1997). Inhibition of Recombinant Ca2+ Channels by Benzothiazepines and Phenylalkylamines: Class-Specific Pharmacology and Underlying Molecular Determinants. *Molecular Pharmacology*, *51*(5), 872–881. https://doi.org/10.1124/mol.51.5.872

Calcium. (2021, January 1). Linus Pauling Institute. https://lpi.oregonstate.edu/mic/minerals/calcium#RDA

Calcium channels. (2021, May 25). Nature Portfolio. https://www.nature.com/subjects/calcium-channels

Calderón-Rivera, A., Andrade, A., Hernández-Hernández, O., González-Ramírez, R., Sandoval, A., Rivera, M., Gomora, J. C., & Felix, R. (2012). Identification of a disulfide bridge essential for structure and function of the voltage-gated Ca2+ channel α2δ-1 auxiliary subunit. *Cell Calcium*, *51*(1), 22–30. https://doi.org/10.1016/j.ceca.2011.10.002

Calorio, C., Gavello, D., Guarina, L., Salio, C., Sassoè-Pognetto, M., Riganti, C., Bianchi, F. T., Hofer, N. T., Tuluc, P., Obermair, G. J., Defilippi, P., Balzac, F., Turco, E., Bett, G. C., Rasmusson, R. L., & Carbone, E. (2019). Impaired chromaffin cell excitability and exocytosis in autistic Timothy syndrome TS2-neo mouse rescued by L-type calcium channel blockers. *The Journal of Physiology*, *597*(6), 1705–1733. https://doi.org/10.1113/jp277487

Carabelli, V., Giancippoli, A., Baldelli, P., Carbone, E., & Artalejo, A. (2003). Distinct Potentiation of L-Type Currents and Secretion by cAMP in Rat Chromaffin Cells. *Biophysical Journal*, *85*(2), 1326–1337. https://doi.org/10.1016/s0006-3495(03)74567-6

Carabelli, V., Hernández-Guijo, J. M., Baldelli, P., & Carbone, E. (2001). Direct autocrine inhibition and cAMP-dependent potentiation of single L-type Ca 2+ channels in bovine chromaffin cells. *The Journal of Physiology*, *532*(1), 73–90. https://doi.org/10.1111/j.1469-7793.2001.0073g.x

Carabelli, V., Lovallo, M., Magnelli, V., Zucker, H., & Carbone, E. (1996). Voltage-dependent modulation of single N-Type Ca2+ channel kinetics by receptor agonists in IMR32 cells. *Biophysical Journal*, *70*(5), 2144–2154. https://doi.org/10.1016/s0006-3495(96)79780-1

Carabelli, V., Marcantoni, A., Comunanza, V., & Carbone, E. (2007). Fast exocytosis mediated by T- and L-type channels in chromaffin cells: distinct voltage-dependence but similar Ca2+-dependence. *European Biophysics Journal*, *36*(7), 753–762. https://doi.org/10.1007/s00249-007-0138-2

Carbone, E., Carabelli, V., Cesetti, T., Baldelli, P., Hernández-Guijo, J., & Giusta, L. (2001). G-protein- and cAMP-dependent L-channel gating modulation: a manyfold system to control calcium entry in neurosecretory cells. *Pflügers Archiv - European Journal of Physiology*, *442*(6), 801–813. https://doi.org/10.1007/s004240100607

Castellano, A., Wei, X., Birnbaumer, L., & Perez-Reyes, E. (1993). Cloning and expression of a third calcium channel beta subunit. *Journal of Biological Chemistry*, *268*(5), 3450–3455. https://doi.org/10.1016/s0021-9258(18)53715-7

Catterall, W. A. (2000). Structure and Regulation of Voltage-Gated Ca2+Channels. *Annual Review of Cell and Developmental Biology*, *16*(1), 521–555. https://doi.org/10.1146/annurev.cellbio.16.1.521

Catterall, W. A. (2010). Ion Channel Voltage Sensors: Structure, Function, and Pathophysiology. *Neuron*, *67*(6), 915–928. https://doi.org/10.1016/j.neuron.2010.08.021

Catterall, W. A., Leal, K., & Nanou, E. (2013). Calcium Channels and Short-term Synaptic Plasticity. *Journal of Biological Chemistry*, *288*(15), 10742–10749. https://doi.org/10.1074/jbc.r112.411645

Catterall, W. A., Lenaeus, M. J., & Gamal El-Din, T. M. (2020). Structure and Pharmacology of Voltage-Gated Sodium and Calcium Channels. *Annual Review of Pharmacology and Toxicology*, *60*(1), 133–154. https://doi.org/10.1146/annurev-pharmtox-010818-021757

Catterall, W. A., Perez-Reyes, E., Snutch, T. P., & Striessnig, J. (2005). International Union of Pharmacology. XLVIII. Nomenclature and Structure-Function Relationships of Voltage-Gated Calcium Channels. *Pharmacological Reviews*, *57*(4), 411–425. https://doi.org/10.1124/pr.57.4.5

Catterall, W. A., & Swanson, T. M. (2015). Structural Basis for Pharmacology of Voltage-Gated Sodium and Calcium Channels. *Molecular Pharmacology*, *88*(1), 141–150. https://doi.org/10.1124/mol.114.097659

CDC High Blood Pressure Home. (2020, October 22). Centers for Disease Control and Prevention. https://www.cdc.gov/bloodpressure/index.htm

Cesetti, T., Hernández-Guijo, J. M., Baldelli, P., Carabelli, V., & Carbone, E. (2003). Opposite Action of β1- and β2-Adrenergic Receptors on CaV1 L-Channel Current in Rat Adrenal Chromaffin Cells. *The Journal of Neuroscience*, *23*(1), 73–83. https://doi.org/10.1523/jneurosci.23-01-00073.2003

Chan, C. S., Guzman, J. N., Ilijic, E., Mercer, J. N., Rick, C., Tkatch, T., Meredith, G. E., & Surmeier, D. J. (2007). 'Rejuvenation' protects neurons in mouse models of Parkinson's disease. *Nature*, *447*(7148), 1081–1086. https://doi.org/10.1038/nature05865

Chang, C. C., Cao, S., Kang, S., Kai, L., Tian, X., Pandey, P., Dunne, S. F., Luan, C. H., Surmeier, D. J., & Silverman, R. B. (2010). Antagonism of 4-substituted 1,4-dihydropyridine-3,5-dicarboxylates toward voltage-dependent L-type Ca2+ channels CaV1.3 and CaV1.2. *Bioorganic & Medicinal Chemistry*, *18*(9), 3147–3158. https://doi.org/10.1016/j.bmc.2010.03.038

Chen, R., Zeng, X., Zhang, R., Huang, J., Kuang, X., Yang, J., Liu, J., Tawfik, O., Brantley Thrasher, J., & Li, B. (2014). Cav1.3 channel α1D protein is overexpressed and modulates androgen receptor transactivation in prostate cancers11This work was partially supported by grants from DoD PCRP program (W81XWH-09-1-0455) and KUMC Valk Foundation to Dr Benyi Li, and grants from China Natural Science Foundation to Dr Benyi Li (NSFC #81172427) and Dr Jun Yang (NSFC #81101927). This project was also supported by the "Chutian Scholar" program funded by Hubei Province of China dedicated to China Three Gorges University. *Urologic Oncology: Seminars and Original Investigations*, *32*(5), 524–536. https://doi.org/10.1016/j.urolonc.2013.05.011

Chen, X. H., & Tsien, R. W. (1997). Aspartate Substitutions Establish the Concerted Action of P-region Glutamates in Repeats I and III in Forming the Protonation Site of L-type Ca2+ Channels. *Journal of Biological Chemistry*, *272*(48), 30002–30008. https://doi.org/10.1074/jbc.272.48.30002

Chen, X., Liu, D., Zhou, D., Si, Y., Xu, D., Stamatkin, C. W., Ghozayel, M. K., Ripsch, M. S., Obukhov, A. G., White, F. A., & Meroueh, S. O. (2018). Small-molecule CaVα1·CaVβ antagonist suppresses neuronal voltage-gated calcium-channel trafficking. *Proceedings of the National Academy of Sciences*, *115*(45), E10566–E10575. https://doi.org/10.1073/pnas.1813157115

Chen, Y. H., Li, M. H., Zhang, Y., He, L. L., Yamada, Y., Fitzmaurice, A., Shen, Y., Zhang, H., Tong, L., & Yang, J. (2004). Structural basis of the α1–β subunit interaction of voltage-gated Ca2+ channels. *Nature*, *429*(6992), 675–680. https://doi.org/10.1038/nature02641

Cheng, R. C., Tikhonov, D. B., & Zhorov, B. S. (2009). Structural Model for Phenylalkylamine Binding to L-type Calcium Channels. *Journal of Biological Chemistry*, *284*(41), 28332–28342. https://doi.org/10.1074/jbc.m109.027326

Choi, M., Scholl, U. I., Yue, P., Bjorklund, P., Zhao, B., Nelson-Williams, C., Ji, W., Cho, Y., Patel, A., Men, C. J., Lolis, E., Wisgerhof, M. V., Geller, D. S., Mane, S., Hellman, P., Westin, G., Akerstrom, G., Wang, W., Carling, T., & Lifton, R. P. (2011). K+ Channel Mutations in Adrenal Aldosterone-Producing Adenomas and Hereditary Hypertension. *Science*, *331*(6018), 768–772. https://doi.org/10.1126/science.1198785

Christie, B. R., Eliot, L. S., Ito, K., Miyakawa, H., & Johnston, D. (1995). Different Ca2+ channels in soma and dendrites of hippocampal pyramidal neurons mediate spike-induced Ca2+ influx. *Journal of Neurophysiology*, *73*(6), 2553–2557. https://doi.org/10.1152/jn.1995.73.6.2553

Chu, P. J., Robertson, H. M., & Best, P. M. (2001). Calcium channel γ subunits provide insights into the evolution of this gene family. *Gene*, *280*(1–2), 37–48. https://doi.org/10.1016/s0378-1119(01)00738-7

Clarke, O. B., & Hendrickson, W. A. (2016). Structures of the colossal RyR1 calcium release channel. *Current Opinion in Structural Biology*, *39*, 144–152. https://doi.org/10.1016/j.sbi.2016.09.002

Cook, D. L., & Hales, N. (1984). Intracellular ATP directly blocks K+ channels in pancreatic B-cells. *Nature*, *311*(5983), 271–273. https://doi.org/10.1038/311271a0

Cooper, G., Kang, S., Perez-Rosello, T., Guzman, J. N., Galtieri, D., Xie, Z., Kondapalli, J., Mordell, J., Silverman, R. B., & Surmeier, D. J. (2020). A Single Amino Acid Determines the Selectivity and Efficacy of Selective Negative Allosteric Modulators of CaV1.3 L-Type Calcium Channels. *ACS Chemical Biology*, *15*(9), 2539–2550. https://doi.org/10.1021/acschembio.0c00577

Cosconati, S., Marinelli, L., Lavecchia, A., & Novellino, E. (2007). Characterizing the 1,4-Dihydropyridines Binding Interactions in the L-Type Ca2+Channel: Model Construction and Docking Calculations. *Journal of Medicinal Chemistry*, *50*(7), 1504–1513. https://doi.org/10.1021/jm061245a

Costé de Bagneaux, P., Campiglio, M., Benedetti, B., Tuluc, P., & Flucher, B. E. (2018). Role of putative voltage-sensor countercharge D4 in regulating gating properties of CaV1.2 and CaV1.3 calcium channels. *Channels*, *12*(1), 249–261. https://doi.org/10.1080/19336950.2018.1482183

Cremer, T., Neefjes, J., & Berlin, I. (2020). The journey of Ca2+ through the cell – pulsing through the network of ER membrane contact sites. *Journal of Cell Science*, *133*(24). https://doi.org/10.1242/jcs.249136

Curtis, B. M., & Catterall, W. A. (1984). Purification of the calcium antagonist receptor of the voltage-sensitive calcium channel from skeletal muscle transverse tubules. *Biochemistry*, *23*(10), 2113–2118. https://doi.org/10.1021/bi00305a001

Curtis, B. M., & Catterall, W. A. (1985). Phosphorylation of the calcium antagonist receptor of the voltage-sensitive calcium channel by cAMP-dependent protein kinase. *Proceedings of the National Academy of Sciences*, *82*(8), 2528–2532. https://doi.org/10.1073/pnas.82.8.2528

Dadi, P. K., Luo, B., Vierra, N. C., & Jacobson, D. A. (2015). TASK-1 Potassium Channels Limit Pancreatic α-Cell Calcium Influx and Glucagon Secretion. *Molecular Endocrinology*, *29*(5), 777–787. https://doi.org/10.1210/me.2014-1321

Damier, P., Hirsch, E. C., Agid, Y., & Graybiel, A. M. (1999). The substantia nigra of the human brain. *Brain*, *122*(8), 1437–1448. https://doi.org/10.1093/brain/122.8.1437

De Jongh, K. S., Colvin, A. A., Wang, K. K. W., & Catterall, W. A. (1994). Differential Proteolysis of the Full-Length Form of the L-Type Calcium Channel α1 Subunit by Calpain. *Journal of Neurochemistry*, *63*(4), 1558–1564. https://doi.org/10.1046/j.1471-4159.1994.63041558.x

De Jongh, K. S., Merrick, D. K., & Catterall, W. A. (1989). Subunits of purified calcium channels: a 212-kDa form of alpha 1 and partial amino acid sequence of a phosphorylation site of an independent beta subunit. *Proceedings of the National Academy of Sciences*, *86*(21), 8585–8589. https://doi.org/10.1073/pnas.86.21.8585

De Jongh, K. S., Murphy, B. J., Colvin, A. A., Hell, J. W., Takahashi, M., & Catterall, W. A. (1996). Specific Phosphorylation of a Site in the Full-Length Form of the α1 Subunit of the Cardiac L-Type Calcium Channel by Adenosine 3‘,5‘-Cyclic Monophosphate-Dependent Protein Kinase†. *Biochemistry*, *35*(32), 10392–10402. https://doi.org/10.1021/bi953023c

de Sevilla, D. F., Nunez, A., Borde, M., Malinow, R., & Buno, W. (2008). Cholinergic-Mediated IP3-Receptor Activation Induces Long-Lasting Synaptic Enhancement in CA1 Pyramidal Neurons. *Journal of Neuroscience*, *28*(6), 1469–1478. https://doi.org/10.1523/jneurosci.2723-07.2008

de Weille, J. R., Schweitz, H., Maes, P., Tartar, A., & Lazdunski, M. (1991). Calciseptine, a peptide isolated from black mamba venom, is a specific blocker of the L-type calcium channel. *Proceedings of the National Academy of Sciences*, *88*(6), 2437–2440. https://doi.org/10.1073/pnas.88.6.2437

DeFronzo, R. A., & Tripathy, D. (2009). Skeletal Muscle Insulin Resistance Is the Primary Defect in Type 2 Diabetes. *Diabetes Care*, *32*(suppl_2), S157–S163. https://doi.org/10.2337/dc09-s302

Degtiar, V. E., Scheller, R. H., & Tsien, R. W. (2000). Syntaxin Modulation of Slow Inactivation of N-Type Calcium Channels. *The Journal of Neuroscience*, *20*(12), 4355–4367. https://doi.org/10.1523/jneurosci.20-12-04355.2000

Deisseroth, K., Heist, E. K., & Tsien, R. W. (1998). Translocation of calmodulin to the nucleus supports CREB phosphorylation in hippocampal neurons. *Nature*, *392*(6672), 198–202. https://doi.org/10.1038/32448

Depil, K., Beyl, S., Stary-Weinzinger, A., Hohaus, A., Timin, E., & Hering, S. (2011). Timothy Mutation Disrupts the Link between Activation and Inactivation in CaV1.2 Protein*. *Journal of Biological Chemistry*, *286*(36), 31557–31564. https://doi.org/10.1074/jbc.m111.255273

des Georges, A., Clarke, O. B., Zalk, R., Yuan, Q., Condon, K. J., Grassucci, R. A., Hendrickson, W. A., Marks, A. R., & Frank, J. (2016). Structural Basis for Gating and Activation of RyR1. *Cell*, *167*(1), 145–157.e17. https://doi.org/10.1016/j.cell.2016.08.075

DETIMARY, P., GILON, P., & HENQUIN, J. C. (1998). Interplay between cytoplasmic Ca2+ and the ATP/ADP ratio: a feedback control mechanism in mouse pancreatic islets. *Biochemical Journal*, *333*(2), 269–274. https://doi.org/10.1042/bj3330269

Devogelaere, B., Beullens, M., Sammels, E., Derua, R., Waelkens, E., van Lint, J., Parys, J., Missiaen, L., Bollen, M., & De Smedt, H. (2007). Protein phosphatase-1 is a novel regulator of the interaction between IRBIT and the inositol 1,4,5-trisphosphate receptor. *Biochemical Journal*, *407*(2), 303–311. https://doi.org/10.1042/bj20070361

Devogelaere, B., Nadif Kasri, N., Derua, R., Waelkens, E., Callewaert, G., Missiaen, L., Parys, J. B., & De Smedt, H. (2006). Binding of IRBIT to the IP3 receptor: Determinants and functional effects. *Biochemical and Biophysical Research Communications*, *343*(1), 49–56. https://doi.org/10.1016/j.bbrc.2006.02.119

Dick, I. E., Joshi-Mukherjee, R., Yang, W., & Yue, D. T. (2016). Arrhythmogenesis in Timothy Syndrome is associated with defects in Ca2+-dependent inactivation. *Nature Communications*, *7*(1). https://doi.org/10.1038/ncomms10370

Dickson, E. J., Falkenburger, B. H., & Hille, B. (2013). Quantitative properties and receptor reserve of the IP3 and calcium branch of Gq-coupled receptor signaling. *Journal of General Physiology*, *141*(5), 521–535. https://doi.org/10.1085/jgp.201210886

Dilmac, N., Hilliard, N., & Hockerman, G. H. (2003). Molecular Determinants of Ca2+ Potentiation of Diltiazem Block and Ca2+-Dependent Inactivation in the Pore Region of Cav1.2. *Molecular Pharmacology*, *64*(2), 491–501. https://doi.org/10.1124/mol.64.2.491

Dilmac, N., Hilliard, N., & Hockerman, G. H. (2004). Molecular Determinants of Frequency Dependence and Ca2+ Potentiation of Verapamil Block in the Pore Region of Cav1.2. *Molecular Pharmacology*, *66*(5), 1236–1247. https://doi.org/10.1124/mol.104.000893

DiMeglio, L. A., Evans-Molina, C., & Oram, R. A. (2018). Type 1 diabetes. *The Lancet*, *391*(10138), 2449–2462. https://doi.org/10.1016/s0140-6736(18)31320-5

Ding, S., Ingleby, L., Ahern, C. A., & Horn, R. (2005). Investigating the Putative Glycine Hinge in Shaker Potassium Channel. *Journal of General Physiology*, *126*(3), 213–226. https://doi.org/10.1085/jgp.200509287

Dixit, S. S., Wang, T., Manzano, E. J. Q., Yoo, S., Lee, J., Chiang, D. Y., Ryan, N., Respress, J. L., Yechoor, V. K., & Wehrens, X. H. T. (2013). Effects of CaMKII-Mediated Phosphorylation of Ryanodine Receptor Type 2 on Islet Calcium Handling, Insulin Secretion, and Glucose Tolerance. *PLoS ONE*, *8*(3), e58655. https://doi.org/10.1371/journal.pone.0058655

Dolmetsch, R. E. (2001). Signaling to the Nucleus by an L-type Calcium Channel-Calmodulin Complex Through the MAP Kinase Pathway. *Science*, *294*(5541), 333–339. https://doi.org/10.1126/science.1063395

Dolphin, A. C. (2003a). Beta-Subunits of Voltage-Gated Calcium Channels. *Journal of Bioenergetics and Biomembranes*, *35*(6), 599–620. https://doi.org/10.1023/b:jobb.0000008026.37790.5a

Dolphin, A. C. (2003b). G Protein Modulation of Voltage-Gated Calcium Channels. *Pharmacological Reviews*, *55*(4), 607–627. https://doi.org/10.1124/pr.55.4.3

Dolphin, A. C. (2016). Voltage-gated calcium channels and their auxiliary subunits: physiology and pathophysiology and pharmacology. *The Journal of Physiology*, *594*(19), 5369–5390. https://doi.org/10.1113/jp272262

Dolphin, A. C. (2018a). Voltage-gated calcium channel α2δ subunits: an assessment of proposed novel roles. *F1000Research*, *7*, 1830. https://doi.org/10.12688/f1000research.16104.1

Dolphin, A. C. (2018b). Voltage-gated calcium channels: Their discovery, function and importance as drug targets. *Brain and Neuroscience Advances*, *2*, 239821281879480. https://doi.org/10.1177/2398212818794805

Döring, F., Degtiar, V. E., Grabner, M., Striessnig, J., Hering, S., & Glossmann, H. (1996). Transfer of L-type Calcium Channel IVS6 Segment Increases Phenylalkylamine Sensitivity of α1A. *Journal of Biological Chemistry*, *271*(20), 11745–11749. https://doi.org/10.1074/jbc.271.20.11745

Drews, G., Krippeit-Drews, P., & Düfer, M. (2010). Electrophysiology of Islet Cells. *Advances in Experimental Medicine and Biology*, 115–163. https://doi.org/10.1007/978-90-481-3271-3_7

Dufer, M., Gier, B., Wolpers, D., Krippeit-Drews, P., Ruth, P., & Drews, G. (2009). Enhanced Glucose Tolerance by SK4 Channel Inhibition in Pancreatic -Cells. *Diabetes*, *58*(8), 1835–1843. https://doi.org/10.2337/db08-1324

e Drigo, R. A., Jacob, S., García-Prieto, C. F., Zheng, X., Fukuda, M., Nhu, H. T. T., Stelmashenko, O., Peçanha, F. L. M., Rodriguez-Diaz, R., Bushong, E., Deerinck, T., Phan, S., Ali, Y., Leibiger, I., Chua, M., Boudier, T., Song, S. H., Graf, M., Augustine, G. J., . . . Berggren, P. O. (2019). Structural basis for delta cell paracrine regulation in pancreatic islets. *Nature Communications*, *10*(1). https://doi.org/10.1038/s41467-019-12258-7

Echevarría, W., Leite, M. F., Guerra, M. T., Zipfel, W. R., & Nathanson, M. H. (2003). Regulation of calcium signals in the nucleus by a nucleoplasmic reticulum. *Nature Cell Biology*, *5*(5), 440–446. https://doi.org/10.1038/ncb980

Efremov, R. G., Leitner, A., Aebersold, R., & Raunser, S. (2014). Architecture and conformational switch mechanism of the ryanodine receptor. *Nature*, *517*(7532), 39–43. https://doi.org/10.1038/nature13916

Eizirik, D. L., Cardozo, A. K., & Cnop, M. (2007). The Role for Endoplasmic Reticulum Stress in Diabetes Mellitus. *Endocrine Reviews*, *29*(1), 42–61. https://doi.org/10.1210/er.2007-0015

Ellis, S. B., Williams, M. E., Ways, N. R., Brenner, R., Sharp, A. H., Leung, A. T., Campbell, K. P., McKenna, E., Koch, W. J., Hui, A., Schwartz, A., & Harpold, M. M. (1988). Sequence and Expression of mRNAs Encoding the α1 and α2 Subunits of a DHP-Sensitive Calcium Channel. *Science*, *241*(4873), 1661–1664. https://doi.org/10.1126/science.2458626

Engisch, K., & Nowycky, M. (1996). Calcium dependence of large dense-cored vesicle exocytosis evoked by calcium influx in bovine adrenal chromaffin cells. *The Journal of Neuroscience*, *16*(4), 1359–1369. https://doi.org/10.1523/jneurosci.16-04-01359.1996

Erne, P., Bürgisser, E., Bühler, F., Dubach, B., Kühnis, H., Meier, M., & Rogg, H. (1984). Enhancement of calcium influx in human platelets by CGP 28392, a novel dihydropyridine. *Biochemical and Biophysical Research Communications*, *118*(3), 842–847. https://doi.org/10.1016/0006-291x(84)91471-2

Ertel, E. A., Campbell, K. P., Harpold, M. M., Hofmann, F., Mori, Y., Perez-Reyes, E., Schwartz, A., Snutch, T. P., Tanabe, T., Birnbaumer, L., Tsien, R. W., & Catterall, W. A. (2000). Nomenclature of Voltage-Gated Calcium Channels. *Neuron*, *25*(3), 533–535. https://doi.org/10.1016/s0896-6273(00)81057-0

Etemad, S., Obermair, G. J., Bindreither, D., Benedetti, A., Stanika, R., Di Biase, V., Burtscher, V., Koschak, A., Kofler, R., Geley, S., Wille, A., Lusser, A., Flockerzi, V., & Flucher, B. E. (2014). Differential Neuronal Targeting of a New and Two Known Calcium Channel 4 Subunit Splice Variants Correlates with Their Regulation of Gene Expression. *Journal of Neuroscience*, *34*(4), 1446–1461. https://doi.org/10.1523/jneurosci.3935-13.2014

Fabiato, A., & Fabiato, F. (1975). Contractions induced by a calcium-triggered release of calcium from the sarcoplasmic reticulum of single skinned cardiac cells. *The Journal of Physiology*, *249*(3), 469–495. https://doi.org/10.1113/jphysiol.1975.sp011026

Fainzilber, M., Lodder, J. C., van der Schors, R. C., Li, K. W., Yu, Z., Burlingame, A. L., Geraerts, W. P. M., & Kits, K. S. (1996). A Novel Hydrophobic ω-Conotoxin Blocks Molluscan Dihydropyridine-Sensitive Calcium Channels. *Biochemistry*, *35*(26), 8748–8752. https://doi.org/10.1021/bi9602674

Fan, G., Baker, M. L., Wang, Z., Baker, M. R., Sinyagovskiy, P. A., Chiu, W., Ludtke, S. J., & Serysheva, I. I. (2015). Gating machinery of InsP3R channels revealed by electron cryomicroscopy. *Nature*, *527*(7578), 336–341. https://doi.org/10.1038/nature15249

Fan, J. S., Yuan, Y., & Palade, P. (2000a). Kinetic effects of FPL 64176 on L-type Ca 2+ channels in cardiac myocytes. *Naunyn-Schmiedeberg's Archives of Pharmacology*, *361*(5), 465–476. https://doi.org/10.1007/s002100000219

Fan, J. S., Yuan, Y., & Palade, P. (2000b). Kinetic effects of FPL 64176 on L-type Ca 2+ channels in cardiac myocytes. *Naunyn-Schmiedeberg's Archives of Pharmacology*, *361*(5), 465–476. https://doi.org/10.1007/s002100000219

Fernández-Quintero, M. L., El Ghaleb, Y., Tuluc, P., Campiglio, M., Liedl, K. R., & Flucher, B. E. (2021). Structural determinants of voltage-gating properties in calcium channels. *ELife*, *10*. https://doi.org/10.7554/elife.64087

Ferreira, M. A. R., O'Donovan, M. C., Meng, Y. A., Jones, I. R., Ruderfer, D. M., Jones, L., Fan, J., Kirov, G., Perlis, R. H., Green, E. K., Smoller, J. W., Grozeva, D., Stone, J., Nikolov, I., Chambert, K., Hamshere, M. L., Nimgaonkar, V. L., Moskvina, V., Thase, M. E., . . . Craddock, N. (2008). Collaborative genome-wide association analysis supports a role for ANK3 and CACNA1C in bipolar disorder. *Nature Genetics*, *40*(9), 1056–1058. https://doi.org/10.1038/ng.209

Ferry, D., Glossmann, H., & Kaumann, A. (1985). Relationship between the stereoselective negative inotropic effects of verapamil enantiomers and their binding to putative calcium channels in human heart. *British Journal of Pharmacology*, *84*(4), 811–824. https://doi.org/10.1111/j.1476-5381.1985.tb17375.x

Ferry, D. R., Goll, A., Gadow, C., & Glossmann, H. (1984). (-)-3H-desmethoxyverapamil labelling of putative calcium channels in brain: autoradiographic distribution and allosteric coupling to 1,4-dihydropyridine and diltiazem binding sites. *Naunyn-Schmiedeberg's Archives of Pharmacology*, *327*(2), 183–187. https://doi.org/10.1007/bf00500915

Findeisen, F., & Minor, D. L. (2009). Disruption of the IS6-AID Linker Affects Voltage-gated Calcium Channel Inactivation and Facilitation. *Journal of General Physiology*, *133*(3), 327–343. https://doi.org/10.1085/jgp.200810143

Fleckenstein, A., & Fleckenstein-Grun, G. (1980). Cardiovascular protection by Ca antagonists. *European Heart Journal*, *1*(suppl 2), 15–21. https://doi.org/10.1093/eurheartj/1.suppl_2.15

Fourbon, Y., Guéguinou, M., Félix, R., Constantin, B., Uguen, A., Fromont, G., Lajoie, L., Magaud, C., Lecomte, T., Chamorey, E., Chatelier, A., Mignen, O., Potier-Cartereau, M., Chantôme, A., Bois, P., & Vandier, C. (2017). Ca2+ protein alpha 1D of CaV1.3 regulates intracellular calcium concentration and migration of colon cancer cells through a non-canonical activity. *Scientific Reports*, *7*(1), 14199. https://doi.org/10.1038/s41598-017-14230-1

Frayn, K. N. (2001). Adipose tissue and the insulin resistance syndrome. *Proceedings of the Nutrition Society*, *60*(3), 375–380. https://doi.org/10.1079/pns200195

Fry, C. H. (1983). The Slow Inward Current and Cardiac Arrhythmias. Edited by D. P. Zipes, J. C. Bailey, V. Elharrar. Martinus Nijhoff Publishers, The Hague, Netherlands (1980) 536 pages, many figures and tables, $65.50 ISBN: 90–247-2380-9. *Clinical Cardiology*, *6*(10), A47–A48. https://doi.org/10.1002/clc.4960061014

Fujimoto, K., Shibasaki, T., Yokoi, N., Kashima, Y., Matsumoto, M., Sasaki, T., Tajima, N., Iwanaga, T., & Seino, S. (2002). Piccolo, a Ca2+ Sensor in Pancreatic β-Cells. *Journal of Biological Chemistry*, *277*(52), 50497–50502. https://doi.org/10.1074/jbc.m210146200

Fujimura, K., & Matsuda, Y. (1989). Autogenous oscillatory potentials in neurons of the guinea pig substantia nigra pars compacta in vitro. *Neuroscience Letters*, *104*(1–2), 53–57. https://doi.org/10.1016/0304-3940(89)90328-5

Galli, C., Meucci, O., Scorziello, A., Werge, T., Calissano, P., & Schettini, G. (1995). Apoptosis in cerebellar granule cells is blocked by high KCl, forskolin, and IGF-1 through distinct mechanisms of action: the involvement of intracellular calcium and RNA synthesis. *The Journal of Neuroscience*, *15*(2), 1172–1179. https://doi.org/10.1523/jneurosci.15-02-01172.1995

Gamelli, A. E., McKinney, B. C., White, J. A., & Murphy, G. G. (2011). Deletion of the L-type calcium channel CaV1.3 but not CaV1.2 results in a diminished sAHP in mouse CA1 pyramidal neurons. *Hippocampus*, *21*(2), 133–141. https://doi.org/10.1002/hipo.20728

Gamper, N. (2004). Phosphotidylinositol 4,5-Bisphosphate Signals Underlie Receptor-Specific Gq/11-Mediated Modulation of N-Type Ca2+ Channels. *Journal of Neuroscience*, *24*(48), 10980–10992. https://doi.org/10.1523/jneurosci.3869-04.2004

Gamper, N., & Shapiro, M. S. (2007). Target-specific PIP2signalling: how might it work? *The Journal of Physiology*, *582*(3), 967–975. https://doi.org/10.1113/jphysiol.2007.132787

Gandasi, N. R., & Barg, S. (2014). Contact-induced clustering of syntaxin and munc18 docks secretory granules at the exocytosis site. *Nature Communications*, *5*(1). https://doi.org/10.1038/ncomms4914

Gandasi, N. R., Yin, P., Riz, M., Chibalina, M. V., Cortese, G., Lund, P. E., Matveev, V., Rorsman, P., Sherman, A., Pedersen, M. G., & Barg, S. (2017). Ca2+ channel clustering with insulin-containing granules is disturbed in type 2 diabetes. *Journal of Clinical Investigation*, *127*(6), 2353–2364. https://doi.org/10.1172/jci88491

Gao, S., & Yan, N. (2020). Structural Basis of the Modulation of the Voltage-Gated Calcium Ion Channel Ca v 1.1 by Dihydropyridine Compounds**. *Angewandte Chemie*, *133*(6), 3168–3174. https://doi.org/10.1002/ange.202011793

Gao, T., Cuadra, A. E., Ma, H., Bünemann, M., Gerhardstein, B. L., Cheng, T., Eick, R. T., & Hosey, M. (2001). C-terminal Fragments of the α1C(CaV1.2) Subunit Associate with and Regulate L-type Calcium Channels Containing C-terminal-truncated α1CSubunits. *Journal of Biological Chemistry*, *276*(24), 21089–21097. https://doi.org/10.1074/jbc.m008000200

García, M., Hernández-Gallegos, Z., Escamilla, J., & Sánchez, J. (2001). Calciseptine, a Ca 2+ Channel Blocker, Has Agonist Actions on L-type Ca 2+ Currents of Frog and Mammalian Skeletal Muscle. *Journal of Membrane Biology*, *184*(2), 121–129. https://doi.org/10.1007/s00232-001-0080-7

García-Palomero, E., Cuchillo-Ibáñez, I., García, A. G., Renart, J., Albillos, A., & Montiel, C. (2000). Greater diversity than previously thought of chromaffin cell Ca2+ channels, derived from mRNA identification studies. *FEBS Letters*, *481*(3), 235–239. https://doi.org/10.1016/s0014-5793(00)01984-0

Geib, S., Sandoz, G., Cornet, V., Mabrouk, K., Fund-Saunier, O., Bichet, D., Villaz, M., Hoshi, T., Sabatier, J. M., & De Waard, M. (2002). The Interaction between the I-II Loop and the III-IV Loop of Cav2.1 Contributes to Voltage-dependent Inactivation in a β-Dependent Manner. *Journal of Biological Chemistry*, *277*(12), 10003–10013. https://doi.org/10.1074/jbc.m106231200

Gembal, M., Gilon, P., & Henquin, J. C. (1992). Evidence that glucose can control insulin release independently from its action on ATP-sensitive K+ channels in mouse B cells. *Journal of Clinical Investigation*, *89*(4), 1288–1295. https://doi.org/10.1172/jci115714

Gerhardstein, B. L., Gao, T., Bünemann, M., Puri, T. S., Adair, A., Ma, H., & Hosey, M. (2000). Proteolytic Processing of the C Terminus of the α1CSubunit of L-type Calcium Channels and the Role of a Proline-rich Domain in Membrane Tethering of Proteolytic Fragments. *Journal of Biological Chemistry*, *275*(12), 8556–8563. https://doi.org/10.1074/jbc.275.12.8556

GERMAN, D. C., MANAYE, K. F., SONSALLA, P. K., & BROOKS, B. A. (1992). Midbrain Dopaminergic Cell Loss in Parkinson's Disease and MPTP-Induced Parkinsonism: Sparing of Calbindin-D28k-Containing Cells. *Annals of the New York Academy of Sciences*, *648*(1 Neurotoxins a), 42–62. https://doi.org/10.1111/j.1749-6632.1992.tb24523.x

Ghosh, D., Syed, A., Prada, M., Nystoriak, M., Santana, L., Nieves-Cintrón, M., & Navedo, M. (2017). Calcium Channels in Vascular Smooth Muscle. *Advances in Pharmacology*, 49–87. https://doi.org/10.1016/bs.apha.2016.08.002

Gilon, P., Chae, H. Y., Rutter, G. A., & Ravier, M. A. (2014). Calcium signaling in pancreatic β-cells in health and in Type 2 diabetes. *Cell Calcium*, *56*(5), 340–361. https://doi.org/10.1016/j.ceca.2014.09.001

Gilon, P., & Henquin, J. (1992). Influence of membrane potential changes on cytoplasmic Ca2+ concentration in an electrically excitable cell, the insulin-secreting pancreatic B-cell. *Journal of Biological Chemistry*, *267*(29), 20713–20720. https://doi.org/10.1016/s0021-9258(19)36744-4

Gilon, P., Ravier, M. A., Jonas, J. C., & Henquin, J. C. (2002). Control Mechanisms of the Oscillations of Insulin Secretion In Vitro and In Vivo. *Diabetes*, *51*(Supplement 1), S144–S151. https://doi.org/10.2337/diabetes.51.2007.s144

Gilquin, B., Lecoq, A., Desne, F., Guenneugues, M., Zinn-Justin, S., & Menez, A. (1999). Conformational and functional variability supported by the BPTI fold: Solution structure of the Ca2+ channel blocker calcicludine. *Proteins: Structure, Function, and Genetics*, *34*(4), 520–532. https://pubmed.ncbi.nlm.nih.gov/10081964/

Ginap, T., Dooley, D., & Feuerstein, T. (1993). The non-dihydropyridine L-type voltage-sensitive calcium channel activator FPL 64176 enhances K+-evoked efflux of [3H]norepinephrine from rat neocortical slices. *Neuroscience Letters*, *156*(1–2), 35–38. https://doi.org/10.1016/0304-3940(93)90433-l

Giordano, T. P., Satpute, S. S., Striessnig, J., Kosofsky, B. E., & Rajadhyaksha, A. M. (2006). Up-regulation of dopamine D2L mRNA levels in the ventral tegmental area and dorsal striatum of amphetamine-sensitized C57BL/6 mice: role of Cav1.3 L-type Ca2+channels. *Journal of Neurochemistry*, *99*(4), 1197–1206. https://doi.org/10.1111/j.1471-4159.2006.04186.x

Glossmann, H., & Striessnig, J. (1990). Molecular properties of calcium channels. *Reviews of Physiology, Biochemistry and Pharmacology*, *114*, 1–105. https://doi.org/10.1007/bfb0031018

Goldberg, J. A., Guzman, J. N., Estep, C. M., Ilijic, E., Kondapalli, J., Sanchez-Padilla, J., & Surmeier, D. J. (2012). Calcium entry induces mitochondrial oxidant stress in vagal neurons at risk in Parkinson's disease. *Nature Neuroscience*, *15*(10), 1414–1421. https://doi.org/10.1038/nn.3209

Gomez-Ospina, N., Tsuruta, F., Barreto-Chang, O., Hu, L., & Dolmetsch, R. (2006). The C Terminus of the L-Type Voltage-Gated Calcium Channel CaV1.2 Encodes a Transcription Factor. *Cell*, *127*(3), 591–606. https://doi.org/10.1016/j.cell.2006.10.017

Göpel, S., Kanno, T., Barg, S., Galvanovskis, J., & Rorsman, P. (1999). Voltage-gated and resting membrane currents recorded from B-cells in intact mouse pancreatic islets. *The Journal of Physiology*, *521*(3), 717–728. https://doi.org/10.1111/j.1469-7793.1999.00717.x

Göpel, S., Zhang, Q., Eliasson, L., Ma, X. S., Galvanovskis, J., Kanno, T., Salehi, A., & Rorsman, P. (2004). Capacitance measurements of exocytosis in mouse pancreatic α-, β- and δ-cells within intact islets of Langerhans. *The Journal of Physiology*, *556*(3), 711–726. https://doi.org/10.1113/jphysiol.2003.059675

Gould, R., Murphy, K., & Snyder, S. (1983). Studies on Voltage-operated Calcium Channels Using Radioligands. *Cold Spring Harbor Symposia on Quantitative Biology*, *48*(0), 355–362. https://doi.org/10.1101/sqb.1983.048.01.039

Graef, I. A., Mermelstein, P. G., Stankunas, K., Neilson, J. R., Deisseroth, K., Tsien, R. W., & Crabtree, G. R. (1999). L-type calcium channels and GSK-3 regulate the activity of NF-ATc4 in hippocampal neurons. *Nature*, *401*(6754), 703–708. https://doi.org/10.1038/44378

Graham, F. L., Russell, W. C., Smiley, J., & Nairn, R. (1977). Characteristics of a Human Cell Line Transformed by DNA from Human Adenovirus Type 5. *Journal of General Virology*, *36*(1), 59–72. https://doi.org/10.1099/0022-1317-36-1-59

Green, G. E., Khan, K. M., Beisel, K. W., Drescher, M. J., Hatfield, J. S., & Drescher, D. G. (2002). Calcium Channel Subunits in the Mouse Cochlea. *Journal of Neurochemistry*, *67*(1), 37–45. https://doi.org/10.1046/j.1471-4159.1996.67010037.x

Griessmeier, K., Cuny, H., Rötzer, K., Griesbeck, O., Harz, H., Biel, M., & Wahl-Schott, C. (2009). Calmodulin Is a Functional Regulator of Cav1.4 L-type Ca2+ Channels. *Journal of Biological Chemistry*, *284*(43), 29809–29816. https://doi.org/10.1074/jbc.m109.048082

Groome, J. R., & Bayless-Edwards, L. (2020). Roles for Countercharge in the Voltage Sensor Domain of Ion Channels. *Frontiers in Pharmacology*, *11*. https://doi.org/10.3389/fphar.2020.00160

Gudlur, A., Zeraik, A. E., Hirve, N., & Hogan, P. G. (2019). STIM calcium sensing and conformational change. *The Journal of Physiology*, *598*(9), 1695–1705. https://doi.org/10.1113/jp276524

Guerra, M. L. (2011). *Specific coupling of L-type voltage-gated calcium channels to signaling events in pancreatic β Cells*. https://docs.lib.purdue.edu/dissertations/AAI3479489/

Guex, N., Peitsch, M. C., & Schwede, T. (2009). Automated comparative protein structure modeling with SWISS-MODEL and Swiss-PdbViewer: A historical perspective. *ELECTROPHORESIS*, *30*(S1), S162–S173. https://doi.org/10.1002/elps.200900140

Gustafsson, A. J., Ingelman-Sundberg, H., Dzabic, M., Awasum, J., Hoa, N. K., Östenson, C. G., Pierro, C., Tedeschi, P., Woolcott, O., Chiounan, S., Lund, P. E., Larsson, O., & Islam, M. S. (2004). Ryanodine receptor-operated activation of TRP-like channels can trigger critical Ca 2+ signaling events in pancreatic β-cells. *The FASEB Journal*, *19*(2), 1–23. https://doi.org/10.1096/fj.04-2621fje

Guzman, J. N., Ilijic, E., Yang, B., Sanchez-Padilla, J., Wokosin, D., Galtieri, D., Kondapalli, J., Schumacker, P. T., & Surmeier, D. J. (2018). Systemic isradipine treatment diminishes calcium-dependent mitochondrial oxidant stress. *Journal of Clinical Investigation*, *128*(6), 2266–2280. https://doi.org/10.1172/jci95898

Guzman, J. N., Sanchez-Padilla, J., Chan, C. S., & Surmeier, D. J. (2009). Robust Pacemaking in Substantia Nigra Dopaminergic Neurons. *Journal of Neuroscience*, *29*(35), 11011–11019. https://doi.org/10.1523/jneurosci.2519-09.2009

Guzman, J. N., Sanchez-Padilla, J., Wokosin, D., Kondapalli, J., Ilijic, E., Schumacker, P. T., & Surmeier, D. J. (2010). Oxidant stress evoked by pacemaking in dopaminergic neurons is attenuated by DJ-1. *Nature*, *468*(7324), 696–700. https://doi.org/10.1038/nature09536

Haby, C., Larsson, O., Islam, M. S., Aunis, D., Berggren, P. O., & Zwiller, J. (1994). Inhibition of serine/threonine protein phosphatases promotes opening of voltage-activated L-type Ca2+ channels in insulin-secreting cells. *Biochemical Journal*, *298*(2), 341–346. https://doi.org/10.1042/bj2980341

Haeseleer, F., Williams, B., & Lee, A. (2016). Characterization of C-terminal Splice Variants of Cav1.4 Ca2+ Channels in Human Retina. *Journal of Biological Chemistry*, *291*(30), 15663–15673. https://doi.org/10.1074/jbc.m116.731737

Hagberg, C. E., Mehlem, A., Falkevall, A., Muhl, L., Fam, B. C., Ortsäter, H., Scotney, P., Nyqvist, D., Samén, E., Lu, L., Stone-Elander, S., Proietto, J., Andrikopoulos, S., Sjöholm, K., Nash, A., & Eriksson, U. (2012). Targeting VEGF-B as a novel treatment for insulin resistance and type 2 diabetes. *Nature*, *490*(7420), 426–430. https://doi.org/10.1038/nature11464

Hagiwara, S., Ozawa, S., & Sand, O. (1975). Voltage clamp analysis of two inward current mechanisms in the egg cell membrane of a starfish. *Journal of General Physiology*, *65*(5), 617–644. https://doi.org/10.1085/jgp.65.5.617

Hakamata, Y., Nakai, J., Takeshima, H., & Imoto, K. (1992). Primary structure and distribution of a novel ryanodine receptor/calcium release channel from rabbit brain. *FEBS Letters*, *312*(2–3), 229–235. https://doi.org/10.1016/0014-5793(92)80941-9

Hammond, G. R. V., Fischer, M. J., Anderson, K. E., Holdich, J., Koteci, A., Balla, T., & Irvine, R. F. (2012). PI4P and PI(4,5)P2 Are Essential But Independent Lipid Determinants of Membrane Identity. *Science*, *337*(6095), 727–730. https://doi.org/10.1126/science.1222483

Hanlon, M., Berrow, N., Dolphin, A., & Wallace, B. (1999). Modelling of a voltage-dependent Ca2+channel β subunit as a basis for understanding its functional properties. *FEBS Letters*, *445*(2–3), 366–370. https://doi.org/10.1016/s0014-5793(99)00156-8

Hao, J., Bao, X., Jin, B., Wang, X., Mao, Z., Li, X., Wei, L., Shen, D., & Wang, J. (2015). Ca 2+ channel subunit α 1D promotes proliferation and migration of endometrial cancer cells mediated by 17β-estradiol via the G protein-coupled estrogen receptor. *The FASEB Journal*, *29*(7), 2883–2893. https://doi.org/10.1096/fj.14-265603

Hardingham, G. E., Arnold, F. J. L., & Bading, H. (2001). Nuclear calcium signaling controls CREB-mediated gene expression triggered by synaptic activity. *Nature Neuroscience*, *4*(3), 261–267. https://doi.org/10.1038/85109

Hardingham, G. E., Cruzalegui, F. H., Chawla, S., & Bading, H. (1998). Mechanisms controlling gene expression by nuclear calcium signals. *Cell Calcium*, *23*(2–3), 131–134. https://doi.org/10.1016/s0143-4160(98)90111-7

Harnick, D. J., Jayaraman, T., Ma, Y., Mulieri, P., Go, L. O., & Marks, A. R. (1995). The Human Type 1 Inositol 1,4,5-Trisphosphate Receptor from T Lymphocytes. *Journal of Biological Chemistry*, *270*(6), 2833–2840. https://doi.org/10.1074/jbc.270.6.2833

Harraz, O. F., Hill-Eubanks, D., & Nelson, M. T. (2020a). PIP2: A critical regulator of vascular ion channels hiding in plain sight. *Proceedings of the National Academy of Sciences*, *117*(34), 20378–20389. https://doi.org/10.1073/pnas.2006737117

Harraz, O. F., Hill-Eubanks, D., & Nelson, M. T. (2020b). PIP2: A critical regulator of vascular ion channels hiding in plain sight. *Proceedings of the National Academy of Sciences*, *117*(34), 20378–20389. https://doi.org/10.1073/pnas.2006737117

Hasreiter, J., Goldnagl, L., Böhm, S., & Kubista, H. (2014). Cav1.2 and Cav1.3 L-type calcium channels operate in a similar voltage range but show different coupling to Ca2+-dependent conductances in hippocampal neurons. *American Journal of Physiology-Cell Physiology*, *306*(12), C1200–C1213. https://doi.org/10.1152/ajpcell.00329.2013

He, P., Zhang, H., & Yun, C. C. (2008). IRBIT, Inositol 1,4,5-Triphosphate (IP3) Receptor-binding Protein Released with IP3, Binds Na+/H+ Exchanger NHE3 and Activates NHE3 Activity in Response to Calcium. *Journal of Biological Chemistry*, *283*(48), 33544–33553. https://doi.org/10.1074/jbc.m805534200

Heimberg, H., De Vos, A., Pipeleers, D., Thorens, B., & Schuit, F. (1995). Differences in Glucose Transporter Gene Expression between Rat Pancreatic α- and β-Cells Are Correlated to Differences in Glucose Transport but Not in Glucose Utilization. *Journal of Biological Chemistry*, *270*(15), 8971–8975. https://doi.org/10.1074/jbc.270.15.8971

Heinzel, S. S., Krysan, P. J., Calos, M. P., & DuBridge, R. B. (1988). Use of simian virus 40 replication to amplify Epstein-Barr virus shuttle vectors in human cells. *Journal of Virology*, *62*(10), 3738–3746. https://doi.org/10.1128/jvi.62.10.3738-3746.1988

Hell, J. W., Westenbroek, R. E., Warner, C., Ahlijanian, M. K., Prystay, W., Gilbert, M. M., Snutch, T. P., & Catterall, W. A. (1993). Identification and differential subcellular localization of the neuronal class C and class D L-type calcium channel alpha 1 subunits. *Journal of Cell Biology*, *123*(4), 949–962. https://doi.org/10.1083/jcb.123.4.949

Hell, J., Yokoyama, C., Wong, S., Warner, C., Snutch, T., & Catterall, W. (1993). Differential phosphorylation of two size forms of the neuronal class C L-type calcium channel alpha 1 subunit. *Journal of Biological Chemistry*, *268*(26), 19451–19457. https://doi.org/10.1016/s0021-9258(19)36536-6

Hellman, B., & Angervall, L. (2009). THE FREQUENCY DISTRIBUTION OF THE NUMBER AND VOLUME OF THE ISLETS OF LANGERHANS IN MAN. *Acta Pathologica Microbiologica Scandinavica*, *53*(3), 230–236. https://doi.org/10.1111/j.1699-0463.1961.tb00405.x

Henquin, J. C. (1990). Role of voltage- and Ca2+-dependent K+ channels in the control of glucose-induced electrical activity in pancreatic B-cells. *Pflugers Archiv European Journal of Physiology*, *416*(5), 568–572. https://doi.org/10.1007/bf00382691

Henquin, J. C. (2021). Paracrine and autocrine control of insulin secretion in human islets: evidence and pending questions. *American Journal of Physiology-Endocrinology and Metabolism*, *320*(1), E78–E86. https://doi.org/10.1152/ajpendo.00485.2020

Henquin, J. C., & Meissner, H. P. (1984). Significance of ionic fluxes and changes in membrane potential for stimulus-secretion coupling in pancreatic B-cells. *Experientia*, *40*(10), 1043–1052. https://doi.org/10.1007/bf01971450

Henquin, J. C., Ravier, M. A., Nenquin, M., Jonas, J. C., & Gilon, P. (2003). Hierarchy of the β-cell signals controlling insulin secretion. *European Journal of Clinical Investigation*, *33*(9), 742–750. https://doi.org/10.1046/j.1365-2362.2003.01207.x

Hering, S., Aczél, S., Grabner, M., Döring, F., Berjukow, S., Mitterdorfer, J., Sinnegger, M. J., Striessnig, J., Degtiar, V. E., Wang, Z., & Glossmann, H. (1996). Transfer of High Sensitivity for Benzothiazepines from L-type to Class A (BI) Calcium Channels. *Journal of Biological Chemistry*, *271*(40), 24471–24475. https://doi.org/10.1074/jbc.271.40.24471

Hering, S., Berjukow, S., Sokolov, S., Marksteiner, R., Weiß, R. G., Kraus, R., & Timin, E. N. (2000). Molecular determinants of inactivation in voltage-gated Ca 2+ channels. *The Journal of Physiology*, *528*(2), 237–249. https://doi.org/10.1111/j.1469-7793.2000.t01-1-00237.x

Hering, S., Zangerl-Plessl, E. M., Beyl, S., Hohaus, A., Andranovits, S., & Timin, E. N. (2018). Calcium channel gating. *Pflügers Archiv - European Journal of Physiology*, *470*(9), 1291–1309. https://doi.org/10.1007/s00424-018-2163-7

Hernández, A., Segura-Chama, P., Jiménez, N., García, A. G., Hernández-Guijo, J. M., & Hernández-Cruz, A. (2011). Modulation by endogenously released ATP and opioids of chromaffin cell calcium channels in mouse adrenal slices. *American Journal of Physiology-Cell Physiology*, *300*(3), C610–C623. https://doi.org/10.1152/ajpcell.00380.2010

Hernández-Guijo, J. M., Carabelli, V., Gandía, L., García, A. G., & Carbone, E. (1999). Voltage-independent autocrine modulation of L-type channels mediated by ATP, opioids and catecholamines in rat chromaffin cells. *European Journal of Neuroscience*, *11*(10), 3574–3584. https://doi.org/10.1046/j.1460-9568.1999.00775.x

Hess, P., & Tsien, R. W. (1984). Mechanism of ion permeation through calcium channels. *Nature*, *309*(5967), 453–456. https://doi.org/10.1038/309453a0

Heusser, K., Yuan, H., Neagoe, I., Tarasov, A. I., Ashcroft, F. M., & Schwappach, B. (2006). Scavenging of 14–3-3 proteins reveals their involvement in the cell-surface transport of ATP-sensitive K+ channels. *Journal of Cell Science*, *119*(20), 4353–4363. https://doi.org/10.1242/jcs.03196

Hilgemann, D. W., Dai, G., Collins, A., Larricia, V., Magi, S., Deisl, C., & Fine, M. (2018). Lipid signaling to membrane proteins: From second messengers to membrane domains and adapter-free endocytosis. *Journal of General Physiology*, *150*(2), 211–224. https://doi.org/10.1085/jgp.201711875

Hille, B. (1978). Ionic channels in excitable membranes. Current problems and biophysical approaches. *Biophysical Journal*, *22*(2), 283–294. https://doi.org/10.1016/s0006-3495(78)85489-7

Hille, B., Dickson, E. J., Kruse, M., Vivas, O., & Suh, B. C. (2015). Phosphoinositides regulate ion channels. *Biochimica et Biophysica Acta (BBA) - Molecular and Cell Biology of Lipids*, *1851*(6), 844–856. https://doi.org/10.1016/j.bbalip.2014.09.010

HILLE, BERTIL (TEACHER, UNIVERSITY OF WASHINGTON, USA). (2021). *ION CHANNELS OF EXCITABLE MEMBRANES*. SINAUER ASSOCIATES INC.,U.S.

Hirschfeld, R. M. A. (2010). History and evolution of the monoamine hypothesis of depression. *The Journal of Clinical Psychiatry*, *61*(suppl 6), 4–6. https://doi.org/10.4088/jcp.11096su1c.01

Hockerman, G. H., Dilmac, N., Scheuer, T., & Catterall, W. A. (2000). Molecular Determinants of Diltiazem Block in Domains IIIS6 and IVS6 of L-type Ca2+ Channels. *Molecular Pharmacology*, *58*(6), 1264–1270. https://doi.org/10.1124/mol.58.6.1264

Hockerman, G. H., Johnson, B. D., Abbott, M. R., Scheuer, T., & Catterall, W. A. (1997). Molecular Determinants of High Affinity Phenylalkylamine Block of l-type Calcium Channels in Transmembrane Segment IIIS6 and the Pore Region of the α1Subunit. *Journal of Biological Chemistry*, *272*(30), 18759–18765. https://doi.org/10.1074/jbc.272.30.18759

Hockerman, G. H., Johnson, B. D., Scheuer, T., & Catterall, W. A. (1995). Molecular Determinants of High Affinity Phenylalkylamine Block of L-type Calcium Channels. *Journal of Biological Chemistry*, *270*(38), 22119–22122. https://doi.org/10.1074/jbc.270.38.22119

Hockerman, G. H., Peterson, B. Z., Johnson, and, B. D., & Catterall, W. A. (1997). MOLECULAR DETERMINANTS OF DRUG BINDING AND ACTION ON L-TYPE CALCIUM CHANNELS. *Annual Review of Pharmacology and Toxicology*, *37*(1), 361–396. https://doi.org/10.1146/annurev.pharmtox.37.1.361

Hockerman, G. H., Peterson, B. Z., Sharp, E., Tanada, T. N., Scheuer, T., & Catterall, W. A. (1997). Construction of a high-affinity receptor site for dihydropyridine agonists and antagonists by single amino acid substitutions in a non-L-type Ca2+ channel. *Proceedings of the National Academy of Sciences*, *94*(26), 14906–14911. https://doi.org/10.1073/pnas.94.26.14906

Hof, R. P., Ruegg, U. T., Hof, A., & Vogel, A. (1985). Stereoselectivity at the Calcium Channel. *Journal of Cardiovascular Pharmacology*, *7*(4), 689–693. https://doi.org/10.1097/00005344-198507000-00012

Hofmann, F., Flockerzi, V., Kahl, S., & Wegener, J. W. (2014). L-Type CaV1.2 Calcium Channels: From In Vitro Findings to In Vivo Function. *Physiological Reviews*, *94*(1), 303–326. https://doi.org/10.1152/physrev.00016.2013

Hohaus, A., Beyl, S., Kudrnac, M., Berjukow, S., Timin, E. N., Marksteiner, R., Maw, M. A., & Hering, S. (2005). Structural Determinants of L-type Channel Activation in Segment IIS6 Revealed by a Retinal Disorder. *Journal of Biological Chemistry*, *280*(46), 38471–38477. https://doi.org/10.1074/jbc.m507013200

Hoppa, M. B., Lana, B., Margas, W., Dolphin, A. C., & Ryan, T. A. (2012). α2δ expression sets presynaptic calcium channel abundance and release probability. *Nature*, *486*(7401), 122–125. https://doi.org/10.1038/nature11033

Horton, R. M., Hunt, H. D., Ho, S. N., Pullen, J. K., & Pease, L. R. (1989). Engineering hybrid genes without the use of restriction enzymes: gene splicing by overlap extension. *Gene*, *77*(1), 61–68. https://doi.org/10.1016/0378-1119(89)90359-4

Houamed, K. M., Sweet, I. R., & Satin, L. S. (2010). BK channels mediate a novel ionic mechanism that regulates glucose-dependent electrical activity and insulin secretion in mouse pancreatic β-cells. *The Journal of Physiology*, *588*(18), 3511–3523. https://doi.org/10.1113/jphysiol.2009.184341

Howes, O. D., & Kapur, S. (2009). The Dopamine Hypothesis of Schizophrenia: Version III--The Final Common Pathway. *Schizophrenia Bulletin*, *35*(3), 549–562. https://doi.org/10.1093/schbul/sbp006

Huang, H., Ng, C. Y., Yu, D., Zhai, J., Lam, Y., & Soong, T. W. (2014). Modest CaV1.342-selective inhibition by compound 8 is β-subunit dependent. *Nature Communications*, *5*(1), 1. https://doi.org/10.1038/ncomms5481

Huang, H., Yu, D., & Soong, T. W. (2013). C-Terminal Alternative Splicing of CaV1.3 Channels Distinctively Modulates Their Dihydropyridine Sensitivity. *Molecular Pharmacology*, *84*(4), 643–653. https://doi.org/10.1124/mol.113.087155

Huang, L., Shen, H., Atkinson, M. A., & Kennedy, R. T. (1995). Detection of exocytosis at individual pancreatic beta cells by amperometry at a chemically modified microelectrode. *Proceedings of the National Academy of Sciences*, *92*(21), 9608–9612. https://doi.org/10.1073/pnas.92.21.9608

Hullin, R., Singer-Lahat, D., Freichel, M., Biel, M., Dascal, N., Hofmann, F., & Flockerzi, V. (1992). Calcium channel beta subunit heterogeneity: functional expression of cloned cDNA from heart, aorta and brain. *The EMBO Journal*, *11*(3), 885–890. https://doi.org/10.1002/j.1460-2075.1992.tb05126.x

Hulme, J. T., Konoki, K., Lin, T. W. C., Gritsenko, M. A., Camp, D. G., Bigelow, D. J., & Catterall, W. A. (2005). Sites of proteolytic processing and noncovalent association of the distal C-terminal domain of CaV1.1 channels in skeletal muscle. *Proceedings of the National Academy of Sciences*, *102*(14), 5274–5279. https://doi.org/10.1073/pnas.0409885102

Hulme, J. T., Lin, T. W. C., Westenbroek, R. E., Scheuer, T., & Catterall, W. A. (2003). -Adrenergic regulation requires direct anchoring of PKA to cardiac CaV1.2 channels via a leucine zipper interaction with A kinase-anchoring protein 15. *Proceedings of the National Academy of Sciences, 100*(22), 13093–13098. https://doi.org/10.1073/pnas.2135335100

Hulme, J. T., Yarov-Yarovoy, V., Lin, T. W. C., Scheuer, T., & Catterall, W. A. (2006). Autoinhibitory control of the CaV1.2 channel by its proteolytically processed distal C-terminal domain. *The Journal of Physiology*, *576*(1), 87–102. https://doi.org/10.1113/jphysiol.2006.111799

Hurley, M. J., Brandon, B., Gentleman, S. M., & Dexter, D. T. (2013). Parkinson's disease is associated with altered expression of CaV1 channels and calcium-binding proteins. *Brain*, *136*(7), 2077–2097. https://doi.org/10.1093/brain/awt134

Identification of risk loci with shared effects on five major psychiatric disorders: a genome-wide analysis. (2013). *The Lancet*, *381*(9875), 1371–1379. https://doi.org/10.1016/s0140-6736(12)62129-1

Inagaki, N., Gonoi, T., Clement, J. P., Namba, N., Inazawa, J., Gonzalez, G., Aguilar-Bryan, L., Seino, S., & Bryan, J. (1995). Reconstitution of I(KATP): An Inward Rectifier Subunit Plus the Sulfonylurea Receptor. *Science*, *270*(5239), 1166–1170. https://doi.org/10.1126/science.270.5239.1166

Inobe, T., & Nukina, N. (2016). Rapamycin-induced oligomer formation system of FRB–FKBP fusion proteins. *Journal of Bioscience and Bioengineering*, *122*(1), 40–46. https://doi.org/10.1016/j.jbiosc.2015.12.004

Inui, M., Saito, A., & Fleischer, S. (1987). Isolation of the ryanodine receptor from cardiac sarcoplasmic reticulum and identity with the feet structures. *Journal of Biological Chemistry*, *262*(32), 15637–15642. https://doi.org/10.1016/s0021-9258(18)47774-5

Irwin, N., & Flatt, P. R. (2013). Enteroendocrine hormone mimetics for the treatment of obesity and diabetes. *Current Opinion in Pharmacology*, *13*(6), 989–995. https://doi.org/10.1016/j.coph.2013.09.009

Islam, M. S. (2002). The Ryanodine Receptor Calcium Channel of -Cells: Molecular Regulation and Physiological Significance. *Diabetes*, *51*(5), 1299–1309. https://doi.org/10.2337/diabetes.51.5.1299

Islam, M. S. (2010). *The Islets of Langerhans (Advances in Experimental Medicine and Biology Book 654)* (2010th ed.). Springer.

Isradipine Versus Placebo in Early Parkinson Disease. (2020). *Annals of Internal Medicine*, *172*(9), 591–598. https://doi.org/10.7326/m19-2534

Itoh, R., Hatano, N., Murakami, M., Mitsumori, K., Kawasaki, S., Wakagi, T., Kanzaki, Y., Kojima, H., Kawaai, K., Mikoshiba, K., Hamada, K., & Mizutani, A. (2021). Both IRBIT and long-IRBIT bind to and coordinately regulate Cl−/HCO3− exchanger AE2 activity through modulating the lysosomal degradation of AE2. *Scientific Reports*, *11*(1). https://doi.org/10.1038/s41598-021-85499-6

Iwashima, Y., Pugh, W., Depaoli, A. M., Takeda, J., Seino, S., Bell, G. I., & Polonsky, K. S. (1993). Expression of calcium channel mRNAs in rat pancreatic islets and downregulation after glucose infusion. *Diabetes*, *42*(7), 948–955. https://doi.org/10.2337/diabetes.42.7.948

Jackson, T. R., Patterson, S. I., Thastrup, O., & Hanley, M. R. (1988). A novel tumour promoter, thapsigargin, transiently increases cytoplasmic free Ca2+ without generation of inositol phosphates in NG115-401L neuronal cells. *Biochemical Journal*, *253*(1), 81–86. https://doi.org/10.1042/bj2530081

Jacob, J., Duclohier, H., & Cafiso, D. S. (1999). The Role of Proline and Glycine in Determining the Backbone Flexibility of a Channel-Forming Peptide. *Biophysical Journal*, *76*(3), 1367–1376. https://doi.org/10.1016/s0006-3495(99)77298-x

Jacobo, S. M. P., Guerra, M. L., Jarrard, R. E., Przybyla, J. A., Liu, G., Watts, V. J., & Hockerman, G. H. (2009). The Intracellular II-III Loops of Cav1.2 and Cav1.3 Uncouple L-Type Voltage-Gated Ca2+ Channels from Glucagon-Like Peptide-1 Potentiation of Insulin Secretion in INS-1 Cells via Displacement from Lipid Rafts. *Journal of Pharmacology and Experimental Therapeutics*, *330*(1), 283–293. https://doi.org/10.1124/jpet.109.150672

Jacobson, D. A., Kuznetsov, A., Lopez, J. P., Kash, S., Ämmälä, C. E., & Philipson, L. (2007). Kv2.1 Ablation Alters Glucose-Induced Islet Electrical Activity, Enhancing Insulin Secretion. *Cell Metabolism*, *6*(3), 229–235. https://doi.org/10.1016/j.cmet.2007.07.010

Jacobson, D. A., Mendez, F., Thompson, M., Torres, J., Cochet, O., & Philipson, L. H. (2010a). Calcium-activated and voltage-gated potassium channels of the pancreatic islet impart distinct and complementary roles during secretagogue induced electrical responses. *The Journal of Physiology*, *588*(18), 3525–3537. https://doi.org/10.1113/jphysiol.2010.190207

Jacobson, D. A., Mendez, F., Thompson, M., Torres, J., Cochet, O., & Philipson, L. H. (2010b). Calcium-activated and voltage-gated potassium channels of the pancreatic islet impart distinct and complementary roles during secretagogue induced electrical responses. *The Journal of Physiology*, *588*(18), 3525–3537. https://doi.org/10.1113/jphysiol.2010.190207

Jacobson, D. A., & Philipson, L. H. (2007). Action potentials and insulin secretion: new insights into the role of Kv channels. *Diabetes, Obesity and Metabolism*, *9*(s2), 89–98. https://doi.org/10.1111/j.1463-1326.2007.00784.x

JAHN, H., NASTAINCZYK, W., RoHRKASTEN, A., SCHNEIDER, T., & HOFMANN, F. (1988). Site-specific phosphorylation of the purified receptor for calcium-channel blockers by cAMP- and cGMP-dependent protein kinases, protein kinase C, calmodulin-dependent protein kinase II and casein kinase II. *European Journal of Biochemistry*, *178*(2), 535–542. https://doi.org/10.1111/j.1432-1033.1988.tb14480.x

Janis, R., Rampe, D., Sarmiento, J., & Triggle, D. (1984). Specific binding of a calcium channel activator, [3H]BAY k 8644, to membranes from cardiac muscle and brain. *Biochemical and Biophysical Research Communications*, *121*(1), 317–323. https://doi.org/10.1016/0006-291x(84)90725-3

Jensen, M. V., Joseph, J. W., Ronnebaum, S. M., Burgess, S. C., Sherry, A. D., & Newgard, C. B. (2008). Metabolic cycling in control of glucose-stimulated insulin secretion. *American Journal of Physiology-Endocrinology and Metabolism*, *295*(6), E1287–E1297. https://doi.org/10.1152/ajpendo.90604.2008

Ji, J., Yang, S. N., Huang, X., Li, X., Sheu, L., Diamant, N., Berggren, P. O., & Gaisano, H. Y. (2002). Modulation of L-Type Ca2+ Channels by Distinct Domains Within SNAP-25. *Diabetes*, *51*(5), 1425–1436. https://doi.org/10.2337/diabetes.51.5.1425

Jia, J. D., Jiang, W. G., Luo, X., Li, R. R., Zhao, Y. C., Tian, G., & Li, Y. N. (2021). Vascular endothelial growth factor B inhibits insulin secretion in MIN6 cells and reduces Ca2+ and cyclic adenosine monophosphate levels through PI3K/AKT pathway. *World Journal of Diabetes*, *12*(4), 480–498. https://doi.org/10.4239/wjd.v12.i4.480

Johnson, B. A., Roache, J. D., Ait-Daoud, N., Wells, L. T., & Mauldin, J. B. (2004). Effects of Isradipine on Cocaine-Induced Subjective Mood. *Journal of Clinical Psychopharmacology*, *24*(2), 180–191. https://doi.org/10.1097/01.jcp.0000115662.45074.c3

Johnson, B. D., Brousal, J. P., Peterson, B. Z., Gallombardo, P. A., Hockerman, G. H., Lai, Y., Scheuer, T., & Catterall, W. A. (1997). Modulation of the Cloned Skeletal Muscle L-Type Ca2+Channel by Anchored cAMP-Dependent Protein Kinase. *The Journal of Neuroscience*, *17*(4), 1243–1255. https://doi.org/10.1523/jneurosci.17-04-01243.1997

Johnson, B. D., Hockerman, G. H., Scheuer, T., & Catterall, W. A. (1996). Distinct effects of mutations in transmembrane segment IVS6 on block of L-type calcium channels by structurally similar phenylalkylamines. *Molecular Pharmacology*, *50*(5), 1388–1400. https://pubmed.ncbi.nlm.nih.gov/8913371/

Johnson, B. D., Scheuer, T., & Catterall, W. A. (1994). Voltage-dependent potentiation of L-type Ca2+ channels in skeletal muscle cells requires anchored cAMP-dependent protein kinase. *Proceedings of the National Academy of Sciences*, *91*(24), 11492–11496. https://doi.org/10.1073/pnas.91.24.11492

Johnson, J. D., Ford, E. L., Bernal-Mizrachi, E., Kusser, K. L., Luciani, D. S., Han, Z., Tran, H., Randall, T. D., Lund, F. E., & Polonsky, K. S. (2006). Suppressed Insulin Signaling and Increased Apoptosis in Cd38-Null Islets. *Diabetes*, *55*(10), 2737–2746. https://doi.org/10.2337/db05-1455

Johnson, J. D., Kuang, S., Misler, S., & Polonsky, K. S. (2004). Ryanodine receptors in human pancreatic β cells: localization and effects on insulin secretion. *The FASEB Journal*, *18*(7), 878–880. https://doi.org/10.1096/fj.03-1280fje

Johny, M. B., Yang, P. S., Bazzazi, H., & Yue, D. T. (2013). Dynamic switching of calmodulin interactions underlies Ca2+ regulation of CaV1.3 channels. *Nature Communications*, *4*(1). https://doi.org/10.1038/ncomms2727

Jones, S. W. (1998). Overview of voltage-dependent calcium channels. *Journal of Bioenergetics and Biomembranes*, *30*(4), 299–312. https://doi.org/10.1023/a:1021977304001

Josephson, I., & Sperelakis, N. (1990). Fast activation of cardiac Ca++ channel gating charge by the dihydropyridine agonist, BAY K 8644. *Biophysical Journal*, *58*(5), 1307–1311. https://doi.org/10.1016/s0006-3495(90)82471-1

Joubert, F. J. (1988). Snake venom toxins—II. The primary structures of cytotoxin homologues S3C2 and S4C8 from Aspidelaps scutatus (shield or shield-nose snake) venom. *International Journal of Biochemistry*, *20*(3), 337–345. https://doi.org/10.1016/0020-711x(88)90361-8

JOUBERT, F. J., & STRYDOM, D. J. (1978). Snake Venoms. The Amino-Acid Sequence of Trypsin Inhibitor E of Dendroaspis polylepis polylepis (Black Mamba) Venom. *European Journal of Biochemistry*, *87*(1), 191–198. https://doi.org/10.1111/j.1432-1033.1978.tb12366.x

Juntti-Berggren, L., Larsson, O., Rorsman, P., Ammala, C., Bokvist, K., Wahlander, K., Nicotera, P., Dypbukt, J., Orrenius, S., Hallberg, A., & et, A. (1993). Increased activity of L-type Ca2+ channels exposed to serum from patients with type I diabetes. *Science*, *261*(5117), 86–90. https://doi.org/10.1126/science.7686306

Juntti-Berggren, L., Refai, E., Appelskog, I., Andersson, M., Imreh, G., Dekki, N., Uhles, S., Yu, L., Griffiths, W. J., Zaitsev, S., Leibiger, I., Yang, S. N., Olivecrona, G., Jornvall, H., & Berggren, P. O. (2004). Apolipoprotein CIII promotes Ca2+-dependent cell death in type 1 diabetes. *Proceedings of the National Academy of Sciences*, *101*(27), 10090–10094. https://doi.org/10.1073/pnas.0403551101

Kahn, S. E., Hull, R. L., & Utzschneider, K. M. (2006). Mechanisms linking obesity to insulin resistance and type 2 diabetes. *Nature*, *444*(7121), 840–846. https://doi.org/10.1038/nature05482

Kamp, T. J., & Hell, J. W. (2000). Regulation of Cardiac L-Type Calcium Channels by Protein Kinase A and Protein Kinase C. *Circulation Research*, *87*(12), 1095–1102. https://doi.org/10.1161/01.res.87.12.1095

Kanai, Y., & Hediger, M. A. (2004). The glutamate/neutral amino acid transporter family SLC1: molecular, physiological and pharmacological aspects. *Pflugers Archiv European Journal of Physiology*, *447*(5), 469–479. https://doi.org/10.1007/s00424-003-1146-4

Kanatsuka, A., Makino, H., Ohsawa, H., Tokuyama, Y., Yamaguchi, T., Yoshida, S., & Adachi, M. (1989). Secretion of islet amyloid polypeptide in response to glucose. *FEBS Letters*, *259*(1), 199–201. https://doi.org/10.1016/0014-5793(89)81527-3

Kang, G., Chepurny, O. G., Malester, B., Rindler, M. J., Rehmann, H., Bos, J. L., Schwede, F., Coetzee, W. A., & Holz, G. G. (2006). cAMP sensor Epac as a determinant of ATP-sensitive potassium channel activity in human pancreatic β cells and rat INS-1 cells. *The Journal of Physiology*, *573*(3), 595–609. https://doi.org/10.1113/jphysiol.2006.107391

Kang, G., & Holz, G. G. (2003). Amplification of exocytosis by Ca 2+ -induced Ca 2+ release in INS-1 pancreatic β cells. *The Journal of Physiology*, *546*(1), 175–189. https://doi.org/10.1113/jphysiol.2002.029959

Kang, M. G., & Campbell, K. P. (2003). γ Subunit of Voltage-activated Calcium Channels. *Journal of Biological Chemistry*, *278*(24), 21315–21318. https://doi.org/10.1074/jbc.r300004200

Kang, S., Cooper, G., Dunne, S. F., Dusel, B., Luan, C. H., Surmeier, D. J., & Silverman, R. B. (2012). CaV1.3-selective L-type calcium channel antagonists as potential new therapeutics for Parkinson's disease. *Nature Communications*, *3*(1), 1146. https://doi.org/10.1038/ncomms2149

Kang, S., Cooper, G., Dunne, S. F., Luan, C. H., Surmeier, D. J., & Silverman, R. B. (2013). Structure–Activity Relationship of N,N′-Disubstituted Pyrimidinetriones as CaV1.3 Calcium Channel-Selective Antagonists for Parkinson's Disease. *Journal of Medicinal Chemistry*, *56*(11), 4786–4797. https://doi.org/10.1021/jm4005048

Kang, Y., Huang, X., Pasyk, E. A., Ji, J., Holz, G. G., Wheeler, M. B., Tsushima, R. G., & Gaisano, H. Y. (2002). Syntaxin-3 and syntaxin-1A inhibit L-type calcium channel activity, insulin biosynthesis and exocytosis in beta-cell lines. *Diabetologia*, *45*(2), 231–241. https://doi.org/10.1007/s00125-001-0718-0

Kawaai, K., Ando, H., Satoh, N., Yamada, H., Ogawa, N., Hirose, M., Mizutani, A., Bonneau, B., Seki, G., & Mikoshiba, K. (2017). Splicing variation of Long-IRBIT determines the target selectivity of IRBIT family proteins. *Proceedings of the National Academy of Sciences*, *114*(15), 3921–3926. https://doi.org/10.1073/pnas.1618514114

Keers, R., Farmer, A. E., & Aitchison, K. J. (2009). Extracting a needle from a haystack: reanalysis of whole genome data reveals a readily translatable finding. *Psychological Medicine*, *39*(8), 1231–1235. https://doi.org/10.1017/s0033291708005084

Kellett, G. L. (2011). Alternative perspective on intestinal calcium absorption: proposed complementary actions of Cav1.3 and TRPV6. *Nutrition Reviews*, *69*(7), 347–370. https://doi.org/10.1111/j.1753-4887.2011.00395.x

Khaliq, Z. M., & Bean, B. P. (2010). Pacemaking in Dopaminergic Ventral Tegmental Area Neurons: Depolarizing Drive from Background and Voltage-Dependent Sodium Conductances. *Journal of Neuroscience*, *30*(21), 7401–7413. https://doi.org/10.1523/jneurosci.0143-10.2010

Khanna, R., Yu, J., Yang, X., Moutal, A., Chefdeville, A., Gokhale, V., Shuja, Z., Chew, L. A., Bellampalli, S. S., Luo, S., François-Moutal, L., Serafini, M. J., Ha, T., Perez-Miller, S., Park, K. D., Patwardhan, A. M., Streicher, J. M., Colecraft, H. M., & Khanna, M. (2019). Targeting the CaVα–CaVβ interaction yields an antagonist of the N-type CaV2.2 channel with broad antinociceptive efficacy. *Pain*, *160*(7), 1644–1661. https://doi.org/10.1097/j.pain.0000000000001524

Kim, D. K., & Catterall, W. A. (1997). Ca2+-dependent and -independent interactions of the isoforms of the 1A subunit of brain Ca2+ channels with presynaptic SNARE proteins. *Proceedings of the National Academy of Sciences*, *94*(26), 14782–14786. https://doi.org/10.1073/pnas.94.26.14782

Kim, J., Takahashi, M., Ogura, A., Kohno, T., Kudo, Y., & Sato, K. (1994). Hydroxyl group of Tyr13 is essential for the activity of omega-conotoxin GVIA, a peptide toxin for N-type calcium channel. *Journal of Biological Chemistry*, *269*(39), 23876–23878. https://doi.org/10.1016/s0021-9258(19)51019-5

Kim, M. S., Morii, T., Sun, L. X., Imoto, K., & Mori, Y. (1993). Structural determinants of ion selectivity in brain calcium channel. *FEBS Letters*, *318*(2), 145–148. https://doi.org/10.1016/0014-5793(93)80009-j

Kim, S. J., Lim, W., & Kim, J. (1995). Contribution of L- and N-type calcium currents to exocytosis in rat adrenal medullary chromaffin cells. *Brain Research*, *675*(1–2), 289–296. https://doi.org/10.1016/0006-8993(95)00085-5

Kini, R. (1998). Proline brackets and identification of potential functional sites in proteins: Toxins to therapeutics. *Toxicon*, *36*(11), 1659–1670. https://doi.org/10.1016/s0041-0101(98)00159-7

Kini, R. M., Caldwell, R. A., Wu, Q. Y., Baumgarten, C. M., Feher, J. J., & Evans, H. J. (1998). Flanking Proline Residues Identify the L-Type Ca2+Channel Binding Site of Calciseptine and FS2†. *Biochemistry*, *37*(25), 9058–9063. https://doi.org/10.1021/bi9802723

Klugbauer, N., Lacinová, L., Marais, E., Hobom, M., & Hofmann, F. (1999). Molecular Diversity of the Calcium Channel α2δ Subunit. *The Journal of Neuroscience*, *19*(2), 684–691. https://doi.org/10.1523/jneurosci.19-02-00684.1999

Kobayashi, K., Sasaki, T., Sato, K., & Kohno, T. (2000). Three-Dimensional Solution Structure of ω-Conotoxin TxVII, an L-Type Calcium Channel Blocker,. *Biochemistry*, *39*(48), 14761–14767. https://doi.org/10.1021/bi001506x

Kokoska, R., Rodriguez, E., & Yamamoto, B. (2020). The Role of Alcohol in Hippocampal Calcium Channel (Cav1.2) expression. *Proceedings of IMPRS*, *3*. https://doi.org/10.18060/24670

Kollmar, R., Montgomery, L. G., Fak, J., Henry, L. J., & Hudspeth, A. J. (1997). Predominance of the 1D subunit in L-type voltage-gated Ca2+ channels of hair cells in the chicken's cochlea. *Proceedings of the National Academy of Sciences*, *94*(26), 14883–14888. https://doi.org/10.1073/pnas.94.26.14883

Kordasiewicz, H. B., Thompson, R. M., Clark, H. B., & Gomez, C. M. (2006). C-termini of P/Q-type Ca 2+ channel α1A subunits translocate to nuclei and promote polyglutamine-mediated toxicity. *Human Molecular Genetics*, *15*(10), 1587–1599. https://doi.org/10.1093/hmg/ddl080

Koschak, A., Reimer, D., Huber, I., Grabner, M., Glossmann, H., Engel, J., & Striessnig, J. (2001). α1D (Cav1.3) Subunits Can Form L-type Ca2+ Channels Activating at Negative Voltages. *Journal of Biological Chemistry*, *276*(25), 22100–22106. https://doi.org/10.1074/jbc.m101469200

Koschak, A., Reimer, D., Walter, D., Hoda, J. C., Heinzle, T., Grabner, M., & Striessnig, J. (2003). Cav1.4α1 Subunits Can Form Slowly Inactivating Dihydropyridine-Sensitive L-Type Ca2+Channels Lacking Ca2+-Dependent Inactivation. *The Journal of Neuroscience*, *23*(14), 6041–6049. https://doi.org/10.1523/jneurosci.23-14-06041.2003

Krey, J. F., Paşca, S. P., Shcheglovitov, A., Yazawa, M., Schwemberger, R., Rasmusson, R., & Dolmetsch, R. E. (2013). Timothy syndrome is associated with activity-dependent dendritic retraction in rodent and human neurons. *Nature Neuroscience*, *16*(2), 201–209. https://doi.org/10.1038/nn.3307

Kuang, Q., Purhonen, P., & Hebert, H. (2015). Structure of potassium channels. *Cellular and Molecular Life Sciences*, *72*(19), 3677–3693. https://doi.org/10.1007/s00018-015-1948-5

Kubodera, T., Yokota, T., Ohwada, K., Ishikawa, K., Miura, H., Matsuoka, T., & Mizusawa, H. (2003). Proteolytic cleavage and cellular toxicity of the human α1A calcium channel in spinocerebellar ataxia type 6. *Neuroscience Letters*, *341*(1), 74–78. https://doi.org/10.1016/s0304-3940(03)00156-3

Kunkel, T. A. (1985). Rapid and efficient site-specific mutagenesis without phenotypic selection. *Proceedings of the National Academy of Sciences*, *82*(2), 488–492. https://doi.org/10.1073/pnas.82.2.488

Kushmerick, M. J., Moerland, T. S., & Wiseman, R. W. (1992). Mammalian skeletal muscle fibers distinguished by contents of phosphocreatine, ATP, and Pi. *Proceedings of the National Academy of Sciences*, *89*(16), 7521–7525. https://doi.org/10.1073/pnas.89.16.7521

Lacinová, L. (2005, June 24). Voltage-dependent calcium channels. *Gen Physiol Biophys*, 1–78. https://pubmed.ncbi.nlm.nih.gov/16096350/

Lao, Q. Z., Kobrinsky, E., Liu, Z., & Soldatov, N. M. (2010). Oligomerization of Cavβ subunits is an essential correlate of Ca2+channel activity. *The FASEB Journal*, *24*(12), 5013–5023. https://doi.org/10.1096/fj.10-165381

Larsson, O. (1997). Inhibition of Phosphatases and Increased Ca2+ Channel Activity by Inositol Hexakisphosphate. *Science*, *278*(5337), 471–474. https://doi.org/10.1126/science.278.5337.471

Leach, R. N., Brickley, K., & Norman, R. I. (1996). Cyclic AMP-vepenvent protein kinase phosphorylates residues in the C-terminal domain of the cardiac L-type calcium channel α1 subunit. *Biochimica et Biophysica Acta (BBA) - Biomembranes*, *1281*(2), 205–212. https://doi.org/10.1016/0005-2736(96)00013-2

Lee, C. Y., Tsai, M. C., Tsaur, M. L., Lin, W. W., Carlsson, F. H., & Joubert, F. J. (1985, May). Pharmacological study on angusticeps-type toxins from mamba snake venoms. *Journal of Pharmacology and Experimental Therapeutics*, *233*(2), 491–498. https://jpet.aspetjournals.org/content/233/2/491.long

Lee, K., Kim, J., Köhler, M., Yu, J., Shi, Y., Yang, S. N., Ryu, S. H., & Berggren, P. O. (2018). Blocking Ca2+ Channel β3 Subunit Reverses Diabetes. *Cell Reports*, *24*(4), 922–934. https://doi.org/10.1016/j.celrep.2018.06.086

Lee, K. S., & Tsien, R. W. (1983). Mechanism of calcium channel blockade by verapamil, D600, diltiazem and nitrendipine in single dialysed heart cells. *Nature*, *302*(5911), 790–794. https://doi.org/10.1038/302790a0

Lees, A. J., Hardy, J., & Revesz, T. (2009). Parkinson's disease. *The Lancet*, *373*(9680), 2055–2066. https://doi.org/10.1016/s0140-6736(09)60492-x

Lehnart, S. E., Mongillo, M., Bellinger, A., Lindegger, N., Chen, B. X., Hsueh, W., Reiken, S., Wronska, A., Drew, L. J., Ward, C. W., Lederer, W., Kass, R. S., Morley, G., & Marks, A. R. (2008). Leaky Ca2+ release channel/ryanodine receptor 2 causes seizures and sudden cardiac death in mice. *Journal of Clinical Investigation*. Published. https://doi.org/10.1172/jci35346

Lehnart, S. E., Wehrens, X. H., Laitinen, P. J., Reiken, S. R., Deng, S. X., Cheng, Z., Landry, D. W., Kontula, K., Swan, H., & Marks, A. R. (2004). Sudden Death in Familial Polymorphic Ventricular Tachycardia Associated With Calcium Release Channel (Ryanodine Receptor) Leak. *Circulation*, *109*(25), 3208–3214. https://doi.org/10.1161/01.cir.0000132472.98675.ec

Lenaeus, M. J., Gamal El-Din, T. M., Ing, C., Ramanadane, K., Pomès, R., Zheng, N., & Catterall, W. A. (2017). Structures of closed and open states of a voltage-gated sodium channel. *Proceedings of the National Academy of Sciences*, *114*(15), E3051–E3060. https://doi.org/10.1073/pnas.1700761114

Letts, V. A., Felix, R., Biddlecome, G. H., Arikkath, J., Mahaffey, C. L., Valenzuela, A., Bartlett, F. S., Mori, Y., Campbell, K. P., & Frankel, W. N. (1998). The mouse stargazer gene encodes a neuronal Ca2+-channel γ subunit. *Nature Genetics*, *19*(4), 340–347. https://doi.org/10.1038/1228

Leuranguer, V., Dirksen, R. T., & Beam, K. G. (2003). Potentiated L-type Ca2+ Channels Rectify. *Journal of General Physiology*, *121*(6), 541–550. https://doi.org/10.1085/jgp.200308833

Lew, M. J., Flinn, J. P., Pallaghy, P. K., Murphy, R., Whorlow, S. L., Wright, C. E., Norton, R. S., & Angus, J. A. (1997). Structure-Function Relationships of ω-Conotoxin GVIA. *Journal of Biological Chemistry*, *272*(18), 12014–12023. https://doi.org/10.1074/jbc.272.18.12014

Lieb, A., Scharinger, A., Sartori, S., Koschak, A., Sinnegger-Brauns, M. J., & Striessnig, J. (2012). Structural Determinants of CaV1.3 L-Type Calcium Channel Gating. *Biophysical Journal*, *102*(3), 125a. https://doi.org/10.1016/j.bpj.2011.11.699

Lin, M., Aladejebi, O., & Hockerman, G. H. (2011). Distinct properties of amlodipine and nicardipine block of the voltage-dependent Ca2+ channels Cav1.2 and Cav2.1 and the mutant channels Cav1.2/Dihydropyridine insensitive and Cav2.1/Dihydropyridine sensitive. *European Journal of Pharmacology*, *670*(1), 105–113. https://doi.org/10.1016/j.ejphar.2011.08.005

Lingford-Hughes, A., Welch, S., Peters, L., & Nutt, D. (2012). BAP updated guidelines: evidence-based guidelines for the pharmacological management of substance abuse, harmful use, addiction and comorbidity: recommendations from BAP. *Journal of Psychopharmacology*, *26*(7), 899–952. https://doi.org/10.1177/0269881112444324

Liou, J., Kim, M. L., Do Heo, W., Jones, J. T., Myers, J. W., Ferrell, J. E., & Meyer, T. (2005). STIM Is a Ca2+ Sensor Essential for Ca2+-Store-Depletion-Triggered Ca2+ Influx. *Current Biology*, *15*(13), 1235–1241. https://doi.org/10.1016/j.cub.2005.05.055

Lipscombe, D., Helton, T. D., & Xu, W. (2004). L-Type Calcium Channels: The Low Down. *Journal of Neurophysiology*, *92*(5), 2633–2641. https://doi.org/10.1152/jn.00486.2004

Lipscombe, D., Pan, J. Q., & Gray, A. C. (2002). Functional Diversity in Neuronal Voltage-Gated Calcium Channels by Alternative Splicing of Cavα1. *Molecular Neurobiology*, *26*(1), 021–044. https://doi.org/10.1385/mn:26:1:021

Liss, B., & Striessnig, J. (2019). The Potential of L-Type Calcium Channels as a Drug Target for Neuroprotective Therapy in Parkinson's Disease. *Annual Review of Pharmacology and Toxicology*, *59*(1), 263–289. https://doi.org/10.1146/annurev-pharmtox-010818-021214

Liu, G., Dilmac, N., Hilliard, N., & Hockerman, G. H. (2003). Cav1.3 Is Preferentially Coupled to Glucose-Stimulated Insulin Secretion in the Pancreatic β-Cell Line INS-1. *Journal of Pharmacology and Experimental Therapeutics*, *305*(1), 271–278. https://doi.org/10.1124/jpet.102.046334

Liu, G., Hilliard, N., & Hockerman, G. H. (2004). Cav1.3 Is Preferentially Coupled to Glucose-Induced [Ca2+]i Oscillations in the Pancreatic β Cell Line INS-1. *Molecular Pharmacology*, *65*(5), 1269–1277. https://doi.org/10.1124/mol.65.5.1269

Liu, G., Jacobo, S. M. P., Hilliard, N., & Hockerman, G. H. (2006). Differential Modulation of Cav1.2 and Cav1.3-Mediated Glucose-Stimulated Insulin Secretion by cAMP in INS-1 Cells: Distinct Roles for Exchange Protein Directly Activated by cAMP 2 (Epac2) and Protein Kinase A. *Journal of Pharmacology and Experimental Therapeutics*, *318*(1), 152–160. https://doi.org/10.1124/jpet.105.097477

Liu, L., Gonzalez, P. K., Barrett, C. F., & Rittenhouse, A. R. (2003). The calcium channel ligand FPL 64176 enhances L-type but inhibits N-type neuronal calcium currents. *Neuropharmacology*, *45*(2), 281–292. https://doi.org/10.1016/s0028-3908(03)00153-9

Liu, X., Betzenhauser, M., Reiken, S., Meli, A., Xie, W., Chen, B. X., Arancio, O., & Marks, A. (2012). Role of Leaky Neuronal Ryanodine Receptors in Stress- Induced Cognitive Dysfunction. *Cell*, *150*(5), 1055–1067. https://doi.org/10.1016/j.cell.2012.06.052

Liu, X., Yang, P. S., Yang, W., & Yue, D. T. (2010). Enzyme-inhibitor-like tuning of Ca2+ channel connectivity with calmodulin. *Nature*, *463*(7283), 968–972. https://doi.org/10.1038/nature08766

Liu, Y., Harding, M., Pittman, A., Dore, J., Striessnig, J., Rajadhyaksha, A., & Chen, X. (2014). Cav1.2 and Cav1.3 L-type calcium channels regulate dopaminergic firing activity in the mouse ventral tegmental area. *Journal of Neurophysiology*, *112*(5), 1119–1130. https://doi.org/10.1152/jn.00757.2013

Livneh, A., Cohen, R., & Atlas, D. (2006). A novel molecular inactivation determinant of voltage-gated CaV1.2 L-type Ca2+ channel. *Neuroscience*, *139*(4), 1275–1287. https://doi.org/10.1016/j.neuroscience.2006.01.028

Llinas, R., Sugimori, M., Lin, J. W., & Cherksey, B. (1989). Blocking and isolation of a calcium channel from neurons in mammals and cephalopods utilizing a toxin fraction (FTX) from funnel-web spider poison. *Proceedings of the National Academy of Sciences*, *86*(5), 1689–1693. https://doi.org/10.1073/pnas.86.5.1689

Lombardi, A., Gambardella, J., Du, X. L., Sorriento, D., Mauro, M., Iaccarino, G., Trimarco, B., & Santulli, G. (2017). Sirolimus induces depletion of intracellular calcium stores and mitochondrial dysfunction in pancreatic beta cells. *Scientific Reports*, *7*(1). https://doi.org/10.1038/s41598-017-15283-y

Lombardi, A., Trimarco, B., Iaccarino, G., & Santulli, G. (2017). Impaired mitochondrial calcium uptake caused by tacrolimus underlies beta-cell failure. *Cell Communication and Signaling*, *15*(1). https://doi.org/10.1186/s12964-017-0203-0

Longo, P. A., Kavran, J. M., Kim, M. S., & Leahy, D. J. (2013). Transient Mammalian Cell Transfection with Polyethylenimine (PEI). *Methods in Enzymology*, 227–240. https://doi.org/10.1016/b978-0-12-418687-3.00018-5

Lopez, J. J., Jardin, I., Sanchez-Collado, J., Salido, G. M., Smani, T., & Rosado, J. A. (2020). TRPC Channels in the SOCE Scenario. *Cells*, *9*(1), 126. https://doi.org/10.3390/cells9010126

Lu, M., Hebert, S. C., & Giebisch, G. (2002). Hydrolyzable ATP and PIP2 Modulate the Small-conductance K+ Channel in Apical Membranes of Rat Cortical-Collecting Duct (CCD). *Journal of General Physiology*, *120*(5), 603–615. https://doi.org/10.1085/jgp.20028677

Luciani, D. S., Gwiazda, K. S., Yang, T. L. B., Kalynyak, T. B., Bychkivska, Y., Frey, M. H., Jeffrey, K. D., Sampaio, A. V., Underhill, T. M., & Johnson, J. D. (2008). Roles of IP3R and RyR Ca2+ Channels in Endoplasmic Reticulum Stress and -Cell Death. *Diabetes*, *58*(2), 422–432. https://doi.org/10.2337/db07-1762

Lukyanetz, E. A., & Neher, E. (1999). Different types of calcium channels and secretion from bovine chromaffin cells. *European Journal of Neuroscience*, *11*(8), 2865–2873. https://doi.org/10.1046/j.1460-9568.1999.00707.x

Lund-Johansen, P., & Omvik, P. (1987). Central Hemodynamic Changes of Calcium Antagonists at Rest and During Exercise in Essential Hypertension. *Journal of Cardiovascular Pharmacology*, *10*, S139–S148. https://doi.org/10.1097/00005344-198710001-00026

Maekawa, H., & Inagi, R. (2017). Stress Signal Network between Hypoxia and ER Stress in Chronic Kidney Disease. *Frontiers in Physiology*, *8*. https://doi.org/10.3389/fphys.2017.00074

Magidovich, E., & Yifrach, O. (2004). Conserved Gating Hinge in Ligand- and Voltage-Dependent K+Channels†. *Biochemistry*, *43*(42), 13242–13247. https://doi.org/10.1021/bi048377v

Mahapatra, S., Calorio, C., Vandael, D., Marcantoni, A., Carabelli, V., & Carbone, E. (2012). Calcium channel types contributing to chromaffin cell excitability, exocytosis and endocytosis. *Cell Calcium*, *51*(3–4), 321–330. https://doi.org/10.1016/j.ceca.2012.01.005

Mahapatra, S., Marcantoni, A., Zuccotti, A., Carabelli, V., & Carbone, E. (2012). Equal sensitivity of Cav1.2 and Cav1.3 channels to the opposing modulations of PKA and PKG in mouse chromaffin cells. *The Journal of Physiology*, *590*(20), 5053–5073. https://doi.org/10.1113/jphysiol.2012.236729

Malhi, H. (2014). MicroRNAs in ER Stress: Divergent Roles in Cell Fate Decisions. *Current Pathobiology Reports*, *2*(3), 117–122. https://doi.org/10.1007/s40139-014-0046-y

Mangoni, M. E., Couette, B., Bourinet, E., Platzer, J., Reimer, D., Striessnig, J., & Nargeot, J. (2003a). Functional role of L-type Cav1.3 Ca2+ channels in cardiac pacemaker activity. *Proceedings of the National Academy of Sciences*, *100*(9), 5543–5548. https://doi.org/10.1073/pnas.0935295100

Mangoni, M. E., Couette, B., Bourinet, E., Platzer, J., Reimer, D., Striessnig, J., & Nargeot, J. (2003b). Functional role of L-type Cav1.3 Ca2+ channels in cardiac pacemaker activity. *Proceedings of the National Academy of Sciences*, *100*(9), 5543–5548. https://doi.org/10.1073/pnas.0935295100

Mao, Z. (1999). Neuronal Activity-Dependent Cell Survival Mediated by Transcription Factor MEF2. *Science*, *286*(5440), 785–790. https://doi.org/10.1126/science.286.5440.785

MARCANTONI, A., BALDELLI, P., HERNANDEZGUIJO, J., COMUNANZA, V., CARABELLI, V., & CARBONE, E. (2007). L-type calcium channels in adrenal chromaffin cells: Role in pace-making and secretion. *Cell Calcium*, *42*(4–5), 397–408. https://doi.org/10.1016/j.ceca.2007.04.015

Marcantoni, A., Calorio, C., Hidisoglu, E., Chiantia, G., & Carbone, E. (2020). Cav1.2 channelopathies causing autism: new hallmarks on Timothy syndrome. *Pflügers Archiv - European Journal of Physiology*, *472*(7), 775–789. https://doi.org/10.1007/s00424-020-02430-0

Marcantoni, A., Carabelli, V., Vandael, D. H., Comunanza, V., & Carbone, E. (2008). PDE type-4 inhibition increases L-type Ca2+ currents, action potential firing, and quantal size of exocytosis in mouse chromaffin cells. *Pflügers Archiv - European Journal of Physiology*, *457*(5), 1093–1110. https://doi.org/10.1007/s00424-008-0584-4

Marcantoni, A., Vandael, D. H. F., Mahapatra, S., Carabelli, V., Sinnegger-Brauns, M. J., Striessnig, J., & Carbone, E. (2010). Loss of Cav1.3 Channels Reveals the Critical Role of L-Type and BK Channel Coupling in Pacemaking Mouse Adrenal Chromaffin Cells. *Journal of Neuroscience*, *30*(2), 491–504. https://doi.org/10.1523/jneurosci.4961-09.2010

Margolskee, R. F., McHendry-Rinde, B., & Horn, R. (1993). Panning transfected cells for electrophysiological studies. *Biotechniques*, *15*, 906–911. http://europepmc.org/article/med/7505602

Marks, A. R., Tempst, P., Hwang, K. S., Taubman, M. B., Inui, M., Chadwick, C., Fleischer, S., & Nadal-Ginard, B. (1989). Molecular cloning and characterization of the ryanodine receptor/junctional channel complex cDNA from skeletal muscle sarcoplasmic reticulum. *Proceedings of the National Academy of Sciences*, *86*(22), 8683–8687. https://doi.org/10.1073/pnas.86.22.8683

Markworth, E., Schwanstecher, C., & Schwanstecher, M. (2000). ATP4- mediates closure of pancreatic beta-cell ATP-sensitive potassium channels by interaction with 1 of 4 identical sites. *Diabetes*, *49*(9), 1413–1418. https://doi.org/10.2337/diabetes.49.9.1413

Marras, C., Gruneir, A., Rochon, P., Wang, X., Anderson, G., Brotchie, J., Bell, C. M., Fox, S., & Austin, P. C. (2012). Dihydropyridine calcium channel blockers and the progression of parkinsonism. *Annals of Neurology*, *71*(3), 362–369. https://doi.org/10.1002/ana.22616

Marschallinger, J., Sah, A., Schmuckermair, C., Unger, M., Rotheneichner, P., Kharitonova, M., Waclawiczek, A., Gerner, P., Jaksch-Bogensperger, H., Berger, S., Striessnig, J., Singewald, N., Couillard-Despres, S., & Aigner, L. (2015). The L-type calcium channel Cav1.3 is required for proper hippocampal neurogenesis and cognitive functions. *Cell Calcium*, *58*(6), 606–616. https://doi.org/10.1016/j.ceca.2015.09.007

Marshall, J., Dolan, B. M., Garcia, E. P., Sathe, S., Tang, X., Mao, Z., & Blair, L. A. (2003). Calcium Channel and NMDA Receptor Activities Differentially Regulate Nuclear C/EBPβ Levels to Control Neuronal Survival. *Neuron*, *39*(4), 625–639. https://doi.org/10.1016/s0896-6273(03)00496-3

Marshall, M. R., Clark, J. P., Westenbroek, R., Yu, F. H., Scheuer, T., & Catterall, W. A. (2011). Functional Roles of a C-terminal Signaling Complex of CaV1 Channels and A-kinase Anchoring Protein 15 in Brain Neurons. *Journal of Biological Chemistry*, *286*(14), 12627–12639. https://doi.org/10.1074/jbc.m110.175257

Martínez-Rivera, A., Hao, J., Tropea, T. F., Giordano, T. P., Kosovsky, M., Rice, R. C., Lee, A., Huganir, R. L., Striessnig, J., Addy, N. A., Han, S., & Rajadhyaksha, A. M. (2017). Enhancing VTA Cav1.3 L-type Ca2+ channel activity promotes cocaine and mood-related behaviors via overlapping AMPA receptor mechanisms in the nucleus accumbens. *Molecular Psychiatry*, *22*(12), 1735–1745. https://doi.org/10.1038/mp.2017.9

Masgrau, R., Churchill, G. C., Morgan, A. J., Ashcroft, S. J., & Galione, A. (2003). NAADP. *Current Biology*, *13*(3), 247–251. https://doi.org/10.1016/s0960-9822(03)00041-1

Mastrolia, V., Flucher, S. M., Obermair, G. J., Drach, M., Hofer, H., Renström, E., Schwartz, A., Striessnig, J., Flucher, B. E., & Tuluc, P. (2017a). Loss of α2δ-1 Calcium Channel Subunit Function Increases the Susceptibility for Diabetes. *Diabetes*, *66*(4), 897–907. https://doi.org/10.2337/db16-0336

Mastrolia, V., Flucher, S. M., Obermair, G. J., Drach, M., Hofer, H., Renström, E., Schwartz, A., Striessnig, J., Flucher, B. E., & Tuluc, P. (2017b). Loss of α2δ-1 Calcium Channel Subunit Function Increases the Susceptibility for Diabetes. *Diabetes*, *66*(4), 897–907. https://doi.org/10.2337/db16-0336

Matsuyama, Z., Wakamori, M., Mori, Y., Kawakami, H., Nakamura, S., & Imoto, K. (1999). Direct Alteration of the P/Q-Type Ca2+Channel Property by Polyglutamine Expansion in Spinocerebellar Ataxia 6. *The Journal of Neuroscience*, *19*(12), RC14. https://doi.org/10.1523/jneurosci.19-12-j0004.1999

McCulloch, L. J., van de Bunt, M., Braun, M., Frayn, K. N., Clark, A., & Gloyn, A. L. (2011). GLUT2 (SLC2A2) is not the principal glucose transporter in human pancreatic beta cells: Implications for understanding genetic association signals at this locus. *Molecular Genetics and Metabolism*, *104*(4), 648–653. https://doi.org/10.1016/j.ymgme.2011.08.026

McCusker, P., & Chan, J. D. (2019). Anti-schistosomal action of the calcium channel agonist FPL-64176. *International Journal for Parasitology: Drugs and Drug Resistance*, *11*, 30–38. https://doi.org/10.1016/j.ijpddr.2019.08.006

McDonough, S. I., Mori, Y., & Bean, B. P. (2005). FPL 64176 Modification of CaV1.2 L-Type Calcium Channels: Dissociation of Effects on Ionic Current and Gating Current. *Biophysical Journal*, *88*(1), 211–223. https://doi.org/10.1529/biophysj.104.051714

McHugh, D., Sharp, E. M., Scheuer, T., & Catterall, W. A. (2000). Inhibition of cardiac L-type calcium channels by protein kinase C phosphorylation of two sites in the N-terminal domain. *Proceedings of the National Academy of Sciences*, *97*(22), 12334–12338. https://doi.org/10.1073/pnas.210384297

McKechnie, K., Killingback, P. G., Naya, I., O'Conner, S. E., Smith, G. W., Wattam, D. G., Wells, E., Whitehead, Y. M., & Williams, G. E. (1994). Calcium channel activator properties in a non-dihydropyridine - FPL 64176. *Br J Pharmacol*, *98*, 673. https://bpspubs.onlinelibrary.wiley.com/journal/14765381

McKerr, N., Breen, C., Srivastava, K., Mills, I. G., & McCloskey, K. D. (2018). Abstract 2330: CaV1.3 calcium channel expression in prostate cancer cells during androgen-deprivation conditions. *Molecular and Cellular Biology / Genetics*, 2330. https://doi.org/10.1158/1538-7445.am2018-2330

McLaughlin, S., Wang, J., Gambhir, A., & Murray, D. (2002). PIP2and Proteins: Interactions, Organization, and Information Flow. *Annual Review of Biophysics and Biomolecular Structure*, *31*(1), 151–175. https://doi.org/10.1146/annurev.biophys.31.082901.134259

McRory, J. E. (2004). The CACNA1F Gene Encodes an L-Type Calcium Channel with Unique Biophysical Properties and Tissue Distribution. *Journal of Neuroscience*, *24*(7), 1707–1718. https://doi.org/10.1523/jneurosci.4846-03.2004

Mehlem, A., Palombo, I., Wang, X., Hagberg, C. E., Eriksson, U., & Falkevall, A. (2016). PGC-1α Coordinates Mitochondrial Respiratory Capacity and Muscular Fatty Acid Uptake via Regulation of VEGF-B. *Diabetes*, *65*(4), 861–873. https://doi.org/10.2337/db15-1231

Meir, A., Bell, D. C., Stephens, G. J., Page, K. M., & Dolphin, A. C. (2000). Calcium Channel β Subunit Promotes Voltage-Dependent Modulation of α1B by Gβγ. *Biophysical Journal*, *79*(2), 731–746. https://doi.org/10.1016/s0006-3495(00)76331-4

Mikala, G., Bahinski, A., Yatani, A., Tang, S., & Schwartz, A. (1993). Differential contribution by conserved glutamate residues to an ion-selectivity site in the L-type Ca2+channel pore. *FEBS Letters*, *335*(2), 265–269. https://doi.org/10.1016/0014-5793(93)80743-e

Mitchell, K. J., Lai, F. A., & Rutter, G. A. (2003). Ryanodine Receptor Type I and Nicotinic Acid Adenine Dinucleotide Phosphate Receptors Mediate Ca2+ Release from Insulin-containing Vesicles in Living Pancreatic β-Cells (MIN6). *Journal of Biological Chemistry*, *278*(13), 11057–11064. https://doi.org/10.1074/jbc.m210257200

Mitterdorfer, J., Wang, Z., Sinnegger, M. J., Hering, S., Jörg, S., Grabner, M., & Glossmann, H. (1996). Two Amino Acid Residues in the IIIS5 Segment of L-Type Calcium Channels Differentially Contribute to 1,4-Dihydropyridine Sensitivity. *Journal of Biological Chemistry*, *271*(48), 30330–30335. https://doi.org/10.1074/jbc.271.48.30330

Miyake, Y. (1986). Congenital Stationary Night Blindness With Negative Electroretinogram. *Archives of Ophthalmology*, *104*(7), 1013. https://doi.org/10.1001/archopht.1986.01050190071042

Molleman, A. (2002). *Patch Clamping: An Introductory Guide to Patch Clamp Electrophysiology* (1st ed.). Wiley.

Moosmang, S. (2005). Role of Hippocampal Cav1.2 Ca2+ Channels in NMDA Receptor-Independent Synaptic Plasticity and Spatial Memory. *Journal of Neuroscience*, *25*(43), 9883–9892. https://doi.org/10.1523/jneurosci.1531-05.2005

Morgan, J. I., & Curran, T. (1986). Role of ion flux in the control of c-fos expression. *Nature*, *322*(6079), 552–555. https://doi.org/10.1038/322552a0

Morgenstern, T. J., Park, J., Fan, Q. R., & Colecraft, H. M. (2019). A potent voltage-gated calcium channel inhibitor engineered from a nanobody targeted to auxiliary CaVβ subunits. *ELife*, *8*. https://doi.org/10.7554/elife.49253

Mosa, F. E., C, S., Feng, T., & Barakat, K. (2021). Effects of selective calcium channel blockers on ions' permeation through the human Cav1.2 ion channel: A computational study. *Journal of Molecular Graphics and Modelling*, *102*, 107776. https://doi.org/10.1016/j.jmgm.2020.107776

Moskvina, V., Craddock, N., Holmans, P., Nikolov, I., Pahwa, J. S., Green, E., Owen, M. J., & O'Donovan, M. C. (2008). Gene-wide analyses of genome-wide association data sets: evidence for multiple common risk alleles for schizophrenia and bipolar disorder and for overlap in genetic risk. *Molecular Psychiatry*, *14*(3), 252–260. https://doi.org/10.1038/mp.2008.133

Murphy, K. M., Gould, R. J., Largent, B. L., & Snyder, S. H. (1983). A unitary mechanism of calcium antagonist drug action. *Proceedings of the National Academy of Sciences*, *80*(3), 860–864. https://doi.org/10.1073/pnas.80.3.860

Murphy, T. H., Worley, P. F., & Baraban, J. M. (1991). L-type voltage-sensitive calcium channels mediate synaptic activation of immediate early genes. *Neuron*, *7*(4), 625–635. https://doi.org/10.1016/0896-6273(91)90375-a

Nadasdi, L., Yamashiro, D., Chung, D., Tarczy-Hornoch, K., Adriaenssens, P., & Ramachandran, J. (1995). Structure-Activity Analysis of a Conus Peptide Blocker of N-Type Neuronal Calcium Channels. *Biochemistry*, *34*(25), 8076–8081. https://doi.org/10.1021/bi00025a013

Nagayama, T., Matsumoto, T., Kuwakubo, F., Fukushima, Y., Yoshida, M., Suzuki-Kusaba, M., Hisa, H., Kimura, T., & Satoh, S. (1999). Role of calcium channels in catecholamine secretion in the rat adrenal gland. *The Journal of Physiology*, *520*(2), 503–512. https://doi.org/10.1111/j.1469-7793.1999.00503.x

Nakai, J., Imagawa, T., Hakamata, Y., Shigekawa, M., Takeshima, H., & Numa, S. (1990). Primary structure and functional expression from cDN A of the cardiac ryanodine receptor/calcium release channel. *FEBS Letters*, *271*(1–2), 169–177. https://doi.org/10.1016/0014-5793(90)80399-4

Nakashima, Y., Nishimura, S., Maeda, A., Barsoumian, E. L., Hakamata, Y., Nakai, J., Allen, P. D., Imoto, K., & Kita, T. (1997). Molecular cloning and characterization of a human brain ryanodine receptor1. *FEBS Letters*, *417*(1), 157–162. https://doi.org/10.1016/s0014-5793(97)01275-1

Namkung, Y., Skrypnyk, N., Jeong, M. J., Lee, T., Lee, M. S., Kim, H. L., Chin, H., Suh, P. G., Kim, S. S., & Shin, H. S. (2001). Requirement for the L-type Ca2+ channel α1D subunit in postnatal pancreatic β cell generation. *Journal of Clinical Investigation*, *108*(7), 1015–1022. https://doi.org/10.1172/jci200113310

Napolitano, C., & Antzelevitch, C. (2011). Phenotypical Manifestations of Mutations in the Genes Encoding Subunits of the Cardiac Voltage–Dependent L-Type Calcium Channel. *Circulation Research*, *108*(5), 607–618. https://doi.org/10.1161/circresaha.110.224279

Natarajan, R., Putta, S., & Kato, M. (2012). MicroRNAs and Diabetic Complications. *Journal of Cardiovascular Translational Research*, *5*(4), 413–422. https://doi.org/10.1007/s12265-012-9368-5

Nawrath, H., & Wegener, J. W. (1996). Kinetics and state-dependent effects of verapamil on cardiac L-type calcium channels. *Naunyn-Schmiedeberg's Archives of Pharmacology*, *355*(1), 79–86. https://doi.org/10.1007/pl00004921

Neely, A., Garcia-Olivares, J., Voswinkel, S., Horstkott, H., & Hidalgo, P. (2004). Folding of Active Calcium Channel β1b -Subunit by Size-exclusion Chromatography and Its Role on Channel Function. *Journal of Biological Chemistry*, *279*(21), 21689–21694. https://doi.org/10.1074/jbc.m312675200

Nelson, B. R., Wu, F., Liu, Y., Anderson, D. M., McAnally, J., Lin, W., Cannon, S. C., Bassel-Duby, R., & Olson, E. N. (2013). Skeletal muscle-specific T-tubule protein STAC3 mediates voltage-induced Ca2+ release and contractility. *Proceedings of the National Academy of Sciences*, *110*(29), 11881–11886. https://doi.org/10.1073/pnas.1310571110

Nenquin, M., Szollosi, A., Aguilar-Bryan, L., Bryan, J., & Henquin, J. C. (2004). Both Triggering and Amplifying Pathways Contribute to Fuel-induced Insulin Secretion in the Absence of Sulfonylurea Receptor-1 in Pancreatic β-Cells. *Journal of Biological Chemistry*, *279*(31), 32316–32324. https://doi.org/10.1074/jbc.m402076200

Nesher, R., & Cerasi, E. (2002). Modeling Phasic Insulin Release: Immediate and Time-Dependent Effects of Glucose. *Diabetes*, *51*(Supplement 1), S53–S59. https://doi.org/10.2337/diabetes.51.2007.s53

Nestler, E. J. (2005a). Is there a common molecular pathway for addiction? *Nature Neuroscience*, *8*(11), 1445–1449. https://doi.org/10.1038/nn1578

Nestler, E. J. (2005b). Is there a common molecular pathway for addiction? *Nature Neuroscience*, *8*(11), 1445–1449. https://doi.org/10.1038/nn1578

Newcomb, R., Szoke, B., Palma, A., Wang, G., Chen, X. H., Hopkins, W., Cong, R., Miller, J., Urge, L., Tarczy-Hornoch, K., Loo, J. A., Dooley, D. J., Nadasdi, L., Tsien, R. W., Lemos, J., & Miljanich, G. (1998). Selective Peptide Antagonist of the Class E Calcium Channel from the Venom of the Tarantula Hysterocrates gigas. *Biochemistry*, *37*(44), 15353–15362. https://doi.org/10.1021/bi981255g

Ng, B., Kang, Y., Elias, C. L., He, Y., Xie, H., Hansen, J. B., Wahl, P., & Gaisano, H. Y. (2007). The Actions of a Novel Potent Islet β-Cell–Specific ATP-Sensitive K+Channel Opener Can Be Modulated by Syntaxin-1A Acting on Sulfonylurea Receptor 1. *Diabetes*, *56*(8), 2124–2134. https://doi.org/10.2337/db07-0030

Nichols, C. G. (2006). KATP channels as molecular sensors of cellular metabolism. *Nature*, *440*(7083), 470–476. https://doi.org/10.1038/nature04711

Nilsson, T., Arkhammar, P., Rorsman, P., & Berggren, P. O. (1989). Suppression of Insulin Release by Galanin and Somatostatin Is Meditated by a G-protein. *Journal of Biological Chemistry*, *264*(2), 973–980. https://doi.org/10.1016/s0021-9258(19)85039-1

Nishio, H., Katoh, E., Yamazaki, T., Inui, T., Nishiuchi, Y., & Kimura, T. (1999). Structure-Activity Relationships of Calcicludine and Dendrotoxin-I, Homologous Peptides Acting on Different Targets, Calcium and Potassium Channels. *Biochemical and Biophysical Research Communications*, *262*(2), 319–321. https://doi.org/10.1006/bbrc.1999.1198

Nitert, M. D., Nagorny, C. L. F., Wendt, A., Eliasson, L., & Mulder, H. (2008). CaV1.2 rather than CaV1.3 is coupled to glucose-stimulated insulin secretion in INS-1 832/13 cells. *Journal of Molecular Endocrinology*, *41*(1), 1–11. https://doi.org/10.1677/jme-07-0133

Norris, C. M., Halpain, S., & Foster, T. C. (1998). Reversal of Age-Related Alterations in Synaptic Plasticity by Blockade of L-Type Ca2+Channels. *The Journal of Neuroscience*, *18*(9), 3171–3179. https://doi.org/10.1523/jneurosci.18-09-03171.1998

Nutt, D. J., Lingford-Hughes, A., Erritzoe, D., & Stokes, P. R. A. (2015). The dopamine theory of addiction: 40 years of highs and lows. *Nature Reviews Neuroscience*, *16*(5), 305–312. https://doi.org/10.1038/nrn3939

Olofsson, C. S., Göpel, S. O., Barg, S., Galvanovskis, J., Ma, X., Salehi, A., Rorsman, P., & Eliasson, L. (2002). Fast insulin secretion reflects exocytosis of docked granules in mouse pancreatic B-cells. *Pflügers Archiv*, *444*(1–2), 43–51. https://doi.org/10.1007/s00424-002-0781-5

Olson, P. A. (2005). G-Protein-Coupled Receptor Modulation of Striatal CaV1.3 L-Type Ca2+ Channels Is Dependent on a Shank-Binding Domain. *Journal of Neuroscience*, *25*(5), 1050–1062. https://doi.org/10.1523/jneurosci.3327-04.2005

Opatowsky, Y., Chen, C. C., Campbell, K. P., & Hirsch, J. A. (2004). Structural Analysis of the Voltage-Dependent Calcium Channel β Subunit Functional Core and Its Complex with the α1 Interaction Domain. *Neuron*, *42*(3), 387–399. https://doi.org/10.1016/s0896-6273(04)00250-8

Orci, L., Unger, R. H., Ravazzola, M., Ogawa, A., Komiya, I., Baetens, D., Lodish, H. F., & Thorens, B. (1990). Reduced beta-cell glucose transporter in new onset diabetic BB rats. *Journal of Clinical Investigation*, *86*(5), 1615–1622. https://doi.org/10.1172/jci114883

Ortner, N. J., Bock, G., Dougalis, A., Kharitonova, M., Duda, J., Hess, S., Tuluc, P., Pomberger, T., Stefanova, N., Pitterl, F., Ciossek, T., Oberacher, H., Draheim, H. J., Kloppenburg, P., Liss, B., & Striessnig, J. (2017). Lower Affinity of Isradipine for L-Type Ca2+ Channels during Substantia Nigra Dopamine Neuron-Like Activity: Implications for Neuroprotection in Parkinson's Disease. *The Journal of Neuroscience*, *37*(28), 6761–6777. https://doi.org/10.1523/jneurosci.2946-16.2017

Ortner, N. J., Bock, G., Vandael, D. H., Mauersberger, R., Draheim, H. J., Gust, R., Carbone, E., Tuluc, P., & Striessnig, J. (2014). Pyrimidine-2,4,6-triones are a new class of voltage-gated L-type Ca2+ channel activators. *Nature Communications*, *5*(1), 3897. https://doi.org/10.1038/ncomms4897

Ortner, N. J., Kaserer, T., Copeland, J. N., & Striessnig, J. (2020). De novo CACAN1D Ca2+ channelopathies: clinical phenotypes and molecular mechanism. *Pflügers Archiv - European Journal of Physiology*, *472*(7), 755–773. https://doi.org/10.1007/s00424-020-02418-w

Otsu, K., Willard, H., Khanna, V., Zorzato, F., Green, N., & MacLennan, D. (1990). Molecular cloning of cDNA encoding the Ca2+ release channel (ryanodine receptor) of rabbit cardiac muscle sarcoplasmic reticulum. *Journal of Biological Chemistry*, *265*(23), 13472–13483. https://doi.org/10.1016/s0021-9258(18)77371-7

Ozer, E. K., Gunduz, M. G., El-Khouly, A., Sara, Y., Simsek, R., Iskit, A. B., & Safak, C. (2017). Synthesis of fused 1,4-dihydropyridines as potential calcium channel blockers. *Turkish Journal of Biochemistry*, *43*(6), 578–586. https://doi.org/10.1515/tjb-2016-0247

Pan, J. Y., Yuan, S., Yu, T., Su, C. L., Liu, X. L., He, J., & Li, H. (2016). Regulation of L-type Ca2+ Channel Activity and Insulin Secretion by Huntingtin-associated Protein 1. *Journal of Biological Chemistry*, *291*(51), 26352–26363. https://doi.org/10.1074/jbc.m116.727990

Pantazis, A., Savalli, N., Sigg, D., Neely, A., & Olcese, R. (2014). Functional heterogeneity of the four voltage sensors of a human L-type calcium channel. *Proceedings of the National Academy of Sciences*, *111*(51), 18381–18386. https://doi.org/10.1073/pnas.1411127112

Parekh, A. B., & Putney, J. W. (2005). Store-Operated Calcium Channels. *Physiological Reviews*, *85*(2), 757–810. https://doi.org/10.1152/physrev.00057.2003

Park, S., Shcheynikov, N., Hong, J. H., Zheng, C., Suh, S. H., Kawaai, K., Ando, H., Mizutani, A., Abe, T., Kiyonari, H., Seki, G., Yule, D., Mikoshiba, K., & Muallem, S. (2013). Irbit Mediates Synergy Between Ca2+ and cAMP Signaling Pathways During Epithelial Transport in Mice. *Gastroenterology*, *145*(1), 232–241. https://doi.org/10.1053/j.gastro.2013.03.047

Paşca, S. P., Portmann, T., Voineagu, I., Yazawa, M., Shcheglovitov, A., Paşca, A. M., Cord, B., Palmer, T. D., Chikahisa, S., Nishino, S., Bernstein, J. A., Hallmayer, J., Geschwind, D. H., & Dolmetsch, R. E. (2011). Using iPSC-derived neurons to uncover cellular phenotypes associated with Timothy syndrome. *Nature Medicine*, *17*(12), 1657–1662. https://doi.org/10.1038/nm.2576

Pasternak, B., Svanström, H., Nielsen, N. M., Fugger, L., Melbye, M., & Hviid, A. (2012). Use of Calcium Channel Blockers and Parkinson's Disease. *American Journal of Epidemiology*, *175*(7), 627–635. https://doi.org/10.1093/aje/kwr362

Pathak, M., Kurtz, L., Tombola, F., & Isacoff, E. (2004). The Cooperative Voltage Sensor Motion that Gates a Potassium Channel. *Journal of General Physiology*, *125*(1), 57–69. https://doi.org/10.1085/jgp.200409197

Patmore, L., Duncan, G. P., Clarke, B., Anderson, A. J., Greenhouse, R., & Pfister, J. R. (1990). RS 30026: a potent and effective calcium channel agonist. *British Journal of Pharmacology*, *99*(4), 687–694. https://doi.org/10.1111/j.1476-5381.1990.tb12990.x

Payandeh, J., Scheuer, T., Zheng, N., & Catterall, W. A. (2011). The crystal structure of a voltage-gated sodium channel. *Nature*, *475*(7356), 353–358. https://doi.org/10.1038/nature10238

Peacock, A., Leung, J., Larney, S., Colledge, S., Hickman, M., Rehm, J., Giovino, G. A., West, R., Hall, W., Griffiths, P., Ali, R., Gowing, L., Marsden, J., Ferrari, A. J., Grebely, J., Farrell, M., & Degenhardt, L. (2018). Global statistics on alcohol, tobacco and illicit drug use: 2017 status report. *Addiction*, *113*(10), 1905–1926. https://doi.org/10.1111/add.14234

Peng, W., Shen, H., Wu, J., Guo, W., Pan, X., Wang, R., Chen, S. R. W., & Yan, N. (2016). Structural basis for the gating mechanism of the type 2 ryanodine receptor RyR2. *Science*, *354*(6310), aah5324. https://doi.org/10.1126/science.aah5324

Pereira, C. M. F. (2013). Crosstalk between Endoplasmic Reticulum Stress and Protein Misfolding in Neurodegenerative Diseases. *ISRN Cell Biology*, *2013*, 1–22. https://doi.org/10.1155/2013/256404

Pérez-Alvarez, A., Hernández-Vivanco, A., Caba-González, J. C., & Albillos, A. (2010). Different roles attributed to Cav1 channel subtypes in spontaneous action potential firing and fine tuning of exocytosis in mouse chromaffin cells. *Journal of Neurochemistry*, *116*(1), 105–121. https://doi.org/10.1111/j.1471-4159.2010.07089.x

Perez-Reyes, E. (2003). Molecular Physiology of Low-Voltage-Activated T-type Calcium Channels. *Physiological Reviews*, *83*(1), 117–161. https://doi.org/10.1152/physrev.00018.2002

Perez-Reyes, E., Cribbs, L. L., Daud, A., Lacerda, A. E., Barclay, J., Williamson, M. P., Fox, M., Rees, M., & Lee, J. H. (1998). Molecular characterization of a neuronal low-voltage-activated T-type calcium channel. *Nature*, *391*(6670), 896–900. https://doi.org/10.1038/36110

Perry, R. J., Samuel, V. T., Petersen, K. F., & Shulman, G. I. (2014). The role of hepatic lipids in hepatic insulin resistance and type 2 diabetes. *Nature*, *510*(7503), 84–91. https://doi.org/10.1038/nature13478

Peterson, B. Z., & Catterall, W. A. (1995). Calcium Binding in the Pore of L-type Calcium Channels Modulates High Affinity Dihydropyridine Binding. *Journal of Biological Chemistry*, *270*(31), 18201–18204. https://doi.org/10.1074/jbc.270.31.18201

Peterson, B. Z., DeMaria, C. D., & Yue, D. T. (1999). Calmodulin Is the Ca2+ Sensor for Ca2+-Dependent Inactivation of L-Type Calcium Channels. *Neuron*, *22*(3), 549–558. https://doi.org/10.1016/s0896-6273(00)80709-6

Peterson, B. Z., Johnson, B. D., Hockerman, G. H., Acheson, M., Scheuer, T., & Catterall, W. A. (1997). Analysis of the Dihydropyridine Receptor Site ofl-type Calcium Channels by Alanine-scanning Mutagenesis. *Journal of Biological Chemistry*, *272*(30), 18752–18758. https://doi.org/10.1074/jbc.272.30.18752

Peterson, B. Z., Tanada, T. N., & Catterall, W. A. (1996). Molecular Determinants of High Affinity Dihydropyridine Binding in L-type Calcium Channels. *Journal of Biological Chemistry*, *271*(10), 5293–5296. https://doi.org/10.1074/jbc.271.10.5293

Pichler, M., Cassidy, T. N., Reimer, D., Haase, H., Kraus, R., Ostler, D., & Striessnig, J. (1997). β Subunit Heterogeneity in Neuronal L-type Ca2+Channels. *Journal of Biological Chemistry*, *272*(21), 13877–13882. https://doi.org/10.1074/jbc.272.21.13877

Pinggera, A., Lieb, A., Benedetti, B., Lampert, M., Monteleone, S., Liedl, K. R., Tuluc, P., & Striessnig, J. (2015). CACNA1D De Novo Mutations in Autism Spectrum Disorders Activate Cav1.3 L-Type Calcium Channels. *Biological Psychiatry*, *77*(9), 816–822. https://doi.org/10.1016/j.biopsych.2014.11.020

Pinggera, A., Mackenroth, L., Rump, A., Schallner, J., Beleggia, F., Wollnik, B., & Striessnig, J. (2017). New gain-of-function mutation shows CACNA1D as recurrently mutated gene in autism spectrum disorders and epilepsy. *Human Molecular Genetics*, *26*(15), 2923–2932. https://doi.org/10.1093/hmg/ddx175

Pinggera, A., Negro, G., Tuluc, P., Brown, M. J., Lieb, A., & Striessnig, J. (2018). Gating defects of disease-causing de novo mutations in Cav1.3 Ca2+ channels. *Channels*, *12*(1), 388–402. https://doi.org/10.1080/19336950.2018.1546518

Pitt, G. S., Zühlke, R. D., Hudmon, A., Schulman, H., Reuter, H., & Tsien, R. W. (2001). Molecular Basis of Calmodulin Tethering and Ca2+-dependent Inactivation of L-type Ca2+ Channels. *Journal of Biological Chemistry*, *276*(33), 30794–30802. https://doi.org/10.1074/jbc.m104959200

Pizzo, P., Lissandron, V., Capitanio, P., & Pozzan, T. (2011). Ca2+ signalling in the Golgi apparatus. *Cell Calcium*, *50*(2), 184–192. https://doi.org/10.1016/j.ceca.2011.01.006

Plant, T. D. (1988). Properties and calcium-dependent inactivation of calcium currents in cultured mouse pancreatic B-cells. *The Journal of Physiology*, *404*(1), 731–747. https://doi.org/10.1113/jphysiol.1988.sp017316

Platzer, J., Engel, J., Schrott-Fischer, A., Stephan, K., Bova, S., Chen, H., Zheng, H., & Striessnig, J. (2000). Congenital Deafness and Sinoatrial Node Dysfunction in Mice Lacking Class D L-Type Ca2+ Channels. *Cell*, *102*(1), 89–97. https://doi.org/10.1016/s0092-8674(00)00013-1

Polster, A., Nelson, B. R., Papadopoulos, S., Olson, E. N., & Beam, K. G. (2018). Stac proteins associate with the critical domain for excitation–contraction coupling in the II–III loop of CaV1.1. *Journal of General Physiology*, *150*(4), 613–624. https://doi.org/10.1085/jgp.201711917

Poomvanicha, M., Wegener, J. W., Blaich, A., Fischer, S., Domes, K., Moosmang, S., & Hofmann, F. (2011). Facilitation and Ca2+-dependent Inactivation Are Modified by Mutation of the Cav1.2 Channel IQ Motif. *Journal of Biological Chemistry*, *286*(30), 26702–26707. https://doi.org/10.1074/jbc.m111.247841

Porzig, H., & Becker, C. (1988). Potential-dependent allosteric modulation of 1,4-dihydropyridine binding by d-(cis)-diltiazem and (+/-)-verapamil in living cardiac cells H Porzig 1, C Becker. *Mol Pharmacol*, *34*(2), 172–179.

Pragnell, M., De Waard, M., Mori, Y., Tanabe, T., Snutch, T. P., & Campbell, K. P. (1994). Calcium channel β-subunit binds to a conserved motif in the I–II cytoplasmic linker of the α1-subunit. *Nature*, *368*(6466), 67–70. https://doi.org/10.1038/368067a0

Pragnell, M., Sakamoto, J., Jay, S. D., & Campbell, K. P. (1991). Cloning and tissue-specific expression of the brain calcium channel β-subunit. *FEBS Letters*, *291*(2), 253–258. https://doi.org/10.1016/0014-5793(91)81296-k

Pratt, E. P., Salyer, A. E., Guerra, M. L., & Hockerman, G. H. (2016). Ca2+ influx through L-type Ca2+ channels and Ca2+-induced Ca2+ release regulate cAMP accumulation and Epac1-dependent ERK 1/2 activation in INS-1 cells. *Molecular and Cellular Endocrinology*, *419*, 60–71. https://doi.org/10.1016/j.mce.2015.09.034

Prole, D. L., & Taylor, C. W. (2019). Structure and Function of IP3 Receptors. *Cold Spring Harbor Perspectives in Biology*, *11*(4), a035063. https://doi.org/10.1101/cshperspect.a035063

Putney, J. W., Steinckwich-Besançon, N., Numaga-Tomita, T., Davis, F. M., Desai, P. N., D'Agostin, D. M., Wu, S., & Bird, G. S. (2017). The functions of store-operated calcium channels. *Biochimica et Biophysica Acta (BBA) - Molecular Cell Research*, *1864*(6), 900–906. https://doi.org/10.1016/j.bbamcr.2016.11.028

Putzier, I., Kullmann, P. H. M., Horn, J. P., & Levitan, E. S. (2009). Cav1.3 Channel Voltage Dependence, Not Ca2+ Selectivity, Drives Pacemaker Activity and Amplifies Bursts in Nigral Dopamine Neurons. *Journal of Neuroscience*, *29*(49), 15414–15419. https://doi.org/10.1523/jneurosci.4742-09.2009

Qin, N., Platano, D., Olcese, R., Stefani, E., & Birnbaumer, L. (1997). Direct interaction of G with a C-terminal G -binding domain of the Ca2+ channel 1 subunit is responsible for channel inhibition by G protein-coupled receptors. *Proceedings of the National Academy of Sciences*, *94*(16), 8866–8871. https://doi.org/10.1073/pnas.94.16.8866

Qin, N., Yagel, S., Momplaisir, M. L., Codd, E. E., & D'Andrea, M. R. (2002). Molecular Cloning and Characterization of the Human Voltage-Gated Calcium Channel α2δ-4 Subunit. *Molecular Pharmacology*, *62*(3), 485–496. https://doi.org/10.1124/mol.62.3.485

Qu, Y., Baroudi, G., Yue, Y., El-Sherif, N., & Boutjdir, M. (2005). Localization and modulation of α1D (Cav1.3) L-type Ca channel by protein kinase A. *American Journal of Physiology-Heart and Circulatory Physiology*, *288*(5), H2123–H2130. https://doi.org/10.1152/ajpheart.01023.2004

Quane, K. A., Healy, J., Keating, K. E., Manning, B. M., Couch, F. J., Palmucci, L. M., Doriguzzi, C., Fagerlund, T. H., Berg, K., Ording, H., Bendixen, D., Mortier, W., Linz, U., Muller, C. R., & McCarthy, T. V. (1993). Mutations in the ryanodine receptor gene in central core disease and malignant hyperthermia. *Nature Genetics*, *5*(1), 51–55. https://doi.org/10.1038/ng0993-51

Radhakrishnan, K., Krieger, A., Dibué, M., Hescheler, J., & Schneider, T. (2011). APLP1 and Rab5A Interact with the II-III loop of the Voltage-gated Ca2+-channel Ca(v)2.3 and Modulate its Internalization Differently. *Cellular Physiology and Biochemistry*, *28*(4), 603–612. https://doi.org/10.1159/000335756

Radhakrishnan, V. M., Gilpatrick, M. M., Parsa, N. A., Kiela, P. R., & Ghishan, F. K. (2017). Expression of Cav1.3 calcium channel in the human and mouse colon: posttranscriptional inhibition by IFNγ. *American Journal of Physiology-Gastrointestinal and Liver Physiology*, *312*(1), G77–G84. https://doi.org/10.1152/ajpgi.00394.2016

Rae, J., Cooper, K., Gates, P., & Watsky, M. (1991). Low access resistance perforated patch recordings using amphotericin B. *Journal of Neuroscience Methods*, *37*(1), 15–26. https://doi.org/10.1016/0165-0270(91)90017-t

Rajadhyaksha, A., Barczak, A., Macías, W., Leveque, J. C., Lewis, S. E., & Konradi, C. (1999). L-Type Ca2+Channels Are Essential for Glutamate-Mediated CREB Phosphorylation andc-fosGene Expression in Striatal Neurons. *The Journal of Neuroscience*, *19*(15), 6348–6359. https://doi.org/10.1523/jneurosci.19-15-06348.1999

Rajagopal, S., & Ponnusamy, M. (2017). Calcium Ion in Biological Systems. *Calcium Signaling: From Physiology to Diseases*, 1–14. https://doi.org/10.1007/978-981-10-5160-9_1

Ramadan, O., Qu, Y., Wadgaonkar, R., Baroudi, G., Karnabi, E., Chahine, M., & Boutjdir, M. (2009). Phosphorylation of the Consensus Sites of Protein Kinase A on α1D L-type Calcium Channel. *Journal of Biological Chemistry*, *284*(8), 5042–5049. https://doi.org/10.1074/jbc.m809132200

Rampe, D., Anderson, B., Rapien-Pryor, V., Li, T., & Dage, R. C. (1993). Comparison of the in vitro and in vivo cardiovascular effects of two structurally distinct Ca++ channel activators, BAY K 8644 and FPL 64176. *Journal of Pharmacology and Experimental Therapeutics*, *265*(3), 1125–1130. https://jpet.aspetjournals.org/content/265/3/1125.long

Rampe, D., & Lacerda, A. E. (1991). A new site for the activation of cardiac calcium channels defined by the nondihydropyridine FPL 64176. *Journal of Pharmacology and Experimental Therapeutics*, *259*(3), 982–987. https://jpet.aspetjournals.org/content/259/3/982.short?casa_token=-tlo6W1LAiwAAAAA:fL_9IlcWf1uLd4J3QEVvZRBZE95IqZccUUvEaP38gPONpWo0Re1vetEc0GVqJF1ItHqP6KU25r4

Ran, Y., He, Y., Yang, G., Johnson, J. L., & Yalkowsky, S. H. (2002). Estimation of aqueous solubility of organic compounds by using the general solubility equation. *Chemosphere*, *48*(5), 487–509. https://doi.org/10.1016/s0045-6535(02)00118-2

Randall, A., & Tsien, R. (1995). Pharmacological dissection of multiple types of Ca2+ channel currents in rat cerebellar granule neurons. *The Journal of Neuroscience*, *15*(4), 2995–3012. https://doi.org/10.1523/jneurosci.15-04-02995.1995

Raybaud, A., Baspinar, E. E., Dionne, F., Dodier, Y., Sauvé, R., & Parent, L. (2007). The Role of Distal S6 Hydrophobic Residues in the Voltage-dependent Gating of CaV2.3 Channels. *Journal of Biological Chemistry*, *282*(38), 27944–27952. https://doi.org/10.1074/jbc.m703895200

Reinbothe, T. M., Alkayyali, S., Ahlqvist, E., Tuomi, T., Isomaa, B., Lyssenko, V., & Renström, E. (2012). The human L-type calcium channel Cav1.3 regulates insulin release and polymorphisms in CACNA1D associate with type 2 diabetes. *Diabetologia*, *56*(2), 340–349. https://doi.org/10.1007/s00125-012-2758-z

Remedi, M. S., Rocheleau, J. V., Tong, A., Patton, B. L., McDaniel, M. L., Piston, D. W., Koster, J. C., & Nichols, C. G. (2006). Hyperinsulinism in mice with heterozygous loss of KATP channels. *Diabetologia*, *49*(10), 2368–2378. https://doi.org/10.1007/s00125-006-0367-4

Reuter, H. (1967). The dependence of slow inward current in Purkinje fibres on the extracellular calcium-concentration. *The Journal of Physiology*, *192*(2), 479–492. https://doi.org/10.1113/jphysiol.1967.sp008310

Reuter, H. (1979). Properties of Two Inward Membrane Currents in the Heart. *Annual Review of Physiology*, *41*(1), 413–424. https://doi.org/10.1146/annurev.ph.41.030179.002213

Rewers, M., & Ludvigsson, J. (2016). Environmental risk factors for type 1 diabetes. *The Lancet*, *387*(10035), 2340–2348. https://doi.org/10.1016/s0140-6736(16)30507-4

Ribalet, B., & Beigelman, P. M. (1981). Effects of divalent cations on beta-cell electrical activity. *American Journal of Physiology-Cell Physiology*, *241*(1), C59–C67. https://doi.org/10.1152/ajpcell.1981.241.1.c59

Richards, M. W., Leroy, J., Pratt, W. S., & Dolphin, A. C. (2007). The HOOK-Domain Between the SH3- and the GK-Domains of CaVβ Subunits Contains Key Determinants Controlling Calcium Channel Inactivation. *Channels*, *1*(2), 92–101. https://doi.org/10.4161/chan.4145

Rios, E., & Brum, G. (1987). Involvement of dihydropyridine receptors in excitation–contraction coupling in skeletal muscle. *Nature*, *325*(6106), 717–720. https://doi.org/10.1038/325717a0

Ritz, B., Rhodes, S. L., Qian, L., Schernhammer, E., Olsen, J., & Friis, S. (2009). L-type calcium channel blockers and Parkinson's disease in Denmark. *Annals of Neurology*, n/a. https://doi.org/10.1002/ana.21937

Riz, M., Braun, M., Wu, X., & Pedersen, M. G. (2015). Inwardly rectifying Kir2.1 currents in human β-cells control electrical activity: Characterisation and mathematical modelling. *Biochemical and Biophysical Research Communications*, *459*(2), 284–287. https://doi.org/10.1016/j.bbrc.2015.02.099

Rizzuto, R., & Pozzan, T. (2003). When calcium goes wrong: genetic alterations of a ubiquitous signaling route. *Nature Genetics*, *34*(2), 135–141. https://doi.org/10.1038/ng0603-135

Roberts-Crowley, M. L., Mitra-Ganguli, T., Liu, L., & Rittenhouse, A. R. (2009). Regulation of voltage-gated Ca2+ channels by lipids. *Cell Calcium*, *45*(6), 589–601. https://doi.org/10.1016/j.ceca.2009.03.015

Roberts-Crowley, M. L., & Rittenhouse, A. R. (2018). Modulation of CaV1.3b L-type calcium channels by M1 muscarinic receptors varies with CaVβ subunit expression. *BMC Research Notes*, *11*(1). https://doi.org/10.1186/s13104-018-3783-x

Rocheleau, J. V., Remedi, M. S., Granada, B., Head, W. S., Koster, J. C., Nichols, C. G., & Piston, D. W. (2006). Critical Role of Gap Junction Coupled KATP Channel Activity for Regulated Insulin Secretion. *PLoS Biology*, *4*(2), e26. https://doi.org/10.1371/journal.pbio.0040026

Rodríguez-Prados, M., Rojo-Ruiz, J., Aulestia, F. J., García-Sancho, J., & Alonso, M. T. (2015). A new low-Ca2+ affinity GAP indicator to monitor high Ca2+ in organelles by luminescence. *Cell Calcium*, *58*(6), 558–564. https://doi.org/10.1016/j.ceca.2015.09.002

Roe, M. W., Worley, J. F., Tokuyama, Y., Philipson, L. H., Sturis, J., Tang, J., Dukes, I. D., Bell, G. I., & Polonsky, K. S. (1996). NIDDM is associated with loss of pancreatic beta-cell L-type Ca2+ channel activity. *American Journal of Physiology-Endocrinology and Metabolism*, *270*(1), E133–E140. https://doi.org/10.1152/ajpendo.1996.270.1.e133

Röhrkasten, A., Meyer, H. E., Nastainczyk, W., Sieber, M., & Hofmann, F. (1988). cAMP-dependent protein kinase rapidly phosphorylates serine- 687 of the skeletal muscle receptor for calcium channel blockers. *Journal of Biological Chemistry*, *263*(30), 15325–15329. https://doi.org/10.1016/s0021-9258(19)37591-x

Röhrkasten, A., Nastainczyk, W., Sieber, M., Jahn, H., Regulla, S., & Hofmann, F. (1988). Phosphorylation of the Purified CaCB-Receptor. *Journal of Cardiovascular Pharmacology*, *12*, 43–46. https://doi.org/10.1097/00005344-198806125-00008

Rorsman, P., & Ashcroft, F. M. (2018). Pancreatic β-Cell Electrical Activity and Insulin Secretion: Of Mice and Men. *Physiological Reviews*, *98*(1), 117–214. https://doi.org/10.1152/physrev.00008.2017

Rorsman, P., Eliasson, L., Kanno, T., Zhang, Q., & Gopel, S. (2011). Electrophysiology of pancreatic β-cells in intact mouse islets of Langerhans. *Progress in Biophysics and Molecular Biology*, *107*(2), 224–235. https://doi.org/10.1016/j.pbiomolbio.2011.06.009

Rosa, J. M., de Diego, A. M., Gandía, L., & García, A. G. (2007). L-type calcium channels are preferentially coupled to endocytosis in bovine chromaffin cells. *Biochemical and Biophysical Research Communications*, *357*(4), 834–839. https://doi.org/10.1016/j.bbrc.2007.03.207

Rosa, J. M., Gandía, L., & García, A. G. (2010). Permissive role of sphingosine on calcium-dependent endocytosis in chromaffin cells. *Pflügers Archiv - European Journal of Physiology*, *460*(5), 901–914. https://doi.org/10.1007/s00424-010-0861-x

Rosa, J. M., Nanclares, C., Orozco, A., Colmena, I., de Pascual, R., García, A. G., & Gandía, L. (2012). Regulation by L-Type Calcium Channels of Endocytosis: An Overview. *Journal of Molecular Neuroscience*, *48*(2), 360–367. https://doi.org/10.1007/s12031-012-9786-5

Rossi, G. P., Bernini, G., Caliumi, C., Desideri, G., Fabris, B., Ferri, C., Ganzaroli, C., Giacchetti, G., Letizia, C., Maccario, M., Mallamaci, F., Mannelli, M., Mattarello, M. J., Moretti, A., Palumbo, G., Parenti, G., Porteri, E., Semplicini, A., Rizzoni, D., . . . Mantero, F. (2006). A Prospective Study of the Prevalence of Primary Aldosteronism in 1,125 Hypertensive Patients. *Journal of the American College of Cardiology*, *48*(11), 2293–2300. https://doi.org/10.1016/j.jacc.2006.07.059

Rotman, E., De Jongh, K., Florio, V., Lai, Y., & Catterall, W. (1992). Specific phosphorylation of a COOH-terminal site on the full-length form of the alpha 1 subunit of the skeletal muscle calcium channel by cAMP-dependent protein kinase. *Journal of Biological Chemistry*, *267*(23), 16100–16105. https://doi.org/10.1016/s0021-9258(18)41972-2

Rotman, E. I., Murphy, B. J., & Catterall, W. A. (1995). Sites of Selective cAMP-dependent Phosphorylation of the L-type Calcium Channel α1 Subunit from Intact Rabbit Skeletal Muscle Myotubes. *Journal of Biological Chemistry*, *270*(27), 16371–16377. https://doi.org/10.1074/jbc.270.27.16371

Rotstein, B., Liang, S., Belov, V., Livni, E., Levine, D., Bonab, A., Papisov, M., Perlis, R., & Vasdev, N. (2015). Practical Radiosynthesis and Preclinical Neuroimaging of [11C]isradipine, a Calcium Channel Antagonist. *Molecules*, *20*(6), 9550–9559. https://doi.org/10.3390/molecules20069550

Ruth, P., Rohrkasten, A., Biel, M., Bosse, E., Regulla, S., Meyer, H., Flockerzi, V., & Hofmann, F. (1989). Primary structure of the beta subunit of the DHP-sensitive calcium channel from skeletal muscle. *Science*, *245*(4922), 1115–1118. https://doi.org/10.1126/science.2549640

Sackin, H., Nanazashvili, M., Palmer, L. G., & Li, H. (2006). Role of Conserved Glycines in pH Gating of Kir1.1 (ROMK). *Biophysical Journal*, *90*(10), 3582–3589. https://doi.org/10.1529/biophysj.105.076653

Saddala, M. S., Kandimalla, R., Adi, P. J., Bhashyam, S. S., & Asupatri, U. R. (2017). Novel 1, 4-dihydropyridines for L-type calcium channel as antagonists for cadmium toxicity. *Scientific Reports*, *7*(1). https://doi.org/10.1038/srep45211

Sampieri, A., Santoyo, K., Asanov, A., & Vaca, L. (2018). Association of the IP3R to STIM1 provides a reduced intraluminal calcium microenvironment, resulting in enhanced store-operated calcium entry. *Scientific Reports*, *8*(1). https://doi.org/10.1038/s41598-018-31621-0

Sánchez-Andrés, J. V., Gomis, A., & Valdeolmillos, M. (1995). The electrical activity of mouse pancreatic beta-cells recorded in vivo shows glucose-dependent oscillations. *The Journal of Physiology*, *486*(1), 223–228. https://doi.org/10.1113/jphysiol.1995.sp020804

Sand, O., Chen, B., & Grinnell, A. D. (2001). Contribution of L-type Ca 2+ channels to evoked transmitter release in cultured Xenopus nerve-muscle synapses. *The Journal of Physiology*, *536*(1), 21–33. https://doi.org/10.1111/j.1469-7793.2001.00021.x

Sandoval, A., Duran, P., Gandini, M. A., Andrade, A., Almanza, A., Kaja, S., & Felix, R. (2017). Regulation of L-type CaV1.3 channel activity and insulin secretion by the cGMP-PKG signaling pathway. *Cell Calcium*, *66*, 1–9. https://doi.org/10.1016/j.ceca.2017.05.008

Sang, L., Dick, I. E., & Yue, D. T. (2016). Protein kinase A modulation of CaV1.4 calcium channels. *Nature Communications*, *7*(1). https://doi.org/10.1038/ncomms12239

Sang, L., Vieira, D. C., Yue, D. T., Ben-Johny, M., & Dick, I. E. (2021). The molecular basis of the inhibition of CaV1 calcium-dependent inactivation by the distal carboxy tail. *Journal of Biological Chemistry*, *296*, 100502. https://doi.org/10.1016/j.jbc.2021.100502

Sanguinetti, M. C., & Kass, R. S. (1984). Voltage-dependent block of calcium channel current in the calf cardiac Purkinje fiber by dihydropyridine calcium channel antagonists. *Circulation Research*, *55*(3), 336–348. https://doi.org/10.1161/01.res.55.3.336

Sansbury, F. H., Flanagan, S. E., Houghton, J. A. L., Shuixian Shen, F. L., Al-Senani, A. M. S., Habeb, A. M., Abdullah, M., Kariminejad, A., Ellard, S., & Hattersley, A. T. (2012). SLC2A2 mutations can cause neonatal diabetes, suggesting GLUT2 may have a role in human insulin secretion. *Diabetologia*, *55*(9), 2381–2385. https://doi.org/10.1007/s00125-012-2595-0

Santos-Longhurst, A. (2020, August 15). *Type 2 Diabetes Statistics and Facts*. Healthline. https://www.healthline.com/health/type-2-diabetes/statistics#1

Santulli, G., Lewis, D., des Georges, A., Marks, A. R., & Frank, J. (2018). Ryanodine Receptor Structure and Function in Health and Disease. *Subcellular Biochemistry*, 329–352. https://doi.org/10.1007/978-981-10-7757-9_11

Santulli, G., Lewis, D. R., & Marks, A. R. (2017). Physiology and pathophysiology of excitation–contraction coupling: the functional role of ryanodine receptor. *Journal of Muscle Research and Cell Motility*, *38*(1), 37–45. https://doi.org/10.1007/s10974-017-9470-z

Santulli, G., & Marks, A. (2015). Essential Roles of Intracellular Calcium Release Channels in Muscle, Brain, Metabolism, and Aging. *Current Molecular Pharmacology*, *8*(2), 206–222. https://doi.org/10.2174/1874467208666150507105105

Santulli, G., Nakashima, R., Yuan, Q., & Marks, A. R. (2017). Intracellular calcium release channels: an update. *The Journal of Physiology*, *595*(10), 3041–3051. https://doi.org/10.1113/jp272781

Santulli, G., Pagano, G., Sardu, C., Xie, W., Reiken, S., D'Ascia, S. L., Cannone, M., Marziliano, N., Trimarco, B., Guise, T. A., Lacampagne, A., & Marks, A. R. (2015). Calcium release channel RyR2 regulates insulin release and glucose homeostasis. *Journal of Clinical Investigation*, *125*(5), 1968–1978. https://doi.org/10.1172/jci79273

Sasaki, T., Feng, Z. P., Scott, R., Grigoriev, N., Syed, N. I., Fainzilber, M., & Sato, K. (1999). Synthesis, Bioactivity, and Cloning of the L-Type Calcium Channel Blocker ω-Conotoxin TxVII†. *Biochemistry*, *38*(39), 12876–12884. https://doi.org/10.1021/bi990731f

Sather, W. A., & McCleskey, E. W. (2003). Permeation and Selectivity in Calcium Channels. *Annual Review of Physiology*, *65*(1), 133–159. https://doi.org/10.1146/annurev.physiol.65.092101.142345

Satin, L. S., & Cook, D. L. (1989). Calcium current inactivation in insulin-secreting cells is mediated by calcium influx and membrane depolarization. *Pflugers Archiv European Journal of Physiology*, *414*(1), 1–10. https://doi.org/10.1007/bf00585619

Sato, K., Park, N., Kohno, T., Maeda, T., Kim, J., Kato, R., & Takahashi, M. (1993). Role of Basic Residues for the Binding of ω-Conotoxin GVIA to N-Type Calcium Channels. *Biochemical and Biophysical Research Communications*, *194*(3), 1292–1296. https://doi.org/10.1006/bbrc.1993.1964

Savalli, N., Pantazis, A., Sigg, D., Weiss, J. N., Neely, A., & Olcese, R. (2016). The α2δ-1 subunit remodels CaV1.2 voltage sensors and allows Ca2+ influx at physiological membrane potentials. *Journal of General Physiology*, *148*(2), 147–159. https://doi.org/10.1085/jgp.201611586

Schaller, D., Gündüz, M. G., Zhang, F. X., Zamponi, G. W., & Wolber, G. (2018). Binding mechanism investigations guiding the synthesis of novel condensed 1,4-dihydropyridine derivatives with L-/T-type calcium channel blocking activity. *European Journal of Medicinal Chemistry*, *155*, 1–12. https://doi.org/10.1016/j.ejmech.2018.05.032

Schierberl, K., Giordano, T., Satpute, S., Hao, J., Kaur, G., Hofmann, F., Moosmang, S., Striessnig, J., & Rajadhyaksha, A. (2012a). Cav1.3 L-type Ca2+channels mediate long-term adaptation in dopamine D2L-mediated GluA1 trafficking in the dorsal striatum following cocaine exposure. *Channels*, *6*(1), 11–17. https://doi.org/10.4161/chan.19324

Schierberl, K., Giordano, T., Satpute, S., Hao, J., Kaur, G., Hofmann, F., Moosmang, S., Striessnig, J., & Rajadhyaksha, A. (2012b). Cav1.3 L-type Ca2+channels mediate long-term adaptation in dopamine D2L-mediated GluA1 trafficking in the dorsal striatum following cocaine exposure. *Channels*, *6*(1), 11–17. https://doi.org/10.4161/chan.19324

Schlick, B., Flucher, B., & Obermair, G. (2010). Voltage-activated calcium channel expression profiles in mouse brain and cultured hippocampal neurons. *Neuroscience*, *167*(3), 786–798. https://doi.org/10.1016/j.neuroscience.2010.02.037

Scholl, U. I., Goh, G., Stölting, G., de Oliveira, R. C., Choi, M., Overton, J. D., Fonseca, A. L., Korah, R., Starker, L. F., Kunstman, J. W., Prasad, M. L., Hartung, E. A., Mauras, N., Benson, M. R., Brady, T., Shapiro, J. R., Loring, E., Nelson-Williams, C., Libutti, S. K., . . . Lifton, R. P. (2013). Somatic and germline CACNA1D calcium channel mutations in aldosterone-producing adenomas and primary aldosteronism. *Nature Genetics*, *45*(9), 1050–1054. https://doi.org/10.1038/ng.2695

Schramm, M., Thomas, G., Towart, R., & Franckowiak, G. (1983). Novel dihydropyridines with positive inotropic action through activation of Ca2+ channels. *Nature*, *303*(5917), 535–537. https://doi.org/10.1038/303535a0

Schroeder, L. I. R. C. J. (2013). *Block of Voltage-Gated Calcium Channels by Peptide Toxins - Madame Curie Bioscience Database - NCBI Bookshelf*. NCBI. https://www.ncbi.nlm.nih.gov/books/NBK6148/

Schuit, F., De Vos, A., Farfari, S., Moens, K., Pipeleers, D., Brun, T., & Prentki, M. (1997). Metabolic Fate of Glucose in Purified Islet Cells. *Journal of Biological Chemistry*, *272*(30), 18572–18579. https://doi.org/10.1074/jbc.272.30.18572

Schulla, V. (2003). Impaired insulin secretion and glucose tolerance in cell-selective CaV1.2 Ca2+ channel null mice. *The EMBO Journal*, *22*(15), 3844–3854. https://doi.org/10.1093/emboj/cdg389

Schweitz, H., Heurteaux, C., Bois, P., Moinier, D., Romey, G., & Lazdunski, M. (1994). Calcicludine, a venom peptide of the Kunitz-type protease inhibitor family, is a potent blocker of high-threshold Ca2+ channels with a high affinity for L-type channels in cerebellar granule neurons. *Proceedings of the National Academy of Sciences*, *91*(3), 878–882. https://doi.org/10.1073/pnas.91.3.878

Sculptoreanu, A., Scheuer, T., & Catterall, W. A. (1993). Voltage-dependent potentiation of L-type Ca2+ channels due to phosphorylation by cAMP-dependent protein kinase. *Nature*, *364*(6434), 240–243. https://doi.org/10.1038/364240a0

Segura-Chama, P., Rivera-Cerecedo, C. V., González-Ramírez, R., Felix, R., Hernández-Guijo, J. M., & Hernández-Cruz, A. (2012). Atypical Ca2+ currents in chromaffin cells from SHR and WKY rat strains result from the deficient expression of a splice variant of the α1D Ca2+ channel. *American Journal of Physiology-Heart and Circulatory Physiology*, *302*(2), H467–H478. https://doi.org/10.1152/ajpheart.00849.2011

Seino, S., Chen, L., Seino, M., Blondel, O., Takeda, J., Johnson, J. H., & Bell, G. I. (1992). Cloning of the alpha 1 subunit of a voltage-dependent calcium channel expressed in pancreatic beta cells. *Proceedings of the National Academy of Sciences*, *89*(2), 584–588. https://doi.org/10.1073/pnas.89.2.584

Seino, S., & Shibasaki, T. (2005). PKA-Dependent and PKA-Independent Pathways for cAMP-Regulated Exocytosis. *Physiological Reviews*, *85*(4), 1303–1342. https://doi.org/10.1152/physrev.00001.2005

Seisenberger, C., Specht, V., Welling, A., Platzer, J., Pfeifer, A., Kühbandner, S., Striessnig, J., Klugbauer, N., Feil, R., & Hofmann, F. (2000). Functional Embryonic Cardiomyocytes after Disruption of the L-type α1C (Ca 1.2) Calcium Channel Gene in the Mouse. *Journal of Biological Chemistry*, *275*(50), 39193–39199. https://doi.org/10.1074/jbc.m006467200

Seo, M. D., Enomoto, M., Ishiyama, N., Stathopulos, P. B., & Ikura, M. (2015). Structural insights into endoplasmic reticulum stored calcium regulation by inositol 1,4,5-trisphosphate and ryanodine receptors. *Biochimica et Biophysica Acta (BBA) - Molecular Cell Research*, *1853*(9), 1980–1991. https://doi.org/10.1016/j.bbamcr.2014.11.023

Seydl, K., Kimball, D., Schindler, H., & Romanin, C. (1993). The benzazepine/benzothiazepine binding domain of the cardiac L-type Ca^{2+} channel is accessible only from the extracellular side. *Pflugers Archiv European Journal of Physiology*, *424*(5–6), 552–554. https://doi.org/10.1007/bf00374922

Shaw, R. M., & Colecraft, H. M. (2013). L-type calcium channel targeting and local signalling in cardiac myocytes. *Cardiovascular Research*, *98*(2), 177–186. https://doi.org/10.1093/cvr/cvt021

Shen, H., Zhou, Q., Pan, X., Li, Z., Wu, J., & Yan, N. (2017). Structure of a eukaryotic voltage-gated sodium channel at near-atomic resolution. *Science*, *355*(6328), eaal4326. https://doi.org/10.1126/science.aal4326

Shen, Y., Thillaiappan, N. B., & Taylor, C. W. (2021). The store-operated Ca2+ entry complex comprises a small cluster of STIM1 associated with one Orai1 channel. *Proceedings of the National Academy of Sciences*, *118*(10), e2010789118. https://doi.org/10.1073/pnas.2010789118

Sheng, M., McFadden, G., & Greenberg, M. E. (1990). Membrane depolarization and calcium induce c-fos transcription via phosphorylation of transcription factor CREB. *Neuron*, *4*(4), 571–582. https://doi.org/10.1016/0896-6273(90)90115-v

Sheng, Z. H., Westenbroek, R. E., & Catterall, W. A. (1998). Physical link and functional coupling of presynaptic calcium channels and the synaptic vesicle docking/fusion machinery. Journal of bioenergetics and biomembranes. *Journal of Bioenergetics and Biomembranes*, *30*(4), 335–345. https://doi.org/10.1023/a:1021985521748

Shibasaki, M., Kurokawa, K., & Ohkuma, S. (2010). Upregulation of L-type Cav1 channels in the development of psychological dependence. *Synapse*, *64*(6), 440–444. https://doi.org/10.1002/syn.20745

Shibasaki, T., Sunaga, Y., & Seino, S. (2004). Integration of ATP, cAMP, and Ca2+ Signals in Insulin Granule Exocytosis. *Diabetes*, *53*(Supplement 3), S59–S62. https://doi.org/10.2337/diabetes.53.suppl_3.s59

Shimomura, T., Yonekawa, Y., Nagura, H., Tateyama, M., Fujiyoshi, Y., & Irie, K. (2020). A native prokaryotic voltage-dependent calcium channel with a novel selectivity filter sequence. *ELife*, *9*. https://doi.org/10.7554/elife.52828

Shiota, C., Larsson, O., Shelton, K. D., Shiota, M., Efanov, A. M., Høy, M., Lindner, J., Kooptiwut, S., Juntti-Berggren, L., Gromada, J., Berggren, P. O., & Magnuson, M. A. (2002). Sulfonylurea Receptor Type 1 Knock-out Mice Have Intact Feeding-stimulated Insulin Secretion despite Marked Impairment in Their Response to Glucose. *Journal of Biological Chemistry*, *277*(40), 37176–37183. https://doi.org/10.1074/jbc.m206757200

Shirakabe, K., Priori, G., Yamada, H., Ando, H., Horita, S., Fujita, T., Fujimoto, I., Mizutani, A., Seki, G., & Mikoshiba, K. (2006). IRBIT, an inositol 1,4,5-trisphosphate receptor-binding protein, specifically binds to and activates pancreas-type Na+/HCO3-cotransporter 1 (pNBC1). *Proceedings of the National Academy of Sciences*, *103*(25), 9542–9547. https://doi.org/10.1073/pnas.0602250103

Shuda, M., Kondoh, N., Imazeki, N., Tanaka, K., Okada, T., Mori, K., Hada, A., Arai, M., Wakatsuki, T., Matsubara, O., Yamamoto, N., & Yamamoto, M. (2003). Activation of the ATF6, XBP1 and grp78 genes in human hepatocellular carcinoma: a possible involvement of the ER stress pathway in hepatocarcinogenesis. *Journal of Hepatology*, *38*(5), 605–614. https://doi.org/10.1016/s0168-8278(03)00029-1

Shyng, S. (1998). Membrane Phospholipid Control of Nucleotide Sensitivity of KATP Channels. *Science*, *282*(5391), 1138–1141. https://doi.org/10.1126/science.282.5391.1138

SIEBER, M., NASTAINCZYK, W., ZUBOR, V., WERNET, W., & HOFMANN, F. (1987). The 165-KDa peptide of the purified skeletal muscle dihydropyridine receptor contains the known regulatory sites of the calcium channel. *European Journal of Biochemistry*, *167*(1), 117–122. https://doi.org/10.1111/j.1432-1033.1987.tb13311.x

Singh, A., Gebhart, M., Fritsch, R., Sinnegger-Brauns, M. J., Poggiani, C., Hoda, J. C., Engel, J., Romanin, C., Striessnig, J., & Koschak, A. (2008). Modulation of Voltage- and Ca2+-dependent Gating of CaV1.3 L-type Calcium Channels by Alternative Splicing of a C-terminal Regulatory Domain. *Journal of Biological Chemistry*, *283*(30), 20733–20744. https://doi.org/10.1074/jbc.m802254200

Singh, A., Hamedinger, D., Hoda, J. C., Gebhart, M., Koschak, A., Romanin, C., & Striessnig, J. (2006). C-terminal modulator controls Ca2+-dependent gating of Cav1.4 L-type Ca2+ channels. *Nature Neuroscience*, *9*(9), 1108–1116. https://doi.org/10.1038/nn1751

Sinnegger, M. J., Wang, Z., Grabner, M., Hering, S., Striessnig, J., Glossmann, H., & Mitterdorfer, J. (1997). Nine L-type Amino Acid Residues Confer Full 1,4-Dihydropyridine Sensitivity to the Neuronal Calcium Channel α1ASubunit. *Journal of Biological Chemistry*, *272*(44), 27686–27693. https://doi.org/10.1074/jbc.272.44.27686

Sinnegger-Brauns, M. J., Hetzenauer, A., Huber, I. G., Renström, E., Wietzorrek, G., Berjukov, S., Cavalli, M., Walter, D., Koschak, A., Waldschütz, R., Hering, S., Bova, S., Rorsman, P., Pongs, O., Singewald, N., & Striessnig, J. (2004). Isoform-specific regulation of mood behavior and pancreatic β cell and cardiovascular function by L-type Ca2+ channels. *Journal of Clinical Investigation*, *113*(10), 1430–1439. https://doi.org/10.1172/jci20208

Sklar, P., Smoller, J. W., Fan, J., Ferreira, M. A. R., Perlis, R. H., Chambert, K., Nimgaonkar, V. L., McQueen, M. B., Faraone, S. V., Kirby, A., de Bakker, P. I. W., Ogdie, M. N., Thase, M. E., Sachs, G. S., Todd-Brown, K., Gabriel, S. B., Sougnez, C., Gates, C., Blumenstiel, B., . . . Purcell, S. M. (2008). Whole-genome association study of bipolar disorder. *Molecular Psychiatry*, *13*(6), 558–569. https://doi.org/10.1038/sj.mp.4002151

Smith, P. A., Bokvist, K., Arkhammar, P., Berggren, P. O., & Rorsman, P. (1990). Delayed rectifying and calcium-activated K+ channels and their significance for action potential repolarization in mouse pancreatic beta-cells. *Journal of General Physiology*, *95*(6), 1041–1059. https://doi.org/10.1085/jgp.95.6.1041

Smith, P. A., Rorsman, P., & Ashcroft, F. M. (1989). Modulation of dihydropyridine-sensitive Ca2+ channels by glucose metabolism in mouse pancreatic β -cells. *Nature*, *342*(6249), 550–553. https://doi.org/10.1038/342550a0

Snutch, T. P., Tomlinson, W., Leonard, J. P., & Gilbert, M. M. (1991). Distinct calcium channels are generated by alternative splicing and are differentially expressed in the mammalian CNS. *Neuron*, *7*(1), 45–57. https://doi.org/10.1016/0896-6273(91)90073-9

Soldatov, N. M. (2012). Molecular Determinants of Cav1.2 Calcium Channel Inactivation. *ISRN Molecular Biology*, *2012*, 1–10. https://doi.org/10.5402/2012/691341

SPÄT, A., & HUNYADY, L. (2004). Control of Aldosterone Secretion: A Model for Convergence in Cellular Signaling Pathways. *Physiological Reviews*, *84*(2), 489–539. https://doi.org/10.1152/physrev.00030.2003

Spedding, M. (1982). Assessment of "Ca2+-antagonist" effects of drugs in K+-depolarized smooth muscle. *Naunyn-Schmiedeberg's Archives of Pharmacology*, *318*(3), 234–240. https://doi.org/10.1007/bf00500485

Splawski, I., Timothy, K. W., Decher, N., Kumar, P., Sachse, F. B., Beggs, A. H., Sanguinetti, M. C., & Keating, M. T. (2005). Severe arrhythmia disorder caused by cardiac L-type calcium channel mutations. *Proceedings of the National Academy of Sciences*, *102*(23), 8089–8096. https://doi.org/10.1073/pnas.0502506102

Splawski, I., Timothy, K. W., Sharpe, L. M., Decher, N., Kumar, P., Bloise, R., Napolitano, C., Schwartz, P. J., Joseph, R. M., Condouris, K., Tager-Flusberg, H., Priori, S. G., Sanguinetti, M. C., & Keating, M. T. (2004). CaV1.2 Calcium Channel Dysfunction Causes a Multisystem Disorder Including Arrhythmia and Autism. *Cell*, *119*(1), 19–31. https://doi.org/10.1016/j.cell.2004.09.011

Stein, D. T., Stevenson, B. E., Chester, M. W., Basit, M., Daniels, M. B., Turley, S. D., & McGarry, J. D. (1997). The insulinotropic potency of fatty acids is influenced profoundly by their chain length and degree of saturation. *Journal of Clinical Investigation*, *100*(2), 398–403. https://doi.org/10.1172/jci119546

Stephens, R. F., Guan, W., Zhorov, B. S., & Spafford, J. D. (2015). Selectivity filters and cysteine-rich extracellular loops in voltage-gated sodium, calcium, and NALCN channels. *Frontiers in Physiology*, *6*. https://doi.org/10.3389/fphys.2015.00153

Stotz, S. C., Hamid, J., Spaetgens, R. L., Jarvis, S. E., & Zamponi, G. W. (2000). Fast Inactivation of Voltage-dependent Calcium Channels. *Journal of Biological Chemistry*, *275*(32), 24575–24582. https://doi.org/10.1074/jbc.m000399200

Stotz, S., Spaetgens, R., & Zamponi, G. (2000). Block of Voltage-dependent Calcium Channel by the Green Mamba Toxin Calcicludine. *Journal of Membrane Biology*, *174*(2), 157–165. https://doi.org/10.1007/s002320001040

Striessnig, J., Bolz, H. J., & Koschak, A. (2010). Channelopathies in Cav1.1, Cav1.3, and Cav1.4 voltage-gated L-type Ca2+ channels. *Pflügers Archiv - European Journal of Physiology*, *460*(2), 361–374. https://doi.org/10.1007/s00424-010-0800-x

Strom, T. M., Nyakatura, G., Apfelstedt-Sylla, E., Hellebrand, H., Lorenz, B., Weber, B. H. F., Wutz, K., Gutwillinger, N., Rüther, K., Drescher, B., Sauer, C., Zrenner, E., Meitinger, T., Rosenthal, A., & Meindl, A. (1998). An L-type calcium-channel gene mutated in incomplete X-linked congenital stationary night blindness. *Nature Genetics*, *19*(3), 260–263. https://doi.org/10.1038/940

Strübing, C., Hering, S., & Glossmann, H. (1993). Evidence for an external location of the dihydropyridine agonist receptor site on smooth muscle and skeletal muscle calcium channels. *British Journal of Pharmacology*, *108*(4), 884–891. https://doi.org/10.1111/j.1476-5381.1993.tb13482.x

STRYDOM, D. J. (1977). Snake Venom Toxins. The Amino-Acid Sequence of a Short-Neurotoxin Homologue from Dendroaspis polylepis polylepis (Black Mamba) Venom. *European Journal of Biochemistry*, *76*(1), 99–106. https://doi.org/10.1111/j.1432-1033.1977.tb11574.x

Stühmer, W., Conti, F., Suzuki, H., Wang, X., Noda, M., Yahagi, N., Kubo, H., & Numa, S. (1989). Structural parts involved in activation and inactivation of the sodium channel. *Nature*, *339*(6226), 597–603. https://doi.org/10.1038/339597a0

Substance Abuse and Mental Health Services Administration (SAMHSA) & U.S. Department of Health and Human Services (HHS). (2020). *Key Substance Use and Mental Health Indicators in the United States: Results from the 2019 National Survey on Drug Use and Health* (HHS Publication No. PEP20-07-01-001, NSDUH Series H-55). Rockville, MD: Center for Behavioral Health Statistics and Quality, Substance Abuse and Mental Health Services Administration. http://www.samhsa.org/data/

Südhof, T. (2012). The Presynaptic Active Zone. *Neuron*, *75*(1), 11–25. https://doi.org/10.1016/j.neuron.2012.06.012

Südhof, T. (2013). Neurotransmitter Release: The Last Millisecond in the Life of a Synaptic Vesicle. *Neuron*, *80*(3), 675–690. https://doi.org/10.1016/j.neuron.2013.10.022

Sudhof, T. C. (2011). Calcium Control of Neurotransmitter Release. *Cold Spring Harbor Perspectives in Biology*, *4*(1), a011353. https://doi.org/10.1101/cshperspect.a011353

Sudhof, T. C., & Rothman, J. E. (2009). Membrane Fusion: Grappling with SNARE and SM Proteins. *Science*, *323*(5913), 474–477. https://doi.org/10.1126/science.1161748

Suh, B. C., & Hille, B. (2002). Recovery from Muscarinic Modulation of M Current Channels Requires Phosphatidylinositol 4,5-Bisphosphate Synthesis. *Neuron*, *35*(3), 507–520. https://doi.org/10.1016/s0896-6273(02)00790-0

Suh, B. C., & Hille, B. (2008). PIP2Is a Necessary Cofactor for Ion Channel Function:Howand Why? *Annual Review of Biophysics*, *37*(1), 175–195. https://doi.org/10.1146/annurev.biophys.37.032807.125859

Sulzer, D. (2007). Multiple hit hypotheses for dopamine neuron loss in Parkinson's disease. *Trends in Neurosciences*, *30*(5), 244–250. https://doi.org/10.1016/j.tins.2007.03.009

Sumoza-Toledo, A., & Penner, R. (2011). TRPM2: a multifunctional ion channel for calcium signalling. *The Journal of Physiology*, *589*(7), 1515–1525. https://doi.org/10.1113/jphysiol.2010.201855

Sun, J., Cui, J., He, Q., Chen, Z., Arvan, P., & Liu, M. (2015). Proinsulin misfolding and endoplasmic reticulum stress during the development and progression of diabetes. *Molecular Aspects of Medicine*, *42*, 105–118. https://doi.org/10.1016/j.mam.2015.01.001

Surmeier, D. J., Guzman, J. N., Sanchez-Padilla, J., & Goldberg, J. A. (2011). The Origins of Oxidant Stress in Parkinson's Disease and Therapeutic Strategies. *Antioxidants & Redox Signaling*, *14*(7), 1289–1301. https://doi.org/10.1089/ars.2010.3521

Surmeier, D., & Schumacker, P. T. (2013). Calcium, Bioenergetics, and Neuronal Vulnerability in Parkinson's Disease. *Journal of Biological Chemistry*, *288*(15), 10736–10741. https://doi.org/10.1074/jbc.r112.410530

Sutton, K. G., Siok, C., Stea, A., Zamponi, G. W., Heck, S. D., Volkmann, R. A., Ahlijanian, M. K., & Snutch, T. P. (1998). Inhibition of Neuronal Calcium Channels by a Novel Peptide Spider Toxin, DW13.3. *Molecular Pharmacology*, *54*(2), 407–418. https://doi.org/10.1124/mol.54.2.407

Takahashi, M., Seagar, M. J., Jones, J. F., Reber, B. F., & Catterall, W. A. (1987). Subunit structure of dihydropyridine-sensitive calcium channels from skeletal muscle. *Proceedings of the National Academy of Sciences*, *84*(15), 5478–5482. https://doi.org/10.1073/pnas.84.15.5478

Takeshima, H., Nishimura, S., Matsumoto, T., Ishida, H., Kangawa, K., Minamino, N., Matsuo, H., Ueda, M., Hanaoka, M., Hirose, T., & Numa, S. (1989). Primary structure and expression from complementary DNA of skeletal muscle ryanodine receptor. *Nature*, *339*(6224), 439–445. https://doi.org/10.1038/339439a0

Talavera, K., Staes, M., Janssens, A., Klugbauer, N., Droogmans, G., Hofmann, F., & Nilius, B. (2001). Aspartate Residues of the Glu-Glu-Asp-Asp (EEDD) Pore Locus Control Selectivity and Permeation of the T-type Ca2+Channel α1G. *Journal of Biological Chemistry*, *276*(49), 45628–45635. https://doi.org/10.1074/jbc.m103047200

Tan, G. M. Y., Yu, D., Wang, J., & Soong, T. W. (2012). Alternative Splicing at C Terminus of CaV1.4 Calcium Channel Modulates Calcium-dependent Inactivation, Activation Potential, and Current Density. *Journal of Biological Chemistry*, *287*(2), 832–847. https://doi.org/10.1074/jbc.m111.268722

Tanabe, T., Takeshima, H., Mikami, A., Flockerzi, V., Takahashi, H., Kangawa, K., Kojima, M., Matsuo, H., Hirose, T., & Numa, S. (1987). Primary structure of the receptor for calcium channel blockers from skeletal muscle. *Nature*, *328*(6128), 313–318. https://doi.org/10.1038/328313a0

Tang, L., Gamal El-Din, T. M., Payandeh, J., Martinez, G. Q., Heard, T. M., Scheuer, T., Zheng, N., & Catterall, W. A. (2013). Structural basis for Ca2+ selectivity of a voltage-gated calcium channel. *Nature*, *505*(7481), 56–61. https://doi.org/10.1038/nature12775

Tang, L., Gamal El-Din, T. M., Swanson, T. M., Pryde, D. C., Scheuer, T., Zheng, N., & Catterall, W. A. (2016). Structural basis for inhibition of a voltage-gated Ca2+ channel by Ca2+ antagonist drugs. *Nature*, *537*(7618), 117–121. https://doi.org/10.1038/nature19102

Tang, S., Mikala, G., Bahinski, A., Yatani, A., Varadi, G., & Schwartz, A. (1993). Molecular localization of ion selectivity sites within the pore of a human L-type cardiac calcium channel. *Journal of Biological Chemistry*, *268*(18), 13026–13029. https://doi.org/10.1016/s0021-9258(19)38613-2

Tao, X., Finkbeiner, S., Arnold, D. B., Shaywitz, A. J., & Greenberg, M. E. (1998). Ca2+ Influx Regulates BDNF Transcription by a CREB Family Transcription Factor-Dependent Mechanism. *Neuron*, *20*(4), 709–726. https://doi.org/10.1016/s0896-6273(00)81010-7

Taplin, C. E., & Barker, J. M. (2008). Autoantibodies in type 1 diabetes. *Autoimmunity*, *41*(1), 11–18. https://doi.org/10.1080/08916930701619169

Tarasov, A. I., Griffiths, E. J., & Rutter, G. A. (2012). Regulation of ATP production by mitochondrial Ca2+. *Cell Calcium*, *52*(1), 28–35. https://doi.org/10.1016/j.ceca.2012.03.003

Tareilus, E., Roux, M., Qin, N., Olcese, R., Zhou, J., Stefani, E., & Birnbaumer, L. (1997). A Xenopus oocyte subunit: Evidence for a role in the assembly/expression of voltage-gated calcium channels that is separate from its role as a regulatory subunit. *Proceedings of the National Academy of Sciences*, *94*(5), 1703–1708. https://doi.org/10.1073/pnas.94.5.1703

Taylor, C. W., da Fonseca, P. C., & Morris, E. P. (2004). IP3 receptors: the search for structure. *Trends in Biochemical Sciences*, *29*(4), 210–219. https://doi.org/10.1016/j.tibs.2004.02.010

Taylor, J., Pereyra, A., Zhang, T., Messi, M. L., Wang, Z. M., Hereñú, C., Kuan, P. F., & Delbono, O. (2014). The Cavβ1a subunit regulates gene expression and suppresses myogenin in muscle progenitor cells. *Journal of Cell Biology*, *205*(6), 829–846. https://doi.org/10.1083/jcb.201403021

Tenti, G., Parada, E., León, R., Egea, J., Martínez-Revelles, S., Briones, A. M., Sridharan, V., López, M. G., Ramos, M. T., & Menéndez, J. C. (2014). New 5-Unsubstituted Dihydropyridines with Improved CaV1.3 Selectivity as Potential Neuroprotective Agents against Ischemic Injury. *Journal of Medicinal Chemistry*, *57*(10), 4313–4323. https://doi.org/10.1021/jm500263v

Tersey, S. A., Nishiki, Y., Templin, A. T., Cabrera, S. M., Stull, N. D., Colvin, S. C., Evans-Molina, C., Rickus, J. L., Maier, B., & Mirmira, R. G. (2012). Islet -Cell Endoplasmic Reticulum Stress Precedes the Onset of Type 1 Diabetes in the Nonobese Diabetic Mouse Model. *Diabetes*, *61*(4), 818–827. https://doi.org/10.2337/db11-1293

Teyra, J., Huang, H., Jain, S., Guan, X., Dong, A., Liu, Y., Tempel, W., Min, J., Tong, Y., Kim, P. M., Bader, G. D., & Sidhu, S. S. (2017). Comprehensive Analysis of the Human SH3 Domain Family Reveals a Wide Variety of Non-canonical Specificities. *Structure*, *25*(10), 1598–1610.e3. https://doi.org/10.1016/j.str.2017.07.017

Thorens, B., Weir, G. C., Leahy, J. L., Lodish, H. F., & Bonner-Weir, S. (1990). Reduced expression of the liver/beta-cell glucose transporter isoform in glucose-insensitive pancreatic beta cells of diabetic rats. *Proceedings of the National Academy of Sciences*, *87*(17), 6492–6496. https://doi.org/10.1073/pnas.87.17.6492

Tikhonov, D. B., & Zhorov, B. S. (2009). Structural Model for Dihydropyridine Binding to L-type Calcium Channels. *Journal of Biological Chemistry*, *284*(28), 19006–19017. https://doi.org/10.1074/jbc.m109.011296

Tikhonov, D. B., & Zhorov, B. S. (2020). Molecular Modeling in Studies of Ion Channels and their Modulation by Ligands. *Neuroscience and Behavioral Physiology*, *50*(7), 928–937. https://doi.org/10.1007/s11055-020-00987-y

Tong, X., Kono, T., & Evans-Molina, C. (2015). Nitric oxide stress and activation of AMP-activated protein kinase impair β-cell sarcoendoplasmic reticulum calcium ATPase 2b activity and protein stability. *Cell Death & Disease*, *6*(6), e1790. https://doi.org/10.1038/cddis.2015.154

Trinquet, E., Bouhelal, R., & Dietz, M. (2011). Monitoring Gq-coupled receptor response through inositol phosphate quantification with the IP-One assay. *Expert Opinion on Drug Discovery*, *6*(10), 981–994. https://doi.org/10.1517/17460441.2011.608658

Trube, G., Rorsman, P., & Ohno-Shosaku, T. (1986). Opposite effects of tolbutamide and diazoxide on the ATP-dependent K+ channel in mouse pancreatic beta-cells. *Pflugers Archiv European Journal of Physiology*, *407*(5), 493–499. https://doi.org/10.1007/bf00657506

Tsien, R., Lipscombe, D., Madison, D., Bley, K., & Fox, A. (1988). Multiple types of neuronal calcium channels and their selective modulation. *Trends in Neurosciences*, *11*(10), 431–438. https://doi.org/10.1016/0166-2236(88)90194-4

Tuluc, P., Benedetti, B., Coste de Bagneaux, P., Grabner, M., & Flucher, B. E. (2016). Two distinct voltage-sensing domains control voltage sensitivity and kinetics of current activation in CaV1.1 calcium channels. *Journal of General Physiology*, *147*(6), 437–449. https://doi.org/10.1085/jgp.201611568

Tuluc, P., Yarov-Yarovoy, V., Benedetti, B., & Flucher, B. (2016). Molecular Interactions in the Voltage Sensor Controlling Gating Properties of Ca V Calcium Channels. *Structure*, *24*(2), 261–271. https://doi.org/10.1016/j.str.2015.11.011

Uhrig, S., Vandael, D., Marcantoni, A., Dedic, N., Bilbao, A., Vogt, M. A., Hirth, N., Broccoli, L., Bernardi, R. E., Schönig, K., Gass, P., Bartsch, D., Spanagel, R., Deussing, J. M., Sommer, W. H., Carbone, E., & Hansson, A. C. (2016). Differential Roles for L-Type Calcium Channel Subtypes in Alcohol Dependence. *Neuropsychopharmacology*, *42*(5), 1058–1069. https://doi.org/10.1038/npp.2016.266

Van Petegem, F., Clark, K. A., Chatelain, F. C., & Minor, D. L. (2004). Structure of a complex between a voltage-gated calcium channel β-subunit and an α-subunit domain. *Nature*, *429*(6992), 671–675. https://doi.org/10.1038/nature02588

Vandael, D. H. F., Zuccotti, A., Striessnig, J., & Carbone, E. (2012). CaV1.3-Driven SK Channel Activation Regulates Pacemaking and Spike Frequency Adaptation in Mouse Chromaffin Cells. *Journal of Neuroscience*, *32*(46), 16345–16359. https://doi.org/10.1523/jneurosci.3715-12.2012

Vandael, D. H., Marcantoni, A., Mahapatra, S., Caro, A., Ruth, P., Zuccotti, A., Knipper, M., & Carbone, E. (2010). Cav1.3 and BK Channels for Timing and Regulating Cell Firing. *Molecular Neurobiology*, *42*(3), 185–198. https://doi.org/10.1007/s12035-010-8151-3

Vandael, D., Mahapatra, S., Calorio, C., Marcantoni, A., & Carbone, E. (2013). Cav1.3 and Cav1.2 channels of adrenal chromaffin cells: Emerging views on cAMP/cGMP-mediated phosphorylation and role in pacemaking. *Biochimica et Biophysica Acta (BBA) - Biomembranes*, *1828*(7), 1608–1618. https://doi.org/10.1016/j.bbamem.2012.11.013

Varadi, G., Strobeck, M., Koch, S., Caglioti, L., Zucchi, C., & Palyi, G. (1999). Molecular Elements of Ion Permeation and Selectivity within Calcium Channels. *Critical Reviews in Biochemistry and Molecular Biology*, *34*(3), 181–214. https://doi.org/10.1080/10409239991209264

Varnai, P., Thyagarajan, B., Rohacs, T., & Balla, T. (2006). Rapidly inducible changes in phosphatidylinositol 4,5-bisphosphate levels influence multiple regulatory functions of the lipid in intact living cells. *Journal of Cell Biology*, *175*(3), 377–382. https://doi.org/10.1083/jcb.200607116

Varodayan, F. P., de Guglielmo, G., Logrip, M. L., George, O., & Roberto, M. (2017). Alcohol Dependence Disrupts Amygdalar L-Type Voltage-Gated Calcium Channel Mechanisms. *The Journal of Neuroscience*, *37*(17), 4593–4603. https://doi.org/10.1523/jneurosci.3721-16.2017

VASSEUR, M., DEBUYSER, A., & JOFFRE, M. (1987). SENSITIVITY OF PANCREATIC BETA CELL TO CALCIUM CHANNEL BLOCKERS. AN ELECTROPHYSIOLOGIC STUDY OF VERAPAMIL AND NIFEDIPINE. *Fundamental & Clinical Pharmacology*, *1*(2), 95–113. https://doi.org/10.1111/j.1472-8206.1987.tb00549.x

Velasco, J., Petersen, J., & Petersen, O. (1988). Single-channel Ba2+ currents in insulin-secreting cells are activated by glyceraldehyde stimulation. *FEBS Letters*, *231*(2), 366–370. https://doi.org/10.1016/0014-5793(88)80851-2

Verapamil. (2020). Drugs.Com. https://www.drugs.com/monograph/verapamil.html

Vervliet, T. (2018). Ryanodine Receptors in Autophagy: Implications for Neurodegenerative Diseases? *Frontiers in Cellular Neuroscience*, *12*. https://doi.org/10.3389/fncel.2018.00089

Vest, J. A., Wehrens, X. H., Reiken, S. R., Lehnart, S. E., Dobrev, D., Chandra, P., Danilo, P., Ravens, U., Rosen, M. R., & Marks, A. R. (2005). Defective Cardiac Ryanodine Receptor Regulation During Atrial Fibrillation. *Circulation*, *111*(16), 2025–2032. https://doi.org/10.1161/01.cir.0000162461.67140.4c

Viard, P., Butcher, A. J., Halet, G., Davies, A., Nürnberg, B., Heblich, F., & Dolphin, A. C. (2004). PI3K promotes voltage-dependent calcium channel trafficking to the plasma membrane. *Nature Neuroscience*, *7*(9), 939–946. https://doi.org/10.1038/nn1300

Vierra, N. C., Dadi, P. K., Jeong, I., Dickerson, M., Powell, D. R., & Jacobson, D. A. (2015). Type 2 Diabetes–Associated K+Channel TALK-1 Modulates β-Cell Electrical Excitability, Second-Phase Insulin Secretion, and Glucose Homeostasis. *Diabetes*, *64*(11), 3818–3828. https://doi.org/10.2337/db15-0280

Vollmer, K., Holst, J. J., Baller, B., Ellrichmann, M., Nauck, M. A., Schmidt, W. E., & Meier, J. J. (2007). Predictors of Incretin Concentrations in Subjects With Normal, Impaired, and Diabetic Glucose Tolerance. *Diabetes*, *57*(3), 678–687. https://doi.org/10.2337/db07-1124

W. (2021). *Ross and Wilson Anatomy and Physiology in Health and Illness (IE) -13E* (13th ed.). ELSEVIER.

Wahl-Schott, C., Baumann, L., Cuny, H., Eckert, C., Griessmeier, K., & Biel, M. (2006). Switching off calcium-dependent inactivation in L-type calcium channels by an autoinhibitory domain. *Proceedings of the National Academy of Sciences*, *103*(42), 15657–15662. https://doi.org/10.1073/pnas.0604621103

Walker, D., Bichet, D., Campbell, K. P., & De Waard, M. (1998). A β4 Isoform-specific Interaction Site in the Carboxyl-terminal Region of the Voltage-dependent Ca2+ Channel α1A Subunit. *Journal of Biological Chemistry*, *273*(4), 2361–2367. https://doi.org/10.1074/jbc.273.4.2361

Walker, D., Bichet, D., Geib, S., Mori, E., Cornet, V., Snutch, T. P., Mori, Y., & De Waard, M. (1999). A New β Subtype-specific Interaction in α1ASubunit Controls P/Q-type Ca2+ Channel Activation. *Journal of Biological Chemistry*, *274*(18), 12383–12390. https://doi.org/10.1074/jbc.274.18.12383

Walker, D., & De Waard, M. (1998). Subunit interaction sites in voltage-dependent Ca2+ channels: role in channel function. *Trends in Neurosciences*, *21*(4), 148–154. https://doi.org/10.1016/s0166-2236(97)01200-9

Wang, C. Y., Lai, M. D., Phan, N. N., Sun, Z., & Lin, Y. C. (2015). Meta-Analysis of Public Microarray Datasets Reveals Voltage-Gated Calcium Gene Signatures in Clinical Cancer Patients. *PLOS ONE*, *10*(7), e0125766. https://doi.org/10.1371/journal.pone.0125766

Wang, S. P., Wang, J. A., Luo, R. H., Cui, W. Y., & Wang, H. (2008). POTASSIUM CHANNEL CURRENTS IN RAT MESENCHYMAL STEM CELLS AND THEIR POSSIBLE ROLES IN CELL PROLIFERATION. *Clinical and Experimental Pharmacology and Physiology*, *35*(9), 1077–1084. https://doi.org/10.1111/j.1440-1681.2008.04964.x

Wang, W., & MacKinnon, R. (2017). Cryo-EM Structure of the Open Human Ether-à-go-go - Related K + Channel hERG. *Cell*, *169*(3), 422–430.e10. https://doi.org/10.1016/j.cell.2017.03.048

Wang, X., Du, L., & Peterson, B. Z. (2007). Calcicludine Binding to the Outer Pore of L-type Calcium Channels Is Allosterically Coupled to Dihydropyridine Binding. *Biochemistry*, *46*(25), 7590–7598. https://doi.org/10.1021/bi7001696

Wang, Y. (2015). *The L-type voltage-gated calcium channels: The role of Cav1.2 in pancreatic B cells and new perspective on the molecular pharmacology of Cav1.3* (Vol. 3734169). Purdue University, ProQuest Dissertations Publishing.

Wang, Y., Jarrard, R. E., Pratt, E. P., Guerra, M. L., Salyer, A. E., Lange, A. M., Soderling, I. M., & Hockerman, G. H. (2014). Uncoupling of Cav1.2 From Ca2+-Induced Ca2+Release and SK Channel Regulation in Pancreatic β-Cells. *Molecular Endocrinology*, *28*(4), 458–476. https://doi.org/10.1210/me.2013-1094

Wang, Y., Tang, S., Harvey, K. E., Salyer, A. E., Li, T. A., Rantz, E. K., Lill, M. A., & Hockerman, G. H. (2018). Molecular Determinants of the Differential Modulation of Cav1.2 and Cav1.3 by Nifedipine and FPL 64176. *Molecular Pharmacology*, *94*(3), 973–983. https://doi.org/10.1124/mol.118.112441

Wasserstrom, J. A., Wasserstrom, L. A., Lokuta, A. J., Kelly, J. E., Reddy, S. T., & Frank, A. J. (2002). Activation of cardiac ryanodine receptors by the calcium channel agonist FPL-64176. *American Journal of Physiology-Heart and Circulatory Physiology*, *283*(1), H331–H338. https://doi.org/10.1152/ajpheart.00788.2001

Watanabe, T. X., Itahara, Y., Kuroda, H., Chen, Y. N., Kimura, T., & Sakakibara, S. (1995). Smooth Muscle Relaxing and Hypotensive Activities of Synthetic Calciseptine and the Homologous Snake Venom Peptide FS2. *Japanese Journal of Pharmacology*, *68*(3), 305–315. https://doi.org/10.1254/jjp.68.305

Waterhouse, A., Bertoni, M., Bienert, S., Studer, G., Tauriello, G., Gumienny, R., Heer, F. T., de Beer, T. A., Rempfer, C., Bordoli, L., Lepore, R., & Schwede, T. (2018). SWISS-MODEL: homology modelling of protein structures and complexes. *Nucleic Acids Research*, *46*(W1), W296–W303. https://doi.org/10.1093/nar/gky427

Wei, R., Wang, X., Zhang, Y., Mukherjee, S., Zhang, L., Chen, Q., Huang, X., Jing, S., Liu, C., Li, S., Wang, G., Xu, Y., Zhu, S., Williams, A. J., Sun, F., & Yin, C. C. (2016). Structural insights into Ca2+-activated long-range allosteric channel gating of RyR1. *Cell Research*, *26*(9), 977–994. https://doi.org/10.1038/cr.2016.99

Wei, X., Neely, A., Lacerda, A., Olcese, R., Stefani, E., Perez-Reyes, E., & Birnbaumer, L. (1994). Modification of Ca2+ channel activity by deletions at the carboxyl terminus of the cardiac alpha 1 subunit. *Journal of Biological Chemistry*, *269*(3), 1635–1640. https://doi.org/10.1016/s0021-9258(17)42074-6

Weiser, A., Feige, J. N., & De Marchi, U. (2021). Mitochondrial Calcium Signaling in Pancreatic β-Cell. *International Journal of Molecular Sciences*, *22*(5), 2515. https://doi.org/10.3390/ijms22052515

Weiss, S., Keren-Raifman, T., Oz, S., Ben-Mocha, A., Haase, H., & Dascal, N. (2012). Modulation of distinct isoforms of L-type calcium channels by Gq-coupled receptors in Xenopus oocytes. *Channels*, *6*(6), 426–437. https://doi.org/10.4161/chan.22016

Weisskopf, M. G., Bauer, E. P., & LeDoux, J. E. (1999). L-Type Voltage-Gated Calcium Channels Mediate NMDA-Independent Associative Long-Term Potentiation at Thalamic Input Synapses to the Amygdala. *The Journal of Neuroscience*, *19*(23), 10512–10519. https://doi.org/10.1523/jneurosci.19-23-10512.1999

Westenbroek, R. E., Hell, J. W., Warner, C., Dubel, S. J., Snutch, T. P., & Catterall, W. A. (1992). Biochemical properties and subcellular distribution of an N-type calcium hannel α1 subunit. *Neuron*, *9*(6), 1099–1115. https://doi.org/10.1016/0896-6273(92)90069-p

Western blot sample preparation | Abcam. (2021, June 7). Abcam. https://www.abcam.com/protocols/sample-preparation-for-western-blot#lysis-buffer

Wheeler, D., Groth, R., Ma, H., Barrett, C., Owen, S., Safa, P., & Tsien, R. (2012). CaV1 and CaV2 Channels Engage Distinct Modes of Ca2+ Signaling to Control CREB-Dependent Gene Expression. *Cell*, *149*(5), 1112–1124. https://doi.org/10.1016/j.cell.2012.03.041

Whittaker, C. A., & Hynes, R. O. (2002). Distribution and Evolution of von Willebrand/Integrin A Domains: Widely Dispersed Domains with Roles in Cell Adhesion and Elsewhere. *Molecular Biology of the Cell*, *13*(10), 3369–3387. https://doi.org/10.1091/mbc.e02-05-0259

Williams, A. J., Thomas, N. L., & George, C. H. (2018). The ryanodine receptor: advances in structure and organization. *Current Opinion in Physiology*, *1*, 1–6. https://doi.org/10.1016/j.cophys.2017.10.003

Wiser, O., Trus, M., Hernandez, A., Renstrom, E., Barg, S., Rorsman, P., & Atlas, D. (1999). The voltage sensitive Lc-type Ca2+ channel is functionally coupled to the exocytotic machinery. *Proceedings of the National Academy of Sciences*, *96*(1), 248–253. https://doi.org/10.1073/pnas.96.1.248

Wong, A. K. C., Capitanio, P., Lissandron, V., Bortolozzi, M., Pozzan, T., & Pizzo, P. (2013). Heterogeneity of Ca2+ handling among and within Golgi compartments. *Journal of Molecular Cell Biology*, *5*(4), 266–276. https://doi.org/10.1093/jmcb/mjt024

Wu, J., Yan, Z., Li, Z., Qian, X., Lu, S., Dong, M., Zhou, Q., & Yan, N. (2016). Structure of the voltage-gated calcium channel Cav1.1 at 3.6 Å resolution. *Nature*, *537*(7619), 191–196. https://doi.org/10.1038/nature19321

Wu, J., Yan, Z., Li, Z., Yan, C., Lu, S., Dong, M., & Yan, N. (2015). Structure of the voltage-gated calcium channel Cav1.1 complex. *Science*, *350*(6267), aad2395. https://doi.org/10.1126/science.aad2395

Wu, L., Bauer, C. S., Zhen, X. G., Xie, C., & Yang, J. (2002). Dual regulation of voltage-gated calcium channels by PtdIns(4,5)P2. *Nature*, *419*(6910), 947–952. https://doi.org/10.1038/nature01118

Wyatt, C. N., Page, K. M., Berrow, N. S., Brice, N. L., & Dolphin, A. C. (1998). The effect of overexpression of auxiliary Ca2+channel subunits on native Ca2+channel currents in undifferentiated mammalian NG108-15 cells. *The Journal of Physiology*, *510*(2), 347–360. https://doi.org/10.1111/j.1469-7793.1998.347bk.x

Xie, C., Zhen, X. G., & Yang, J. (2005). Localization of the Activation Gate of a Voltage-gated Ca2+ Channel. *Journal of General Physiology*, *126*(3), 205–212. https://doi.org/10.1085/jgp.200509293

Xie, L., Dolai, S., Kang, Y., Liang, T., Xie, H., Qin, T., Yang, L., Chen, L., & Gaisano, H. Y. (2016). Syntaxin-3 Binds and Regulates Both R- and L-Type Calcium Channels in Insulin-Secreting INS-1 832/13 Cells. *PLOS ONE*, *11*(2), e0147862. https://doi.org/10.1371/journal.pone.0147862

Xu, L., Li, D., Tao, L., Yang, Y., Li, Y., & Hou, T. (2016). Binding mechanisms of 1,4-dihydropyridine derivatives to L-type calcium channel Cav1.2: a molecular modeling study. *Molecular BioSystems*, *12*(2), 379–390. https://doi.org/10.1039/c5mb00781j

Xu, W., & Lipscombe, D. (2001). Neuronal CaV1.3α1L-Type Channels Activate at Relatively Hyperpolarized Membrane Potentials and Are Incompletely Inhibited by Dihydropyridines. *The Journal of Neuroscience*, *21*(16), 5944–5951. https://doi.org/10.1523/jneurosci.21-16-05944.2001

Yamada, N., Makino, Y., Clark, R. A., Pearson, D. W., Mattei, M. G., Guénet, J. L., Ohama, E., Fujino, I., Miyawaki, A., Furuichi, T., & MIKOSHIBA, K. (1994). Human inositol 1,4,5-trisphosphate type-1 receptor, InsP3R1: structure, function, regulation of expression and chromosomal localization. *Biochemical Journal*, *302*(3), 781–790. https://doi.org/10.1042/bj3020781

Yamada, T., McGeer, P., Baimbridge, K., & McGeer, E. (1990). Relative sparing in Parkinson's disease of substantia nigra dopamine neurons containing calbindin-D28K. *Brain Research*, *526*(2), 303–307. https://doi.org/10.1016/0006-8993(90)91236-a

Yamaguchi, S., Okamura, Y., Nagao, T., & Adachi-Akahane, S. (2000). Serine Residue in the IIIS5-S6 Linker of the L-type Ca2+ Channel α1C Subunit Is the Critical Determinant of the Action of Dihydropyridine Ca2+Channel Agonists. *Journal of Biological Chemistry*, *275*(52), 41504–41511. https://doi.org/10.1074/jbc.m007165200

Yamaguchi, S., Zhorov, B. S., Yoshioka, K., Nagao, T., Ichijo, H., & Adachi-Akahane, S. (2003). Key Roles of Phe1112 and Ser1115 in the Pore-Forming IIIS5-S6 Linker of L-Type Ca2+ Channel α1C Subunit (CaV 1.2) in Binding of Dihydropyridines and Action of Ca2+ Channel Agonists. *Molecular Pharmacology*, *64*(2), 235–248. https://doi.org/10.1124/mol.64.2.235

Yamakage, M., & Namiki, A. (2002). Calcium channels — basic aspects of their structure, function and gene encoding; anesthetic action on the channels — a review. *Canadian Journal of Anesthesia/Journal Canadien d'anesthésie*, *49*(2), 151–164. https://doi.org/10.1007/bf03020488

Yamamoto, W. R., Bone, R. N., Sohn, P., Syed, F., Reissaus, C. A., Mosley, A. L., Wijeratne, A. B., True, J. D., Tong, X., Kono, T., & Evans-Molina, C. (2019). Endoplasmic reticulum stress alters ryanodine receptor function in the murine pancreatic β cell. *Journal of Biological Chemistry*, *294*(1), 168–181. https://doi.org/10.1074/jbc.ra118.005683

Yamamoto-Hino, M., Sugiyama, T., Hikichi, K., Mattei, M. G., Furuichi, T., Hasegawa, K., Sekine, S., Sakurada, K., Miyawaki, A., Furuichi, T., & Hasegawa, M. (1994). Cloning and characterization of human type 2 and type 3 inositol 1,4,5-trisphosphate receptors. *Recept Channels.*, *2*(1), 9–22. https://pubmed-ncbi-nlm-nih-gov.ezproxy.lib.purdue.edu/8081734/

Yan, Z., Bai, X. C., Yan, C., Wu, J., Li, Z., Xie, T., Peng, W., Yin, C. C., Li, X., Scheres, S. H. W., Shi, Y., & Yan, N. (2014). Structure of the rabbit ryanodine receptor RyR1 at near-atomic resolution. *Nature*, *517*(7532), 50–55. https://doi.org/10.1038/nature14063

Yan, Z., Zhou, Q., Wang, L., Wu, J., Zhao, Y., Huang, G., Peng, W., Shen, H., Lei, J., & Yan, N. (2017). Structure of the Na v 1.4-β1 Complex from Electric Eel. *Cell*, *170*(3), 470–482.e11. https://doi.org/10.1016/j.cell.2017.06.039

Yang, D., Shcheynikov, N., Zeng, W., Ohana, E., So, I., Ando, H., Mizutani, A., Mikoshiba, K., & Muallem, S. (2008). IRBIT coordinates epithelial fluid and HCO3–secretion by stimulating the transporters pNBC1 and CFTR in the murine pancreatic duct. *Journal of Clinical Investigation*. Published. https://doi.org/10.1172/jci36983

Yang, F., Ma, H., Butler, M. R., & Ding, X. (2020). Potential contribution of ryanodine receptor 2 upregulation to cGMP/PKG signaling-induced cone degeneration in cyclic nucleotide-gated channel deficiency. *The FASEB Journal*, *34*(5), 6335–6350. https://doi.org/10.1096/fj.201901951rr

Yang, G., Shi, Y., Yu, J., Li, Y., Yu, L., Welling, A., Hofmann, F., Striessnig, J., Juntti-Berggren, L., Berggren, P. O., & Yang, S. N. (2014). CaV1.2 and CaV1.3 channel hyperactivation in mouse islet β cells exposed to type 1 diabetic serum. *Cellular and Molecular Life Sciences*, *72*(6), 1197–1207. https://doi.org/10.1007/s00018-014-1737-6

Yang, H., Yu, Y., Hu, X., Wang, W., Yang, X., Liu, H., Ren, L., Zhang, X., Feng, X., & Liu, L. (2020). Association Between the Overall Risk of Prostate Cancer and Use of Calcium Channel Blockers: A Systematic Review and Meta-analysis. *Clinical Therapeutics*, *42*(9), 1715–1727.e2. https://doi.org/10.1016/j.clinthera.2020.06.021

Yang, J., Elllnor, P. T., Sather, W. A., Zhang, J. F., & Tsien, R. W. (1993). Molecular determinants of Ca2+ selectivity and ion permeation in L-type Ca2+ channels. *Nature*, *366*(6451), 158–161. https://doi.org/10.1038/366158a0

Yang, L., Liu, G., Zakharov, S. I., Bellinger, A. M., Mongillo, M., & Marx, S. O. (2007). Protein Kinase G Phosphorylates Ca v 1.2 α 1c and β 2 Subunits. *Circulation Research*, *101*(5), 465–474. https://doi.org/10.1161/circresaha.107.156976

Yang, N., George, A. L., & Horn, R. (1996). Molecular Basis of Charge Movement in Voltage-Gated Sodium Channels. *Neuron*, *16*(1), 113–122. https://doi.org/10.1016/s0896-6273(00)80028-8

Yang, N., & Horn, R. (1995). Evidence for voltage-dependent S4 movement in sodium channels. *Neuron*, *15*(1), 213–218. https://doi.org/10.1016/0896-6273(95)90078-0

Yang, P. S., Alseikhan, B. A., Hiel, H., Grant, L., Mori, M. X., Yang, W., Fuchs, P. A., & Yue, D. T. (2006). Switching of Ca2+-Dependent Inactivation of CaV1.3 Channels by Calcium Binding Proteins of Auditory Hair Cells. *Journal of Neuroscience*, *26*(42), 10677–10689. https://doi.org/10.1523/jneurosci.3236-06.2006

Yang, S. N., & Berggren, P. O. (2005). β-Cell CaV channel regulation in physiology and pathophysiology. *American Journal of Physiology-Endocrinology and Metabolism*, *288*(1), E16–E28. https://doi.org/10.1152/ajpendo.00042.2004

Yang, S. N., & Berggren, P. O. (2006). The Role of Voltage-Gated Calcium Channels in Pancreatic β-Cell Physiology and Pathophysiology. *Endocrine Reviews*, *27*(6), 621–676. https://doi.org/10.1210/er.2005-0888

Yang, S. N., Larsson, O., Branstrom, R., Bertorello, A. M., Leibiger, B., Leibiger, I. B., Moede, T., Kohler, M., Meister, B., & Berggren, P. O. (1999). Syntaxin 1 interacts with the LD subtype of voltage-gated Ca2+ channels in pancreatic beta cells. *Proceedings of the National Academy of Sciences*, *96*(18), 10164–10169. https://doi.org/10.1073/pnas.96.18.10164

Yang, S. N., Shi, Y., Yang, G., Li, Y., Yu, J., & Berggren, P. O. (2014). Ionic mechanisms in pancreatic β cell signaling. *Cellular and Molecular Life Sciences*, *71*(21), 4149–4177. https://doi.org/10.1007/s00018-014-1680-6

Yarov-Yarovoy, V., DeCaen, P. G., Westenbroek, R. E., Pan, C. Y., Scheuer, T., Baker, D., & Catterall, W. A. (2011). Structural basis for gating charge movement in the voltage sensor of a sodium channel. *Proceedings of the National Academy of Sciences*, *109*(2), E93–E102. https://doi.org/10.1073/pnas.1118434109

Yasuda, O., Morimoto, S., Chen, Y., Jiang, B., Kimura, T., Sakakibara, S., Koh, E., Fukuo, K., Kitano, S., & Ogihara, T. (1993). Calciseptine Binding to a 1,4-Dihydropyridine Recognition Site of the L-Type Calcium Channel of Rat Synaptosomal Membranes. *Biochemical and Biophysical Research Communications*, *194*(2), 587–594. https://doi.org/10.1006/bbrc.1993.1862

Yasuda, O., Morimoto, S., Jiang, B., Kuroda, H., Kimura, T., Sakakibara, S., Fukuo, K., Chen, S., Tamatani, M., & Ogihara, T. (1994). FS2. a mamba venom toxin, is a specific blocker of the L-type calcium channels. *Artery*, *21*(5), 287–302. https://pubmed.ncbi.nlm.nih.gov/8826098/

Yasuda, T., Shibasaki, T., Minami, K., Takahashi, H., Mizoguchi, A., Uriu, Y., Numata, T., Mori, Y., Miyazaki, J. I., Miki, T., & Seino, S. (2010). Rim2α Determines Docking and Priming States in Insulin Granule Exocytosis. *Cell Metabolism*, *12*(2), 117–129. https://doi.org/10.1016/j.cmet.2010.05.017

Yen, H. Y., Hoi, K. K., Liko, I., Hedger, G., Horrell, M. R., Song, W., Wu, D., Heine, P., Warne, T., Lee, Y., Carpenter, B., Plückthun, A., Tate, C. G., Sansom, M., & Robinson, C. V. (2018). PtdIns(4,5)P_2 stabilizes active states of GPCRs and enhances selectivity of G-protein coupling. *Nature*, *559*(7714), 423–427. https://doi.org/10.1038/s41586-018-0325-6

Yosida, M., Dezaki, K., Uchida, K., Kodera, S., Lam, N. V., Ito, K., Rita, R. S., Yamada, H., Shimomura, K., Ishikawa, S. E., Sugawara, H., Kawakami, M., Tominaga, M., Yada, T., & Kakei, M. (2014). Involvement of cAMP/EPAC/TRPM2 Activation in Glucose- and Incretin-Induced Insulin Secretion. *Diabetes*, *63*(10), 3394–3403. https://doi.org/10.2337/db13-1868

Young, K., Lin, S., Sun, L., Lee, E., Modi, M., Hellings, S., Husbands, M., Ozenberger, B., & Franco, R. (1998a). Identification of a calcium channel modulator using a high throughput yeast two-hybrid screen. *Nature Biotechnology*, *16*(10), 946–950. https://doi.org/10.1038/nbt1098-946

Young, K., Lin, S., Sun, L., Lee, E., Modi, M., Hellings, S., Husbands, M., Ozenberger, B., & Franco, R. (1998b). Identification of a calcium channel modulator using a high throughput yeast two-hybrid screen. *Nature Biotechnology*, *16*(10), 946–950. https://doi.org/10.1038/nbt1098-946

Yuan, Q., Yang, J., Santulli, G., Reiken, S. R., Wronska, A., Kim, M. M., Osborne, B. W., Lacampagne, A., Yin, Y., & Marks, A. R. (2016). Maintenance of normal blood pressure is dependent on IP3R1-mediated regulation of eNOS. *Proceedings of the National Academy of Sciences*, *113*(30), 8532–8537. https://doi.org/10.1073/pnas.1608859113

Yunker, A. M. R., & McEnery, M. W. (2003). Low-Voltage-Activated ("T-Type") Calcium Channels in Review. *Journal of Bioenergetics and Biomembranes*, *35*(6), 533–575. https://doi.org/10.1023/b:jobb.0000008024.77488.48

Zafra, F., Hengerer, B., Leibrock, J., Thoenen, H., & Lindholm, D. (1990). Activity dependent regulation of BDNF and NGF mRNAs in the rat hippocampus is mediated by non-NMDA glutamate receptors. *The EMBO Journal*, *9*(11), 3545–3550. https://doi.org/10.1002/j.1460-2075.1990.tb07564.x

Zagotta, W. N., Hoshi, T., & Aldrich, R. W. (1994). Shaker potassium channel gating. III: Evaluation of kinetic models for activation. *Journal of General Physiology*, *103*(2), 321–362. https://doi.org/10.1085/jgp.103.2.321

Zagotta, W. N., Hoshi, T., Dittman, J., & Aldrich, R. W. (1994). Shaker potassium channel gating. II: Transitions in the activation pathway. *Journal of General Physiology*, *103*(2), 279–319. https://doi.org/10.1085/jgp.103.2.279

Zalk, R., Clarke, O. B., des Georges, A., Grassucci, R. A., Reiken, S., Mancia, F., Hendrickson, W. A., Frank, J., & Marks, A. R. (2014). Structure of a mammalian ryanodine receptor. *Nature*, *517*(7532), 44–49. https://doi.org/10.1038/nature13950

Zamponi, G. W., Striessnig, J., Koschak, A., & Dolphin, A. C. (2015). The Physiology, Pathology, and Pharmacology of Voltage-Gated Calcium Channels and Their Future Therapeutic Potential. *Pharmacological Reviews*, *67*(4), 821–870. https://doi.org/10.1124/pr.114.009654

Zerangue, N., Schwappach, B., Jan, Y. N., & Jan, L. Y. (1999). A New ER Trafficking Signal Regulates the Subunit Stoichiometry of Plasma Membrane KATP Channels. *Neuron*, *22*(3), 537–548. https://doi.org/10.1016/s0896-6273(00)80708-4

Zhang, L., Liu, Y., Song, F., Zheng, H., Hu, L., Lu, H., Liu, P., Hao, X., Zhang, W., & Chen, K. (2011). Functional SNP in the microRNA-367 binding site in the 3'UTR of the calcium channel ryanodine receptor gene 3 (RYR3) affects breast cancer risk and calcification. *Proceedings of the National Academy of Sciences*, *108*(33), 13653–13658. https://doi.org/10.1073/pnas.1103360108

Zhang, M., Meng, X. Y., Cui, M., Pascal, J. M., Logothetis, D. E., & Zhang, J. F. (2014). Selective phosphorylation modulates the PIP2 sensitivity of the CaM–SK channel complex. *Nature Chemical Biology*, *10*(9), 753–759. https://doi.org/10.1038/nchembio.1592

Zhang, Q., Bengtsson, M., Partridge, C., Salehi, A., Braun, M., Cox, R., Eliasson, L., Johnson, P. R., Renström, E., Schneider, T., Berggren, P. O., Göpel, S., Ashcroft, F. M., & Rorsman, P. (2007). R-type Ca2+-channel-evoked CICR regulates glucose-induced somatostatin secretion. *Nature Cell Biology*, *9*(4), 453–460. https://doi.org/10.1038/ncb1563

Zhang, Q., Chibalina, M. V., Bengtsson, M., Groschner, L. N., Ramracheya, R., Rorsman, N. J. G., Leiss, V., Nassar, M. A., Welling, A., Gribble, F. M., Reimann, F., Hofmann, F., Wood, J. N., Ashcroft, F. M., & Rorsman, P. (2014). Na + current properties in islet α- and β-cells reflect cell-specific Scn3a and Scn9a expression. *The Journal of Physiology*, *592*(21), 4677–4696. https://doi.org/10.1113/jphysiol.2014.274209

Zhang, R., Dzhura, I., Grueter, C. E., Thiel, W., Colbran, R. J., & Anderson, M. E. (2005). A dynamic α-β inter-subunit agonist signaling complex is a novel feedback mechanism for regulating L-type Ca 2+ channel opening. *The FASEB Journal*, *19*(11), 1573–1575. https://doi.org/10.1096/fj.04-3283fje

Zhang, Y., Garcia, E., Sack, A. S., & Snutch, T. P. (2020). L-type calcium channel contributions to intrinsic excitability and synaptic activity during basolateral amygdala postnatal development. *Journal of Neurophysiology*, *123*(3), 1216–1235. https://doi.org/10.1152/jn.00606.2019

Zhao, Y., Huang, G., Wu, J., Wu, Q., Gao, S., Yan, Z., Lei, J., & Yan, N. (2019). Molecular Basis for Ligand Modulation of a Mammalian Voltage-Gated Ca2+ Channel. *Cell*, *177*(6), 1495–1506.e12. https://doi.org/10.1016/j.cell.2019.04.043

Zhao, Y., Yarov-Yarovoy, V., Scheuer, T., & Catterall, W. A. (2004). A Gating Hinge in Na+ Channels. *Neuron*, *41*(6), 859–865. https://doi.org/10.1016/s0896-6273(04)00116-3

Zheng, W., Rampe, D., & Triggle, D. J. (1991). Pharmacological, radioligand binding, and electrophysiological characteristics of FPL 64176, a novel nondihydropyridine Ca2+ channel activator, in cardiac and vascular preparations. *Mol Pharmacol*, *40*, 734–741. https://molpharm-aspetjournals-org.ezproxy.lib.purdue.edu/content/40/5/734.long

Zhong, H., Yokoyama, C. T., Scheuer, T., & Catterall, W. A. (1999). Reciprocal regulation of P/Q-type Ca2+ channels by SNAP-25, syntaxin and synaptotagmin. *Nature Neuroscience*, *2*(11), 939–941. https://doi.org/10.1038/14721

Zhou, Z., & Misler, S. (1995). Action Potential-induced Quantal Secretion of Catecholamines from Rat Adrenal Chromaffin Cells. *Journal of Biological Chemistry*, *270*(8), 3498–3505. https://doi.org/10.1074/jbc.270.8.3498

Zhu, J., Shang, Y., Xia, C., Wang, W., Wen, W., & Zhang, M. (2011). Guanylate kinase domains of the MAGUK family scaffold proteins as specific phospho-protein-binding modules. *The EMBO Journal*, *30*(24), 4986–4997. https://doi.org/10.1038/emboj.2011.428

Zubcevic, L., Bavro, V. N., Muniz, J. R., Schmidt, M. R., Wang, S., De Zorzi, R., Venien-Bryan, C., Sansom, M. S., Nichols, C. G., & Tucker, S. J. (2014). Control of KirBac3.1 Potassium Channel Gating at the Interface between Cytoplasmic Domains. *Journal of Biological Chemistry*, *289*(1), 143–151. https://doi.org/10.1074/jbc.m113.501833

Zuccotti, A., Clementi, S., Reinbothe, T., Torrente, A., Vandael, D. H., & Pirone, A. (2011). Structural and functional differences between L-type calcium channels: crucial issues for future selective targeting. *Trends in Pharmacological Sciences*, *32*(6), 366–375. https://doi.org/10.1016/j.tips.2011.02.012

Zühlke, R. D., Pitt, G. S., Deisseroth, K., Tsien, R. W., & Reuter, H. (1999). Calmodulin supports both inactivation and facilitation of L-type calcium channels. *Nature*, *399*(6732), 159–162. https://doi.org/10.1038/20200

Zühlke, R. D., Pitt, G. S., Tsien, R. W., & Reuter, H. (2000). Ca2+-sensitive Inactivation and Facilitation of L-type Ca2+ Channels Both Depend on Specific Amino Acid Residues in a Consensus Calmodulin-binding Motif in theα1C subunit. *Journal of Biological Chemistry*, *275*(28), 21121–21129. https://doi.org/10.1074/jbc.m002986200

VITA

Education

Purdue University, West Lafayette, IN

2016-present Ph.D. Candidate, Medicinal Chemistry & Molecular Pharmacology

2012-2016 Bachelor of Science, Pharmaceutics and Drug Design, College of Pharmacy

2014-2016 Bachelor of Science, Applied Statistics, College of Science, Purdue University

Research Experience

Purdue University, West Lafayette, IN

2016-present Graduate Research Assistant (Advisor: Dr. Gregory G. Hockerman)

Thesis title: Differentiation of the $Ca_v1.2$ and $Ca_v1.3$ pharmacology and role of RyR2 in pancreatic β-cell electrophysiology.

2014-2016 Undergraduate Research Assistant (Advisor: Dr. Richard M. van Rijn)

Project title: Identification of a novel interaction site of the delta-mu opioid receptor heteromers in relation to alcohol behaviors and chronic pain.

2013-2014 Undergraduate Research Assistant (Advisor: Dr. Nancy Pelaez)

Project title: Different ion fluxes and antioxidant quercetin effect on hog pulmonary contraction

Publications

1. **Tang S**, Wang Y, Hockerman G (2018). Molecular Determinants of the Differential Modulation of $Ca_v1.2$ and $Ca_v1.3$ by Nifedipine and FPL 64176. Mol Pharmacol. 2018 Sep;94(3):973-983.
2. **Tang S**, Sun Y, Hockerman G. Differentiated regulation of beta-3 subunit on L-type voltage-gated channel alpha-1 subunits at intracellular II-III loop. (in preparation.)
3. Alongkronrusmee D, **Tang S**, van Rijn RM. Identification of a novel interaction site of the delta-mu opioid receptor heteromers (in final preparation.)
4. Harvey K, Rantz E, **Tang S**, Hockerman G. RyR2 regulation insulin secretion, electrical activity, and IP3 receptor activation in INS-1 cells. (in final preparation)

Teaching & Mentoring Experience

Purdue University, West Lafayette, IN

2020-2021 Graduate Teaching Assistant, Examsoft

2018 Graduate Teaching Assistant, Therapeutics (PHRM 844)

2016 Graduate Teaching Assistant, Organic Chemistry I (MCMP 204)

2015 Undergraduate Teaching Assistant, Organic Chemistry II (MCMP 205)

2014 Undergraduate Teaching Assistant**,** Development, Structure and Function of Organisms (BIOL 131)

2013 Tutor, Introduction to Chinese, Purdue International Center

Professional Experience

2014 Shadowing at Eli Lilly, Pantheon and Bristol-Myers Squibb

2013-2014 Shadowing at Cardinal Health nuclear pharmacy, IU Arnett hospital (Pharmacy, Infectious Disease, anesthesiology), Walgreen Pharmacy, Purdue Veterinary Pharmacy, Indiana Veteran's Home

Poster Presentations

1. **Tang S**, Wang Y, Hockerman G. Molecular Determinants of the Differential Modulation of $Ca_v1.2$ and $Ca_v1.3$ by Nifedipine and FPL 64176. Mol Pharmacol.

   Health & Disease Poster Session, Purdue University, 2019

   Interdisciplinary Graduate Program, Purdue University, 2019

   Sigma Xi Graduate Student Research Awards Competition Poster Session, Purdue University, 2019

   Hitchhiker's Guide to the Biomolecular Galaxy Symposium, Purdue University, 2019

   College of Pharmacy Poster Session, Purdue University, 2017-2019

   Turkey Run Retreat Poster Session, Purdue University, 2018-2019

2. **Tang S**, Sun Y, Krusemark C, Hockerman G. Differentiated regulation of beta-3 subunit on L-type voltage-gated channel alpha-1 subunits at intracellular II-III loop

   Health & Disease Poster Session, Purdue University, 2020

   Interdisciplinary Graduate Program, Purdue University, 2020

   Sigma Xi Graduate Student Research Awards Competition Poster Session, Purdue University, 2020

3. Harvey K, Rantz E, **Tang S**, Hockerman G. RyR2 regulation insulin secretion, electrical activity, and IP3 receptor activation in INS-1 cells

   12th Annual Midwest Islet Club (MIC)- University of Michigan, Ann Arbor, 2019

4. Alongkronrusmee D, **Tang S**, Ghomi HT, Lill MA, van Rijn RM. Identification of a novel interaction site of the delta-mu opioid receptor heteromers.

   Experimental Biology- San Diego, CA 2016

   Undergraduate Research Awards Competition Poster Session, Purdue University, 2016

Oral Presentations

1. **Tang S**, Calcium Channel Subtype Differentiation: Selectively Treating Parkinson's Disease Beyond Hypertension, Hitchhiker's Guide to the Biomolecular Galaxy Symposium, Purdue University, 2019 (**invited talk**)
2. **Tang S**. Identification of a novel interaction site of the delta-mu opioid receptor heteromers. Dean's Summer Undergraduate Research Program. 2015

Awards/Honors/Certificate

2020-2021	Completion of Graduate Online Data Science Connector Modules (In Progress)
2020	Completion of Schrödinger's "Introduction to Molecular Modeling in Drug Discovery"
2018	First place in College of Pharmacy T-shirt design competition
2016-2017	First place in College of Pharmacy Christmas ornament design
2016	BSPS (Bachelor of Science Pharmaceutical Science) Research recognition award

2016 Dr. Frank Brown Jr Travel Award

2015 Dean's Summer Undergraduate Research Program

2015 Charles V. and Madonna Dienhart Flemming Pharmacy Fund

2012-2016 Semester Honor & Dean's List

Professional Memberships

2020-present American Association for the Advancement of Science (AAAS)

2016-present American Society for Pharmacology and Experimental Therapeutics (ASPET)

2012-2016 National Student Pharmaceutical Association

Academic Service

2018-2019 Judge, Science in Schools, Purdue University

2013-2015 Media Officer, Co-founder of Purdue Anime, Comics, Game Association, Purdue University

2014-2015 Purdue Musical organization

2012-2016 Purdue Photography Club